Optimization and Application of CRISPR/Cas-based *in planta* Gene Targeting Technologies

Zur Erlangung des akademischen Grades einer

DOKTORIN DER NATURWISSENSCHAFTEN

(Dr. rer. nat.)

von der KIT-Fakultät für Chemie und Biowissenschaften

des Karlsruher Instituts für Technologie (KIT)

genehmigte

DISSERTATION

von

M. Sc. Seda Yaşar

1. Referent: Prof. Dr. Holger Puchta
2. Referent: Prof. Dr. Peter Nick

Tag der mündlichen Prüfung: 21.07.2026

“For everything in the world, whether material or spiritual,

and for life and success, the truest guide is science.”

Mustafa Kemal Atatürk

Acknowledgement

First and foremost, I would like to express my sincere gratitude to my doctoral supervisor, Prof. Dr. Holger Puchta, for giving me the opportunity to carry out my dissertation in his research group and to work on a wide range of interesting topics within this framework at the Joseph Gottlieb Kölreuter Institute for Plant Sciences, Department of Molecular Biology, Karlsruhe Institute of Technology. I am also very grateful to him for the excellent opportunities to publish in reputable journals and for the chance to present our work at an international conference. Furthermore, I would like to thank him for the generous resources he provided and for involving me in a collaboration with another research institute. I sincerely thank him for his interest in and strong support of my scientific training and development.

I would like to thank Prof. Dr. Peter Nick for kindly agreeing to serve as co-referee for my dissertation.

I gratefully acknowledge the financial support provided by the Study Abroad Postgraduate Education Scholarship (YLSY), awarded by the Republic of Türkiye Ministry of National Education, during my doctoral studies.

I sincerely thank to Prof. Dr. Andreas Houben of the Leibniz Institute of Plant Genetics and Crop Plant Research for the fruitful collaboration, which led to valuable results and provided the opportunity to publish our findings in a renowned journal.

My sincere thanks go to Dr. Laura Merker for her comprehensive introduction to the intricacies of *ip*GT and, for her supervision during the initial phase of my work.

I would especially like to thank Dr. Niklas Capdeville for proofreading this work, but above all for his personal and emotional support during the final year of my doctoral studies, especially during the final months. Thank you for your motivating words, your encouragement, and the many scientific and non-scientific conversations.

I would like to thank Lena Rady for her dedicated and reliable technical support. I am very proud to have had the opportunity to accompany her during her professional training. In addition, I would like to thank all members of the working group for the pleasant working atmosphere and team spirit, and for their constant support. Beyond being colleagues, many of you became friends, and I am truly grateful for the time we shared both in the offices and outside of work. You made my experience in Germany much more enjoyable, meaningful, and memorable.

I would also like to thank the staff of the JKIP experimental facility for the careful cultivation and maintenance of my plants. In particular, I would like to express my sincere thanks to Ms. Sabine Wöhle, Ms. Solène Schreck, and Mr. Kevin Malakowsky.

I would like to express my deep gratitude to my family and friends for their constant moral support and their motivating and encouraging words. My greatest thanks go to my parents for their trust and support.

I would also like to thank my late grandmother, whose endless love and memory will always remain in my heart.

Finally, I would like to acknowledge my own perseverance and resilience, and thank myself for not giving up during this challenging journey.

Publications

Somasundaram, S., **Yaşar, S.**, Fuchs, J., Cuacos, M., Claassen, J., Weiss, O., Kochevenko, A., Lamb, J.C., Li, T., Capdeville, N., Puchta, H., Houben, A., 2026. Targeted CENH3 protein depletion in egg cells enables highly efficient haploid induction. Plant Comm 0. https://doi.org/10.1016/j.xplc.2026.101837

Wirsiy, E.L., Pulat, E., Arslantürk, A.H., **Yaşar, S.**, Çakır, Ö., 2025. Small RNA sequencing reveals important miRNA function in *Arabidopsis thaliana* calli in response to combined drought and nitrogen deficiency. Acta Bot. Bras. 39, e20240147. https://doi.org/10.1590/1677-941X-ABB-2024-0147

Yaşar, S., Pulat, E., Çakır, Ö., 2024. Effects of nitrogen deficiency and drought stresses on miRNA expressions in Arabidopsis thaliana. Plant Cell Tiss Organ Cult 157, 42. https://doi.org/10.1007/s11240-024-02754-0

Review

Yaşar, S., Gehrke, F., Capdeville, N., Puchta, H., 2026. Recent progress in plant genome engineering: from large insertions to chromosome number changes. Current Opinion in Biotechnology 97, 103426. https://doi.org/10.1016/j.copbio.2025.103426

TABLE OF CONTENTS

LIST OF FIGURES

LIST OF TABLES

LIST OF ABBREVIATIONS

aNHEJ	alternative NHEJ
Cas	CRISPR-associated
cNHEJ	classical NHEJ
CRISPR	clustered regularly interspaced short palindromic repeats
crRNA	CRISPR-RNA
D-loop	displacement-loop
DSB	Double-strand break
dsDNA	double-stranded DNA
gDNA	genomic DNA
gRNA	guide RNA
GT	Gene Targeting
HR	Homologous Recombination
*ip*GT	*in planta* GT
MMEJ	Microhomology-Mediated end-joining
NHEJ	Non-homologous end joining
PAM	Protospacer Adjacent Motif
pre-crRNA	precursor crRNA
scFv	single-chain variable fragment
sfGFP	superfolder-Green Fluorescent Protein
sgRNA	single guide RNA
SSA	single strand annealing
ssDNA	single-stranded DNA
SunTag	SuperNova tagging
tracrRNA	trans-activating crRNA
ttLbCas12a-i	intron-containing temperature-tolerant LbCas12a

1 INTRODUCTION

All living organisms are constantly exposed to environmental factors that can induce DNA damage. Among them, plants are particularly vulnerable due to their sessile lifestyle. As phototropic organisms, plants experience continuous exposure to various sources of genotoxic stress, including ultraviolet (UV) radiation, reactive oxygen species (ROS) and, site-specific biotic and abiotic stresses. Consequently, the frequency and diversity of DNA lesions that occur throughout a plant's life cycle are typically higher than in most other organisms (Beying et al., 2021). These DNA lesions are processed by DNA repair mechanisms, which may introduce mutations depending on the pathway involved. As a result, such mutations can enhance survival (Chatterjee and Walker, 2017).

For thousands of years, humans have relied on classical breeding techniques to naturally select for desirable traits in plants, such as improved yield or resilience (Beying et al., 2021). Thereby, these agronomically interesting traits can be achieved via spontaneous mutations (Krishna et al., 2023). The work of Joseph Gottlieb Kölreuter, who showed that offspring inherit traits from both parents (Kölreuter, 1761), along with Gregor Mendel's later clarification of the inheritance principles (Mendel, 1866), established the basis for targeted crossbreeding and hybrid breeding aimed at combining advantageous traits from separate varieties. Later, mutation breeding approaches were developed using physical mutagens such as X-rays (Muller, 1927; Stadler, 1928) or chemical mutagens (Auerbach and Robson, 1946; Loveless, 1958), which were first shown in non-plant organisms to increase mutation rates and were subsequently adopted for use in plants to enhance genetic variability. However, both traditional selection and induced mutagenesis are inherently complex and time-consuming processes. Since mutations occur in an uncontrolled, random manner, identifying individuals with the desired traits demands intensive screening, and additional unintended mutations may remain hidden in the genome (Beying et al., 2021; Shi and Lai, 2015).

1.1 DNA Double-Strand Break Repair Mechanism

DNA double-strand breaks (DSBs) represent one of the most harmful types of DNA lesions, as they can trigger cell cycle arrest, cell death, and compromise genomic stability. Mis-repaired DSBs give rise to genomic alterations, whereas unpaired breaks may lead to chromosomal rearrangements, genome instability or lethality. Therefore, DSB repair must be tightly controlled and precisely regulated to maintain genomic integrity and ensure optimal cellular function (Ceccaldi and Cejka, 2025; Chiolo et al., 2025; Krenning et al., 2019; Stinson and Loparo, 2021; Xue and Greene, 2021). In eukaryotic cells, DSBs are repaired through several pathways that can be grouped into two main classes: error-prone non-homologous end-joining (NHEJ) and error-free homologous recombination (HR) (Beying et al., 2021; Scully et al., 2019; Xue and Greene, 2021).

1.1.1 Non-homologous end-joining repair mechanism

Between the two major pathways, the error-prone NHEJ pathway constitutes the primary pathway for DSB repair across most cell-cycle phases (Karanam et al., 2012; Rodgers and McVey, 2016; Stinson and Loparo, 2021). In the past, NHEJ was considered to be active throughout the entire cell cycle, with its predominant function occurring in G0/G1 (Lieber et al., 2003). A subsequent study, however, has refined this view by demonstrating in human cells that, even when both NHEJ and HR are fully operational, NHEJ remains the dominant repair pathway in both G1 and G2 (Karanam et al., 2012).

NHEJ is further subdivided into two mechanistically distinct branches: classical or canonical NHEJ (cNHEJ) and alternative NHEJ (aNHEJ), also referred to as microhomology-mediated end joining (MMEJ) (Beying et al., 2021; Tamura et al., 2002).

KU-dependent classical NHEJ repair mechanism

The primary pathway for repairing DSBs in both proliferating and non-dividing somatic cells is NHEJ (Scully et al., 2019). Classical NHEJ (cNHEJ) repair (Figure 1.1A) is initiated by the rapid recognition and binding of the KU70/KU80 heterodimer to DNA ends, a critical step that prevents nucleolytic degradation and preserves end stability (Chang et al., 2017; Scully et al., 2019). KU, composed of ~70 and ~80 kDa subunits, binding also triggers the recruitment of core NHEJ factors, ultimately enabling end ligation mediated by the X-RAY REPAIR COMPLEMENTING 1 (XRCC4)-DNA LIGASE IV (LIG4) complex. In plants, PAXX (PARALOG OF XRCC4) and its functional interactions with XRCC4 and KU proteins

contribute to the repair process (Andres et al., 2007; Khan and Ochi, 2023; Mari et al., 2006; Nick McElhinny et al., 2000; Tamura et al., 2002; Zhao et al., 2020). Additionally, mammalian cNHEJ involves Artemis endonuclease and the DNA-dependent protein kinase catalytic subunit (DNA-PKcs), which assist in processing diverse DNA end configurations such as 3' and 5' overhangs (Chang et al., 2016; Waters et al., 2014). Interestingly, homologs of DNA-PKcs and Artemis factors have not yet been identified in plants, and no clear function for these factors has been described within the plant NHEJ pathway (Charbonnel et al., 2010; Molinier et al., 2004). However, *in vitro* studies in mammalian cells have shown that these factors are not essential for cNHEJ and that their roles can be taken over by the MRN (MRE11-RAD50-NBS1) complex. Thus, cNHEJ prioritizes rapid end-rejoining over sequence fidelity. As a result, cNHEJ is intrinsically error-prone and frequently leads to insertions and/or deletions (InDels) at the repair junction and extensive genomic rearrangements such as translocations or improper chromosomal fusions (Kieffer and Lowndes, 2022; Zhao et al., 2020).

Alternative NHEJ repair mechanisms

The high abundance of the KU70/KU80 heterodimer and its rapid interaction with DNA ends ensure that most DSBs are repaired through the cNHEJ pathway. However, if the cNHEJ pathway is impaired, either due to disruptions in its components or depending on the cell cycle phase, cells can instead activate alternative end-joining mechanisms (Beying et al., 2021; Sfeir and Symington, 2015). This KU-independent repair route appears in the literature under several names, including back-up NHEJ, alternative NHEJ (aNHEJ), microhomology-mediated end-joining (MMEJ) and POLYMERASE THETA (POLθ)-mediated end-joining (TMEJ). It remains uncertain whether these terms describe a single repair pathway or several distinct pathways. Nevertheless, the use of short (5-25 bp) microhomologies (MHs) close to the break site is a common characteristic shared across these mechanisms (Beying et al., 2021; Chang et al., 2017; Seol et al., 2018; Sfeir and Symington, 2015). In yeast, repair based on MHs of 3-16 nucleotides have been observed, whereas in human cells, repair events involving MHs of only 1-4 nucleotides have been reported (Boulton and Jackson, 1996; Roth and Wilson, 1986).

aNHEJ requires the activity of POLθ (Figure 1.1B), encoded by *POLQ*, and may also involve POLY (ADP-RIBOSE) POLYMERASE 1 (PARP1), C-terminal binding protein interacting protein (CtIP), and the MRN complex (Chang et al., 2017; Sfeir and Symington, 2015). PARP1 serves as an ADP-ribosylation enzyme that promotes aNHEJ and detects DNA damage (Robert et al., 2009). The endonuclease activity of MRN complex plays only a minor role in end-joining when KU is present (Makharashvili et al., 2014). In plant cells, MRN complex recognize the DNA damage and initiates DNA end resection together with COM1 which is the ortholog of

mammalian CtIP (Asik et al., 2026; Lee and Paull, 2004; Sartori et al., 2007; Uanschou et al., 2007). Following DNA end resection, very short MH (2-6 bp) on the 3' single-stranded DNA (ssDNA) overhangs anneal to each other. Polθ stabilizes the alignment of 3' ssDNA overhangs, using one overhang as the template (Boulton and Jackson, 1996; C. Li et al., 2023; Roth and Wilson, 1986). In cells carrying Polθ mutations, aNHEJ activity is significantly diminished and becomes nearly undetectable, highlighting its key role in this repair mechanism (Chang et al., 2017). A more stable intermediate is then formed through ligation by DNA ligase I (LIG1) or DNA ligase III (LIG3). The polymerase activity of Polθ limits extensive end resection, thereby reducing deletion size. Furthermore, due to its terminal transferase activity, Polθ is capable of adding nucleotides without any template potentially creating MHs between the break ends (Kent et al., 2016; Seol et al., 2018). Repair outcomes of aNHEJ are characterized by deletions, insertions, and mutations at the DNA break site (C. Li et al., 2023). However, this pathway frequently generates templated insertions, typically <25 bp in length, derived from sequences flanking the DSB and associated with Polθ activity (Sfeir et al., 2024).

Given the error-prone nature of NHEJ-based repair mechanisms, cells also rely on HR, a precise pathway that requires longer homologous sequences to accurately repair DNA DSBs (Deng et al., 2014; Sfeir et al., 2024).

1.1.2 Homologous recombination

Homologous recombination is responsible for repairing DNA DSBs that occur during meiosis and requires sister chromatids or another homologous template to repair breaks without errors. This limits HR to the S and G2 phases of the cell cycle in many organisms (Gehrke et al., 2021; Stinson and Loparo, 2021). Homologous recombination is particularly important for chromosome segregation, recombination, and the exchange of genetic information in meiotic tissues (Beying et al., 2021).

DSB repair via homologous recombination is initiated by the recognition of DNA damage, and this step plays key role in determining repair pathway choice. The MRN complex competes with KU at DNA ends, and the initiation of end resection renders these ends incompatible with KU binding, thereby directing repair towards HR (Symington and Gautier, 2011; Tan et al., 2023). Although the initiation of the resection is shared among multiple repair pathways, they can be differed in their genetic dependencies and the length of homologous sequences involved. Typically, single-strand annealing (SSA) and HR require more extensive end resection and

depend on longer regions of homology (20-100 nucleotides) to ensure accurate repair, in contrast to aNHEJ (Deng et al., 2014; Kamoen et al., 2025; Sfeir and Symington, 2015).

The MRN complex has many different roles in DNA repair. First, it structurally stabilizes DNA ends at DSB sites via RAD50 (Symington and Gautier, 2011; Tan et al., 2023). After the recognition phase, the complex regulates the end resection phase, which is critical for homologous recombination. Following the assembly of MRN, MRE11 nuclease activity, together with BRCA1, performs a 5'-3' directional cut to create a 3'-end ssDNA. This 5'-3' end resection cleavage performed by the MRN complex is common to all HR pathways (Beying et al., 2021; Gnügge and Symington, 2021; Symington, 2016). In this end resection phase, considered a highly sensitive stage, the heterotrimeric Replication protein A (RPA A) complex covers the single-stranded 3'-overhangs, protecting them from nucleolytic degradation (Eschbach and Kobbe, 2014). The ssDNA-binding protein RPA removes secondary structures in DNA by binding to the DSB region, thereby facilitating the formation of the RAD51 nuclear filament (Tan et al., 2023; Toh and Ngeow, 2021; Wright et al., 2018). The RAD51 filament formation results in suppression repair via aNHEJ as well as SSA, thereby ensuring that canonical HR is favoured (Feng et al., 2011; Gallagher et al., 2020; Ma et al., 2017; Sung, 1997; Symington and Gautier, 2011).

The specific characteristics of the homologous sequence and the proteins involved determine how the HR pathway branches into distinct repair mechanisms. The most critical of these mechanisms include SSA, as well as the RAD51-mediated pathways Synthesis-Dependent Strand Annealing (SDSA), Double-Strand Break Repair (DSBR), and Dissolution (Beying et al., 2021).

Single-strand annealing (SSA)

Single-Strand Annealing (SSA) is a specialized, non-conservative sub-pathway of homologous recombination that functions independently (Bhargava et al., 2016; Sfeir and Symington, 2015). If the 3' ssDNA overhangs generated by the MRN complex contain more than 20 bp of homologous sequence, SSA can be used to repair the DSB. SSA is highly similar to aNHEJ, particularly in its reliance on ssDNA overhangs and its error-prone nature. The key difference from aNHEJ is that SSA involves longer regions of homology (Figure 1.1C). However, SSA requires long-range end resection to generate extended ssDNA overhangs (>1000 nucleotides). End resection proceeds with RPA coating the ssDNA overhangs, followed by RAD52 binding to homologous sequences at both DSB ends to mediate annealing (Xue and Greene, 2021). Processing of non-homologous tails constitutes the final step of SSA. In this stage, heterologous

3’ overhangs are removed as in aNHEJ, and the resulting gaps are subsequently filled (Bhargava et al., 2016). These 3’ overhangs are excised by the XPF-ERCC1 endonuclease. A dimer composed of RAD1 and RAD10 proteins then trims the overhangs and ligates the DNA strands. This ligation step, which results in the loss of genetic information between homologous sequences, makes SSA the only example of non-conservative HR (Knoll et al., 2014a).

Synthesis-dependent-strand annealing (SDSA), Double-strand break repair (DSBR) and Dissolution

If no flanking repetitive homology is present at the break site, HR repair through other sub-pathways requires a homologous repair template. These pathways, Synthesis-Dependent Strand Annealing (SDSA), Double-Strand Break Repair (DSBR), and Dissolution are all dependent on RAD51 filament assembly and strand invasion (H. Chen et al., 2013; Salas et al., 2006).

Following end resection, the resulting ssDNA is initially coated by RPA. Subsequently, RAD51 is recruited to the ssDNA through BRCA2-mediated loading, and replaces RPA on the ssDNA to forms RAD51 filaments that mediate homology search required for the repair. In mammalian, RAD51 is recruited to the DSB through its interaction with BRCA2, which is connected to BRCA1 via the bridging protein PALB2. After recruitment, RAD51 dissociates from BRCA2 and assembles into a nucleoprotein filament capable of invading homologous dsDNA, using the homologous sequence as a template for DNA synthesis and repair (Renkawitz et al., 2013; Toh and Ngeow, 2021; Wright et al., 2018; Yamamoto and Hirasawa, 2022). In different organisms, this process is facilitated by distinct factors, including RAD52 in yeast, BRCA2 in mammals, and RAD51 paralogs such as XRCC2, RAD51B and RAD51D in *Arabidopsis thaliana* (Feng et al., 2011; Gallagher et al., 2020; Ma et al., 2017; Serra et al., 2013; Sung, 1997; Wolter et al., 2021). The invading strand can invade a homologous sequence within the donor duplex, displacing one of its strands and forming a displacement loop (D-loop). The invading strand then extends by using the homologous sequence as a template, thereby driving the strand-invasion process forward. Following this step, the stability of the D-loop and the extent of DNA synthesis govern the subsequent choice of repair pathway, determining whether the break will be processed through SDSA, DSBR, or ultimately resolved by dissolution. In SDSA, the D-loop is dissolved, and the newly extended invading strand anneals with the second, processed end of the DSB (Figure 1.1D). Because synthesis is restricted to a single strand, SDSA exclusively yields non-crossover (NCO) products. If the invading strand extends excessively, the displaced strand from the D-loop may anneal to the complementary strand at the second DSB end, a process known as second-end capture, commonly observed during

meiosis. This leads to the formation of a double Holliday junction (dHJ) intermediate (Szostak et al., 1983). The dHJ can be resolved through DSBR or through dissolution. In classical DSBR, symmetrical cleavage at both junctions separates the DNA molecules, and the orientation of these cuts determines whether crossover (CO) or NCO products are generated (Figure 1.1E). The alternative pathway, Dissolution (Figure 1.1F), is catalyzed by the RTR complex and represents the predominant mechanism in eukaryotes. The RTR complex, which consists of a Type IA topoisomerase, a RECQ helicase, and the structural proteins RMI1 and RMI2, is highly conserved across eukaryotic species (Chen et al., 2014; Knoll et al., 2014b). In *Arabidopsis*, RECQ4A, TOP3α, and RMI1/RMI2 have been identified and their *in vivo* interactions have been experimentally confirmed (Bonnet et al., 2013; Dorn et al., 2018; Hartung et al., 2008; Röhrig et al., 2018; Schröpfer et al., 2014; Séguéla-Arnaud et al., 2015). During dissolution, the helicase migrates the dHJ towards itself, forming a hemicatenane intermediate (Chen et al., 2014). The topoisomerase then relaxes the resulting DNA supercoils and resolves the hemicatenane structure (Chen et al., 2014). Dissolution preserves genome integrity because it yields only NCO products, ensuring that chromosomes are separated without exchanging genetic material (Knoll et al., 2014b).

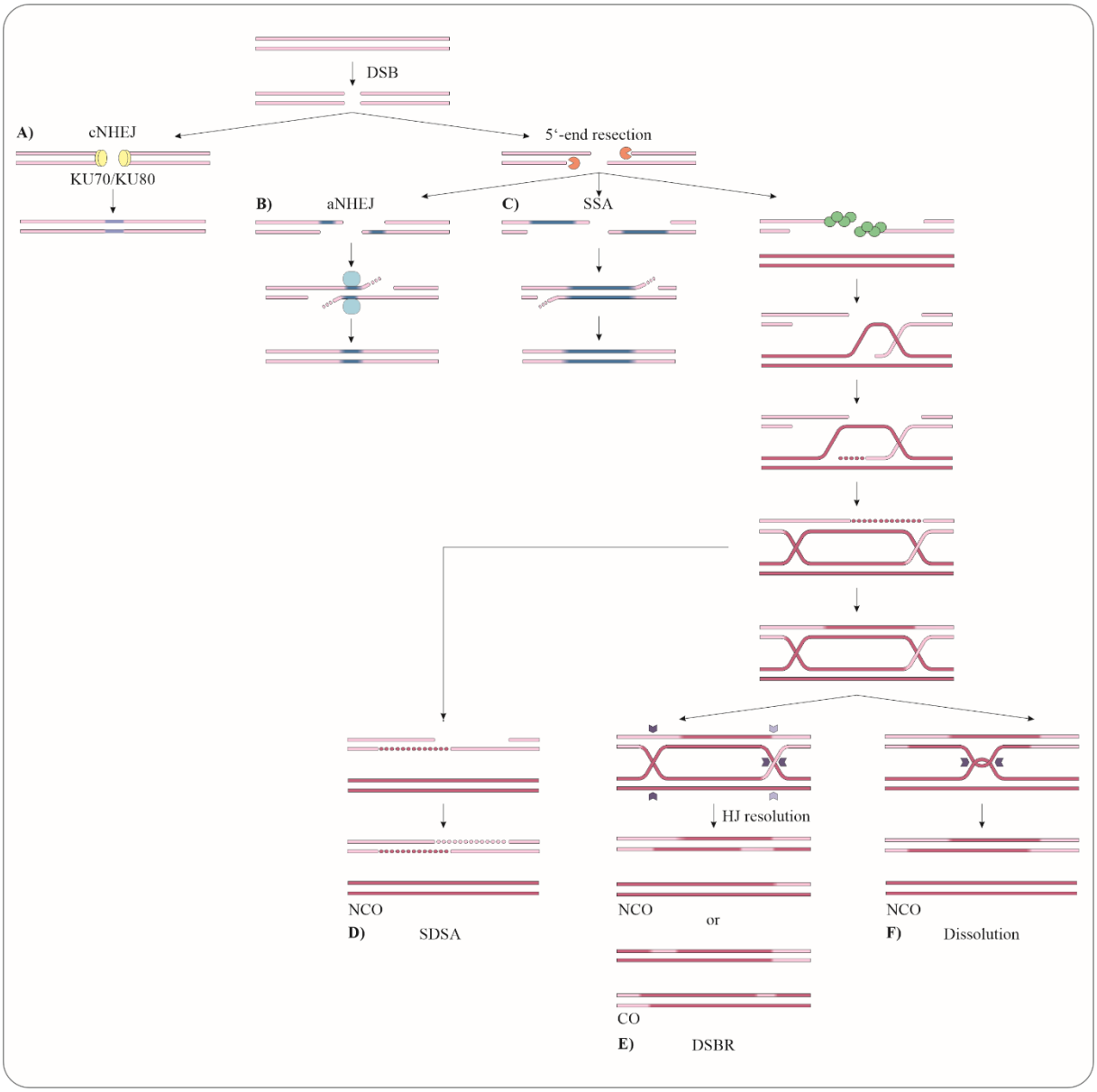

Figure 1.1: Double-strand break (DSB) repair pathways.

DSBs can be repaired through several pathways. Classical non-homologous end-joining (cNHEJ) can directly ligate DNA ends without prior processing. **A) cNHEJ.** Following DSB induction, the KU heterodimer (KU70/KU80) (yellow) rapidly binds to DNA ends and protects them from resection. The DNA ends are subsequently processed if necessary and ligated to restore DNA integrity. **B) Alternative NHEJ (aNHEJ).** The other pathways including aNHEJ require 5'-end resections initiated by the MRN complex (MRE11-RAD50-NBS1) (orange), generating 3' single-stranded overhangs. End resection exposes short microhomology sequences (blue), which can anneal through the activity of polymerase POLθ (light blue). Remaining gaps are filled and non-homologous overhangs are removed before ligation. **C) Single-strand annealing (SSA).** In SSA, longer homologous sequences (blue) exposed by end resection anneal with each other. The intervening DNA is removed, and the remaining gaps are filled to complete repair. **D) Synthesis-dependent strand annealing (SDSA).** After end resection, the 3' overhang invades a homologous DNA template through RAD51-mediated strand exchange (green), forming a displacement loop (D-loop). DNA synthesis extends the invading strand, which subsequently dissociates from template and anneals with the other end of the break, resulting in a non-crossover (NCO) repair product. **E) DSB Repair (DSBR).** If the second DSB-end also engages the homologous template, a double Holliday Junction (dHJ) intermediate forms. Resolution of the dHJ by resolvases can generate either crossover (CO) or NCO products depending on the cleavage orientation. **F) Dissolution.** Alternatively, the dHJ intermediate can be dissolved by the RTR complex, which resolves the junction without cleavage and exclusively produces NCO repair products.

1.2 The CRISPR/Cas system

Genome editing relies on the induction of site-specific DNA DSBs by engineered nucleases. These breaks are subsequently repaired by cellular mechanisms, resulting in insertions, deletions, or sequence replacements (Doudna and Charpentier, 2014). These new genome editing techniques rely on engineered nucleases and are removing barriers to plant breeding (Gao, 2018; Tuncel et al., 2025). In plant biotechnology, the Clustered Regularly Interspaced Short Palindromic Repeats (CRISPR)/CRISPR-associated endonuclease (Cas) system has become a widely used genome editing tool due to its low-cost, time efficiency and high predictability (Gao, 2018). The CRISPR/Cas system is a revolutionary tool in biology, originally discovered as an immune system in prokaryotes. Different CRISPR/Cas systems mediate the recognition, binding, and subsequent cleavage of invading nucleic acids, thereby ensuring their inactivation (Doudna and Charpentier, 2014; Jinek et al., 2012; Makarova et al., 2025).

Naturally, CRISPR/Cas systems function as RNA-guided adaptive immune mechanisms in bacteria and archaea, providing defence against invading genetic elements such as bacteriophages and plasmids (Bhaya et al., 2011; Terns and Terns, 2011; Wiedenheft et al., 2012). Genomically, these systems are characterized by CRISPR loci, which consist of a repeat-spacer array and adjacent *cas* gene operons. The array is composed of conserved direct repeats (21-48 bp) separated by variable, foreign-derived spacers (26-72 bp), the number of which varies significantly across species and strains (Hwarari et al., 2024; Loureiro and da Silva, 2019; Makarova et al., 2022, 2020). During the immune response, the array is transcribed and processed into small CRISPR-derived RNAs (crRNAs) that direct Cas effector proteins – encoded by the associated *cas* operons – to mediate sequence-specific recognition and subsequent cleavage of complementary target sequences (Newsom et al., 2021; Wiedenheft et al., 2012). Thus, the *cas* genes provide the enzymatic machinery required for spacer acquisition, crRNA biogenesis, and interference (Makarova et al., 2022).

The CRISPR/Cas-mediated immune response is structured into three functional phases: adaptation, expression, and interference (Jinek et al., 2012). During adaptation stage, fragments of invading nucleic acids, known as protospacers, are captured and integrated into the CRISPR array, establishing a heritable genetic memory of prior infections and, this process depends on the recognition of a Protospacer Adjacent Motif (PAM), which both directs spacer acquisition and enables self-non-self-discrimination (Feng et al., 2021; Jinek et al., 2012; Makarova et al.,

2025, 2020). In the subsequent expression phase, the CRISPR locus is transcribed into a long precursor RNA (pre-crRNA), which undergoes enzymatic cleavage to generate individual mature crRNAs. This mature crRNAs serve as guides within effector complexes (Awan et al., 2022; Makarova et al., 2025, 2022; Paul and Montoya, 2020). Finally, in the interference stage, these Ribonucleoprotein (RNP) complexes utilize the crRNAs as guides to identify complementary targets, typically via PAM-dependent interactions, and induce site-specific cleavage of the invading genome. Thereby neutralizing the invading genome (Jiang and Doudna, 2017; Jinek et al., 2012; Makarova et al., 2025, 2020). Understanding these natural constraints in RNA-guided recognition and enzymatic activation provides the necessary framework for subsequent strategies aimed at optimizing CRISPR/Cas-based biotechnological tools.

1.2.1 The classification and diversity of CRISPR/Cas system

The discovery of CRISPR elements originated from the identification of atypical repetitive sequences in bacterial genomes. In 1987, short, regularly spaced 32-nucleotide repeats located downstream of the *alkaline phosphatase (iap)* gene in *Escherichia coli* K-12 was reported (Ishino et al., 1987). Over the following years, structurally similar repeat-spacer arrays were reported in other species (Hermans et al., 1991; Nakata et al., 1989). The presence of comparable loci in archaeal genomes further indicated a widespread distribution across prokaryotes (Mojica et al., 2000). However, the functional significance of these elements remained unclear for more than a decade and the characterization of *cas* genes provided the first indication of a linked protein machinery (Jansen et al., 2002). Subsequent genome-wide analyses established the conserved organization of repeat-spacer arrays and cas operons (Haft et al., 2005), culminating in the experimental demonstration that CRISPR/Cas systems mediate immunity against bacteriophages (Barrangou et al., 2007).

The growing number of identified CRISPR/Cas loci revealed an unexpected level of diversity, which ultimately led to the development of a comprehensive classification framework. The current scheme, which is continuously refined to keep pace with new discoveries, recognizes over 50 distinct Cas protein families, reflecting the remarkable evolutionary diversification of CRISPR/Cas systems. Based on effector composition and mechanism, the CRISPR/Cas system has been categorized into two major classes (1 and 2) and seven types (I-VII). Class 1 systems (comprising Type I, III, IV, and VII) are characterized by multi-subunit effector complexes where various Cas proteins cooperate to mediate pre-crRNA processing and interference (Jinek et al., 2012; Makarova et al., 2025). The structural backbone of these complexes is typically

formed by multiple, paralogous proteins from the Repeat-Associated Mysterious Protein (RAMP) family, specifically Cas5 and Cas7 (Makarova et al., 2022, 2015, 2011). Within this class, Type I systems are the most diverse and are defined by signature gene *cas3*, which encodes a helicase-nuclease responsible for target DNA degradation (Makarova et al., 2020).

In contrast, Class 2 systems (comprising Type II, V, and VI) utilize a single, large, multidomain effector protein – such as Cas9, Cas12, or Cas13 – to perform all activities required for targeted interference (Makarova et al., 2025). This structural simplicity is the primary reason of their widespread use as biotechnological tools (Hwarari et al., 2024; Makarova et al., 2022). Type II systems are defined by the presence of Cas9 (Nishimasu et al., 2014) and Type V systems, encompassing Cas12 proteins (Makarova et al., 2020).

Lastly, Type VI systems represent the only variety that exclusively targets RNA through the activity of Cas13 (Makarova et al., 2020). By 2025, Type VI systems continue to be classified among the 46 CRISPR/Cas subtypes identified through computational analyses and are strategically significant in RNA diagnostic platforms owing to their collateral RNase activity (Makarova et al., 2025). These subtypes are defined according to differences in operon organization and the distribution of accessory genes, reflecting lineage-specific evolutionary adaptations among diverse prokaryotic hosts. Within Type II systems, for example, Subtype II-A is distinguished by the presence of the signature *csn2* gene and includes the extensively applied *Streptococcus pyogenes* Cas9 (SpCas9), whereas Subtype II-C exhibits a more reduced gene architecture and is commonly linked to smaller Cas9 orthologs. Likewise, the expansion of Type V into multiple subtypes – including the Subtype V-A represented by Cas12a – has generated a functionally specialized repertoire characterized by distinct PAM specificities and cleavage properties (Fonfara et al., 2016; Makarova et al., 2025). This diversity of CRISPR/Cas systems offers various applications in biotechnology, most notably those involving Cas9 and Cas12a endonucleases.

Structure and mechanism of CRISPR/Cas9 system

The operational efficiency of Class 2 CRISPR/Cas systems is fundamentally rooted in their single-protein effector architecture, which facilitates targeted interference through a highly coordinated series of structural rearrangements (Makarova et al., 2022). Within this class, the Type II effector, Cas9, represents the most extensively characterized model, particularly the ortholog from SpCas9 (Altae-Tran et al., 2021; Makarova et al., 2025, 2020).

The functional activation of Cas9 is a multi-step process that begins with the hybridization of a trans-activating CRISPR RNA (tracrRNA) to the pre-crRNA repeats, a process mediated by the

host's RNase III in the presence of the Cas9 protein itself. Later, Cas9 was programmed using a single chimeric RNA to mimic the tracrRNA:crRNA duplex, enabling to targeted DNA cleavage. This single chimeric RNA, commonly referred to as a single guide RNA (sgRNA), was engineered as a single transcript. In combination with the Cas9 nuclease, the sgRNA efficiently introduce sequence-specific cleavage of the target DNA. These findings demonstrate that sgRNA can be utilized to program the Cas9 endonuclease and can be preferred as a biotechnological tool due to its versatility, efficiency and programmability (Jinek et al., 2012).

Structural analysis has revealed that SpCas9 is composed of six primary functional domains: the Recognition lobe (comprising REC I and REC II), an arginine-rich bridge helix, the PAM Interacting (PI) domain, and the HNH and RuvC nuclease domains (Anders et al., 2014; Jinek et al., 2012; Nishimasu et al., 2014). Subtype II-A constitutes the most commonly applied subtype within Type II CRISPR systems. Despite its widespread use, the large coding sequence presents challenges for vector packaging and may compromise delivery efficiency in systems where cargo size is restricted (Makarova et al., 2025, 2020).

The REC I domain serves as the primary scaffold for binding the guide RNA (gRNA), while the PI domain is responsible for monitoring the DNA for a specific PAM, which for SpCas9 is typically a 5'-NGG-3' sequence. However, this stringent PAM requirement substantially restricts the range of genomic targets, as DNA cleavage is limited to sequences located immediately adjacent to these specific motifs. (Anders et al., 2014; Jinek et al., 2012; Nishimasu et al., 2014). In this context, Subtype II-C effectors have gained considerable interest due to their comparatively small Cas9 orthologs, including *Staphylococcus aureus* Cas9 (SaCas9), which comprises approximately 1053 amino acids (Nishimasu et al., 2015; Ran et al., 2015).

Recognition of the PAM is achieved within the PI domain that engage the DNA major groove, thereby triggering the initiation of catalytic activity via the arginine-rich bridge helix. Upon PAM engagement, the Cas9-RNA complex aligns the target DNA duplex so that it promotes the initiation of local strand separation (Anders et al., 2014). Following successful R-loop formation, the HNH domain cleaves the DNA strand complementary to the gRNA, while the RuvC-like domain cleaves the non-complementary strand at positions approximately 3 bp upstream of the PAM, resulting in mostly blunt-ended DSBs (Figure 1.2) (Gasiunas et al., 2012; Jinek et al., 2012; Nishimasu et al., 2014; Wiedenheft et al., 2009). Although Cas9 catalytic activity generates predominantly blunt-ends, the formation of 1-3 nt 5' overhangs has also been reported (Shou et al., 2018). The stability of the R-loop, particularly across the PAM-proximal 8-12 bp seed region, plays a critical role in defining targeting specificity. While mismatches

within this seed region are largely disruptive to cleavage activity, PAM distal mismatches can be partially tolerated and may contribute to unintended off-target effects. (Jiang and Doudna, 2017).

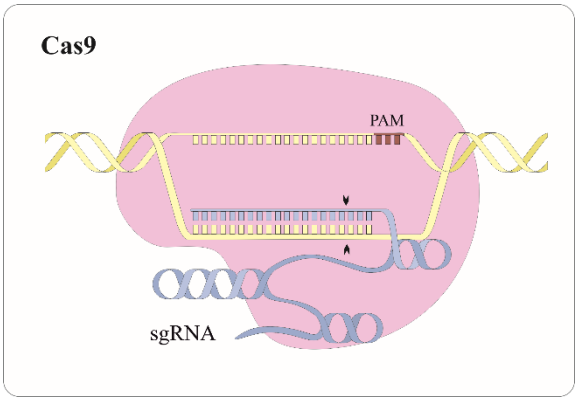

Figure 1.2: Mechanism of CRISPR/Cas9 target recognition and DNA cleavage.

The Cas9 endonuclease forms a complex with the single-guide RNA (sgRNA), which directs Cas9 to a complementary DNA target sequence. Target recognition requires the presence of a protospacer adjacent motif (PAM) located downstream of the target sequence. After PAM recognition, the sgRNA hybridizes with the complementary DNA strand, forming an RNA-DNA heteroduplex and displacing the non-target strand. Cas9 subsequently introduces a double-strand break in 3 bp upstream of PAM sequence at the target DNA.

However, functional diversification of Cas9 has been achieved through targeted mutations within its two nuclease domains, RuvC and HNH. Introduction of a single point mutation in either the RuvC domain (D10A) or the HNH domain (H840A) generates a Cas9 nickase (nCas9), which cleaves only one DNA strand. In contrast, simultaneous inactivation of both catalytic domains (D10A and H840A) completely abolishes nuclease activity, resulting in deadCas9 (dCas9) (Jinek et al., 2012; Piatek et al., 2015; L. S. Qi et al., 2013). Although dCas9 lacks endonuclease activity, it retains its ability to bind DNA in a sequence-specific manner guided by gRNA. This property allows its use in transcriptional regulation, including CRISPR-mediated activation (CRISPRa) and CRISPR interference (CRISPRi) (McCarty et al., 2020; L. S. Qi et al., 2013). In CRISPRi applications, dCas9 represses transcription by hindering RNA polymerase binding or by blocking transcriptional elongation when targeted within the open reading frame (ORF). To expand the scope of gene regulation, multiplexing strategies can be employed, in which multiple gRNAs are used simultaneously to target different genomic loci. In the context of dCas9-based systems, multiplexing provides coordinated regulation of multiple genes without inducing DNA cleavage. In contrast, when catalytically active Cas9 endonuclease is utilized, multiplexing can facilitate simultaneously DNA cleavage at several target sites for genome editing purposes (McCarty et al., 2020).

Structure and mechanism of CRISPR/Cas12a system

In contrast to the dual-nuclease architecture of Cas9, the Type V effector, Cas12a (formerly Cpf1), employs a distinct catalytic logic characterized by a single RuvC-like nuclease domain responsible for the consecutive cleavage of both DNA strands (Fonfara et al., 2016; Makarova et al., 2022). A defining functional hallmark of Cas12a is its intrinsic ribonuclease activity; unlike Cas9, which requires external factors for RNA maturation, Cas12a is a dual-nuclease capable of processing its own pre-crRNA independently of tracrRNA or RNase III. This self-processing occurs upstream of a characteristic hairpin structure, significantly streamlining the delivery of multiple guides for multiplexing applications (Fonfara et al., 2016; Gupta et al., 2019; Swarts et al., 2017). The short mature crRNAs (42-44 nt in length) are processed from the pre-crRNA transcripts derived from CRISPR arrays (Zetsche et al., 2015). While type II CRISPR/Cas systems typically consist of 20-24 nt of spacer sequences followed by 22 nt direct repeats, the crRNA structure of Cas12a systems contains 23-25 nt spacers followed by 19 nt direct repeats (Chylinski et al., 2013; Deltcheva et al., 2011; Zetsche et al., 2015). Most notably, Cas12a recognizes T-rich PAM sequences located upstream of the protospacer, typically 5'-TTTV-3' (V = A, C, or G) (see Figure 1.3), although some orthologues such as *F. novicida* (FnCas12a) accept the shorter 5'-TTV-3' motif. This upstream PAM orientation contrasts with Cas9, which recognizes PAMs on the 3' side of the target sequence. The T-rich PAM preference enables efficient targeting of AT-rich genomic regions that may be inaccessible to SpCas9 (Chen et al., 2019; Malzahn et al., 2019; Tuncel et al., 2025; Zetsche et al., 2015).

Structurally, Cas12a also differs in its cleavage pattern. Following PAM recognition and R-loop formation, Cas12a introduces staggered DSBs distal to the PAM, typically generating 5' overhangs of approximately 4-5 nucleotides located around 18 nt away from the PAM (Chen et al., 2019; Zetsche et al., 2015). These fundamental mechanistic differences between Cas9 and Cas12a have direct implications for their performance in eukaryotic environments. In contrast to the predominantly blunt-ended DSBs generated by Cas9, the staggered DNA breaks produced by Cas12a have been suggested to provide a potentially more favorable substrate for certain targeted insertion strategies (Chen et al., 2019; Jinek et al., 2012; Malzahn et al., 2019; Zetsche et al., 2015). For plant science, where the goal often shifts from simple gene knockouts to precise sequence replacement these natural enzymatic properties must be further optimized.

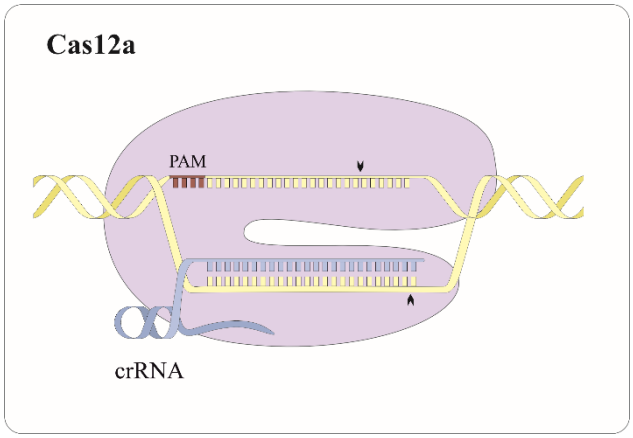

Figure 1.3: Mechanism of CRISPR/Cas12a-mediated DNA recognition and cleavage.

Cas12a forms a ribonucleoprotein complex with a CRISPR RNA (crRNA), which guides the nuclease to the complementary DNA target sequence. Target recognition requires the presence of a protospacer adjacent motif (PAM) located upstream of the target sequence. Following PAM recognition, the crRNA pairs with the complementary DNA strand, resulting in the formation of an RNA-DNA hybrid and displacement of the non-target strand. Cas12a subsequently cleaves the target DNA distal to the PAM site, with non-target strand typically cleaved at 18 nt and the target strand at 23 nt downstream of the PAM, generating a double-strand break with staggered ends and 5 nt 5`overhangs.

1.2.2 CRISPR/Cas-mediated Genome Engineering in plants

The adaptation of CRISPR/Cas systems from their original role in bacterial adaptive immunity into programmable genome engineering tools has profoundly reshaped strategies for targeted DNA modification across biological systems. In prokaryotes, CRISPR arrays and associated Cas proteins operate as an RNA-guided defence machinery that detects and cleaves invading nucleic acids, including bacteriophages and plasmids. Following the biochemical demonstration that RNA-guided nucleases can be harnessed for site-specific DNA cleavage, CRISPR/Cas technologies were rapidly repurposed into versatile genome editing platforms applicable to a wide range of eukaryotic organisms, including plants (Chen et al., 2019; Doudna and Charpentier, 2014; Jinek et al., 2012). This conceptual breakthrough was particularly significant because, unlike earlier sequence-specific nucleases such as zinc-finger nucleases (ZFNs) and transcription activator-like effector nucleases (TALENs), CRISPR-based targeting can be reprogrammed simply by altering the guide RNA sequence rather than re-engineering the protein scaffold for each genomic locus (Doudna and Charpentier, 2014; Malzahn et al., 2019; Voytas, 2013). A defining mechanistic hallmark of CRISPR/Cas gene editing is the induction of site-specific DNA DSB. These breaks are the primary triggers for genome modification because they recruit endogenous DNA repair machinery. Once a Cas endonuclease generates a DSB at a target locus (Chen et al., 2019; Malzahn et al., 2019; Symington and Gautier, 2011), NHEJ is frequently produces small Indels at the cleavage site, making it highly effective for gene knockout strategies (Malzahn et al., 2019). In contrast, HDR enables precise sequence

replacement or targeted insertion when a homologous donor template is supplied; however, the efficiency of such gene targeting (GT) approaches in plants is often limited due to cell-cycle dependence and the relatively low activity of HDR pathways in many plant tissues. Consequently, genome editing outcomes in plants are largely shaped by the nature of the nuclease-induced DNA break and by the relative activities of endogenous repair pathways (Atkins and Voytas, 2020; Chen et al., 2019; Malzahn et al., 2019; Voytas, 2013).

Despite the extensive diversity of CRISPR/Cas systems in nature, genome engineering applications have been dominated by Class 2 systems, which employ single, multidomain effector nucleases guided by RNA (Jiang and Doudna, 2015; Makarova et al., 2020; Tao et al., 2023). This single-effector organization simplifies system design and deployment in genome engineering applications (Doudna and Charpentier, 2014; Makarova et al., 2020; Tuncel et al., 2025). Consistent with these advantages, CRISPR/Cas9 technology has been widely adopted for genome editing in plants, with SpCas9 emerging as the most widely utilized system among Class 2 nucleases (Chen et al., 2019; Gürel et al., 2020). This widespread use is partly attributable to its PAM compatibility, as SpCas9 recognizes not only the canonical NGG PAM, but also noncanonical PAMs, including NAG in plant system (Meng et al., 2018). In addition to target recognition, DNA repair outcomes further influence genome editing efficiency. Given that DSBs in plant systems are predominantly repaired through the NHEJ pathway, this intrinsic repair bias represents an important mechanistic factor when selecting CRISPR nucleases for specific genome engineering applications (Atkins and Voytas, 2020; Malzahn et al., 2019).

Optimization and expansion of the CRISPR/Cas toolbox: Cas9 orthologues, Cas12a and its improvements

As plant genome engineering applications expanded, several limitations associated with the canonical SpCas9 system became apparent. In particular, its requirements for the presence of a 5’-NGG-3’ PAM adjacent to the target site, can limit access to certain genomic regions. This constraint may be especially relevant in AT-rich genomic contexts, including many plant promoter regions, where suitable NGG sites occur less frequently (Chen et al., 2019; Hillary and Ceasar, 2023; Zetsche et al., 2015). To expand the editable sequence space, considerable effort has therefore been directed toward the identification of naturally occurring Cas9 orthologues as well as the engineering of SpCas9 variants with altered PAM specificities (Chen et al., 2019; Tuncel et al., 2025). Multiple orthologues from subtypes of Cas9 have been successfully utilized in plant genome engineering (Tuncel et al., 2025). In parallel, different variants have been engineered to loosen PAM requirements and further broadened the targeting range across plant genomes (Chen et al., 2019; Tuncel et al., 2025). However, expanding PAM

compatibility can be accompanied by changes in editing efficiency or target specificity, indicating that nuclease performance remains context-dependent and may require case-specific optimization (Chen et al., 2019; Hillary and Ceasar, 2023).

In addition to Cas9 diversification, type V CRISPR systems – particularly Cas12a – have emerged as important complementary genome editing tools (Chen et al., 2019; Malzahn et al., 2019). Cas12a exhibits several mechanistic differences from Cas9 that are highly relevant for plant genome engineering (Yan et al., 2019). Moreover, engineered Cas12a variants with improved editing performance or more flexible PAM recognition have been developed (Tuncel et al., 2025).The most widely used Cas12a orthologues in plants include *Acidaminococcus* sp. *BV3L6* (AsCas12a), LbCas12a, and FnCas12a, all of which have demonstrated functionality in species such as rice, *Arabidopsis thaliana* and maize (A. Endo et al., 2016; Hu et al., 2017; Tang et al., 2017; Xu et al., 2017; Zhong et al., 2018). However, practical deployment of Cas12a has revealed system-specific constraints, particularly temperature sensitivity (Moreno-Mateos et al., 2017). Plant transformation and regeneration are commonly performed at approximately 20-25 °C, yet several studies have shown that Cas12a editing efficiency can decline at these ambient temperatures. Experimental evidence indicates that optimal Cas12a activity in rice cells often requires temperatures of approximately 28 °C or higher, and certain orthologues such as AsCas12a display particularly strong temperature dependence (Malzahn et al., 2019). These observations highlighted temperature sensitivity as a key bottleneck limiting broader adoption of Cas12a in plant systems. To address this limitation, temperature-tolerant LbCas12a (ttLbCas12a) derivatives were engineered (Schindele and Puchta, 2020). Notably, the enhanced variant enLbCas12a exhibits improved activity at moderately reduced temperatures, while the strongly ttLbCas12a demonstrates robust editing efficiency under conditions typical of plant tissue culture (Schindele and Puchta, 2020). These engineered nucleases substantially reduce the need for elevated-temperature treatments and improve the practical applicability of Cas12a-based genome editing in plants. Such protein-level optimization represents an important step toward improving the performance of Cas12a under standard plant growth conditions.

Beyond protein engineering, further improvements in Cas12a performance have also been achieved through expression-level optimization. An intron-containing version of ttLbCas12a (ttLbCas12a-i) was shown to significantly enhance both gene editing and gene targeting efficiencies in *A. thaliana* (Schindele et al., 2023). This enhancement is consistent with the well-established phenomenon of intron-mediated enhancement (IME) in plants, whereby the presence of introns can promote messenger RNA (mRNA) processing, nuclear export, and transcript accumulation (Laxa, 2017; Rose, 2008; Shaul, 2017). Increased transcript abundance

is expected to elevate the intracellular levels of functional nuclease, thereby improving overall editing outcomes. These findings indicate that effective deployment of Cas12a in plants often requires integrated optimization strategies that combine protein engineering, expression tuning, and guide design.

In addition to these optimization strategies, off-target effects are also one of the major challenges for the improvement of CRISPR/Cas technologies. Off-target effects are characterized by unwanted genomic manipulations at loci that share high sequence homology with the target site. These events typically occur when the Cas nuclease-gRNA complex recognizes a sequence with several mismatches, particularly outside the seed region PAM, where perfect complementarity is most vital for cleavage specificity (Allen et al., 2025; Hajiahmadi et al., 2019; Rananaware et al., 2023; Rohatgi et al., 2024). Off-target activity can lead to genomic instability, undesired gene disruption, or unintended phenotypic changes in plants, making its management essential for ensuring precision of modern breeding (H. Zhang et al., 2021; S. Zhang et al., 2021).

Various strategies have been developed to enhance the accuracy of these molecular tools. One effective approach is the utilization of nCas9, which induces single-strand breaks (SSBs) rather than DSBs, thereby reducing the possible error-prone repair at non-target sites. Additionally, the use of paired nCas9, which can be positioned on the opposite DNA strands to introduce two breaks, can generate a staggered DSB at the target site while significantly enhancing specificity (Ran et al., 2013). This paired nCas9 nuclease system has been utilized in rice calli to investigate off-target effects, demonstrating that the system can induce mutations more specifically at the intended target sites (Mikami et al., 2016). Furthermore, the transition toward DNA-free genome editing has proven successfully. By delivering pre-assembled RNPs into plant cells, such as immature wheat embryos, researchers have achieved high editing efficiency with no detectable off-target effects. This primarily attributed to transient expression of the nuclease, which performs the desired edit and is rapidly degraded before it can act on sub-optimal genomic sites (Liang et al., 2017).

The choice of nuclease also significantly impacts specificity. A comparative study in tomato cells involving SpCas9, AsCas12a, FnCas12a and LbCas12a demonstrated that LbCas12a possesses the lowest off-target activity, highlighting the inherent high specificity of Cas12a-mediated systems (Baranova et al., 2025; Slaman et al., 2024). Additionally, engineering the sgRNA scaffold has been shown to improve outcomes; for instance, targeting genes in rice using optimized Cas12b complexes resulted in reduced off-target mutations (Gurel

et al., 2023). Finally, the integration of computational prediction tools has become standard practice for pre-identification and avoidance of high risk off-target sites (Hwarari et al., 2024; Naeem and Alkhnbashi, 2023). However, editing efficiency in plants is strongly context dependent and influenced by multiple factors, including DNA repair pathway bias, chromatin status and accessibility, chromosome region, nuclease expression levels, nuclear localization efficiency, and temperature conditions (Lowder et al., 2015; Malzahn et al., 2019; Weiss et al., 2022; Zhang et al., 2019). Continued refinement of Cas nucleases and their expression architectures therefore remains essential for advancing plant genome engineering and for enabling broader applications in modern plant breeding (Capdeville et al., 2023; Zhu et al., 2020). These technological improvements have contributed to establishment of CRISPR/Cas systems as robust and versatile tools for plant genome engineering applications.

1.3 Applications of CRISPR/Cas for plant breeding aspects

The history of plant breeding has been defined by the pursuit of generating and harnessing genetic variation (Evenson and Gollin, 2003). Traditional breeding methodologies, while successful in doubling global grain yields during Green Revolution, have reached a plateau in productivity due to the inherent constraints of natural genetic recombination (Pingali, 2012). The integration of CRISPR/Cas technology into plant biotechnology represents a fundamental transition from the passive natural genetic diversity to active, high-precision engineering of specific genomic loci (Voytas and Gao, 2014). This evolution represents more than an expansion of the conventional breeding paradigms, it fundamentally redefines the temporal efficiency and the genomic scope of crop improvement strategies (Zhu et al., 2020). The application of CRISPR/Cas in plants is harnessed for different aspects for plant breeding.

1.3.1 Targeted Mutagenesis

Targeted mutagenesis is widely adopted in the application of CRISPR/Cas systems in plant biotechnology, allowing to induce several DSB simultaneously (Li et al., 2024). Targeted mutagenesis often categorized as Site-Directed Nuclease-1 (SDN-1), this approach focuses on introducing site-specific genomic disruption resulting in loss-of-function alleles (Atia et al., 2024; Authority (EFSA) et al., 2021). The predominant NHEJ-mediated repair of cleaved DNA frequently introduces small InDels at the target site leading to frameshift or nonsense mutations (Jinek et al., 2012; Kalter et al., 2025; Kosicki et al., 2022; Lieber, 2010).

In modern plant breeding, the inherent limitations of conventional breeding approaches, particularly with respect to time efficiency, genetic variability, and interspecific cross compatibility, have established targeted mutagenesis for *de novo* domestication strategies (Li et al., 2024; J. Zhang et al., 2023). Through the application of CRISPR/Cas-based genome editing systems, researchers can efficiently introduce key domestication traits and modulate the fruit number, morphology, size and nutritional composition thereby accelerating the genetic improvement of crop species (Zsögön et al., 2018). Using CRISPR/Cas-mediated genome engineering six domestication-associated loci were targeted in wild *Solanum pimpinellifolium*, resulting in threefold enhancement in fruit size and a tenfold enhancement in fruit number (Zsögön et al., 2018). Furthermore, this strategy was successfully implemented in diverse crop species, including rice (Yu et al., 2021) and tomato (T. Li et al., 2018), where it has facilitated the targeted introduction of domestication-related traits. Beyond yield and quality-associated characteristics, the same approach has also been applied in studies aiming to enhance tolerance to abiotic stresses such as salinity (Zsögön et al., 2017). While these established strategies demonstrated the power of targeted mutagenesis, they often face limitations in achieving the specific deletion sizes necessary for optimal trait modulation. To address this, the SuperNova-tag (SunTag)-mediated recruitment of the 3'-5' exonuclease human THREE PRIME REPAIR EXONUCLEASE 1 (HsTREX1) has emerged as a superior tool (Capdeville et al., 2024). The SunTag system is allow for the simultaneous recruitment of multiple copies of a protein through the interaction between a peptide epitope array and its corresponding antibody (Tanenbaum et al., 2014). In this approach, a 19-amino-acid peptide derived from the leucine zipper motif of the GCN4 transcription factor from *Saccharomyces cerevisiae* is used as the epitope. Tandem repeats of this peptide, separated by short 22-amino-acid GS linkers, can be fused to a Cas nuclease, thereby creating a scaffold that allows the recruitment of multiple effector proteins via GCN4-specific antibodies (Wörn et al., 2000). To ensure efficient intercellular functionality, the system employs single-chain-variable-fragment (scFv) antibodies instead of full-length antibodies, which often exhibit improper folding in the cytoplasm. These scFv fragments are generated by linking the variable regions of the heavy and light chains, resulting in improved solubility and expression in intracellular environments (Marks et al., 1991). However, the GCN4-specific antibody variant originally optimized for yeast expression was found to aggregate at higher concentrations in human cells. To overcome this limitation, the antibody was further engineered by adding superfolder Green Fluorescent Protein (sfGFP) (Pédelacq et al., 2006) and the B1 immunoglobulin-binding domain of protein G (GB1) from group C *Streptococci* (Gronenborn et al., 1991) to its C-terminus (see

Figure 1.4). These modifications enhance proper folding and increase the stability of resulting fusion constructs (Tanenbaum et al., 2014). In the study, SunTag-mediated recruitment of HsTREX1 exonuclease enabled the efficient induction of 20 to 40 bp deletions that are ideally suited for the functional dissection and fine-tuning of cis-regulatory elements (Capdeville et al., 2024).

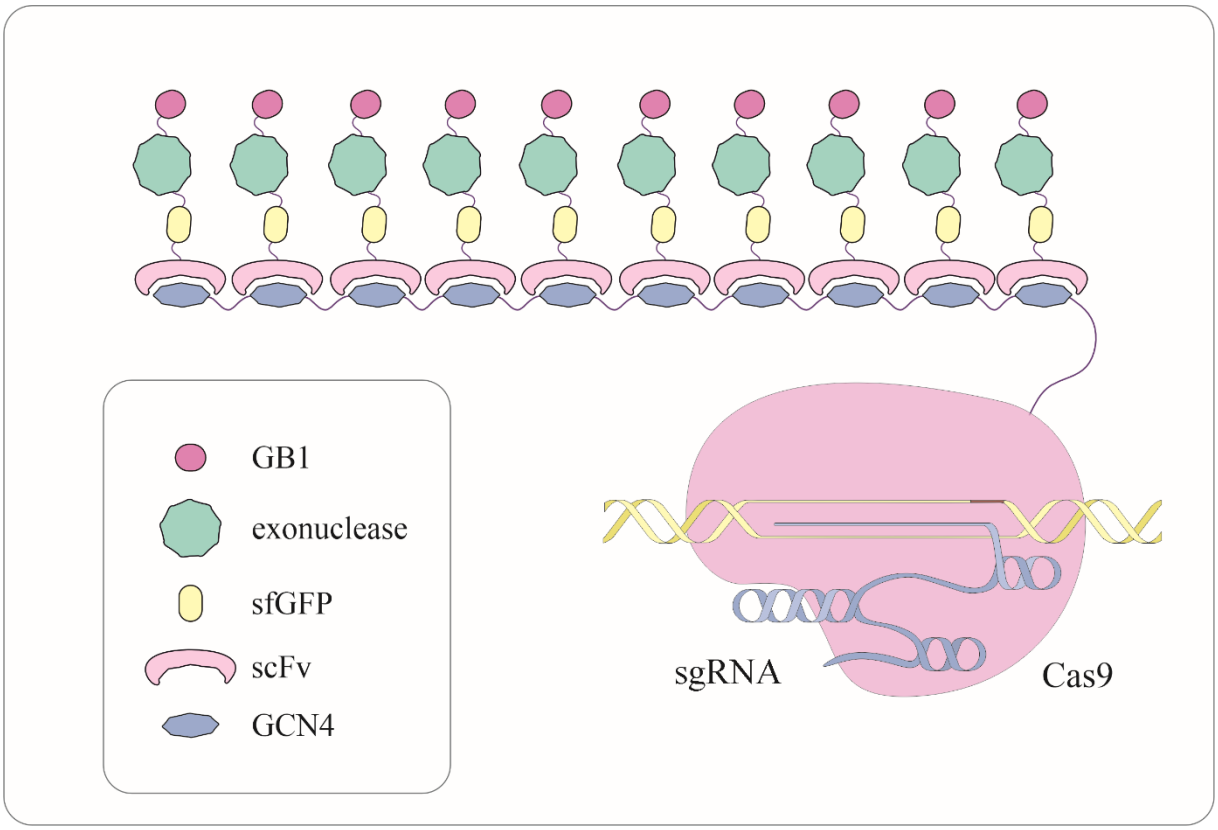

Figure 1.4: The SuperNova tagging (SunTag)-mediated recruitment system.

The SunTag system is based on a repeating array of peptide epitopes that are recognized by specific single-chain variable fragment (scFv) antibodies. In this system, a tandem array of GCN4-derived peptide epitopes is fused to the CRISPR-associated protein 9 (Cas9), enabling the recruitment of multiple copies of effector proteins to a defined genomic locus in a sequence-specific manner via single-guide RNA (sgRNA)-guided DNA targeting. Each GCN4 epitope consists of a 19-amino-acid peptide derived from the leucine zipper motif of the transcription factor GCN4 from *Saccharomyces cerevisiae*. The recruited effector proteins are fused to an scFv antibody that specifically recognizes the GCN4 epitopes. To enhance protein stability and prevent aggregation, the fusion construct includes a superfolder green fluorescent protein (sfGFP) and the B1 domain of protein G (GB1). In the system, multiple copies of any protein of interest are recruited to the Cas9, thereby amplifying the local enzymatic activity at the target site. This modular design allows efficient and tunable recruitment of functional proteins to specific genomic regions for targeted mutagenesis.

Nevertheless, despite these advances and improvement in targeted mutagenesis, it remains limited in its ability to introduce random mutations, and the development of alternative or complementary genome editing tools enables predefined modifications (Yu and Li, 2022).

1.3.2 Base Editing

While CRISPR/Cas-mediated targeted mutagenesis primarily relies on DSB formation followed by error-prone repair, recent advances have enabled precise nucleotide substitutions without introducing DSBs (Eid et al., 2018). These precise nucleotide substitutions are important for plant breeding as they increase crop yield, enhance stress tolerance, and promote agronomic sustainability. Furthermore, CRISPR/Cas systems can be used to induce targeted mutagenesis to improve genetic diversity and facilitate the development of crops with desirable traits (Kumar et al., 2024). Targeted mutagenesis enables the generation of gene knockouts through the induction of insertions or deletions, whereas accurate single-nucleotide polymorphisms (SNPs) can be introduced using Base Editing (BE). In contrast, BE facilitates efficient and targeted nucleotide substitutions by binding to the genomic locus without generating DSB, thereby providing a site-specific genome engineering approach in plant systems (Eid et al., 2018; Hess et al., 2017). Catalytically inactivated Cas9 endonuclease (dCas9) has been widely utilized as a programmable DNA-binding platform for diverse applications, including transcriptional regulation, epigenetic modification, and the recruitment of DNA-modifying enzymes such as deaminases (Eid et al., 2018; Piatek et al., 2015). BE systems exploit the nCas9 variant fused to a cytidine or adenosine deaminase to mediate site-specific, single nucleotide conversion for genome engineering (Eid et al., 2018). The historical foundation of BE began with the fusion of a rat cytidine deaminase (APOBEC1) to a dCas9 to achieve cytosine (C) to thymine (T) transitions (Komor et al., 2016), followed by the development of the first adenine base editor using a laboratory-evolved TadA protein (Gaudelli et al., 2017). Cytosine Base Editors (CBEs) employ cytidine deaminases to catalyze the hydrolytic deamination of cytosine to uracil (U), generating a U:G mismatch within genomic DNA (Komor et al., 2018). In biological systems, uracil is interpreted as thymine during DNA replication, ultimately resulting in a permanent C:G to T:A transition (Komor et al., 2018; Rees and Liu, 2018). However, endogenous uracil DNA glycosylase (UNG), initiates base excision repair to remove uracil and restore the original base pairing. To suppress this reversal, modern CBE designs incorporate a uracil glycosylase inhibitor (UGI), which inhibits UNG activity and promotes retention of U:G intermediate until replication-dependent fixation into a T:A base pair (Komor et al., 2018; Rees and Liu, 2018). Base transversion systems are not only limited to C-to-T base editing. To enhance the diversity in the system for enabling variable edits, additionally, base editors such as C-to-G base editors (Sretenovic et al., 2021) and A-to-Y or G-to-Y base editors (Y = C or T) (Y. Li et al., 2023; L. Liu et al., 2024) have also been developed (Tuncel et al., 2025). Conversely, Adenine Base Editors (ABEs) utilize an engineered TadA domain to convert adenine (A) into inosine (I),

which is recognized as guanine (G) during replication, thereby facilitating A:T to G:C transitions. ABEs are often more robust in plants due to the absence of competitive Inosine Glycosylase activity (Gaudelli et al., 2017). These tools have been successfully applied to engineer agronomically important traits. For example, point mutations introduced into *Acetolactate Synthase (ALS)* gene can confer herbicide resistance in rice (Dong et al., 2021; Kuang et al., 2020). To further improve ABE efficiency, engineered dual base deaminase variants such as TadDE have been developed. TadDE contains tandemly evolved TadA domains that enhance catalytic activity and increase editing efficiency (Neugebauer et al., 2023). In addition, dual base editing systems such as saturated targeted endogenous mutagenesis editors (STEME) (Li et al., 2020a), simultaneous and wide editing induced by a single system (SWISS) (Li et al., 2020b) and multiplexed orthogonal base editor (MoBe) (A. Zhang et al., 2023) have been developed to perform base editing in plants by employing two different deamination activities within a single construct (Tuncel et al., 2025). Although Cas9 has been the dominant nuclease used in this field, its application remains limited (Gaillochet et al., 2023). Additionally, base editing systems have also been adapted to CRISPR/Cas12a system to further overcome Cas9 PAM sequence requirements and targeting limitations (Gaillochet et al., 2023; X. Li et al., 2018).

Nevertheless, the narrow editing window of BE limits their efficiency. Another approach to increase the number of editable bases is to broaden this editing window. To achieve this, the BE-PLUS (Base editing for programming larger C-to-U (T) scope) system was developed to enhance editing capacity (Jiang et al., 2018). In the BE-PLUS system, up to ten deaminase molecules can be recruited to the target site via the SunTag system, thereby expanding the effective editing window and increasing the number of editable bases (Jiang et al., 2018). Despite these developments and advances, the restriction of BE to C-to-T and A-to-G transitions and the inability to generate all desired nucleotide substitutions have driven the development of alternative genome editing technologies (Lee et al., 2025).

1.3.3 Prime Editing

Prime editing (PE) was developed to overcome the limitations, including small editing windows in the region of spacer and its requirement of PAM sequence, associated with both nuclease-based and BE technologies, providing a versatile and accurate approach for genome modification (Lee et al., 2025). PE, first described for enabling all twelve types of base-to-base conversions, as well as small-scale insertions and deletions, without the requirements of DSBs

or exogenous donor DNA templates. This versatility gives PE a more favorable profile for genome editing than BE (Anzalone et al., 2019).

The PE machinery consists of a fusion protein comprising an RNA-programmable nCas9 and an engineered Reverse Transcriptase (RT). The system is directed by a specialized prime editing guide RNA (pegRNA), which is structurally more complex than a standard sgRNA. The pegRNA contains a 5' spacer sequence for target recognition, a 3' Primer Binding Site (PBS) that anneals to the exposed 3' end of the nicked DNA strand, and a reverse transcription template encoding the desired genetic edit. Following PAM recognition and nicking of the target strand by nCas9, the PBS hybridizes with the 3' DNA end, enabling the RT to extend the DNA using the pegRNA as a template and thereby introducing the programmed edit at the target locus (Anzalone et al., 2019).

Various improvements have been introduced to the components of PE system in order to enhance its efficiency, improve the editing mechanism, reduce off-target effects, and increase the size range of insertions and deletions that can be introduced (Anzalone et al., 2019; Lee et al., 2025). The first-generation prime editors (PE1) consist of a fusion between nCas9 and the wild-type RT from Moloney Murine Leukaemia Virus (M-MLV) (Anzalone et al., 2019). Later, PE2 system with improved editing efficiency especially for targeted insertions and deletions was introduced (Anzalone et al., 2019; Arezi and Hogrefe, 2009; Baranauskas et al., 2012). Furthermore, the PE3 system introduces an additional nick in the non-edited DNA strand, promoting mismatch repair (MMR) and increasing editing efficiency approximately threefold compared to PE2 (Anzalone et al., 2019). Further improvements included PE4 and PE5 systems which increased the prime editing efficiency in plants (Y. Jiang et al., 2022; Li et al., 2024).

Additionally, further enhancement of pegRNA stability within the cellular environment (Yan et al., 2024) were established. Because pegRNAs are prone to degradation, which can reduce editing efficiency, engineered pegRNAs (epegRNAs) were subsequently developed to enhance pegRNA stability and improve prime editing performance (Nelson et al., 2022). Additionally, engineered plant prime editor (ePPE) and ePPEplus were developed to increase the efficiency of prime editing in plants (Ni et al., 2023; Zong et al., 2022a).

To broaden the range of potential applications and ensure large-scale genomic modifications, additional PE strategies have also been introduced (Anzalone et al., 2022; Choi et al., 2022; Hwang et al., 2024; T. Jiang et al., 2022; Kweon et al., 2023; Lee et al., 2025; Tao et al., 2022b, 2022a; Wang et al., 2022; Yarnall et al., 2023). Although several of these advanced PE-derived strategies have been demonstrated in both animals and plants, their applicability in plants

remains comparatively limited due to low efficiency. For instance, although the dual ePPE system has facilitated the targeted integration of the green fluorescent protein (*GFP*) gene in plants (Sun et al., 2024), the efficiency of integration was relatively low. In contrast, systems such as PE Cas9-based deletion (PRIME-DEL) and PE Cas9-based deletion and repair (PEDAR) have achieved accurate deletions of up to 10 kb in mammalian cells (Choi et al., 2022; T. Jiang et al., 2022), but their functionality in plant genomes has not yet been experimentally validated (Li et al., 2024). In plants, strategies to enhanced PE efficiency have mainly focused on several technical parameters including codon optimization of the nCas9-H840A RT (Lin et al., 2020a), improved expression of the pegRNA (Y. Jiang et al., 2022), adjustment of the PBS melting temperature (Lin et al., 2020a), and modifications to prime editor structure (Zong et al., 2022b). Additional approaches involve the use of paired pegRNAs (Lin et al., 2021) and the modulation of DNA MMR pathways (X. Liu et al., 2024; Tuncel et al., 2025). In monocot species, improved PE systems such as ePE5max (Y. Jiang et al., 2022), PE6 (Cao et al., 2024; Xu et al., 2024), and ePPEplus (Ni et al., 2023) have enabled the generation of homozygous mutations in T0 plants of rice, wheat and maize, although editing efficiencies remain dependent on the specific target locus and type of edit (Tuncel et al., 2025). In dicot plants, the combination of optimized prime editor components with viral replicon systems has advanced the generation of heritable edits in tomato and *A. thaliana* (Vu et al., 2024). Despite these advances, PE efficiency remains strongly target-site dependent, and its broader application is still limited in many plant species, particularly in dicots.

1.3.4 HDR-mediated gene targeting for precision trait engineering

The ability to introduce precise modifications into plant genomes has become a widely used strategy in modern biotechnology and crop improvement. On the one hand, traditional breeding and random mutagenesis approaches generate genetic variation but lack the precision required to introduce specific alleles or defined genomic modifications. On the other hand, while BE and PE allow precise but relatively small-scale nucleotide changes, HDR-based GT enables larger, scar-free and precise genomic changes, such as gene replacements and targeted gene insertions (Huang and Puchta, 2019; Tuncel et al., 2025; Zhang et al., 2019; Zhou et al., 2025).

GT is a technology that allows genome modification based on HR (Huang and Puchta, 2019). HR-based gene targeting occurs between the genomic target locus and the donor DNA template carrying the desired mutation flanked by homology arms, guiding the repair machinery to incorporate the desired genetic modification at the target locus (Fauser et al., 2014; Mao et al., 2008; Schubert et al., 2021). With this mechanism, desired nucleotide changes, gene knock-ins,

or allele replacement, among many other changes ranging from small to large, can be achieved (Fauser et al., 2014).

The conceptual basis of gene targeting in plants emerged from early studies demonstrating homologous recombination between introduced DNA and genomic sequences. The first evidence that HR could mediate gene targeting in plants emerged in the late 1980s. Firstly, HR between introduced DNA and chromosomal sequences in tobacco protoplasts was demonstrated, establishing the conceptual basis for GT in plants (Paszkowski et al., 1988). Following this, it was shown that *Agrobacterium*-mediated transformation could deliver donor DNA templates capable of recombining with genomic sequences in tobacco protoplasts (Offringa et al., 1990). However, early GT experiments revealed that HR events occurred at extremely low frequencies in plants and this constraint mainly arises from the predominance of NHEJ repair pathways in plant cells (Puchta and Hohn, 1991a, 1991b; Swoboda et al., 1994). Although GT in plants remained technically challenging for decades, the utilization of sequence-specific nucleases (SSNs) has made GT much more accessible (Čermák et al., 2015; Fauser et al., 2014; Sun et al., 2016).

A major conceptual milestone in plant molecular biology was the discovery that targeted DNA DSBs can strongly promote HR in plant cells (Puchta et al., 1993). Building upon this discovery, the complexity of plant DNA repair was further elucidated by the identification of two distinct but related pathways for HR: DSBR and SSA (Puchta et al., 1996). Together these findings proved that site-specific DSBs could be used to strategically activate endogenous DNA repair pathways, including both NHEJ and HR, which remain the core principle underlying current CRISPR/Cas-based genome editing technologies.

Genome engineering was truly transformed with the introduction of the CRISPR/Cas system, which is simpler to design, more versatile, and more efficient than previous nuclease-based technologies. The first demonstrations of CRISPR/Cas-mediated GT in plants showed that Cas9-induced DSBs could stimulate HR events when donor templates were provided (Doudna and Charpentier, 2014; Schiml et al., 2014). Since then, CRISPR/Cas-based systems have become the dominant technology for HR-mediated genome engineering (J. Chen et al., 2022; Doudna and Charpentier, 2014). Moreover, It has been already showed several improvements to achieve efficient DSB at the target site according to which Cas protein will be utilized and its optimizations to enhance break induction (Fauser et al., 2012; Huang et al., 2021; Merker et al., 2020a; Schindele et al., 2023; Schindele and Puchta, 2020).

Despite these technological advances, HR-mediated GT remains challenging in most plant species (Puchta et al., 1996). Because NHEJ repair mechanism operates more rapidly and is generally favored over HR in plant cells (Kozak et al., 2009), most DSBs generated by CRISPR/Cas systems are repaired through NHEJ rather than HR. Consequently, this strong preference for NHEJ considerably reduces the efficiency of precise GT (Huang and Puchta, 2019; Voytas, 2013). To overcome the limitations, several biological and technical innovations have been developed to promote HR-mediated gene targeting in plants (Cardi et al., 2023). One approach involves manipulating proteins involved in HR pathways. For instance, overexpression of HR-associated proteins such as yeast RAD54 has been shown to enhance HR frequencies in plants (Shaked et al., 2005). Similarly, enhancing HR-promoting factors to specific cell types can improve GT efficiency. Expression of recombination factors in reproductive cells or early embryos may enhance HDR frequency (Even-Faitelson et al., 2011). Another strategy focused on suppressing key components of NHEJ factors. Mutations in key NHEJ factors such as KU70 and LIG4 have been shown to increase GT efficiency in plants (M. Endo et al., 2016; Y. Qi et al., 2013). These proteins play essential roles in NHEJ-mediated repair, and their disruption can reduce NHEJ activity. However, long-term suppression of NHEJ can lead to genome instability, which limits the practical application of this strategy in crop improvement (Liao et al., 2024; Merker et al., 2024). Additionally, controlling the cellular context of genome editing activity can improve HDR efficiency. HR is most active during the G2 and S phases of the cell cycle, when sister chromatids are available as templates (Butler et al., 2016; Schmidt et al., 2019). HDR-mediated GT often occurs at low frequency due to cell cycle limitations during repair events (González et al., 2025). Therefore, inducing DSB formation during reproductive or early embryonic stages can improve HDR efficiency. For example, egg-cell-specific (EC1) expression of Cas9 and Cas12a as well as expression of the Cas9 endonuclease under early embryo-specific DD45 promoter have been reported to enhance gene targeting efficiency in Arabidopsis (Miki et al., 2018; Schindele et al., 2023; Wolter et al., 2018; Wolter and Puchta, 2019).

In addition to manipulating the cellular context of genome editing, engineering the genome editing machinery itself has also been explored to enhance HDR efficiency. For example, fusing Class 2 Cas proteins with 5’ exonucleases, such as Herpes virus exonucleases and T7 bacteriophage exonucleases, can inhibit the ligation of DSBs at the target site and thereby promote gene targeting efficiency and enabling scare-free knock-in events (Schreiber et al., 2024).

Besides engineering the genome editing machinery, strategies focusing on the controlled availability of donor templates represent another key strategy for improving HDR efficiency. In plant cells, donor DNA molecules are typically present at relatively low copy numbers, reducing the probability that they will participate in repair events. As a result, increasing donor template availability during the DNA repair process has become an important strategy for improving HDR efficiency. One such approach involves the use of geminivirus-derived viral replicon systems, which can amplify the donor DNA to high copy numbers within plant cells and thereby increase the frequency of recombination events (Baltes et al., 2014). Subsequent studies have further refined replicon-based systems, demonstrating improved GT efficiency across various plant species (Butler et al., 2016; Dahan-Meir et al., 2018; Vu et al., 2020; Wang et al., 2017). In addition, the design of donor templates can also be optimized to achieve high GT efficiency. Successful sequence alterations at a targeted genomic locus via HDR requires the presence of an HR donor template containing regions of sequence homology that flank the cut site (Mao et al., 2008; Schubert et al., 2021). While single-stranded oligodeoxynucleotide (ssODN) donors are typically used for small edits, long ssDNA or dsDNA/plasmid donors with longer homology arms are preferred for larger insertions (J. Chen et al., 2022; González et al., 2025; Schubert et al., 2021). It was suggested that homology arms of at least 600 bp are required to achieve efficient recombination in plants (Merker et al., 2020b), and studies have shown that longer homology arms enhance GT efficiency in various plants (Barco et al., 2025; J. Chen et al., 2022). Among the approaches developed to improve availability of donor templates, *in planta* Gene Targeting (*ip*GT) represent a particularly powerful strategy. In this approach, donor templates are first integrated into plant genome and subsequently released through nuclease-mediated cleavage. This approach ensures that donor templates are physically present in the nucleus when DSBs occur, and can be used as a HR template (Fauser et al., 2012). The *ip*GT system was first demonstrated to boost efficiency in plants (Fauser et al., 2012), and has since been successfully used for targeted gene modifications in Arabidopsis and tobacco (Fauser et al., 2014; Huang et al., 2021; Merker et al., 2020a; Wolter and Puchta, 2019).

The *ip*GT system requires the establishment of a robust and reliable selection system, as it enables the determination and direct comparison of GT efficiencies. Thereby, an established system based on the ACETOLACTATE SYNTHASE (ALS; EC 2.2.1.6) (Lonhienne et al., 2020) also known as acetohydroxyacid synthase (AHAS), encoded by the *Acetolactate Synthase* gene (*AT3G48560*) (Pan et al., 2026), has been widely utilized (Fauser et al., 2012; Merker et al., 2020b; Schindele et al., 2023; Wolter and Puchta, 2019). The ALS enzyme catalyzes the first step in the biosynthesis of branched-chain amino acids (BCAAs) including

leucine, valine and isoleucine (Pan et al., 2026). Importantly, ALS can be inhibited by herbicides of the imidazolinone (IMI) and sulfonylurea (SU) classes (Garcia et al., 2017; LaRossa and Schloss, 1984; Shaner et al., 1984). Herbicide resistance has been successfully achieved through various amino acid substitutions in ALS (Pan et al., 2026). For example, substitution of a serine with an asparagine at position 653 (S653N) confers resistance to the herbicide imazapyr (IM) (Chang and Duggleby, 1998). Therefore, this mutation has been widely exploited as a selectable marker for GT events (Wolter et al., 2018).

In a typical *ip*GT assay, a CRSPR/Cas-mediated DSB is induced within the *ALS* gene and a donor DNA template that contains homologous regions to the ALS sequence as well as the mutation encoding the S653N amino acid substitution is provided (see Figure 1.5 and 1.6). Two protospacer sequences, each accompanied by a PAM sequence, are incorporated at the 5' and 3' ends of the donor sequence (see Figure 1.6B and D). This design facilitates the excision of the donor from the T-DNA integration site through CRISPR/Cas-mediated DSB formation (see Figure 1.5B) (Fauser et al., 2012; Merker et al., 2020b). In case of HR-mediated DSB repair, the donor can be used as a template, resulting in precise incorporation of the mutation. To prevent re-cleavage of the edited locus following successful GT, silent mutations are strategically positioned within the PAM or the seed region of the protospacer to disrupt CRISPR/Cas recognition and cleavage (see Figure 1.6C). The IM-resistant plants can be readily identified through viability and phenotypic selection on IM-containing medium by the *ip*GT experiment workflow (Fauser et al., 2012; Merker et al., 2020b).

The *ip*GT construct has undergone progressive optimization based on earlier designs that enabled reliable GT analysis (Fauser et al., 2012; Merker et al., 2020a, 2020b; Schiml et al., 2014; Schindele et al., 2023; Wolter et al., 2018; Wolter and Puchta, 2019). Subsequent studies introduced key improvements at multiple levels, particularly in nuclease choice and expression strategies. A major improvement was the implementation of oocyte-specific expression using EC.1.1 (AT1G76750) (EC promoter) system fused to an enhancer of EC1.2, which was selected in combination with the *Pisum sativum* rbcS E9 terminator (rbcS terminator) (see Figure 1.5A) (Sprunck et al., 2012; Wang et al., 2015). The oocyte-specific Cas9 expression significantly increased the heritable GT efficiency compared to constitutive expression of Cas9 (Wang et al., 2015; Wolter et al., 2018). Building on this, further improvements were achieved through iterative replacement and engineering of Cas nucleases, progressing from SaCas9 to LbCas12a (Merker et al., 2020b; Wolter and Puchta, 2019), then to ttLbCas12a (Merker et al., 2020a), and finally ttLbCas12a-i (Schindele et al., 2023), each step resulting in increased GT efficiency. These cumulative developments formed the basis for the *ip*GT construct.

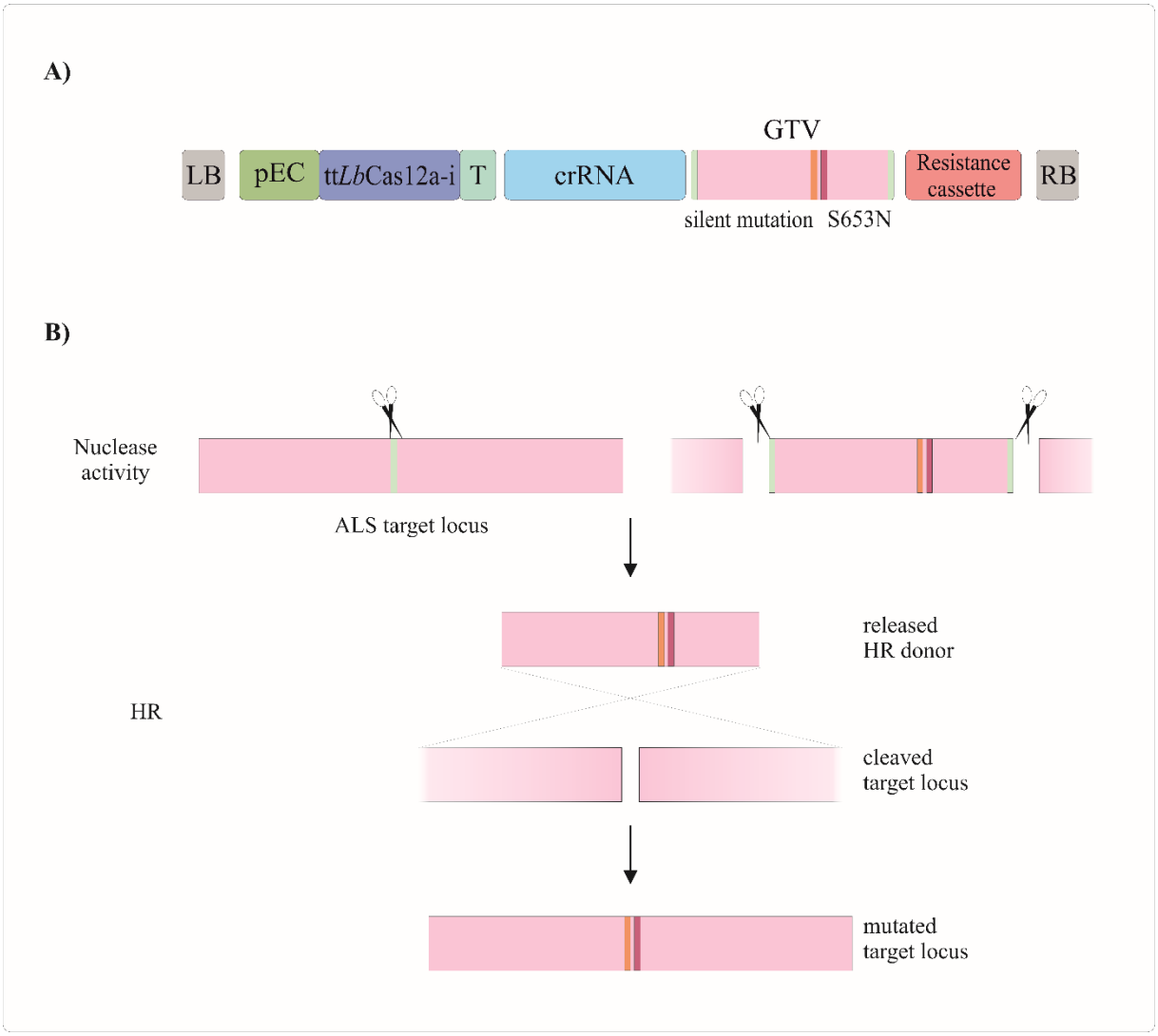

Figure 1.5: Outline of the *in planta* Gene Targeting (*ip*GT) system (adapted from (Merker et al., 2020b)).

A) *in planta* Gene Targeting (*ip*GT) construct. The *ip*GT construct consists of a T-DNA which harbours a Cas expression cassette composed of an oocyte-specific promoter (pEC), the ttLbCas12a-i coding sequence, and the rbcS E9 terminator (T) from *Pisum sativum*. In addition, a gRNA expression cassette is included, consisting of the CRISPR RNA (crRNA) sequence driven by the *Arabidopsis U6 SMALL NUCLEOLAR RNA26* (U6-26) promoter and terminated by Poly-T signal, which contains the spacer sequence. Furthermore, the construct contains a donor template, GT vector (GTV), comprising homologous arms flanked by protospacer sequences, along with a silent mutation and the desired sequence change. To facilitate selection of primary transformants, a resistance cassette is also incorporated into the construct. The *ip*GT construct is flanked by the left and right borders (LB and RB), enabling integration into the plant genome via *Agrobacterium*-mediated transformation of *Arabidopsis thaliana*. **B) The mechanism of the *ip*GT system.** The Cas nuclease, expressed under the control of the pEC, induces double-strand breaks (DSBs) both at the genomic target locus and at the flanking sites of the GT vector (GTV). The GTV is designed to contain the same target sequence and PAM motifs at its 5' and 3' ends, enabling Cas-mediated excision and release of the donor template. Following cleavage, the released donor DNA serves as a repair template for homology-directed repair (HDR) at the genomic target site, resulting in the precise integration of the desired mutations.

In addition to these improvements in *ip*GT construct design, the use of *ku70* mutant Arabidopsis lines further promotes HR-mediated repair by blocking the cNHEJ repair pathway, thereby enhancing GT efficiency compared to wild-type Columbia-0 (Col-0) plants (Merker et al., 2024).

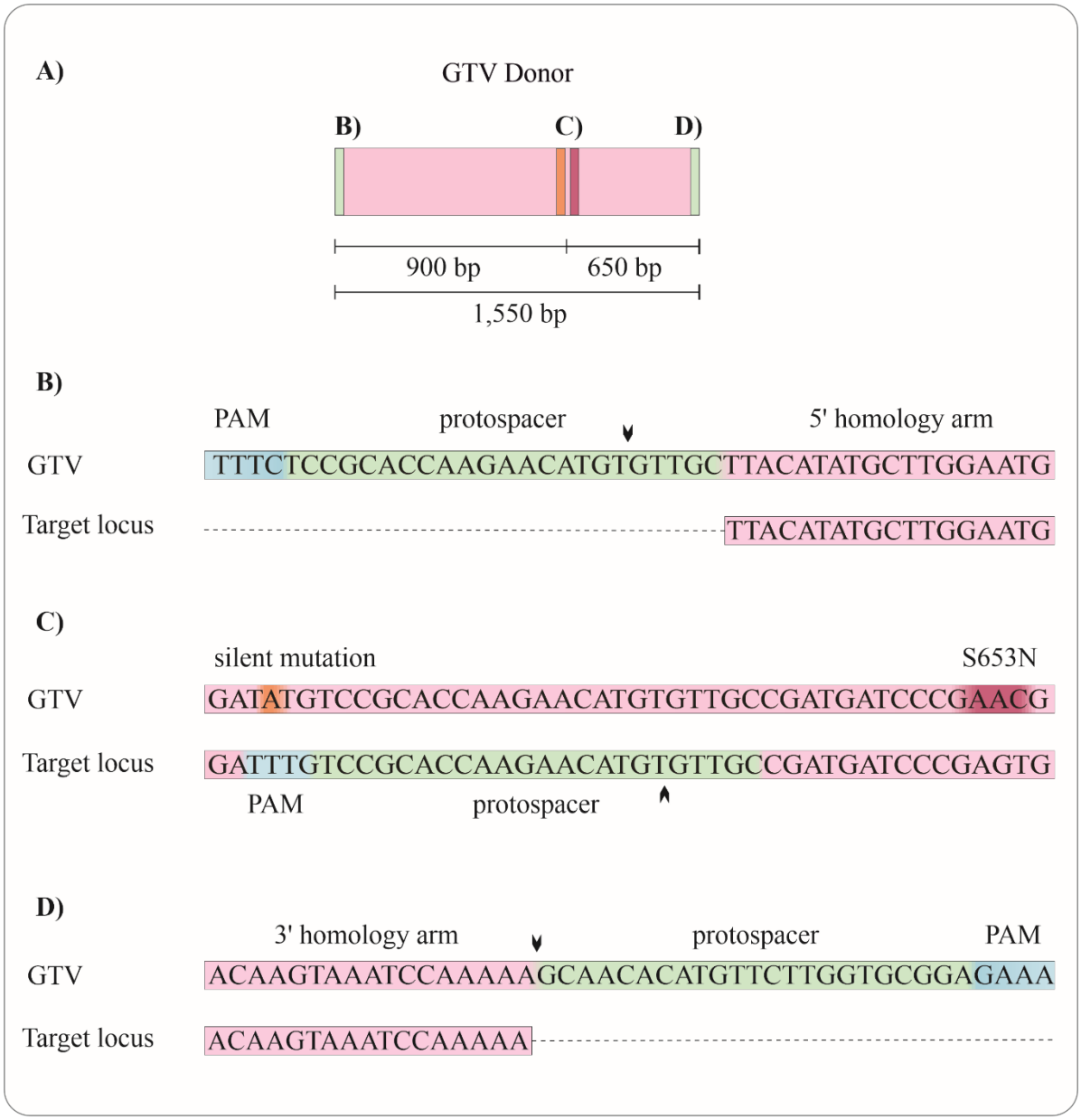

Figure 1.6: Donor design.

A) Schematic representation of the gene targeting vector (GTV), exemplified by the ttLbCas12a-i-based construct (*Lb*GTV). The donor sequence contains homology arms corresponding to the *ALS* locus, approximately 900 bp and 650 bp in length, resulting in a total donor size of approximately 1,550 bp. The donor is flanked by protospacer sequences (light green) to enable its excision from the T-DNA integration site. In addition, a silent mutation (orange) is incorporated into the donor sequence to prevent double-strand break (DSB) induction within the donor itself. To confer imidazolinone (IM) herbicide resistance, the donor sequence includes the mutation encoding the S653N amino acid substitution (magenta). **B) Left border of the donor.** The orientation of the PAM (light blue) and protospacer sequences were designed such that, following DSB induction, the majority of the protospacer sequence is removed. This ensures the release of a donor sequence that is predominantly homologous to the target locus. Accordingly, the PAM was positioned upstream of the protospacer sequence. After DSB induction, the donor retains only five non-homologous bases on the strand non-complementary to the spacer sequence. **C) Region of the DSB induction site.** To prevent DSB formation within the donor sequence, a silent mutation is introduced into the PAM (T → A). Downstream of the DSB site lies the mutation encoding the S653N amino acid substitution, which differs from the target sequence by two nucleotide changes (G → A and T → C). **D) Right border of the donor.** As for the left border, the PAM and protospacer sequences were oriented to maximize the homologous region. For this purpose, the PAM sequence was positioned downstream of the protospacer sequence. Following DSB induction, the donor similarly retains only five non-homologous bases.

Overall, the development of efficient GT strategies has enabled the precise introduction of desired mutations and the integration of large DNA fragments into plant genomes. Although the *ip*GT system still works at low efficiency and needs improvements, it allows for the precise induction of large, predefined sequence changes. These advantages make *ip*GT widely applicable, as it accelerates research by reducing time requirements and offers a flexible, easy applicable, and readily designable platform for generation of genome-edited lines.

1.4 Haploid induction

The presented gene editing tools provide efficient strategies for targeted mutagenesis and precise genome modifications. However, generating homozygous lines can be time-consuming and requires considerable effort.

Haploid induction represents a central strategy in modern plant breeding, enabling the rapid generation of homozygous lines through doubled haploid (DH) technology. Haploids can be produced either via *in vitro* culture of gametophytic tissues or through selective elimination following inter- or intraspecific hybridization. The resulting DH plants significantly enhance breeding process while decreasing both time and cost (Demidov et al., 2022; Jacquier et al., 2020; Kalinowska et al., 2019). The DH process depends on two key steps: the induction of haploid embryos or plantlets and subsequent chromosome doubling to restore diploidy (Forster and Thomas, 2005; Maluszynski et al., 2003). Even though chromosome doubling is challenging, the fundamental bottleneck in DH technology is the insufficient availability of reliable haploid induction systems, due to their genotype-dependent structure, and economical restrictions (Demidov et al., 2022; Dunwell, 2010; Forster et al., 2007; Jacquier et al., 2020).

Traditional haploid induction methods are largely based on *in vitro* techniques, such as anther or microspore culture, first demonstrated in *Datura* in the 1970s (Guha and Maheshwari, 1964). Despite the improvements in efficiency, the *in vitro* protocols remain limited to a narrow range of species (Jacquier et al., 2020). To overcome these limitations, *in planta* haploid induction systems have been developed, allowing haploid embryos to be generated directly through intra-specific crosses without tissue culture. Haploid inducer lines represent specialized genotypes capable of triggering genome elimination, and these systems can be broadly divided into centromere-based and non-centromere-based approaches (Jacquier et al., 2020; Somasundaram et al., 2026). Among these, centromere-based haploid induction, particularly via manipulation of the CENTROMERIC HISTONE H3 (CENH3), has emerged as the most

effective *in vivo* strategy, especially in *A. thaliana* (Quiroz et al., 2024; Somasundaram et al., 2026). CENH3, also known as centromere protein A (CENP-A) in human, is essential especially in meiosis and mitosis for enabling chromosome segregation (Jacquier et al., 2020; Ravi and Chan, 2010). Alterations to CENH3, such as a GFP-tailswap modification, can result in structurally impaired centromeres. In this construct, hypervariable N-terminal region of CENH3 is replaced with the corresponding domain from conventional H3, allowing the rescue of the lethal phenotype of the *cenh3-1* mutant in *Arabidopsis thaliana*, thereby enabling the complete replacement of endogenous CENH3 (Ravi and Chan, 2010). When these modified plants are crossed with wild-type individuals, chromosomes carrying defective centromeres are selectively eliminated during early embryogenesis, leading to haploid embryo formation (Comai and Tan, 2019; Wang and Dawe, 2018). This centromere-mediated genome elimination mechanism highlights the importance of precise genetic modifications in controlling chromosome behavior. However, current CENH3-based systems still face several limitations, including low efficiency in certain genetic backgrounds and reduced effectiveness when transmitted through the male parent (Comai and Tan, 2019; Jacquier et al., 2020). For example, haploid induction was achieved in maize with <1% frequency by using a tailswap strategy (Kelliher et al., 2016). Furthermore, alternative approaches, such as engineered CENH3 degradation systems, require complex transgenic setups and are not yet suitable for practical breeding applications (Comai and Tan, 2019; Demidov et al., 2022; Somasundaram et al., 2026). For instance, targeted degradation of enhanced yellow fluorescent protein (EYFP)-tagged CENH3, mediated by engineered E3 ligases expressed from the paternal genome, has been demonstrated to induce maternal chromosome elimination in Arabidopsis. Nevertheless, compared to established CENH3 manipulation methods, this paternal-driven strategy indicates extremely low efficiency and resulted in transgenic haploid progeny unsuitable for breeding (Demidov et al., 2022). Consequently, achieving stable and efficient CENH3 depletion while producing non-transgenic haploids requires further improvements in the modular design of the degradation system.

Overall, the *ip*GT system represents an important advancement by facilitating HR-mediated, predefined modifications of endogenous loci and offering strong potential for establishing robust, non-transgenic haploid induction platforms. Although the GT remains challenging due to its low efficiency, further optimization of the *ip*GT system is necessary to enhance its efficiency for advanced breeding applications.

1.5 Aim of this Study

Precise genome modification is a major objective in modern plant biotechnology, as it enables both the targeted improvement of plant traits and the functional analysis of endogenous genes. In plants, GT provides defined sequence modifications to be introduced at specific genomic loci through HR. However, the efficiency of GT in somatic plant cells remains limited, mainly due to the low frequency of HR. Therefore, improving the efficiency of *ip*GT is critical for enabling the broader application of precise genome engineering strategies in plants. For this reason, investigating *ip*GT efficiency and evaluating alternative strategies to enhance GT in plants are essential for overcoming these limitations. One such strategy involves the direct or indirect fusion/recruitment of end-processing exonucleases to Cas nucleases in order to assess the stability of Cas nucleases and their effects together on GT efficiency. In this context, previous reports showing that N-terminal fusion of the 5'-3' exonucleases HSVUL12 and its ortholog PapE to Cas nucleases can enhance HR-mediated GT efficiency. However, the overall efficiency of precise GT remains relatively low. Therefore, this thesis aimed to combine exonuclease-assisted Cas strategies with the *ip*GT system in order to test whether targeted exonuclease recruitment could further enhance precise GT efficiency. Additionally, it has been reported that an indirect approach, such as SunTag-mediated exonuclease recruitment, can increase mutation efficiency and allow larger deletions when combined with the 3'-5' human exonuclease TREX1 (HsTREX1). Therefore, the aim of this study was further to investigate the effects of SunTag-mediated recruitment of PapE, HSVUL12, and HsTREX1 on *ip*GT efficiency. In parallel, the exonucleases selected for SunTag-mediated recruitment in *ip*GT approaches were to be further characterized with regard to their genome editing activity. This included the analysis of editing efficiency and deletion frequency at the corresponding target sites. In addition to analysing the influence of exonuclease recruitment, this study aimed to apply the *ip*GT system to enable endogenous CENH3-based haploidization for crop improvement and trait selection. The CENH3-mediated haploid induction depends on the elimination of chromosomes carrying compromised or depleted CENH3 during early embryogenesis. Since randomly integrated transgenes may be affected by position effects, variable expression levels, and background-dependent activity, *ip*GT was to be used to establish a precise endogenous ALFA-tagged CENH3 system. This approach was intended to assess whether endogenous CENH3 tagging provides a more controlled genetic background for egg-cell-specific CENH3 depletion and thereby supports more efficient and reliable haploid induction.

2 MATERIAL AND METHODS

2.1 Material

2.1.1 Chemicals, Enzymes, Kits and Supplies

Unless stated otherwise, all chemicals used in this study were of analytical grade and obtained from following suppliers: AppliChem GmbH (Darmstadt), Carl Roth GmbH + Co. KG (Karlsruhe), Duchefa Biochemie B.V. (Haarlem, Netherlands), New England Bioblas (Frankfurt am Main), Merck (Darmstadt), Roche Diagnostics (Mannheim), SERVA Electrophoresis (Heidelberg), and VWR International (Darmstadt). Therefore, they are not listed separately here.

Chemicals:

- Acetosyringone (Merck, Darmstadt)
- Beef extract (GERBU Biotechnik GmbH, Heidelberg)
- Benzylaminopurine (Duchefa Biochemie B.V., Haarlem, Netherlands)
- dNTP Mix Set 10 mM (Thermo Fisher Scientific, Braunschweig)
- Ethidium bromide (Carl Roth GmbH + Co. KG, Karlsruhe)
- GeneRuler™ 1 kb DNA Ladder (Thermo Fisher Scientific, Braunschweig)
- GeneRuler™ Low Range DNA Ladder (Thermo Fisher Scientific, Braunschweig)
- Imazapyr PESTANAL® (Merck, Darmstadt)
- Glyphosate (Duchefa Biochemie B.V., Haarlem, Netherlands)
- Murashige & Skoog ready-made medium (Duchefa Biochemie B.V., Haarlem, Netherlands)
- Sodium hypochlorite solution 12% (Carl Roth GmbH + Co. KG, Karlsruhe)
- Pepton (Duchefa Biochemie B. V., Haarlem, Netherlands)
- Plant Agar (Duchefa Biochemie B. V., Haarlem, Netherlands)
- Tryptone (Duchefa Biochemie B. V., Haarlem, Netherlands)
- Tween-20 (Serva Electrophoresis GmbH, Heidelberg)
- Yeast Extract (Duchefa Biochemie B. V., Haarlem, Netherlands)

- SOC medium (MP Biomedicals, USA)
- PeqGOLD Agarose (VWR International, Darmstadt)
- Silwet Gold L-77 (Hermann Meyer KG, Rellingen)
- DMSO (Merck, Darmstadt)

Enzymes and enzyme master mixes:

- Antarctic Phosphatase (New England Biolabs, Frankfurt am Main)
- DreamTaq DNA Polymerase (Thermo Fisher Scientific GmbH, Braunschweig)
- Gateway® LR Clonase® II Enzyme Mix (Thermo Fisher Scientific GmbH, Braunschweig)
- Gibson Assembly® Cloning Kit (New England Biolabs, Frankfurt am Main)
- Instant Sticky-end Ligase Master Mix (New England Biolabs, Frankfurt am Main)
- NEBuilder® HiFi DNA Assembly (New England Biolabs, Frankfurt am Main)
- Proteinase K (Thermo Fisher Scientific GmbH, Braunschweig)
- Q5® High-Fidelity DNA Polymerase (New England Biolabs, Frankfurt am Main)
- Restriction endonucleases (New England Biolabs, Frankfurt am Main)
- T4 DNA Ligase (Thermo Fisher Scientific GmbH, Braunschweig)

Kits and consumables:

- Electroporation cuvette, 2 mm electrode gap (VWR International, Darmstadt)
- peqGOLD Cycle Pure Kit (VWR International, Darmstadt)
- peqGOLD Gel Extraction Kit (VWR International, Darmstadt)
- peqGOLD Plasmid Miniprep Kit (VWR International, Darmstadt)
- E.Z.N.A.® Cycle Pure Kit (Omega Biotech, Norcross, USA)
- E.Z.N.A.® Gel Extraction Kit (Omega Biotech, Norcross, USA)
- E.Z.N.A.® Plasmid DNA Mini Kit II (Omega Biotech, Norcross, USA)
- Qubit® dsDNA Broad Range Assay Kit (Thermo Fisher Scientific, Braunschweig)

2.1.2 Antibiotics and Herbicides

The antibiotics and herbicides used in this study were stored as stock solutions at -20 °C and added to the autoclaved media at their respective final concentrations after cooling below 50 °C. The stock concentrations, final concentrations, corresponding solvents, and target organisms for each compound are summarized in Table 2.1.

Table 2.1: Overview of Antibiotics and Herbicides Used

The table lists the antibiotics and herbicides used in this study, along with their respective solvents, stock solution concentrations, and the working concentrations applied for each organism.

Antibiotics/Herbicides	Solvent	Stock solution [mg/mL]	*E. coli* [mg/L]	*A. tumefaciens* [mg/L]	*A. thaliana* [mg/L]
Ampicillin	H_2O	100	100		
Cefotaxime	H_2O	250			500
Gentamicin	H_2O	100		20	60
Imazapyr	H_2O	0.98			1.3
Kanamycin	H_2O	100	100		30
Phosphinothricin (PPT)	H_2O	20			6
Rifampicin	DMSO	100		100	
Spectinomycin	H_2O	100	100	100	

2.1.3 Devices, Software and Databanks

Incubators, growth chambers, shakers, heating blocks and drying cabinets

- Incubation shaker 3032 (GFL Gesellschaft für Labortechnik GmbH, Burgwedel, Germany)
- Incubation shaker Certomat® IS (Sartorius Stedim Biotech GmbH, Göttingen, Germany)
- Incubation shaker Ecotron (Infors AG, Bottmingen, Switzerland)
- Growth chamber CU-36L4 (Percival Scientific, Perry, Iowa, USA)
- Growth chamber polyklima PK-520 (Poly Klima GmbH, Freising, Germany)
- Heating block TDB-120 (lab4you, Berlin, Germany)
- Heating block Thermomixer comfort (Eppendorf AG, Hamburg, Germany)
- Drying cabinet Heratherm™ OMH 750 (Thermo Fisher Scientific GmbH, Braunschweig, Germany)
- Drying cabinet, models UE 500 and UL 50 (Memmert GmbH + Co. KG, Schwabach, Germany)

Safety cabinets and clean benches

- MaxiSafe 2020 1.5 Class II Biological Safety Cabinet (Thermo Fisher Scientific GmbH, Braunschweig, Germany)

- Clean bench, types HF and KVF (BDK Luft- und Reinraumtechnik, Sonnenbühl-Genkingen, Germany)
- Biological Safety Cabinet NU-480-500E (NuAire, Plymouth, USA)

Thermocyclers

- Labcycler 48 (SensoQuest GmbH, Göttingen, Germany)
- SimpliAmp™ Thermocycler (Thermo Fisher Scientific GmbH, Braunschweig, Germany)
- Tpersonal Thermocycler (Analytik Jena, Jena, Germany)
- T100™ Thermal Cycler (Bio-Rad Laboratories GmbH, Feldkirchen, Germany)
- MyCyler™ (Bio-Rad Laboratories, München)
- SensoQuest Labcycler 48 (SensoQuest GmbH, Göttingen)
- T100™ Thermocycler (Bio-Rad Laboratories, München) o Tpersonal Thermocycler (Analytik Jena, Jena) o LightCycler 480 (Roche Diagnostics, Mannheim)

Centrifuges

- Mini centrifuge IKA® mini G (IKA®-Werke GmbH + Co. KG, Staufen, Germany)
- Refrigerated centrifuge SIGMA 6-16K (Sigma Laborzentrifugen GmbH, Osterode am Harz, Germany)
- Micro Star 12 centrifuge (VWR International, Darmstadt, Germany)
- MiniSpin® centrifuge (Eppendorf AG, Hamburg, Germany)
- Centrifuge with vortexer (neoLab Migge Laborbedarf, Heidelberg, Germany)
- Centrifuge Z 216 M (Hermle Labortechnik, Wehingen, Germany)
- Refrigerated centrifuge Z 233 MK-2 (Hermle Labortechnik, Wehingen, Germany)
- Refrigerated centrifuge Z 383 K (Hermle Labortechnik, Wehingen, Germany)

Additional devices

- Consort EV1450 gel electrophoresis power source (Consort bvba, Turnhout, Belgium)
- FiveEasy pH meter (Mettler-Toledo GmbH, Gießen, Germany)
- Gel iX Imager documentation system (Intas Science Imaging Instruments GmbH, Göttingen, Germany)

- GenePulser II electroporation system (Bio-Rad Laboratories GmbH, Feldkirchen, Germany)
- Invitrogen Q32857 Qubit™ fluorometer (Thermo Fisher Scientific GmbH, Braunschweig, Germany)
- Mixer Mill MM 400 (Retsch GmbH, Haan, Germany)
- NanoDrop™ Lite spectrophotometer (Thermo Fisher Scientific GmbH, Braunschweig, Germany)
- PURELAB Classic ultrapure water system (ELGA LabWater, Celle, Germany)
- VWR LA Classic precision scale (VWR International GmbH, Darmstadt)
- VX-75 Autoclave (Systec GmbH, Linden)

Software for DNA Sequence Visualization and Primer Design

- ApE – A Plasmid Editor v3.0.4 and v3.1.8.1 (M. Wayne Davis, Salt Lake City, Utah, USA)
- Integrated Genome Browser 9.1.10 (Freese et al., 2016)
- SnapGene Viewer 6.1.2 (GSL Biotech, Boston, Massachusetts, USA)
- NCBI BLASTn: (https://blast.ncbi.nlm.nih.gov/Blast.cgi)
- NEBuilder® Assembly Tool (https://nebuilder.neb.com/#!/, New England Biolabs GmbH, Frankfurt am Main, Germany)
- NEB Tm Calculator (https://tmcalculator.neb.com/#!/main, New England Biolabs GmbH, Frankfurt am Main, Germany)

Databases

- NCBI – National Center for Biotechnology Information (http:://ncbi.nlm.nih.gov/)
- TAIR – The Arabidopsis Information Resources (http:://www.arabidopsis.org/)

Software for the Analysis of Sequencing Data from Modified DNA Sequences

- CRISPResso2 (Clement et al., 2019)
- Cas-Analyzer/Cas-OFFinder, CRISPR RGEN Tools (http:://www.rgenome.net/, (Park et al., 2017))
- ICE CRISPR Analysis Tool (synthego.com/products/bioinformatics/analysis, (Conant et al., 2022))

- Indigo Rapid InDel Discovery in Sanger Chromatograms | Gear (https://www.gear-genomics.com/, (Rausch et al., 2020))
- OriginLabs 2023 (OriginLab Corporation, Northampton, USA)
- RStudio 2022.12.0 Build 353 (Posit Software, PBC, Boston, Massachusetts, USA)
- R 4.1.2 (R Foundation for Statistical Computing, Vienna, Austria)

The last access to the online resources mentioned above was on 02.06.2026.

2.1.4 Medium, Solutions and Buffers

Unless otherwise specified, all media, solutions, and buffers used throughout this study were prepared using double-distilled water (ddH_2O) and sterilized by autoclaving prior to use. Heat-sensitive substances, such as antibiotics and herbicides, were sterilized separately and introduced only after the temperature dropped below 50 °C.

Media for the cultivation and transformation of *Arabidopsis thaliana*

Germination medium (GM)	4.9 g/L Murashige & Skoog basal medium 10 g/L Sucrose 8 g/L Plant agar (for solid medium) pH adjusted to 5.7 with KOH
Infiltration medium	2.5 g/l Murashige & Skoog basal medium 50 g/L sucrose 5.25 µL/L benzylaminopurine (1 mg/mL stock) 1 mL/L acetosyringone (100 mg/mL in DMSO) 500 µL/L Silwet Gold

Infiltration medium was freshly prepared and not autoclaved.

Media for bacterial cultivation

Luria-Bertani (LB) medium	10 g/L peptone 5 g/L yeast extract 10 g/L NaCl 17.5 g/L plant agar (for solid medium)
Yeast Extract Broth (YEB) medium	5 g/L beef extract 5 g/L peptone 1 g/L yeast extract

	5 g/L sucrose
	493 mg/L $MgSO_4$
	12 g/L plant agar (for solid medium)
SOC medium	31 g/L SOC medium Powder

Buffers and solutions for plant genomic DNA extraction

DNA extraction buffer	63.76 g/L sorbitol
	12.11 g/L Tris
	1.86 g/L EDTA
	pH adjusted to 7.5 with HCl
Nuclei lysis buffer	24.22 g/L Tris
	18.61 g/L EDTA
	116.88 g/L NaCl
	20 g/L CTAB
	pH adjusted to 8.0 with HCl
5% Sarkosyl solution	50 g/L N-lauroylsarcosine
Isolation buffer	8 g sodium disulfite dissolved in 80 mL ddH_2O
	420 mL DNA extraction buffer
	420 mL nuclei lysis buffer
	80 mL 5% Sarkosyl solution

The buffer was freshly prepared and not autoclaved.

Tris-EDTA (TE) buffer	10 mM Tris-HCl (pH 9.0)
	1 mM EDTA
	pH adjusted to 8.0 with HCl

Buffers and solutions for agarose gel electrophoresis:

6× Loading buffer	10% (v/v) glycerol
	60 mM EDTA
	0.2% (w/v) Orange G
	0.05% (w/v) xylene cyanol

Sodium borate (SB) buffer (20×)	8 g/L NaOH 47 g/L boric acid pH adjusted to 8.0 with boric acid
0.9% SB gel	9 g/L agarose dissolved in 1× SB buffer 37.5 µL/L ethidium bromide [1% stock solution]
Tris-Acetate-EDTA (TAE) buffer (50×)	242 g/L Tris 57.1 mL/L glacial acetic acid 100 mL/L EDTA [500 mM] pH adjusted to 8.0 with glacial acetic acid
0.9% TAE gel	9 g/L agarose dissolved in 1× TAE buffer 37.5 µL/L ethidium bromide [1% stock solution]

2.1.5 Oligonucleotides and Plasmids

Oligonucleotides

The oligonucleotides used in this study were obtained in desalted form from Eurofins Genomics GmbH (Ebersberg) or Microsynth AG (Switzerland) and dissolved in ddH_2O to a final concentration of 100 µM before use. The sequence information for all oligonucleotides used in this work is provided in Tables 7.3-7.8 in the Supplementary Information.

Plasmids

Cloning experiments conducted in this study were based on the following plasmids:

- pEn-Sa-Chimera (Steinert et al., 2015)
- pEn-Sa-Chimera-HsTREX1(Capdeville et al., 2024)
- pEn-SpsgRNA+UBI-scFv-sfGFP-GB1-nosT (Capdeville et al., 2024)
- pEn-SasgRNA+UBI-scFv-sfGFP-GB1-nosT (BioCat GmbH, Heidelberg)
- pEn-RZ-LbcrRNA (Wolter and Puchta, 2019)
- pDe-UBI-SaCas9 (Steinert et al., 2015)
- pDe-EC-LbCas12a-ALS-GTVc12 (Wolter and Puchta, 2019)
- pDe-UBI-ttLbCas12a-i-nosT+ccdB+PPTR (Schindele et al., 2023)
- pDe-EC-ttLbCas12a-i-rbcST+ccdB+PPTR (Schindele et al., 2023)
- pDe-EC-ttLbCas12a-rbcST+ccdB+PPTR (Schindele, 2020)
- pDe-UBI-Omega-SaCas9-GCN4-pea3A+ccdB+PPTR (Capdeville et al., 2024)

- pDe-UBI-Omega-SaCas9-pea3A+ccdB+PPTR (Capdeville et al., 2024)
- pAGT8175 (Schreiber et al., 2024)
- pAGT9782 (Schreiber et al., 2024)
- pUC57-Simple-GTV-ALFA-CENH3-T1 (BioCat GmbH, Heidelberg)
- pUC57-Simple-GTV-ALFA-CENH3-T3 (BioCat GmbH, Heidelberg)

All vectors constructed during this study are summarized in Supplementary Tables 7.1 and 7.2, and the corresponding DNA sequences of the synthetic constructs are provided in the Supplementary Information.

2.1.6 Organisms

Escherichia coli

- NEB5α (New England Biolabs, Frankfurt a.M.)
  This strain was used for plasmid propagation and standard cloning procedures (genotype: *fhuA2::IS2 Δ(mmuP-mhpD)169 ΔphoA8 glnX44 ϕ80d[ΔlacZ58(M15)] rfbD1 gyrA96 luxS11 recA1 endA1 rphWT thiE1 hsdR17*).
- One Shot™ ccdB Survival™ (*E. coli*) (Thermo Fisher Scientific, Braunschweig)
  This strain was used for the propagation of destination vectors containing the *ccdB* gene (genotype: F^- *mcr*A Δ(*mrr-hsd*RMS-*mcr*BC) Φ80*lac*ZΔM15 Δ*lac*X74 *rec*A1 *ara*Δ139 Δ(*ara-leu*)7697 *gal*U *gal*K *rps*L (Str^R) *end*A1 *nup*G *fhu*A*::IS2*).

Agrobacterium tumefaciens

- GV3101::pMP90
  This strain was utilized for stable *Arabidopsis thaliana* transformation. Selection was achieved through chromosomal rifampicin resistance and gentamicin resistance conferred by the Ti-plasmid (De Saeger et al., 2021; Koncz and Schell, 1986).

Arabidopsis thaliana

- Columbia-0 (Col-0)
  In this study, the *A. thaliana* ecotype Columbia-0 was used as the model plant.
- *Ku70-1* (*ku70*) mutant in the Col-0 background
  For this work, *ku70* mutant (Jia et al., 2012) derived from the Col-0 background was employed.

2.2 Methods

2.2.1 Microbiological Methods

Transformation and cultivation of *E. coli*

Competent *E. coli* cells applied in this study were maintained at -80 °C until use and thawed on ice immediately prior to transformation. For transformation, 3-10 µL of plasmid DNA was gently mixed with 100-150 µL of competent cells and incubated on ice for 10-30 minutes. The cells were then subjected to a heat shock at 42 °C for 60 seconds, followed by rapid cooling on ice for 2-5 minutes.

Following the heat shock treatment, 500 µL of LB or SOC medium was added to the transformation mixture, which was subsequently incubated at 37 °C for 1 hour with shaking at 650 rpm to allow for recovery and expression of the antibiotic resistance marker. The cell suspension was then centrifuged at 6000 rpm for 2 minutes, and 500 µL of the supernatant was removed. The pellet was resuspended in the remaining medium and spread onto solid LB agar plates containing the appropriate selective antibiotic. Plates were incubated overnight at 37 °C to allow colony propagation.

Individual colonies were inoculated into liquid LB medium supplemented with the corresponding selection marker and incubated overnight at 37 °C with shaking at 190 rpm to ensure the growth of positively transformed cells. For long-term preservation, 700 µL of each liquid culture was mixed with 300 µL of 99% glycerol, vortexed thoroughly, and stored at -80 °C.

Transformation and cultivation of *A. tumefaciens*

A. tumefaciens transformation was carried out using the electroporation method. Competent cells stored at -80 °C were thawed on ice, and 1 µL of plasmid DNA diluted in 5 µL of ddH_2O was mixed with 50 µL of the bacterial suspension. The mixture was transferred to a pre-cooled electroporation cuvette, ensuring the absence of air bubbles. Electroporation was performed at 2.5 kV, 25 µF, and 200 Ω for 5 seconds using an electroporator. Immediately after the pulse, the cuvettes were placed on ice for 2 minutes to allow cell recovery and then transferred into 500 µL of liquid YEB medium. The cells were subsequently incubated at 28 °C for 30 minutes with shaking at 650 rpm for regeneration.

Following regeneration, 80 µL of the transformed cell suspension was spread onto solid YEB medium supplemented with Gentamicin, Rifampicin and Spectinomycin antibiotics, and

incubated at 28 °C for two nights to allow colony formation. To propagate positively transformed colonies, single colonies were transferred into 10 mL of liquid YEB medium containing the corresponding selection antibiotics to establish pre-cultures, which were incubated overnight at 28 °C with shaking at 200 rpm. For long-term storage, 700 µL of each pre-culture was mixed thoroughly with 300 µL of 99% glycerol and stored at -80 °C.

Main cultures used for *Agrobacterium*-mediated transformation of *A. thaliana* were initiated either from these pre-cultures or directly from glycerol stocks. For this purpose, 1 mL of pre-culture or glycerol stock was inoculated into 400 mL of liquid YEB medium containing the respective selection markers and incubated overnight at 28 °C with shaking at 200 rpm.

2.2.2 Plant-specific Methods

Storage, Surface sterilization, and stratification of seeds

Storage of seeds

Arabidopsis seeds were stored dry, in the dark, and in air-permeable bags at room temperature.

Surface sterilization and stratification of seeds

For sterilization, 1 mL of 70% ethanol was added to the Arabidopsis seeds under sterile conditions. The seeds were vigorously shaken for 1 minute and subsequently centrifuged at 6000 rpm for 1 minute. The supernatant was discarded. Next, 1 mL of 8% sodium hypochlorite (NaOCl) supplemented with Tween-20 (1/1000) was added to the seeds, and the samples were shaken for 5 minutes. Following this step, the seeds were centrifuged for 1 minute, and the supernatant was carefully removed.

After sterilization, the seeds were washed three times with 1 mL ddH_2O. Each washing step involved shaking for 1 minute, followed by centrifugation at 6000 rpm for 1 minute, after which the supernatant was discarded.

Finally, sterilized seeds were stratified overnight at 4 °C in 1 mL of ddH_2O or 0.1% agarose water.

Plant cultivation

Plant cultivation in the S1 greenhouse

Stratified seeds or two-week-old Arabidopsis plants were transferred onto soil substrate in 5 × 5 cm pots. The substrate consisted of equal parts Floraton 3 (Floragard Vertriebs GmbH, Oldenburg) and vermiculite with a grain size of 2 mm to 3 mm (Deutsche Vermiculite

Dämmstoff GmbH, Sprockhövel), in a 1:1 ratio. Plants were grown at 22 °C, at a relative humidity 50-60%, and under a day/night cycle of 16 hours light and 8 hours dark.

Plant cultivation in the growth room

For cultivation in the growth room, surface-sterilized and stratified Arabidopsis seeds were sown under sterile conditions on GM solid medium using a 0.1% agarose water. Plates were cultivated for 14 days at approximately 22 °C under a 16 h light / 8 h dark photoperiod. Cultivation in the growth room was used for the selection of primary transformants and identification of GT plants. After two weeks, depending on the experimental requirements, seedlings were either transferred to the botanical garden for further growth or used for genomic DNA (gDNA) extraction for subsequent analysis.

Determination of the seed weight for GT experiment

To determine the number of *Arabidopsis thaliana* seeds, the seeds from each harvested plant were processed individually. First, respective Eppendorf tubes for each sample were labelled, and their empty weights were recorded. The seeds from each individual line were then cleaned to remove residual plant material and transferred into the corresponding tubes. Subsequently, the total weight of each tube containing seeds was measured. The number of seeds was estimated by dividing the total seed weight by the approximate weight of a single seed. To estimate the total number of seeds required for GT efficiency calculations, the seed weight measurements are provided in Supplementary Figures 7.1 and 7.2.

Primary transformant selection and seed sowing on herbicide-containing medium

To obtain plants with stable integration of T-DNA into the genome, a primary transformant selection was performed. Approximately 15,000 seeds from bulk harvest were surface-sterilized and sown on 10 150 x 20 mm size, 10 Petri dishes containing GM solid medium supplemented with appropriate antibiotic. Additionally, the antibiotic cefotaxime was included in the medium to prevent the growth of *Agrobacterium* that might be present on the seeds. The plates were maintained in a growth room at approximately 22 °C under a 16 h light / 8 h dark cycle. Surviving primary transformants were then transferred to the soil and further cultivated as individual lines in the botanical garden until seed maturity. Seeds from each line were subsequently harvested separately.

For GT experiments, all surface-sterilized, stratified seeds from one line were sown on IM-containing GM solid medium and cultivated in the growth room. After 14 days, viable GT plants were counted and normalized to the total number of germinated seeds, allowing accurate

comparison of GT efficiencies across lines. GT events were subsequently verified at the molecular level. Confirmed GT plants were transferred to the botanical garden for further cultivation.

For the bulk screening method, the protocol described by Rönspies *et al.* (2022) was adapted. Seeds from each individual line were cleaned from remained plant materials and subsequently surface-sterilized and stratified. Following this, 40 seeds per line were sown on herbicide containing GM solid medium. Each line was sown on two to three Petri dishes. After 14 days, one leaf from each viable plant was collected and pooled for subsequent analyses.

A. tumefaciens*-mediated transformation of *A. thaliana

Stable transformation of *A. thaliana* was performed using the *floral-dip* method according to Clough and Bent (1998). For this purpose, 400 mL of YEB liquid medium containing the appropriate antibiotics was inoculated with Agrobacteria carrying the desired plasmid DNA. For inoculation, either 1 ml of glycerol stock or 1 ml of liquid culture was used. The culture was incubated overnight at 28 °C with shaking at 200 rpm until reaching a maximum OD_{600} of 1.7. To obtain a bacterial pellet, the culture was centrifuged at 4500 rpm for 15 minutes at 20 °C. The pellet was resuspended in infiltration medium to OD_{600} approximately 0.8 by adding 800 mL of infiltration medium.

Prior to transformation, approximately four-week-old plants were prepared by removing all open flowers and developed siliques. For transformation, the plants were submerged up to the rosette for approximately 20 seconds in Agrobacteria suspension. The transformed plants were then kept in the dark overnight at room temperature. The following day, the plants were sprayed with H_2O and grown in the S1 greenhouse until seed maturity. Seeds were subsequently collected as a bulk harvest.

***In planta* gene targeting workflow**

The *ip*GT workflow was performed in this study based on a previously established protocol (Merker et al., 2020b), integrating the procedures described above (see Figure 2.1). Briefly, cloned *ip*GT constructs were introduced into *Arabidopsis thaliana* via Agrobacterium-mediated transformation (see Figure 2.1A), and primary transformants (T_1) were selected on herbicide-containing medium. Selected lines were transferred to soil, grown to maturity, and harvested individually to maintain line-specific resolution (see Figure 2.1B).

To assess GT events, T_2 seeds derived from each line were screened on IM-containing medium, allowing the identification of successfully targeted individuals (see Figure 2.1C). GT efficiency

was calculated as the proportion of resistant seedlings relative to the total number of viable seeds, with normalization applied to account for differences in germination rates and to enable reliable comparison between wild-type and *ku70* mutant backgrounds (see Figure 2.1D). Line exhibiting GT efficiencies exceeding 70% were considered to originate from GT events in the T_1 generation and were excluded from further analysis. The resulting GT efficiencies were subsequently used to evaluate variation across independent lines and were visualized as a distribution (Figure 2.1E).

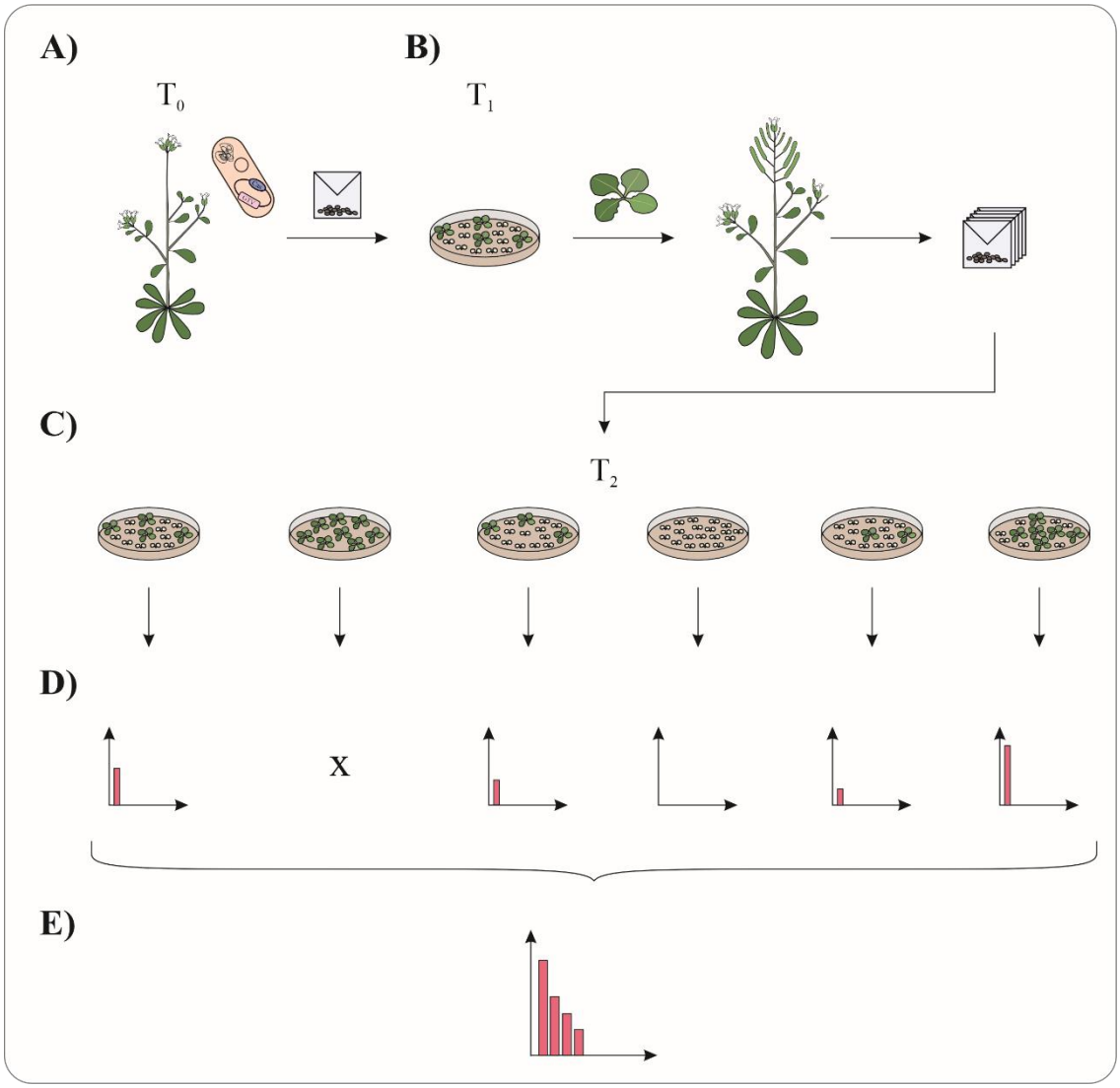

Figure 2.1: *In planta* Gene Targeting (*ip*GT) experiments.

A) Transformation of *Arabidopsis thaliana* plants (T_0 generation) with *ip*GT constructs via *Agrobacterium*-mediated floral dip. B) Selection of primary transformant (T_1 generation) on herbicide-containing medium, followed by transfer to soil, growth to maturity, and individual harvesting of T2 seeds from T-DNA-integrated lines. C) Screening of T2 seeds from individual lines on imidazolinone (IM)-containing medium to identify GT events. D) Determination of GT efficiency for each line by calculating the ratio of viable, herbicide-resistant seedlings to the total number of seeds, with normalization based on seed number and germination rate. Line with GT efficiencies above 70% were considered to result from GT events in the T_1 generation and were excluded from subsequent analysis. E) Distribution of GT efficiencies across independent lines, including only lines with detectable GT events, to enable comparative analysis between genotypes.

2.2.3 Molecular biology Methods

Polymerase chain reaction (PCR)

Polymerase chain reaction (PCR) was employed to amplify specific DNA fragments. When amplification was required for cloning or sequencing purposes, reactions were carried out using the Q5® High-Fidelity DNA Polymerase. The amplification procedure followed the manufacturer's instructions, and the GC enhancer provided in the kit was included when the target fragment exhibited a high GC content.

For all other amplifications, DNA amplification was performed using DreamTaq™ DNA Polymerase according to the manufacturer's instructions. The annealing temperature (T_A) for each primer pair was determined using the NEB Tm Calculator to ensure optimal specificity and efficiency.

Colony PCR

Colony PCR was performed to identify colonies carrying the desired construct. Positive colonies were distinguished by the amplification of the target DNA fragment. For this purpose, bacterial colonies were used directly as templates in the PCR reactions. Primer pairs were designed specifically for the intended cloning product, and the size of the resulting amplicons was analyzed to confirm the presence of the correct construct.

Two-step PCR

A two-step PCR method was used to add overhangs to a DNA fragment that would be complementary to a vector which had been linearized by a restriction enzyme digestion for Gibson Assembly. This approach differs from conventional PCR by including two distinct cycling phases. The first phase consisted of 15-20 cycles with an T_A determined according to the primer sequences complementary to the target DNA fragment. The second phase consisted of 25 additional cycles in which the overhang sequences were included in the calculation of the T_A. For both amplification phases, annealing temperatures were calculated using the NEB Tm Calculator.

DNA extraction and purification

Plasmid DNA extraction from *E. coli*

Plasmid DNA extraction from *E. coli* was performed using the peqGOLD Plasmid Miniprep Kit according to the manufacturer's instructions. Plasmid DNA was isolated from 4 mL of liquid culture and eluted in 50 µL of ddH_2O. The DNA concentration was measured using a

NanoDrop™ Lite spectrophotometer, and the cloned plasmids were verified by Sanger sequencing.

Genomic DNA extraction from *A. thaliana* with Shorty method

For the rapid extraction of genomic DNA from *A. thaliana*, the Shorty method (Edwards et al., 1991) was applied. In this procedure, either a single leaf or an entire plant was used as starting material. The plant tissue was mechanically disrupted in a 1.5 mL microcentrifuge tube using a plastic pestle, followed by the addition of 500 µL of Shorty DNA extraction buffer to complete the chemical lysis step. The samples were then centrifuged at >13,000 × g for 5 minutes to pellet cell debris.

After centrifugation, 400 µL of the supernatant was transferred to a new microcentrifuge tube and mixed with 400 µL of isopropanol. To precipitate the genomic DNA, the samples were centrifuged again at >13,000 × g for 10 minutes. The supernatant was carefully removed, and the resulting DNA pellet was air-dried overnight at room temperature or dried at 37 °C for 1 hour. The dried DNA pellet was then resuspended in 50-100 µL of TE buffer and shaken at 200 rpm for 30 minutes to ensure complete dissolution. For further experiments, genomic DNAs were stored at -80 °C.

Separation of DNA fragments using agarose gel electrophoresis

Agarose gels containing ethidium bromide (EtBr) in 0.9% or 2% TAE gels were used for verification and subsequent extraction of PCR amplificons and DNA fragments from restriction enzyme-digested plasmid DNA. For routine analysis of PCR amplification products, 0.9% or 2% SB gels were employed. Gels with a concentration of 0.9% were preferred for the separation if fragments larger than 1,000 bp.

Electrophoresis was performed in a gel chamber filled with corresponding running buffer at a final concentration of 1x. DNA samples were loaded into the wells, and electrophoresis was carried out for 20-50 minutes at voltages ranging from 80 V to 200 V, depending on fragment size and gel type. DNA bands were visualized using a gel documentation system. The GeneRuler™ 1 kb DNA Ladder and the GeneRuler™ Low Range DNA Ladder were used as molecular size markers.

Purification of DNA fragments

PCR amplicons and fragments obtained by restriction endonuclease digestion were purified for further usage. Buffers, enzymes, loading dyes and DNA fragments smaller than 50 bp were

removed using peqGOLD Cycle Pure Kit or E.Z.N.A.® Cycle Pure Kit, following the manufacturers' instructions.

For the purification of DNA fragments generated by restriction endonuclease digestion, which resulted in multiple fragments larger than 50 bp, the corresponding DNA band was excised from the agarose gel and purified by peqGOLD Gel Extraction Kit or E.Z.N.A.® Gel Extraction Kit, according to manufacturers' instructions. In both purification approaches, DNA was eluted in 30 µl ddH_2O. DNA concentration and purity were subsequently determined using NanoDrop™ Lite spectrophotometer.

Cloning Methods

Classical cloning

Restriction enzymes were employed to generate constructs by exchanging or removing specific DNA sequences. Type II restriction endonucleases were used throughout this study, as they cleave within or in close proximity to their recognition sequences. When cloning involved a single restriction enzyme, the vector backbone was dephosphorylated using Antarctic Phosphatase (New England Biolabs, Frankfurt am Main) to prevent self-ligation.

Following restriction digestion, DNA fragments were purified as described above. The insert and backbone fragments were subsequently ligated using T4 DNA ligase (Thermo Fisher Scientific, Braunschweig). The ligation reaction was prepared at 1:2, 1:3, 1:4, 1:5 or 1:6 molar ratio of backbone to insert, with 50-100 ng of backbone DNA per reaction. Ligation mixtures were incubated for 1 hour or overnight at room temperature (RT) and then transformed into *E. coli* NEB5α competent cells (see Chapter 2.2.1). When a destination vector containing the *ccdB* gene was used as the backbone, the ligation mixture was transformed into *E. coli ccdB*-resistant cells (One Shot™ ccdB Survival™ competent cells). Successful cloning events were confirmed by colony PCR and DNA sequencing.

Cloning with Gibson Assembly

Gibson Assembly was utilized for cloning when restriction enzyme-based cloning was not feasible or multiple inserts were to be simultaneously integrated into a single vector backbone. This method requires a linearized backbone and insert fragments possessing overlapping sequences that are complementary either to the backbone or, in the case of multiple inserts, to each other.

For Gibson Assembly, the linearized backbone and inserts were combined with NEBuilder® HiFi DNA Assembly Master Mix (New England Biolabs, Frankfurt am Main) according to the

manufacturer's instructions and incubated for 1 hour at 50 °C. The Master Mix contains an exonuclease that nucleolytically cleaves the 5' ends of DNA fragments, thereby generating complementary 3' overhangs. These overhangs anneal to homologous regions of adjacent fragments, after which a DNA polymerase fills the remaining gaps and a DNA ligase covalently joins the fragments. Successful assemblies were verified by colony PCR, and DNA sequencing.

CRISPR Cloning

CRISPR constructs were generated by using a recombination system derived from bacteriophage λ. The LR Clonase® II enzyme mix (Thermo Fisher Scientific, Braunschweig) recognizes specific recombination sequences, known as attachment sites (*att* sites), and catalyzes the exchange of DNA regions located between them. To utilize this system, entry vectors (pEn) and destination vectors (pDe) were utilized both containing *att* sites flanking the sequences to be recombined. In the pEn vector the gRNA cassette, including the *BbsI* recognition site for spacer integration, is positioned between the *att* sites. The pDe vector contains the T-DNA constructs with a *ccdB* counterselection cassette flanked by *att* sites.

In the first step, oligonucleotides were designed for spacer insertion. For Cas12a constructs, oligonucleotides with the sequences 5'-AGAT-spacer-3' and 5'-GGCC-reverse-spacer-3' were employed**.** Equimolar amount (2 µM each) of oligonucleotides were mixed and incubated for 5 minutes at 95 °C, followed by gradual cooling to room temperature for 20 minutes to anneal the oligonucleotides. The hybridized oligonucleotides were then ligated into *BbsI*-digested pEn vectors. For each ligation reaction, 3 µl of annealed oligonucleotides were combined with 10 ng of digested pEn and ligated using the Instant Sticky-end Ligase Master Mix prior to transformation into *E. coli* NEB5α competent cells (see Chapter 2.2.1). Successful spacer integration was confirmed by colony PCR and sequencing.

Gateway Reaction

For the LR recombination reaction, a mixture containing 200 ng of pEn, 150 ng of pDe and 1 µl of Gateway® LR Clonase® II Enzyme Mix was prepared and adjusted to total volume of 10 µl with TE buffer (pH 8.0). The reaction was incubated for 3 hours at room temperature and subsequently terminated by adding Proteinase K (Thermo Fisher Scientific, Braunschweig). The resulting mixture was transformed into *E. coli* NEB5α cells (see Chapter 2.2.1).

Replacement of *ccdB* cassette ensures that only bacteria containing an expected expression vector (pEx) with the integrated gRNA expression cassette can survive. All CRISPR constructs were validated by colony PCR and DNA sequencing.

Cloning for *ip*GT constructs

The CRISPR cloning strategy described above was applied to generate plasmid constructs suitable for applications such as mutagenesis frequency analysis. However, to perform gene targeting (GT) experiments, a donor sequence for HR must be provided together with the CRISPR/Cas expression cassette. For this purpose, donor sequences were either synthesized by BioCat GmbH (Heidelberg, Germany) or excised from a plasmid vector containing corresponding donor sequence via restriction endonuclease digestion (see Chapter 2.2.3). The resulting donor fragments were subsequently integrated into the destination vector via restriction digestion followed by ligation. The donor sequences utilized in this study are listed in Chapter 7.2 of the Supplementary Information, except for the previously described ALS HR donor sequence (Merker et al., 2020b; Wolter and Puchta, 2019).

Sequencing

Sanger Sequencing

Sanger sequencing was used to verify cloned plasmid constructs. Sequencing results were provided by Eurofins Genomics GmbH (Ebersberg, Germany) using the *SupremeRun* service or by Microsynth AG (Switzerland) using the *Economy Run* service. Samples and primers were prepared and shipped according to the companies' specifications.

Oxford Nanopore Technologies (ONT) Sequencing

Oxford Nanopore Technologies (ONT) was conducted to analyze amplified genomic region from plant DNA using ONT sequencing service (Microsynth AG, Switzerland). For this purpose, a LongPCR approach was employed for ONT sequencing. For each experimental setup, gDNA samples were obtained from 30 individual plants. These samples were divided into three biological pools, each consisting of gDNA from 10 plants and approximately 50 ng of gDNA were used as the template to amplify ~2000 bp amplicons. LongPCR amplification was performed using the Q5® High-Fidelity DNA Polymerase (New England Biolabs, Frankfurt am Main) following the manufacturer's protocol. Primer pairs were designed to maintain approximately equal distances from the target region, with the expected cleavage site positioned near the center of the amplified fragment to ensure balanced coverage during sequencing. The annealing temperature for each primer pair was calculated using the NEB Tm Calculator. The oligonucleotide sequences used for amplifications are listed in Table 7.2.

Data processing and initial analysis were conducted employing CRISPResso2 with default parameters.

Molecular Analysis

To identify GT events also at the molecular level, a leaf sample was collected from each GT plant for gDNA extraction using the Shorty method. The modified genomic region was then amplified by PCR using the primers 5'-CCAATGTCTGATTAGTGCTTCTGG-3' (forward) and 5'- AGTACGTTGATGGGGCTGG-3' (reverse) and subsequently sequenced (see Figure 2.1). Analysis of the resulting chromatograms enabled discrimination between homozygous and heterozygous GT events using *Indigo Rapid InDel Discovery in Sanger Chromatograms* Gear Genomics; available at: https://www.gear-genomics.com/. To prevent amplification of residual donor sequences originating from T-DNA integration, the primers were designed to anneal outside the donor region, exclusively within the genomic target locus (Figure 2.2A). Accordingly, both primers bind outside the homology arms. This primer design allows differentiation between perfect, one-sided, and ectopic GT events. A perfect GT event is characterized by the presence of the S653N mutation together with unaltered junctions, where the junctions refer to the transitions between homologous and non-homologous regions between the target locus and the donor sequence. In contrast, one-sided GT events exhibit sequence alterations at one of the junction sites (Figure 2.2B). If sequencing reveals no modifications – neither the S653N mutation, nor the introduced silent mutation – the event is classified as ectopic. In such cases, HR may result in the transfer of a portion of the target sequence to the donor. The resulting extended donor sequence may subsequently integrate into the genome via NHEJ (Figure 2.2C). This process can restore the selection marker, thereby conferring IM resistance without modifying the endogenous target locus.

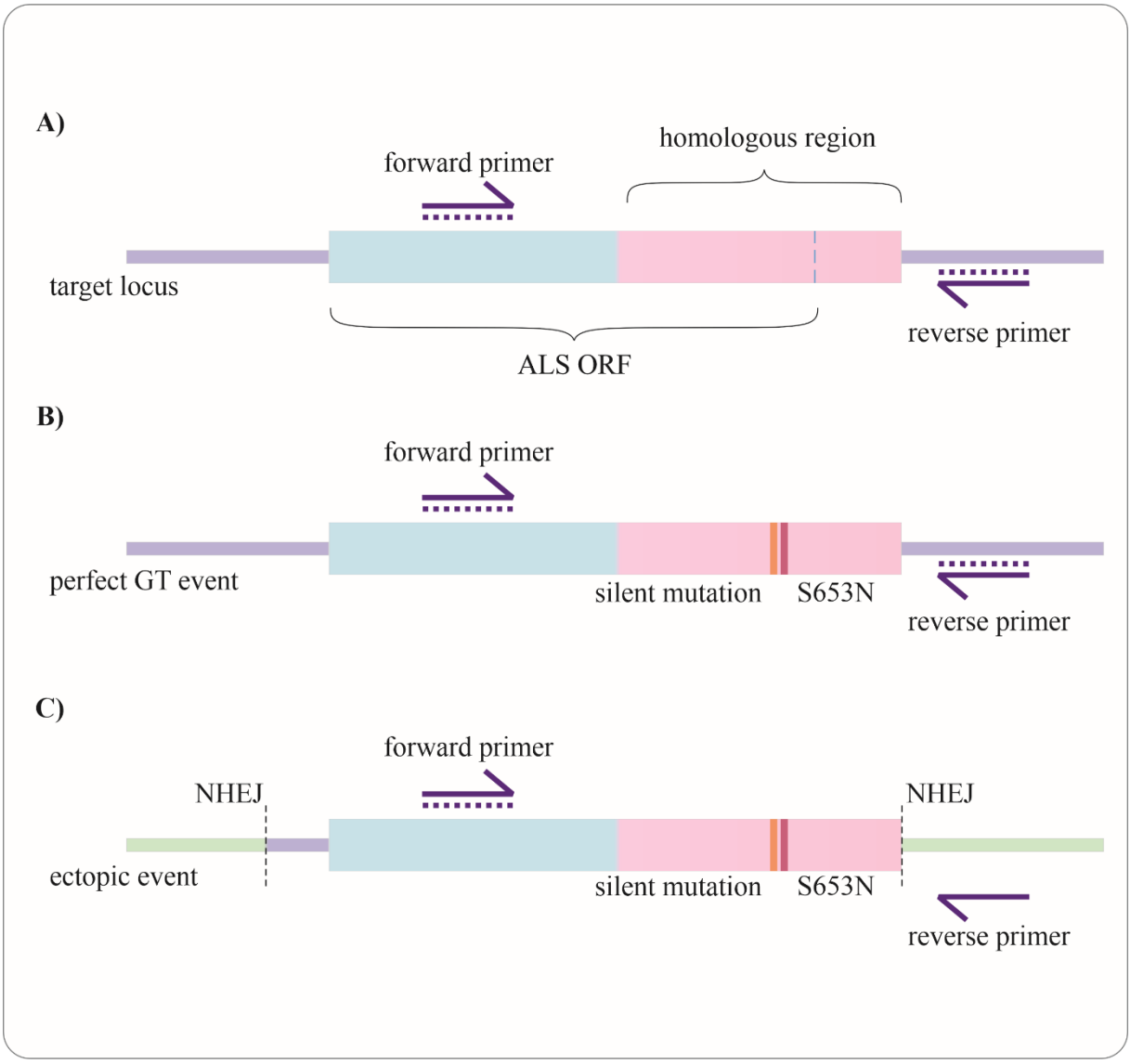

Figure 2.2: Molecular analysis of *in planta* Gene Targeting (*ip*GT).

A) For the amplification of the target sequence, primers were designed to anneal outside the homologous region, represents the homologous sequence between the target locus and the donor template. The forward primer is located within the *ALS* open reading frame (ORF), upstream of the homologous region, whereas the reverse primer is positioned outside the *ALS* ORF, downstream of the homologous region. B) In the case of a perfect GT event, amplification yields a fragment containing the coding sequence for the S653N mutation and, where applicable, additional silent mutations, with no alterations at the junction sites. C) An ectopic event is defined by restoration of the selection marker within the donor sequence through sequence information derived from the target locus. The restored donor can subsequently integrate into a random genomic location via NHEJ.

.

3 RESULTS

The introduction of specific modifications into plant genomes is of main interest for modern biotechnology and crop improvements. Although conventional breeding and random mutagenesis approaches have been widely applied, they have remained insufficient for the precise induction of predefined sequence changes, highlighting the need for further technological advancements. While approaches such as BE and PE have enabled precise GT, due to the underlying mechanisms of these systems, their applications have largely remained limited to small-scale modifications (Huang and Puchta, 2019; Tuncel et al., 2025; Zhang et al., 2019; Zhou et al., 2025). In contrast, HR-based GT approaches provide the advantage of introducing larger and more precise insertions and genomic modifications (Atkins and Voytas, 2020). Nevertheless, the efficiency of HR-based GT methods in plants remains relatively low, and this efficiency can potentially be improved through the use of CRISPR/Cas systems and further advancements in these technologies (Zhu et al., 2020).

3.1 Direct fusion of exonucleases to ttLbCas12a-i

HR enables the scar-free insertion or replacement of large DNA fragments in plants, however, its efficiency remain relatively low (Schreiber et al., 2024). Therefore, alternative strategies need to be explored to improve the GT efficiency. All HDR-mediated repair pathways of DSBs require end resection to generate extended 3’ ssDNA overhangs (>25 bp), which are essential for strand invasion and HR (Lieber, 2010; Schmidt et al., 2019). Even though Cas12a endonucleases inherently produce staggered DNA ends, the direct fusion of exonucleases to CRISPR/Cas nucleases has been proposed as a strategy to further extend 3’ overhangs, thereby potentially enhancing HDR efficiency (Schreiber et al., 2024). Previous studies have demonstrated that fusion of exonucleases to endonucleases can result in increased deletion sizes, suggesting enhanced end processing activity (Certo et al., 2012; Clements et al., 2017; Lainšček et al., 2022; Ordon et al., 2023; Weiss et al., 2020; Wu et al., 2020; Zhang et al., 2020). More importantly, several reports indicate that the fusion of 5’ exonucleases to Cas9 or Cas12a

can significantly improve HDR frequencies (Hackley, 2021; Schreiber et al., 2024; Zhang et al., 2022).

In particular, the use of 5’ exonucleases derived from the herpes virus (HSV) family in fusion with Cas9 or Cas12a has been shown to enhance HR efficiency more than 10-fold in stable knock-ins (KIs) in Arabidopsis (Schreiber et al., 2024). For instance, fusion of the 5’-3’ exonuclease *Papiine alpha herpesvirus 2* (PapE) to intronized SpCas9 (SpCas9i) resulted in a substantial increase in GT efficiency in tobacco. Similarly, fusion of the UL12 exonuclease from Herpes Simplex Virus 1 (HSVUL12) (Bronstein and Weber, 1996; Chung and Hsu, 1996) to ttLbCas12a-i led to an improvement compared to Cas12a alone. Furthermore, targeting the *thiC* locus in Arabidopsis using the PapE-Cas9 fusion demonstrated a significant increase in GT efficiency (Schreiber et al., 2024). Based on these findings, HSVUL12 and its ortholog from PapE were selected for further investigation of *ip*GT efficiency. Notably, the N-terminal domain of UL12 (amino acids 1-26) has been reported to interact with MRN complex, a key component involved in the initiation of DNA repair pathways (Balasubramanian et al., 2010; Schreiber et al., 2024). Incorporation of this MRN-recruiting domain (N1-126) into a Cas9 fusion construct was demonstrated to result in an increase in HR efficiency in human cells (Reuven et al., 2019).

To investigate whether the direct fusion of exonucleases could further improve GT efficiency beyond the most advanced *ip*GT approach currently available, the 5’-3’ exonucleases were individually fused to ttLbCas12a-i. In this study, the ttLbCas12a-i and fused exonuclease sequences were placed under the control of the EC promoter with a rbcS terminator, while the crRNA was driven by the *A. thaliana* U6-26 promoter. Specifically, PapE and HSVUL12 exonucleases were fused to the N-terminus of the Cas12a endonuclease using flexible 4 × glycine-serine (GS) linkers (X. Chen et al., 2013). This linker selection was informed by the comparable activity and efficiency of N- and C- terminal fusion configurations reported previously (Schreiber et al., 2024). Accordingly, the pAGT8175 HSVUL12-ttLbCas12a-i and pAGT9782 PapE-ttLbCas12a-i plasmids (Schreiber et al., 2024) were utilized as templates to clone expression vectors. These vectors also contained an HR donor sequence incorporating both the silent mutation and the desired mutation to the *ALS* locus, flanked by PAM and spacer sequence. For primary transformant selection, a gentamicin resistance cassette (GentR) was included within the T-DNA.

For the cloning of *ip*GT vectors, pEx-EC-ttLbCas12a-i+ALS+GTVc12+GentR expression vector was used (Schindele et al., 2023). The coding sequence for ttLbCas12a-i was excised using the restriction enzyme AscI to be replaced by the HSVUL12-ttLbCas12a-i or

PapE-ttLbCas12a-i sequences via Gibson Assembly. HSVUL12-ttLbCas12a-i from pAGT8175 HSVUL12-tt*Lb*Cas12a-i, and PapE-ttLbCas12a-i from pAGT9782 PapE-tt*Lb*Cas12a-i were amplified with overhangs (OHs). The expression clones resulting are pEx-EC-HSVUL12-ttLbCas12a-i+ALS+GTVc12+GentR and pEx-EC-PapE-ttLbCas12a-i+ALS+GTVc12+GentR, respectively.

To investigate the effect of the direct fusion of the exonucleases on the GT efficiency, the *ip*GT protocol described in Chapter 2.2.2 was applied. For this purpose, T2 seeds were obtained from *Arabidopsis* Col-0 plants transformed with the respective T-DNAs, and the number of viable seedlings was determined using IM-containing selection medium. Two replicates were performed for each construct, with each replicate comprising between 16 and 20 independent lines. In Col-0, a total of 40 independent lines were analyzed for the approach based on ttLbCas12a-i alone, and 39 independent lines each for PapE-ttLbCas12a-i and HSVUL12-ttLbCas12a-i fusions.

The GT efficiency for ttLbCas12a-i was initially calculated based on seed weight and subsequently normalized to the baseline viable plants/total seeds ratio of wild-type Col-0 plants, resulting in an observed value of 0.98%. Interestingly, GT efficiency decreased upon direct fusion of exonucleases in Col-0, dropping to 0.29% and 0.58% for PapE-ttLbCas12a-i and HSVUL12-ttLbCas12a-i, respectively. Furthermore, the ttLbCas12a-i construct exhibited a higher frequency of GT-positive independent lines (87.5%) compared to the exonuclease-fused variants. In comparison, the HSVUL12-ttLbCas12a-i approach resulted in 69.3% positive lines. Notably, for the PapE-ttLbCas12a-i based approach, only 17 lines (43.6%) showed at least one GT events, whereas no GT events were detected in the remaining 22 individual lines, representing more than half of the tested population (56.4%) (see Table 3.1).

The effect of exonucleases on GT efficiency becomes more apparent when comparing the efficiencies across individual lines. For this purpose, GT efficiencies in Col-0 plants for each construct are presented in Figure 3.1, where values are illustrated from highest to lowest. The highest GT efficiency among individual lines was observed for HSVUL12-ttLbCas12a-i at 5.67%, while the other two constructs reached 4.81%. However, only 10.26% of the exonuclease-fusion lines exhibited GT efficiencies above 1%, whereas this proportion reached 45% in ttLbCas12a-i lines, representing the highest frequency.

Comparison of normalized average GT efficiencies revealed that, relative to ttLbCas12a-i in Col-0, PapE-ttLbCas12a-i and HSVUL12-ttLbCas12a-i showed 3.38-fold and 1.69-fold decreases, respectively.

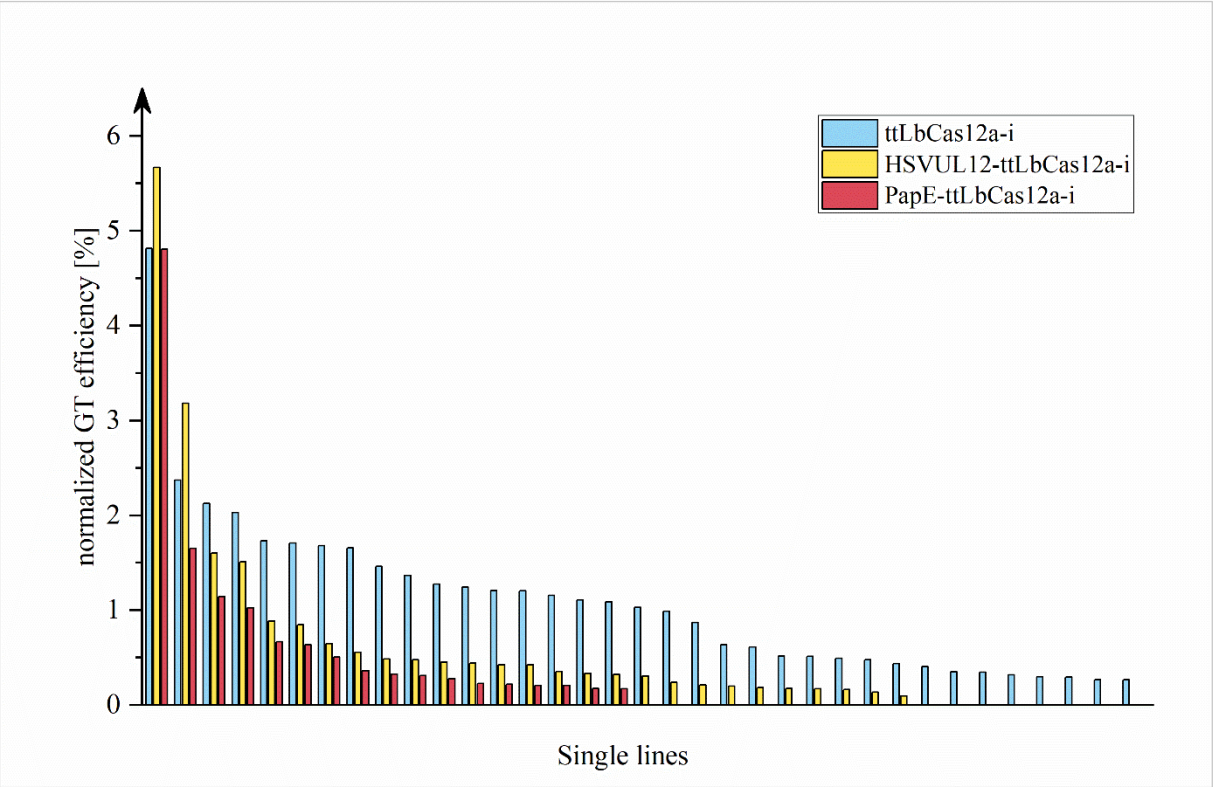

Figure 3.1: Gene targeting distribution of direct fusion of exonucleases compared to normal GT approach in *Arabidopsis* Col-0.

The normalized GT efficiencies of individual lines in Col-0 plants are shown for ttLbCas12a-i (blue), PapE-ttLbCas12a-i (red), and HSVUL12-ttLbCas12a-i (yellow). The highest GT efficiency was 4.81% for both ttLbCas12a-i and PapE-ttLbCas12a-i, whereas HSVUL12-ttLbCas12a-i reached a maximum GT efficiency of 5.7%. At least one GT event was observed in 35 individual lines out of 40 individual lines for ttLbCas12a-i (87.5%), 17 out of 39 lines for PapE-ttLbCas12a-I (43.6%), and 27 out of 39 lines for HSVUL12-ttLbCas12a-i (69.2%).

In addition to these findings, previous study have demonstrated that GT efficiency increases when the predominant cNHEJ repair pathway is suppressed following DSB formation (Merker et al., 2024). Therefore, to assess the behavior of exonuclease fusions under impaired cNHEJ conditions, the *ip*GT protocol was also applied in *ku70* mutant *Arabidopsis* plants. T_2 seeds were generated according to the protocol in Chapter 2.2.2, and GT efficiency was evaluated by sowing seeds on IM-containing medium. Two replicates were performed per construct, each comprising 16 to 20 independent lines. In *ku70* mutant plants, 37 individual lines were analyzed for ttLbCas12a-i, 33 for PapE-ttLbCas12a-i, and 39 for HSVUL12-ttLbCas12a-i. The percentages of lines showing at least one GT event were 83.8% for ttLbCas12a-i, 36.4% for PapE-ttLbCas12a-i and 53.9% for HSVUL12-ttLbCas12a-i (see Table 3.1).

As observed in Col-0, normalized average GT efficiency was highest for ttLbCas12a-i in *ku70* mutants at 2.10%, whereas PapE-ttLbCas12a-i and HSVUL12-ttLbCas12a-i exhibited efficiencies of 0.25% and 0.43%, respectively (see Table 3.1). Only a single PapE-ttLbCas12a-i

line displayed a GT efficiency above 1% (3.66%), while all other positive lines remained below 1%. Furthermore, 63.6% of PapE-ttLbCas12a-i lines showed no GT events.

When comparing average GT efficiencies between *ku70* mutants and Col-0 in ttLbCas12a-i, a 2.14-fold increase was observed in *ku70*. However, notably, exonuclease fusion resulted in reduced efficiencies in both genotypes and exhibited similar GT efficiency levels relative to each other (see Table 3.1).

The distribution of GT efficiencies across individual lines in *ku7*0 mutant plants is presented in Figure 3.2.

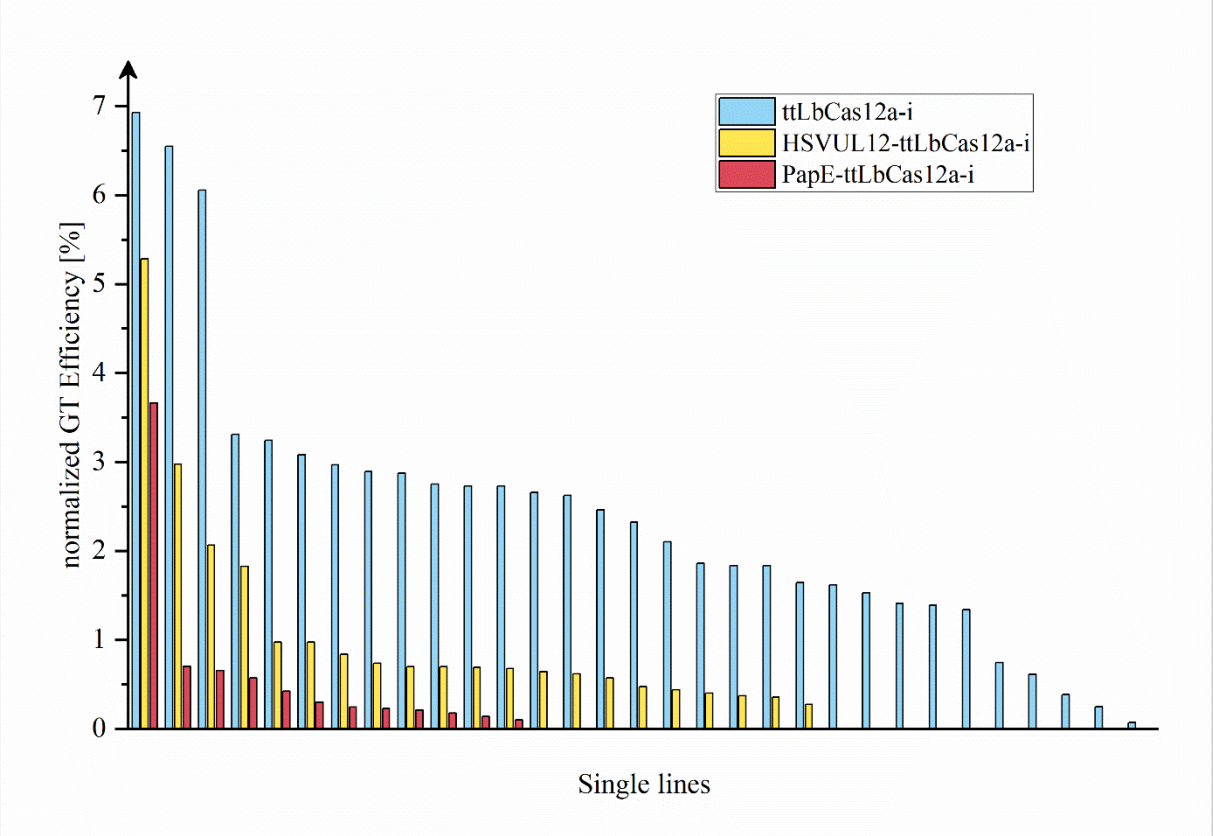

Figure 3.2: Gene targeting distribution of direct fusion of exonucleases compared to normal GT approach in *Arabidopsis ku70*.

The normalized GT efficiencies of individual lines in *ku70* mutant plants are shown for ttLbCas12a-i (blue), PapE-ttLbCas12a-i (red), and HSVUL12-ttLbCas12a-i (yellow). The highest GT efficiency in an individual line was 6.93% for ttLbCas12a-i, 3.66% for PapE-ttLbCas12a-i, and 5.28% for HSVUL12-ttLbCas12a-i. GT efficiencies were calculated based on normalized values of individual lines. At least one GT event was observed in 31 individual lines for ttLbCas12a-i, 12 lines for PapE-ttLbCas12a-i, and 21 lines for HSVUL12-ttLbCas12a-i.

Analysis of the proportion of lines exhibiting positive GT events in both Col-0 and *ku70* backgrounds showed that the ttLbCas12a-i control approaches yielded the highest frequencies (87.50% and 83.8%, respectively), compared to PapE (43.6% and 36.4%, respectively) and HSVUL12 (69.2% and 53.9%, respectively) fusion approaches. Moreover, the proportion of

negative lines was higher for PapE (63.6%) and HSVUL12 (46.2%) exonuclease fusions in the *ku70* background compared to Col-0.

Table 3.1: Quantitative outcomes of GT approaches of direct fusion of PapE and HSVUL12 exonucleases to ttLbCas12a-i with a comparison of ttLbCas12a-i in Col-0 and *ku70* genotypes.

For all tested approaches, the number of individual lines, the number of positive lines, the total number of approximately analyzed seeds, the number of positive seeds, as well as the GT efficiency (%) and normalized GT efficiency (%) are presented in the table.

Genotype	Approaches	Number of T_1 lines	Number of positive lines	Positive lines (%)	Number of analyzed seeds	Number of analyzed positive seeds	GT efficiency (%)	Normalized GT efficiency (%)
Col-0	ttLbCas12a-i	40	35	87.50	~41,400	359	0.87	0.98
	PapE-ttLbCas12a-i	39	17	43.59	~28,500	72	0.25	0.29
	HSVUL12-ttLbCas12a-i	39	27	69.23	~26,800	137	0.51	0.58
ku70	ttLbCas12a-i	37	31	83.78	~37,900	748	1.97	2.10
	PapE-ttLbCas12a-i	33	12	36.36	~17,600	42	0.24	0.25
	HSVUL12-ttLbCas12a-i	39	21	53.85	~32,700	131	0.40	0.43

To confirm GT events, molecular analyses described in Chapter 2.2.3 were performed. These analyses revealed that 43%, 15%, and 44% of the examined Col-0 lines carrying ttLbCas12a-i, PapE-ttLbCas12a-i, and HSVUL12-ttLbCas12a-i approaches, respectively, exhibited perfect GT events. In the *ku70* background, the frequencies of perfect GT event were 71%, 38%, and 55% for ttLbCas12a-i, PapE-ttLbCas12a-i, and HSVUL12-ttLbCas12a-i approaches, respectively. Consistent with GT efficiency data, PapE-ttLbCas12a-i showed reduced performance in both Col-0 and *ku70* backgrounds, whereas HSVUL12-ttLbCas12a-i did not show a notable change in Col-0.

Interestingly, analysis of homozygous perfect GT events revealed that, in *ku70* background, ttLbCas12a-i and PapE fusion approaches resulted in 14% and 19%, respectively. Overall, each approach in the *ku70* background achieved higher perfect GT efficiencies compared to the corresponding approaches in the Col-0 genotype (see Table 3.2).

Since direct fusion of exonucleases reduced GT efficiency compared with the control in both genotypes and yielded very similar efficiencies among the tested exonuclease approaches, this strategy appeared to offer limited improvement. Therefore, an alternative recruitment strategy was considered to overcome this limitation in GT efficiency.

Table 3.2: Molecular analysis of GT Events of ttLbCas12a-i with comparison of direct fusion of PapE and HSVUL12 exonucleases in Col-0 and *ku70*.

For the six tested approaches, the number of analyzed T_2 plants, the number of T_2 plants exhibiting a GT event, the proportion of perfect GT events, the number of homozygous GT events, and their corresponding proportion are listed.

Genotype	Approaches	Number of analyzed T_2 plants	Number of T_2 plants with Perfect GT event	Perfect GT Events (%)	Number of homozygous GT event	Homozygous GT event (%)
Col-0	ttLbCas12a-i	23	10	43	-	-
	PapE-ttLbCas12a-i	13	2	15	-	-
	HSVUL12-ttLbCas12a-i	25	11	44	1	4
ku70	ttLbCas12a-i	28	20	71	4	14
	PapE-ttLbCas12a-i	21	8	38	4	19
	HSVUL12-ttLbCas12a-i	22	12	55	-	-

3.2 SunTag-mediated exonuclease recruitment of gene targeting efficiency

The SunTag-mediated exonuclease recruitment system was adopted to increase the local accumulation of multiple exonucleases near the cleavage site and to test whether multivalent recruitment could overcome this limitation in GT efficiency. The SunTag system has been employed previously as a strategy to enhance targeted deletion sizes through the recruitment of exonucleases. Notably, SunTag-mediated recruitment of *Homo sapiens* TREX2 (HsTREX2) resulted in a higher mean deletion size compared with direct fusion of the 3' exonuclease human TREX2, and additionally led to an increase in insertion events (Capdeville et al., 2024). Therefore, this system was applied in Arabidopsis to investigate whether recruitment of multiple exonucleases could improve the GT efficiency.

Based on the previous results obtained from the direct fusion experiments, PapE and HSVUL12 were selected for further investigation using the SunTag-mediated recruitment system. Additionally, the human 3'-5' exonuclease TREX1 (HsTREX1) was included as another candidate to evaluate whether the SunTag-mediated exonuclease recruitment of this exonuclease could also affect the GT efficiency. Previously, SunTag-mediated recruitment of HsTREX1 via SpCas9 revealed an increase in mean deletion size from 12 bp to 52 bp (Capdeville et al., 2024). HsTREX1 contains a C-terminal endoplasmic reticulum (ER) localization signal peptide, however, a truncated variant lacking this signal sequence ($HsTREX1_{1-293}$, hereafter referred to as HsTREX1) has been reported to exhibit increased catalytic activity (Lindahl et al., 2009). Therefore, this truncated form was used in the previous study and was also included in the present study.

To evaluate *ip*GT efficiency of SunTag-mediated exonuclease recruitment, the 5'-3' exonucleases HSVUL12 and its ortholog PapE, as well as the 3'-5' exonuclease HsTREX1, were recruited to LbCas12a-induced DSBs via the SunTag system.

To generate the destination plasmids, multiple cloning strategies were applied sequentially. Initially, the GTV donor sequence GTVc12 from the previous expression vector pEx-EC-ttLbCas12a-i+ALS+GTVc12+GentR was transferred onto the destination vector pDe-EC-ttLbCas12a-i-rbcST+ccdB+PPTR (Schindele et al., 2023) via a classical cloning approach based on the restriction enzyme PacI, resulting in the destination vector pDe-EC-ttLbCas12a-i-rbcST+ccdB+GTVc12+PPTR.

Subsequently, an intermediate cloning step involving an entry vector was performed to facilitate further plasmid construction via restriction digestion and ligation. For this purpose, the pEn-RZ-LbcrRNA (Wolter and Puchta, 2019) was digested with BbsI and the ALS target protospacer sequence was inserted into the crRNA cassette. The resulting construct was designated pEn-RZ-LbcrRNA-ALS. In the next step, both the pEn-RZ-LbcrRNA-ALS and pDe-EC-ttLbCas12a-i-rbcST+ccdB+GTVc12+PPTR plasmid were digested with MluI restriction digestion enzyme. The crRNA cassette containing the ALS target sequence was subsequently inserted into the destination vector via T4 DNA Ligase (Thermo Fisher Scientific GmbH, Braunschweig) mediated ligation. The resulting plasmid was named pDe-EC-ttLbCas12a-i-rbcST+ccdB+ALS+GTVc12+PPTR.

In a further modification step, the pDe-Omega-SaCas9-GCN4+PPTR plasmid was digested using EcoRI and AscI to excise the Omega RBC sequence between the recognition sites of these enzymes, as well as the GCN4 sequence linked to the SaCas9 coding sequence. The coding sequence of the ttLbCas12a-i in the pDe-EC-ttLbCas12a-i-rbcST+ccdB+ALS+GTVc12+PPTR plasmid was replaced via AscI-mediated excision and subsequent Gibson Assembly with the Omega RBC, ttLbCas12a-i, and 10 x GCN4 coding sequences, whereby the first and the latter sequences were derived from pDe-Omega-SaCas9-GCN4+PPTR. The resulting final destination plasmid was designated as pDe-EC-Omega-ttLbCas12a-i-GCN4-rbcST+ccdB+ALS+GTVc12+PPTR.

For the cloning of the entry vectors, the pEn-SagRNA+UBI-scFv-sfGFP-GB1-nosT (BioCat GmbH, Heidelberg) plasmid was used as the initial vector. Firstly, the SagRNA cassette was removed from the plasmid using the Bsu36I restriction enzyme, and resulting in the generation of the plasmid pEn-UBI-scFv-sfGFP-GB1-nosT. Subsequently, digestion with EcoRI resulted in the removal of the *Petroselinum crispum* UBIQUITIN4-2 promoter (UBI) and linearization

of the backbone. The pDe-EC-ttLbCas12a-i-rbcST+ccdB+PPTR (Schindele et al., 2023) plasmid was digested with EcoRI to obtain the EC promoter fragment. First, EC promoter was ligated into EcoRI-digested backbone using classical ligation, yielding the pEn-EC-scFv-sfGFP-GB1-nosT plasmid. Subsequently, the rbcS terminator fragment was excised from pDe-EC-ttLbCas12a-i-rbcST+ccdB+PPTR using SacI digestion. The resulting rbcS terminator sequence was amplified by PCR for use in Gibson Assembly. The pEn-EC-scFv-sfGFP-GB1-nosT plasmid was linearized with AvrII, to remove terminator sequence of *nopaline synthase* (*nos*) gene from *Agrobacterium tumefaciens* (nosT), and the rbcS terminator was inserted via Gibson Assembly, resulting in the pEn-EC-scFv-sfGFP-GB1-rbcST plasmid. This plasmid was used as the primary vector for exonuclease integration and also served as the final entry vector for generating the expression clone via Gateway reaction for the SunTag control construct.

HSVUL12, PapE, and HsTREX1 exonuclease sequences were obtained from the plasmids generated in Chapter 3.1, and from the pEn-Sa-Chimera-HsTREX1 plasmid. The plasmids obtained from Chapter 3.1 were digested with AscI and amplified by PCR to include OHs compatible with Gibson Assembly. Meanwhile, the pEn-EC-scFv-sfGFP-GB1-rbcST plasmid linearized with BamHI. The BamHI digested pEn-Sa-Chimera-HsTREX1 plasmid was ligated via classical ligation, and the OH-HSVUL12 and OH-PapE fragments were assembled into the final entry vector using Gibson Assembly. The resulting plasmids were designated as pEn-EC-scFv-sfGFP-HsTREX1-GB1-rbcST, pEn-EC-scFv-sfGFP-HSVUL12-GB1-rbcST, and pEn-EC-scFv-sfGFP-PapE-GB1-rbcST, respectively.

To generate the final expression vectors, the destination vector pDe-EC-Omega-ttLbCas12a-i-GCN4-rbcST+ccdB+ALS+GTVc12+PPTR was combined with the final entry vector using the Gateway LR recombination reaction. The final expression constructs were named as follows:

pEx-EC-Omega-ttLbCas12a-i-GCN4+scFv-sfGFP-HsTREX1-GB1+ALS+GTVc12+PPTR,
pEx-EC-Omega-ttLbCas12a-i-GCN4+scFv-sfGFP-HSVUL12-GB1-ALS-GTVc12+PPTR,
pEx-EC-Omega-ttLbCas12a-i-GCN4+scFv-sfGFP-PapE-GB1+ALS+GTVc12+PPTR,
pEx-EC-Omega-ttLbCas12a-i-GCN4+scFv-sfGFP-GB1+ALS+GTVc12+PPTR.

The constructs were hereafter referred to as SunTag-HsTREX1, SunTag-HSVUL12, SunTag-PapE, and the SunTag control, respectively (see Figure 3.3).

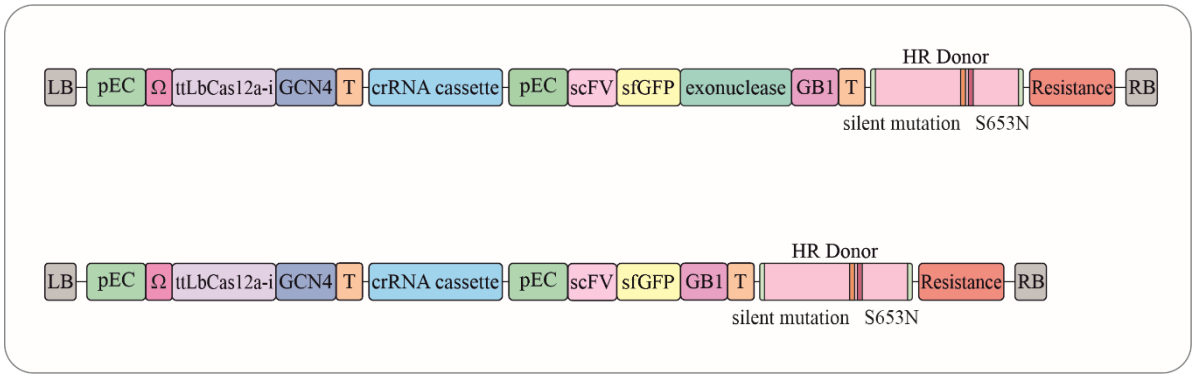

Figure 3.3: The *ip*GT constructs for SunTag-mediated exonuclease recruitment of ttLbCas12a-i.

The constructs consist of sequences flanked by the left and right borders (LB and RB). Shown are the expression constructs for the recruitment of the 5' exonucleases Herpes Simplex Virus UL12 (HSVUL12) and *Papiine alpha herpesvirus 2* (PapE), and 3' exonuclease human THREE PRIME REPAIR EXONUCLEASE 1 (HsTREX1) to intronized temperature tolerant Cas12a (ttLbCas12a-i) coding sequence for *ip*GT. For SunTag-mediated recruitment, GCN4 epitope was cloned at the 3' end of the ttLbCas12a-i coding sequence. The constructs contain single-chain variable fragment (scFv) antibodies that bind to GCN4 epitopes. The fusion construct incorporates a superfolder green fluorescent protein (sfGFP) and B1 domain of protein G (GB1) to improve protein stability and reduce aggregation. A corresponding antibody fusion construct enables the recruitment of the three exonucleases. Through this system, multiple copies of selected exonucleases can be recruited to Cas12a. (top). To compare the GT efficiency of the SunTag system recruited to ttLbCas12a-i, the respective construct was also cloned (bottom). Expression of the fusion constructs is driven by the oocyte-specific promoter (pEC) with *Pisum sativum* rbcS E9 terminator (T). The constructs additionally contain the Omega (Ω) translational enhancer sequence from Tobacco mosaic virus. The CRISPR RNA (crRNA) cassette driven by the *Arabidopsis U6 SMALL NUCLEOLAR RNA26* (U6-26) promoter and terminated by Poly-T signal, which incorporates the ALS target sequence. Additionally, the constructs contain a Homologous Recombination donor (HR donor) template, including homologous arms flanked by ALS target sequences, together with silent mutation and the coding sequence for S653N substitution. An herbicide resistance cassette is also placed in the constructs as a selection marker.

To analyze GT efficiency, the *ip*GT protocol described in Chapter 2.2.2 was applied. The cloned vectors were transformed into *Arabidopsis* wild-type Col-0 and *ku70* plants. T_2 seeds were plated on IM-selection medium, and the number of viable seedlings was recorded. For each line, the seed weight was measured individually, and the approximate seed number of each individual line was calculated according to the total seed weight of the corresponding single-line groups. GT efficiencies were then determined by comparing the calculated seed numbers with the number of viable seedlings.

In Col-0 plants, five replicates were performed for each approach, and these replicates included between 2 and 22 single lines. In total, 71, 80, 57, and 75 individual T1 lines were analyzed for the SunTag approach, SunTag-HsTREX1, SunTag-PapE, and SunTag-HSVUL12, respectively (see Table 3.3).

Prior to the analysis, the viable seed/total seed ratio calculated separately for each approach was used to normalize the GT efficiency results. The normalized GT efficiency of the SunTag approach was 0.71% on average, whereas reduced efficiencies were observed for SunTag-HsTREX1 (0.36%) and SunTag-PapE (0.59%). In contrast, the GT efficiency of

SunTag-HSVUL12 increased to 1.12% compared to the control. Accordingly, the highest average GT efficiency in Col-0 lines was observed in the single lines carrying the SunTag-HSVUL12 approach. When the occurrence of at least one GT event was examined, the single lines of the SunTag-HsTREX1 approach showed the lowest proportion of positive lines in Col-0 plants, with 35 positive single lines out of 80 (43.8%), whereas the remaining SunTag control, SunTag-PapE and SunTag-HSVUL12 approaches showed 74.7%, 86.0%, and 79.7%, respectively (see Table 3.3).

The distribution of GT efficiencies among individual lines in Col-0 plants is shown in Figure 3.4. Interestingly, only 3.75% of SunTag-HsTREX1 single lines exhibited GT efficiencies greater than 1%, representing the lowest proportion among all approaches. Furthermore, the maximum GT efficiency observed for this approach was 2.31% for a single line, which was also comparatively low relative to the other approaches. On the other hand, 28.38% of SunTag-HSVUL12 lines displayed GT efficiencies above 1%. This proportion was slightly higher than that observed in the control SunTag approach (22.54%).

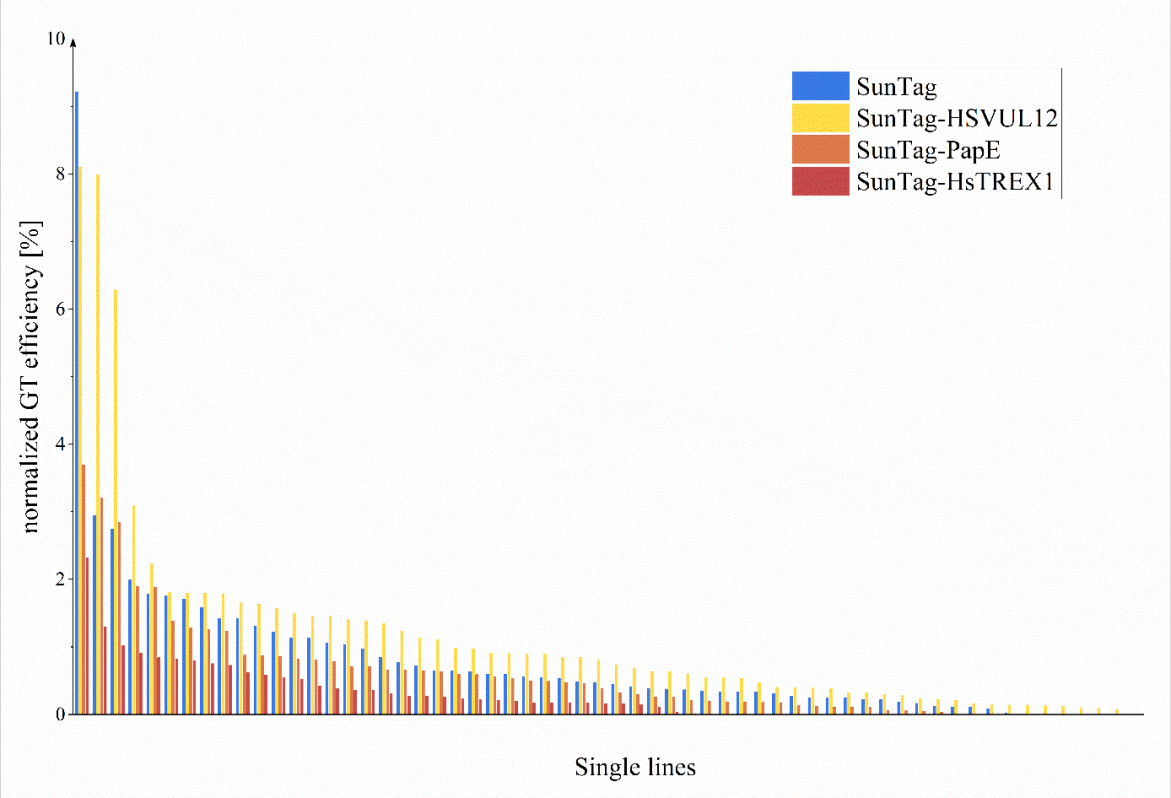

Figure 3.4: Gene targeting distribution of SunTag-mediated exonuclease recruitments in *Arabidopsis* Col-0.

The normalized GT efficiencies of individual lines in Col-0 plants are shown for SunTag approach (blue), SunTag-HsTREX1 (red), SunTag-PapE (orange) and SunTag-HSVUL12 (yellow). The highest GT efficiency was 9.22% for the SunTag approach, followed bySunTag-HSVUL12 with 8.10%. However, SunTag-PapE and SunTag-HsTREX1 showed low GT efficiencies with 3.70% and 2.32%, respectively. GT efficiencies were calculated based on normalized values of individual lines. At least one GT event was observed in 53 individual lines for SunTag, 35 lines for SunTag-HsTREX1, 49 lines for SunTag-PapE and 59 lines for SunTag-HSVUL12.

As for the direct fusion approach, the influence of KU-mediated end protection on GT efficiency following SunTag-mediated exonuclease recruitment was analyzed. In the *ku70* Arabidopsis plants, the approaches were performed with 4-5 replicates and included the analysis of groups containing between 3 and 35 single lines. In total, 62, 61, 57, and 69 individual lines were analyzed for the SunTag approach, SunTag-HsTREX1, SunTag-PapE, and SunTag-HSVUL12 applications, respectively (see Table 3.3).

In *ku70* mutants, the normalized GT efficiency of the SunTag approach was 0.81%, whereas a decrease to 0.61% was observed for SunTag-HsTREX1. Meanwhile, slight increases were detected for SunTag-PapE (1%) and SunTag-HSVUL12 (0.90%). Among the four applications, SunTag-HsTREX1 again showed the lowest proportion of lines with GT efficiencies above 1%, corresponding to 11.5%, while the remaining applications, including the SunTag control approach (29%), SunTag-PapE (33.4%), and SunTag-HSVUL12 (24.6%) showed higher proportions of lines with GT efficiencies above 1%.

The distribution of GT efficiencies among individual lines in *ku70* mutants is presented in Figure 3.5.

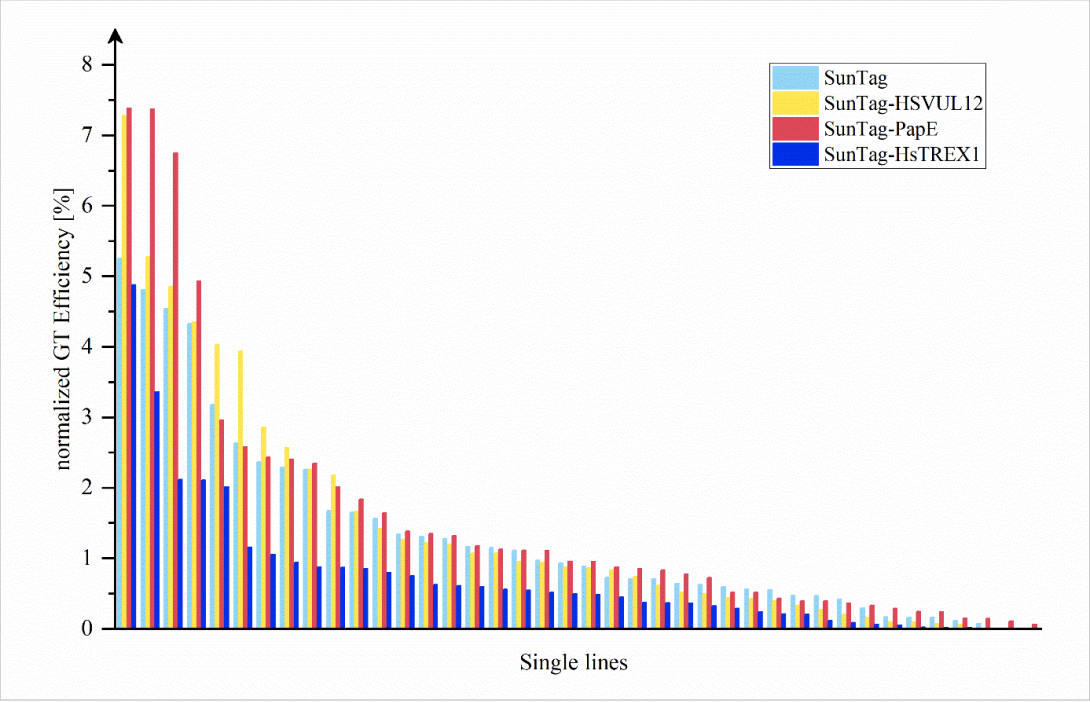

Figure 3.5: Gene targeting distribution of SunTag-mediated exonuclease recruitments in *Arabidopsis ku70* mutants.

The normalized GT efficiencies of individual lines in *ku70* plants are shown for the SunTag approach (light blue), SunTag-HsTREX1 (dark blue), SunTag-PapE (red) and SunTag-HSVUL12 (yellow). The two highest GT efficiency was 7.38% for SunTag-PapE (shown in two individual lines), followed by SunTag-HSVUL12 with 7.28%. GT efficiencies were calculated based on normalized values of individual lines. At least one GT event was observed in 38 individual lines for SunTag, 37 lines for SunTag-HsTREX1 and SunTag-HSVUL12 and 40 lines for SunTag-PapE.

When the proportion of positive lines in *ku70* mutants was examined, SunTag approach, SunTag-HsTREX1, SunTag-PapE and SunTag-HSVUL12 showed 61.3%, 60.7%, 70.2% and 53.6%, respectively (see Table 3.3). Although all approaches exhibited positive line frequencies above 50%, the proportion observed for SunTag-HsTREX1 (60.7%) was similar to that of the control SunTag approach (61.3%). However, despite SunTag-HSVUL12 showing the lowest positive line ratio at 53.6%, its average GT efficiency did not decrease and instead showed a slight increase compared to the control, likely due to the relatively high proportion (14.5%) of single lines exhibiting GT efficiencies greater than 2%.

When the proportions of lines exhibiting GT efficiencies above 2% were compared between Col-0 and *ku70* plants, the frequencies in Col-0 ranged between 1.25% and 6.76%, whereas in *ku70* plants these values ranged between 8.20% and 17.54%. This observation indicates that, compared to wild-type plants, *ip*GT applications in *ku70* mutants resulted in a higher proportion of lines exhibiting elevated GT efficiencies above 2%.

Table 3.3: Quantitative outcomes of GT approaches of SunTag-mediated exonuclease recruitment via CRISPR/Cas12a in *Arabidopsis* Col-0 and *ku70* plants.

For all tested approaches, the number of individual lines, the number of positive lines, the total number of approximately analyzed seeds, the number of positive seeds, as well as the GT efficiency (%) and normalized GT efficiency (%) are presented in the table.

Genotype	Approaches	Number of T1 lines	Number of positive lines	Positive lines (%)	Number of analyzed seeds	Number of analyzed positive seeds	GT efficiency (%)	Normalized GT efficiency (%)
Col-0	SunTag approach	71	53	74.65	~328,200	1500	0.46	0.71
	SunTag-HsTREX1	80	35	43.75	~406,400	1219	0.30	0.36
	SunTag-PapE	57	49	85.96	~254,200	1002	0.39	0.59
	SunTag-HSVUL12	74	59	79.73	~251,800	1924	0.76	1.12
ku70	SunTag approach	62	38	61.29	~251,100	1491	0.59	0.81
	SunTag-HsTREX1	61	37	60.66	~274,400	1337	0.49	0.61
	SunTag-PapE	57	40	70.18	~113,000	816	0.72	1.00
	SunTag-HSVUL12	69	37	53.62	~201,500	1131	0.56	0.90

GT events were confirmed by the molecular analyses described in Chapter 2.2.3. These analyses revealed that 23%, 57%, 55%, and 29% of the tested Col-0 lines exhibited perfect GT events in the SunTag approach, SunTag-HsTREX1, SunTag-PapE, and SunTag-HSVUL12, respectively. Relative to the control, SunTag-HsTREX1 and SunTag-PapE showed notable increases in perfect GT events, corresponding to 2.48-fold and 2.39-fold increases, respectively. In contrast, SunTag-HSVUL12 exhibited only a slight increase, corresponding to a 1.26-fold increase relative to the control (see Table 3.4).

When perfect GT event in *ku70* were analyzed, SunTag-HsTREX1 (60%), SunTag-PapE (53%) and SunTag-HSVUL12 (48%) indicated 1.67-fold, 1.47-fold and 1.33-fold increases, respectively, relative to the control group (36%).

When homozygous GT events were examined, an increase in the proportion of homozygous GT events was observed in *ku70* lines compared to Col-0 for all approaches except SunTag-HSVUL12. In contrast, while SunTag-HSVUL12 displayed homozygous GT events at a frequency of 13% in Col-0 plants, no homozygous GT events were detected in *ku70* mutant plant (see Table 3.4).

Overall, SunTag-mediated exonuclease recruitment resulted in distinct genotype-dependent effects on GT efficiency. SunTag-HsTREX1 recruitment reduced GT efficiency relative to the corresponding control groups in both the Col-0 and *ku70* backgrounds. In contrast, SunTag-HSVUL12 recruitment increased GT efficiency in both genotypes, although the extent of this increase was lower in the *ku70* background. Meanwhile, SunTag-PapE recruitment resulted in reduced GT efficiency in the Col-0 background but increased GT efficiency relative to the control in ku70 lines. These observations indicate that the impact of exonuclease recruitment on GT efficiency depends on both the recruited exonuclease and the genetic background.

Table 3.4: Molecular analysis of GT Events of SunTag-mediated exonuclease recruitment via CRISPR/Cas12a in Col-0 and *ku70*.

For the eight tested approaches, the number of analyzed T_2 plants, the number of T_2 plants exhibiting a GT event, the proportion of perfect GT events, the number of homozygous GT events, and their corresponding proportion are listed.

Genotype	Approaches	Number of analyzed T_2 plants	Number of T_2 plants with Perfect GT event	Perfect GT Events (%)	Number of homozygous GT event	Homozygous GT event (%)
Col-0	SunTag approach	35	8	23	-	-
	SunTag-HsTREX1	42	24	57	2	5
	SunTag-PapE	49	27	55	3	6
	SunTag-HSVUL12	31	9	29	4	13
ku70	SunTag approach	39	14	36	4	10
	SunTag-HsTREX1	48	29	60	4	8
	SunTag-PapE	30	16	53	4	13
	SunTag-HSVUL12	29	14	48	-	-

3.3 SunTag-mediated exonuclease recruitment of DSB induction

To further characterize the effects of the tested exonuclease-based approaches, the constructs used in the GT experiments were additionally adapted and evaluated in a mutagenesis-based assay. To investigate whether the recruitment of a nuclease together with exonucleases would influence DNA repair outcomes and promote the induction of larger deletions, the 5'-3' exonucleases HSVUL12 and PapE, as well as 3'-5' exonuclease HsTREX1 were recruited to DSBs generated by the ttLbCas12a-i via the SunTag system.

To evaluate the mutagenesis efficiency and deletion distribution induced by SunTag-mediated exonuclease recruitment at DSBs, different target loci were selected within the *A. thaliana* genome. The selected targets included the heterochromatic region of Centromere 4 (Cen4), *ER-type Ca^{2+}-ATPase 3* (*ECA3,* AT1G10130) and *ALCOHOL DEHYDROGENASE 1* (*ADH1,* AT1G77120). Protospacer sequences designed for these loci were individually cloned into BbsI-digested linear pEn-RZ-LbcrRNA plasmid. The resulting constructs were designated as pEn-RZ-LbcrRNA-Cen4 for the Cen4 target, pEn-RZ-LbcrRNA-ECA3 for *ECA3*, and pEn-RZ-LbcrRNA-ADH1 for *ADH1*.

The experimental design incorporated a destination vector system in which expression was driven under the control of the UBIQUITIN4-2 (UBI) promoter from *Petroselinum crispum* and terminated by the 3A terminator (pea3A) from *Pisum sativum*. The UBI promoter was selected due to its constitutive activity across all cell types and its suitability for analyzing outcomes in the T_1 generation (Steinert et al., 2015).

For the construction of destination vectors, the plasmid pDe-UBI-Ω-SaCas9-GCN4-pea3A was used as the initial backbone and digested with AscI to remove the SaCas9-GCN4 fragment. In parallel, the plasmid generated in Chapter 3.2, pDe-EC-Omega-ttLbCas12a-i-GCN4-rbcST+ccdB+ALS+GTVc12+PPTR, was also digested with AscI, to excise the ttLbCas12a-i-GCN4 fragments. Subsequently, the isolated ttLbCas12a-i-GCN4 fragment was ligated into AscI-digested backbone using classical restriction-ligation cloning, resulting in pDe-UBI-Omega-ttLbCas12a-i-GCN4-pea3A+ccdB+PPTR vector. The resulting plasmid was first digested with MluI to facilitate the insertion of appropriate crRNA cassettes. Subsequently, the crRNA cassettes with Cen4, ECA3 and ADH1 targets were inserted via classical ligation. The final destination vectors for Cen4, *ECA3* and *ADH1* targets were identified as follows, respectively:

pDe-UBI-Omega-ttLbCas12a-i-GCN4-pea3A+ccdB+Cen4+PPTR,
pDe-UBI-Omega-ttLbCas12a-i-GCN4-pea3A+ccdB+ECA3+PPTR,
pDe-UBI-Omega-ttLbCas12a-i-GCN4-pea3A+ccdB+ADH1+PPTR.

To generate the final entry vectors required for Gateway reaction of expression clones, the initial plasmid pEn-UBI-scFv-sfGFP-GB1-nosT (obtained in Chapter 3.3) was linearized by BamHI digestion. The HsTREX1, HSVUL12 and PapE fragments, previously amplified with Gibson-compatible OHs, were assembled into this backbone using Gibson Assembly, producing the following constructs: pEn-UBI+scFv-sfGFP-HsTREX1-GB1-nosT, pEn-UBI+scFv-sfGFP-HSVUL12-GB1-nosT and pEn-UBI+scFv-sfGFP-PapE-GB1-nosT.

To build the final expression vectors, each destination vector was combined with the corresponding entry vector using the Gateway reaction. The resulting expression constructs were assigned as follows:

pEx-UBI-Omega-ttLbCas12a-i-GCN4-pea3A+Cen4+scFv-sfGFP-HsTREX1-GB1+PPTR,
pEx-UBI-Omega-ttLbCas12a-i-GCN4-pea3A+Cen4+scFv-sfGFP-HSVUL12-GB1+PPTR,
pEx-UBI-Omega-ttLbCas12a-i-GCN4-pea3A+Cen4+scFv-sfGFP-PapE-GB1+PPTR,
pEx-UBI-Omega-ttLbCas12a-i-GCN4-pea3A+Cen4+scFv-sfGFP-GB1+PPTR,
pEx-UBI-Omega-ttLbCas12a-i-GCN4-pea3A+ECA3+scFv-sfGFP-HsTREX1-GB1+PPTR,
pEx-UBI-Omega-ttLbCas12a-i-GCN4-pea3A+ECA3+scFv-sfGFP-HSVUL12-GB1+PPTR,
pEx-UBI-Omega-ttLbCas12a-i-GCN4-pea3A+ECA3+scFv-sfGFP-PapE-GB1+PPTR,
pEx-UBI-Omega-ttLbCas12a-i-GCN4-pea3A+ECA3+scFv-sfGFP-GB1+PPTR,
pEx-UBI-Omega-ttLbCas12a-i-GCN4-pea3A+ADH1+scFv-sfGFP-HsTREX1-GB1+PPTR,
pEx-UBI-Omega-ttLbCas12a-i-GCN4-pea3A+ADH1+scFv-sfGFP-HSVUL12-GB1+PPTR,
pEx-UBI-Omega-ttLbCas12a-i-GCN4-pea3A+ADH1+scFv-sfGFP-PapE-GB1+PPTR,
pEx-UBI-Omega-ttLbCas12a-i-GCN4-pea3A+ADH1+scFv-sfGFP-GB1+PPTR.

Hereafter, the constructs together with the corresponding target loci will be referred to throughout the remainder of the text as SunTag-HsTREX1, SunTag-HSVUL12, SunTag-PapE, and the SunTag approach (see Figure 3.6).

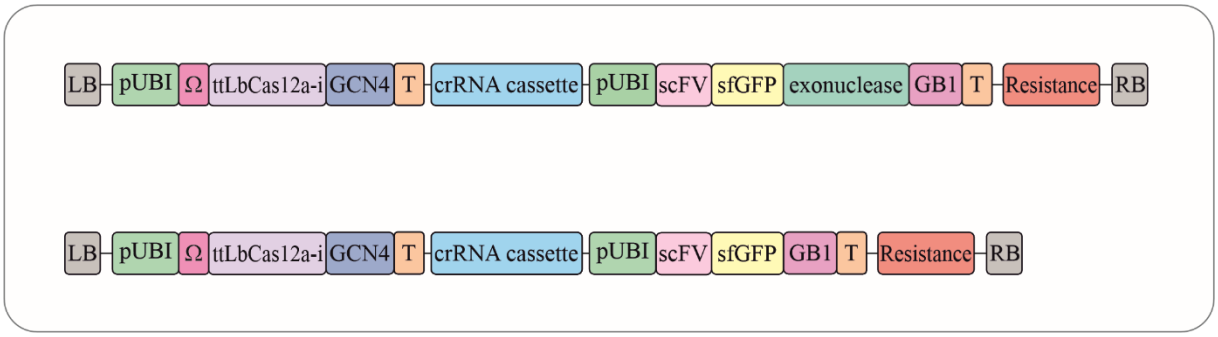

Figure 3.6: The constructs for the SunTag-mediated exonuclease recruitment via ttLbCas12a-i-induced double-strand break (DSB) formation.

Shown are the expression constructs designed for the SunTag-mediated recruitment of exonucleases to Cas12a-induced DSBs in Arabidopsis Col-0 plants. For the SunTag-mediated recruitment, the coding sequence of a peptide array containing ten copies of the GENERAL CONTROL NON-DEREPRESSIBLE 4 (GCN4) epitope was fused to the 3' end of the ttLbCas12a-i coding sequence. A corresponding antibody fusion construct containing a single-chain variable fragment (scFv) enables recruitment of the exonuclease through specific interaction with the GCN4 peptide array from *Saccharomyces cerevisiae* (upper construct). The recruited protein fusion additionally contains a superfolder green fluorescent protein (sfGFP) and the B1 immunoglobulin-binding domain of bacterial protein G (GB1) to enhance protein stability and reduce aggregation. To evaluate the effect of exonuclease recruitment, a corresponding control construct lacking the exonuclease coding sequence was generated (lower construct). Expression of all fusion constructs is driven by the *Petroselinum crispum* UBIQUITIN4-2 promoter (pUBI). The constructs additionally contain the OMEGA (Ω) translational enhancer sequence derived from Tobacco mosaic virus. Sequence specificity of DSB induction is mediated by the CRISPR RNA (crRNA) expression cassette. For Agrobacterium-mediated transformation and subsequent selection of transgenic plants, the constructs are flanked by left and right border (LB and RB) T-DNA recognition sequences and contain an herbicide resistance cassette.

The cloned constructs were transformed into *A. thaliana* Col-0 plants via Agrobacterium-mediated transformation, and transformed plants were cultivated in the green house until seed maturity for subsequent T_1 seed collection. T_1 seeds were sown on herbicide-containing medium for the selection of primary transformants, and 30 plants were selected for each approach after 14 days of cultivation in growth room. gDNA from each primary transformant was extracted individually using the Shorty method. Subsequently, gDNA from 10 plants was pooled into a single reaction tube for PCR amplification, resulting in three replicates for each target and approach. ONT sequencing was then performed according to the protocol described in Chapter 2.2.3. The obtained sequences were analyzed using CRISPResso2 (Clement et al., 2019) to determine mutagenesis efficiency and deletion profile at the target loci. Additionally, mutation frequencies (%) were statistically evaluated using one-way ANOVA followed by Tukey's multiple comparison test in OriginLab.

For the heterochromatic target locus Cen4, all approaches exhibited mutagenesis efficiencies ranging from 33.7% to 36.5% (see Figure 3.7). Compared to the control approach, SunTag-mediated exonuclease recruitment did not result in a substantial increase in editing efficiency at this heterochromatic target region.

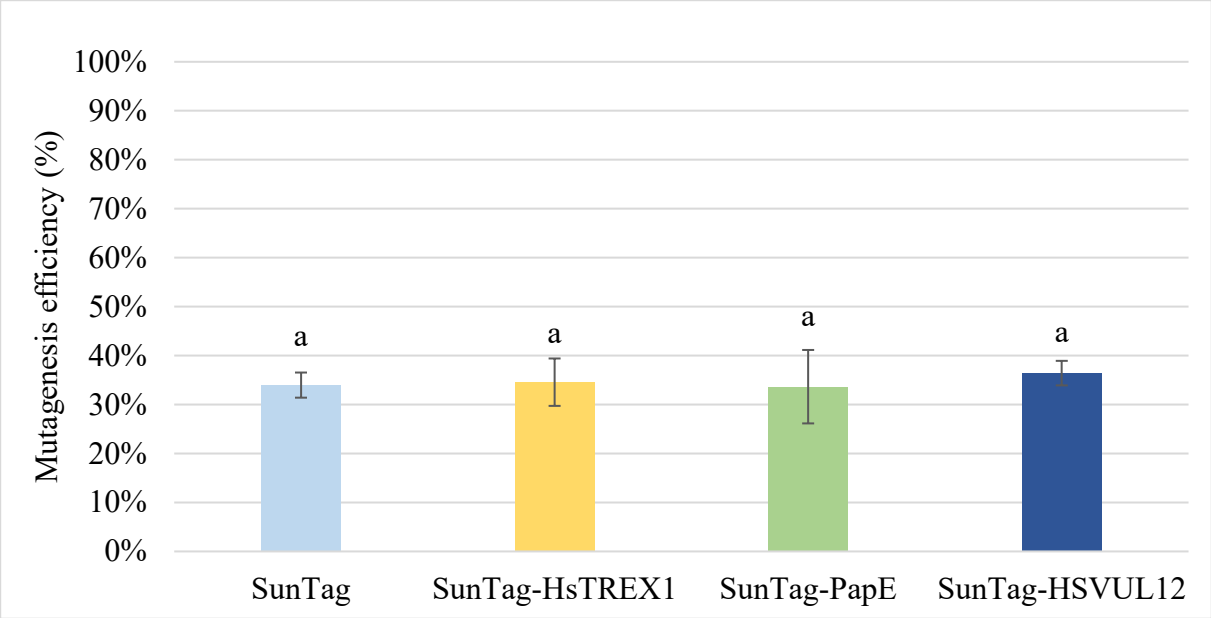

Figure 3.7: Mutagenesis efficiency following SunTag-mediated exonuclease recruitment using CRISPR/Cas12a at the Cen4 target locus.

Mutagenesis efficiencies of the SunTag-mediated recruitment of up to then copies of the 5'-3' exonucleases Herpes Simplex Virus UL12 (HSVUL12) and *Papiine alpha herpesvirus 2* (PapE), and human 3'-5' exonuclease THREE PRIME REPAIR EXONUCLEASE 1 lacking the C-terminal endoplasmic reticulum localization signal peptide ($HsTREX1_{1-293}$, hereafter referred to as HsTREX1) are analyzed at *Arabidopsis thaliana* Centromere 4 (Cen4). Mutation frequency was calculated as the proportion of Oxford Nanopore Technology (ONT) sequencing reads containing sequence alterations relative to the total number of reads using CRISPResso2 (Clement et al., 2019). Error bars represent mean ± SD of biological replicates. Statistical analysis was performed using One-Way ANOVA followed by Tukey's multiple comparison test for p-value adjustment. Different letters indicate statistically significant differences ($p < 0.05$). All tested approaches showed no significant changes between treatments. Mean ONT reads analyzed were: $n_{SunTag} = 1623$, $n_{SunTag\text{-}HsTREX1} = 2087$, $n_{SunTag\text{-}PapE} = 1428$, $n_{SunTag\text{-}HSVUL12} = 912$.

The positional distribution of deletions further revealed that all approaches generated deletion hotspots centred around the DSB site. The deletion profiles revealed slightly elevated deletion for SunTag-HsTREX1 within the -5 to +5 bp region surrounding the cleavage site compared with the other applications (see Figure 3.8).

In contrast to the gradual increase observed toward the cleavage site, deletion frequencies collapsed rapidly on the PAM-distal side following DSB induction. Following the cleavage site, deletion frequencies decreased sharply toward the PAM-distal side of the target sequence. For example, in the SunTag control approach, deletion frequencies declined from 46.2% at the cleavage site to 30.4% at position +1 and further to 9.9% at position +5. Comparable rapid decay patterns were observed for all tested approaches.

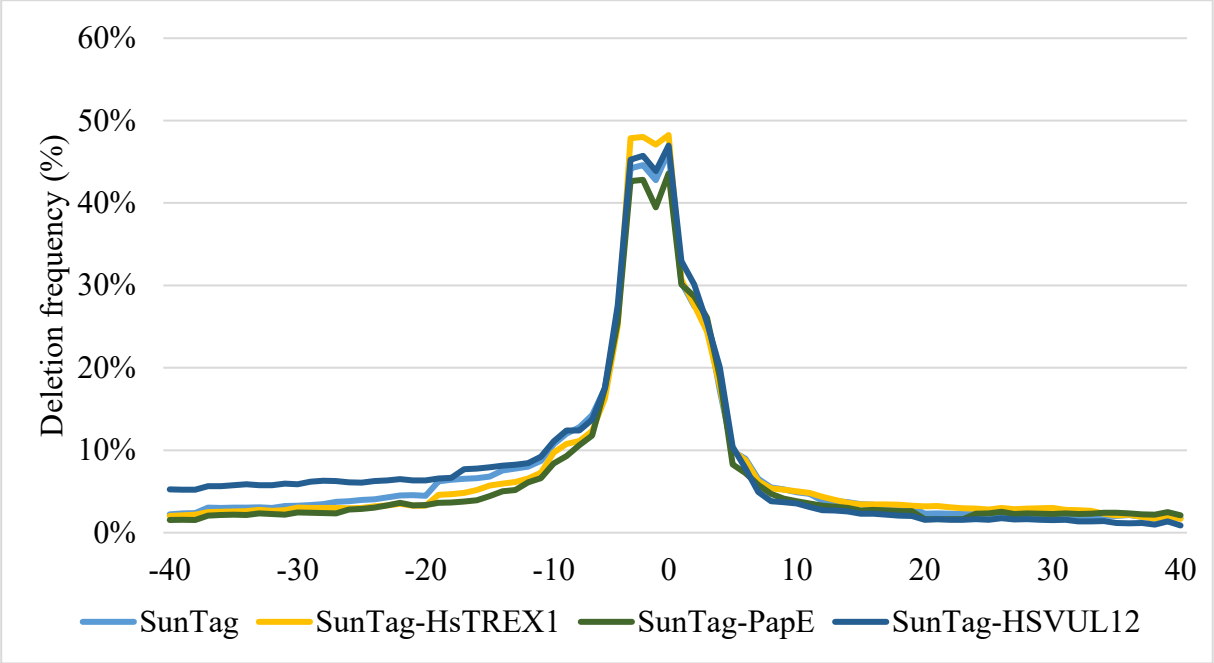

Figure 3.8: Deletion profiles following SunTag-mediated exonuclease recruitment at a Cas12a-induced DSB in *Arabidopsis thaliana Cen4* locus.

Shown is the position of deleted bases relative to the cleavage site within an 80 bp region surrounding the Cas12a-mediated DSB at the *Arabidopsis thaliana Centromere 4* (*Cen4*) target locus. Deletion profiles following SunTag-mediated recruitment of up to ten copies of the 5'-3' exonucleases Herpes Simplex Virus UL12 (HSVUL12) and *Papiine alpha herpesvirus 2* (PapE), as well as the human 3'-5' exonuclease THREE PRIME REPAIR EXONUCLEASE 1 lacking the C-terminal endoplasmic reticulum localization signal peptide ($HsTREX1_{1-293}$, hereafter referred to as HsTREX1), were analyzed and compared with the SunTag control. All approaches resulted in a largely symmetrical processing of the DNA break ends, with the highest deletion frequencies concentrated around the cleavage site. Graphs indicate the proportion of Oxford Nanopore Technology (ONT) sequencing reads containing deletions at a specific position relative to the total number of reads, analyzed using CRISPResso2 (Clement et al., 2019). The cleavage site is defined as position zero; negative values indicate positions on the PAM-proximal break end, whereas positive values indicate positions on the PAM-distal break end. Mean ONT reads analyzed were: $n_{SunTag} = 1623$, $n_{SunTag\text{-}HsTREX1} = 2087$, $n_{SunTag\text{-}PapE} = 1428$, $n_{SunTag\text{-}HSVUL12} = 912$.

When euchromatic target loci were analyzed, the ECA3 and ADH1 targets exhibited higher mutagenesis efficiencies compared to heterochromatic Cen4 target region.

For ECA3, editing efficiencies of 59.9%, 43.7%, 75.5%, and 59.8% were obtained for the SunTag approach, SunTag-HsTREX1, SunTag-PapE, and SunTag-HSVUL12, respectively. Although the proportion of edited sequences showed 0.73-fold decrease for SunTag-HsTREX1 and 1.26-fold increase for SunTag-PapE relative to the control group, as for the Cen4 target, the different approaches yielded comparable mutagenesis efficiencies at the *ECA3* target albeit the recruitment of PapE showed the highest frequency at 75.5% (see Figure 3.9).

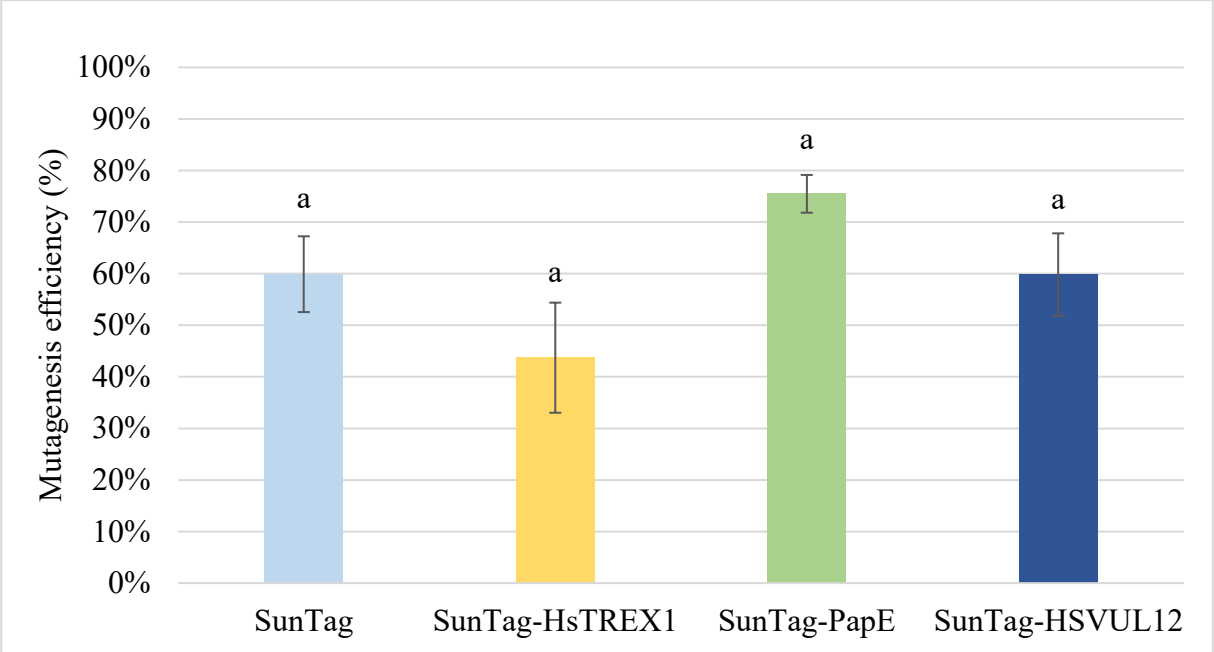

Figure 3.9: Mutagenesis efficiency following SunTag-mediated exonuclease recruitment using CRISPR/Cas12a at the ECA3 target locus.

Mutagenesis efficiencies of the SunTag-mediated recruitment of up to then copies of the 5'-3' exonucleases Herpes Simplex Virus UL12 (HSVUL12) and *Papiine alpha herpesvirus 2* (PapE), and human 3'-5' exonuclease THREE PRIME REPAIR EXONUCLEASE 1 lacking the C-terminal endoplasmic reticulum localization signal peptide ($HsTREX1_{1-293}$, hereafter referred to as HsTREX1) are analyzed at the *Arabidopsis thaliana ER-type Ca^{2+}-ATPase 3* (*ECA3*) target. Mutation frequency was calculated as the proportion of Oxford Nanopore Technology (ONT) sequencing reads containing sequence alterations relative to total number of reads using CRISPResso2 (Clement et al., 2019). Error bars represent mean ± SD of biological replicates. Statistical analysis was performed using One-Way ANOVA followed by Tukey's multiple comparison test for p-value adjustment. Different letters indicate statistically significant differences ($p < 0.05$). All tested approaches shared the same letter, indicating no significant changes between treatments. Mean ONT reads analyzed were: $n_{SunTag} = 1796$, $n_{SunTag\text{-}HsTREX1} = 1306$, $n_{SunTag\text{-}PapE} = 1374$, $n_{SunTag\text{-}HSVUL12} = 1549$.

Analysis of deletion distributions surrounding the cleavage site demonstrated that deletion frequencies were strongly concentrated around the Cas12a-induced DSB site. SunTag-PapE exhibited the highest deletion frequencies within the -5 to +5 bp region surrounding the cleavage site, whereas SunTag-HsTREX1 showed the lowest frequencies in this region. Meanwhile, SunTag-HSVUL12 did not indicate a pronounced difference compared with the control approach (see Figure 3.10).

All approaches displayed a progressive increase in deletion frequency toward the Cas12a cleavage site, reaching maximal levels directly at or immediately adjacent to the cut position. Following this peak, deletion frequencies dropped sharply within the first nucleotides toward the PAM-distal side. This effect was particularly pronounced in the SunTag-PapE approach, where deletion frequencies decreased from 73.5% at the position 18 of protospacer sequence to 48.5% at position +2 and further to 32% at position +3. Similar rapid decay patterns were

observed for the remaining approaches, indicating that deletions were highly concentrated around the immediate DSB region with a narrow mutation window.

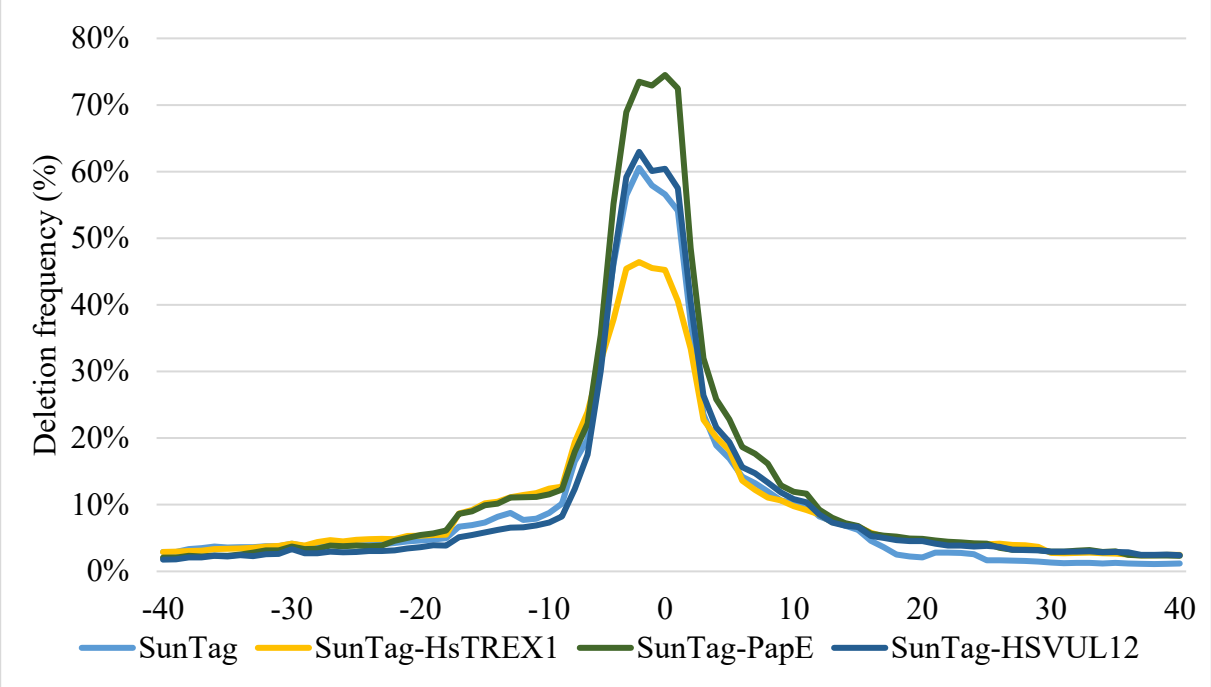

Figure 3.10: Deletion profiles following SunTag-mediated exonuclease recruitment at a Cas12a-induced DSB in *Arabidopsis thaliana ECA3* locus.

Shown is the position of deleted bases relative to the cleavage site within an 80 bp region surrounding the Cas12a-mediated DSB at the *Arabidopsis thaliana ER-type Ca^{2+}-ATPase 3* (*ECA3*) target locus. Deletion profiles following SunTag-mediated recruitment of up to ten copies of the 5'-3' exonucleases Herpes Simplex Virus UL12 (HSVUL12) and *Papiine alpha herpesvirus 2* (PapE), as well as the human 3'-5' exonuclease THREE PRIME REPAIR EXONUCLEASE 1 lacking the C-terminal endoplasmic reticulum localization signal peptide ($HsTREX1_{1-293}$, hereafter referred to as HsTREX1), were analyzed and compared with the SunTag control. All approaches resulted in a largely symmetrical processing of the DNA break ends, with the highest deletion frequencies concentrated around the cleavage site. Recruitment of PapE resulted in the highest deletion frequencies directly adjacent to the cleavage site, whereas HsTREX1 recruitment showed a comparatively broader distribution of deletions surrounding the Double-strand break. Graphs indicate the proportion of Oxford Nanopore Technology (ONT) sequencing reads containing deletions at a specific position relative to the total number of reads, analyzed using CRISPResso2 (Clement et al., 2019). The cleavage site is defined as position zero; negative values indicate positions on the PAM-proximal break end, whereas positive values indicate positions on the PAM-distal break end. Mean ONT reads analyzed were: $n_{SunTag} = 1796$, $n_{SunTag\text{-}HsTREX1} = 1306$, $n_{SunTag\text{-}PapE} = 1374$, $n_{SunTag\text{-}HSVUL12} = 1549$.

At the ADH1 target locus, the four tested approaches exhibited editing efficiencies ranging from 63.9% to 75.3%. The SunTag control approach showed an editing frequency of 63.9%, whereas the SunTag-exonuclease applications ranged between 65.8% and 75.3%. Similar to the Cen4 and ECA3 targets, the tested applications exhibited overall comparable mutagenesis efficiencies at the ADH1 target (see Figure 3.11).

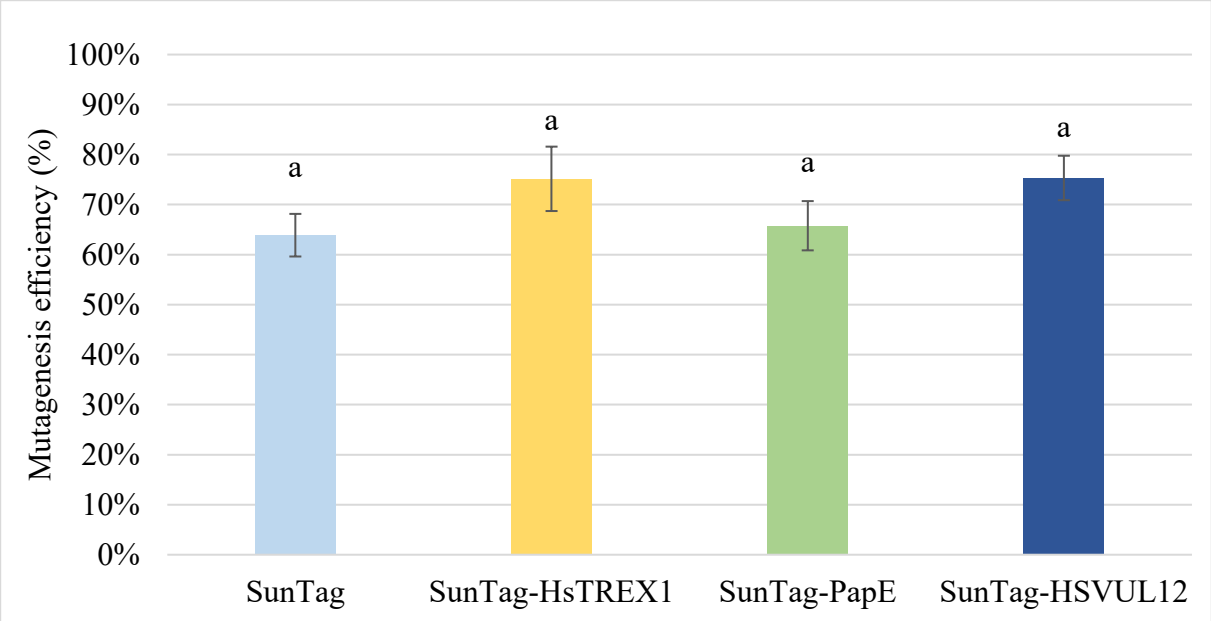

Figure 3.11: Mutagenesis efficiency following SunTag-mediated exonuclease recruitment using CRISPR/Cas12a at the ADH1 target locus.

Mutagenesis efficiencies of the SunTag-mediated recruitment of up to then copies of the 5'-3' exonucleases Herpes Simplex Virus UL12 (HSVUL12) and *Papiine alpha herpesvirus 2* (PapE), and human 3'-5' exonuclease THREE PRIME REPAIR EXONUCLEASE 1 lacking the C-terminal endoplasmic reticulum localization signal peptide ($HsTREX1_{1-293}$, hereafter referred to as HsTREX1) are analyzed at the *Arabidopsis thaliana ALCOHOL DEHYDROGENASE 1* (*ADH1*). Mutation frequency was calculated as the proportion of Oxford Nanopore Technology (ONT) sequencing reads containing sequence alterations relative to total number of reads using CRISPResso2 (Clement et al., 2019). Error bars represent mean ± SD of biological replicates. Statistical analysis was performed using One-Way ANOVA followed by Tukey's multiple comparison test for p-value adjustment. Different letters indicate statistically significant differences ($p < 0.05$). All tested approaches shared the same letter, indicating no significant changes between treatments. Mean ONT reads analyzed were: $n_{SunTag} = 393$, $n_{SunTag\text{-}HsTREX1} = 343$, $n_{SunTag\text{-}PapE} = 465$, $n_{SunTag\text{-}HSVUL12} = 333$.

When the distribution of deletion frequencies surrounding the DSB region at the ADH1 target locus was examined, an accumulation of deletions around the cleavage site was again observed, similar to the patterns detected at the other target loci. Deletion frequencies gradually increased toward the cleavage position and reached maximal levels directly at or adjacent to the cut site. However, a sharp decline in deletion frequency was consistently observed within the first 5-6 nucleotides toward the 3' region from the cleavage site. For example, in the SunTag-HsTREX1 approach, deletion frequencies decreased from 79.7% at the Cas12a cleavage site corresponding to position 19 of the protospacer and 76.3% at the cleavage site corresponding to position 20 of the protospacer to 38.0% at position +5 and 31.5% at position +7. Similar rapid decay patterns were observed for all tested approaches. The highest deletion frequencies were observed at position 19 of the protospacer sequence with 65.6% for SunTag approach, 79.7% for SunTag-HsTREX1, 68% for SunTag-Pape and 74.8% for SunTag-HSVUL12 (see Figure 3.12).

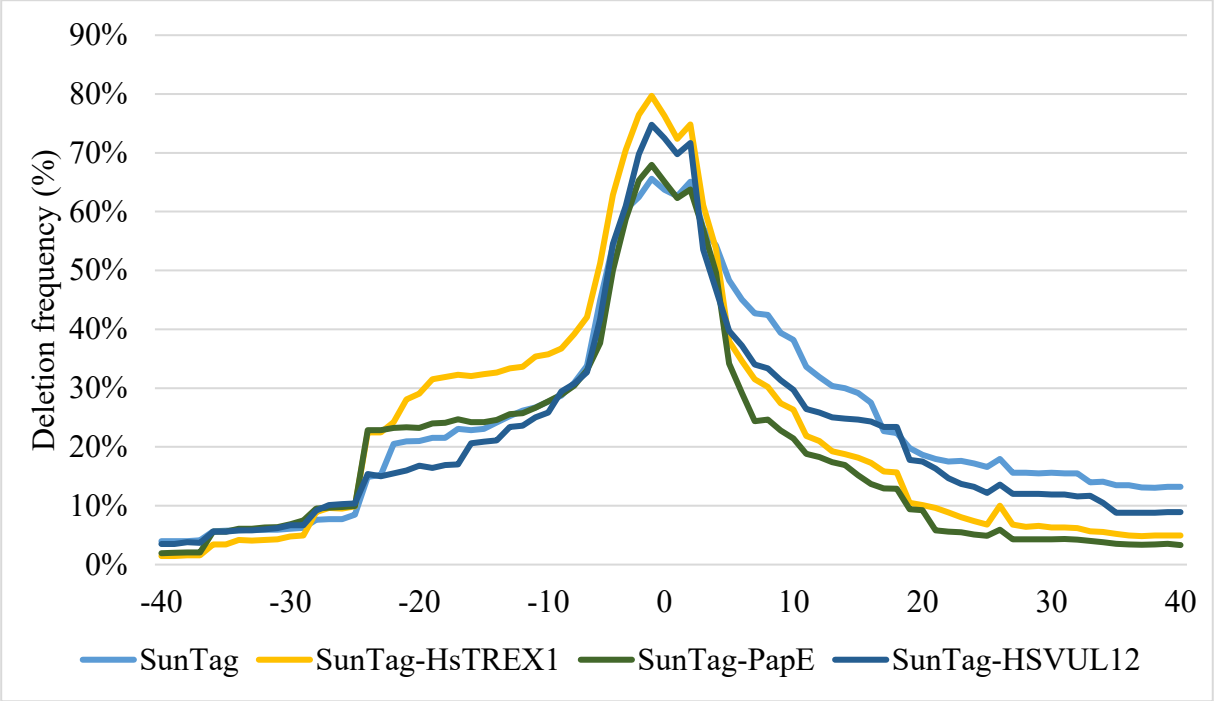

Figure 3.12: Deletion profiles following SunTag-mediated exonuclease recruitment at a Cas12a-induced DSB in *Arabidopsis thaliana ADH1* locus.

Shown is the position of deleted bases relative to the cleavage site within an 80 bp region surrounding the Cas12a-mediated DSB at the *Arabidopsis thaliana ALCOHOL DEHYDROGENASE 1* (*ADH1*) target locus. Deletion profiles following SunTag-mediated recruitment of up to ten copies of the 5'-3' exonucleases Herpes Simplex Virus UL12 (HSVUL12) and *Papiine alpha herpesvirus 2* (PapE), as well as the human 3'-5' exonuclease THREE PRIME REPAIR EXONUCLEASE 1 lacking the C-terminal endoplasmic reticulum localization signal peptide (hereafter referred to as HsTREX1), were analyzed and compared with the SunTag control. All approaches resulted in a largely symmetrical processing of the DNA break ends, with the highest deletion frequencies concentrated around the cleavage site. Graphs indicate the proportion of Oxford Nanopore Technology (ONT) sequencing reads containing deletions at a specific position relative to the total number of reads, analyzed using CRISPResso2 (Clement et al., 2019). The cleavage site is defined as position zero; negative values indicate positions on the PAM-proximal break end, whereas positive values indicate positions on the PAM-distal break end. Mean ONT reads analyzed were: $n_{SunTag} = 393$, $n_{SunTag\text{-}HsTREX1} = 343$, $n_{SunTag\text{-}PapE} = 465$, $n_{SunTag\text{-}HSVUL12} = 333$.

Overall, the GT and mutagenesis analysis indicate that SunTag-mediated exonuclease recruitment affects genome editing outcomes in a context-dependent manner. In the GT experiments, efficiency varied depending on both recruited exonuclease and the genetic background, whereas the mutagenesis-based analysis showed broadly comparable Cas12a-mediated editing efficiencies among the tested recruitment approaches. Editing efficiency was more strongly associated with the genomic target, regardless the SunTag-exonuclease recruitment, with the heterochromatic target displaying lower mutagenesis levels than the euchromatic targets. Together, these findings suggest that exonuclease recruitment differentially affects GT efficiency without uniformly altering overall Cas12a-mediated mutagenesis efficiency, highlighting the importance of the recruited exonuclease, genetic background, and target context.

3.4 Application of *ip*GT for a haploidization approach

Given that haploid induction efficiency critically depends on targeted modifications of key genomic loci such as *CENH3*, the development of precise and flexible genome engineering tools has become essential. Accordingly, CRISPR/Cas systems have revolutionized plant molecular biology by enabling targeted, efficient, and cost-effective genome editing across a wide range of species (Gao, 2018; Jacquier et al., 2020). Their ability to introduce defined sequence modifications at specific genomic loci provides new opportunities to refine haploid induction systems and to engineer functional protein variants. The 26.7 kDa Enhanced Yellow Fluorescent Protein (EYFP) tag has previously been used to target CENH3 for the generation of transgenic haploid-inducing plants (Demidov et al., 2022). Specifically, EYFP was incorporated as a marker in transgenic constructs designed to functionally complement *cenh3-1 null* mutant plants. In addition to its use as a fluorescent tag, EYFP provides a molecular target that can be directly and specifically recognized on the protein surface with high affinity by GFP-specific nanobodies fused to engineered E3 ligases. The results obtained in previous studies indicate that, even before the introduction and activation of an engineered E3 ligase system designed to degrade the target proteins in the test genotype, the presence of the EYFP tag itself and/or the genomic position of the transgene may contribute to background haploid induction, with reported frequencies ranging from 5.54% to 20.34% (Demidov et al., 2022; Somasundaram et al., 2026). This effect likely results from the large size tag, which may disrupt the CENH3 protein structure and/or interfere with its loading onto centromeres, thereby leading to inherent protein destabilization. Because this effect is likely associated with structural interference caused by the large tag, the considerably smaller ALFA-tag (1.9 kDa) was selected as an alternative tagging strategy. While ALFA-tagged CENH3 transgenic plants (ALFA-gCENH3) exhibited background haploid induction ranging from 0% to 15.15%, most likely due to the transgene position effects and the resulting variation in expression levels, the ALFA-tag itself proved to be non-disruptive when expressed at appropriate levels (Somasundaram et al., 2026). To eliminate position-dependent transgene effects and establish a more controlled system, the 15-amino-acid ALFA-tag (Götzke et al., 2019) was integrated into the endogenous *AtCENH3* locus employing the *ip*GT technique in combination with CRISPR/Cas systems. The *ip*GT-mediated integration strategy was designed to insert the 45 bp coding sequence (CDS) immediately downstream of the start codon in Exon 1.

To fuse the ALFA-tag to the N-terminus of *At*CENH3, two different target sites were selected based on predictions from Cas-OFFinder and RNAfold (*ViennaRNA Web Services*,

http://rna.tbi.univie.ac.at/). Target regions were chosen within Exon 1. Among three potential candidates, two targets (T1 and T3) exhibiting favorable secondary structures were selected for donor design. For Target 1 (T1), the predicted DSB site is located upstream of the start codon, whereas for Target 3 (T3), it is positioned downstream of the start codon. Donor constructs were designed accordingly for each target. In both cases, the ALFA-tag (45 bp CDS) was positioned directly after the start codon of the *CENH3* gene, flanked by homology arms of 500-to-600 bp in length. To prevent re-cleavage after successful GT, silent mutations were introduced into the GTVs designed for both T1 and T3. Specifically, one silent mutation was placed within the PAM sequence and another at the second position of the protospacer. Additionally, PAM and protospacer sequences were incorporated at 5' and 3' ends of the homology arms to facilitate donor excision (see Figure 3.13). To enable cloning via classical ligation, SpeI restriction sites were added to both ends of the homology arms and the complete donor construct was synthesized by BioCat GmbH, Heidelberg.

For cloning, the plasmid pDe-EC-ttLbCas12a-i-rbcST+PPTR (Schindele et al., 2023) was used as the starting backbone. The GTV fragments were digested with SpeI and ligated into the destination vector linearized with the same enzyme. In parallel, T1 and T3 protospacer sequences were individually cloned into the pEn-RZ-LbcrRNA plasmid following digestion with BbsI. Expression clones were generated via Gateway recombination between the destination vector carrying the GTV and the corresponding target-specific crRNA cassette. The resulting plasmids were identified as follows:

pEx-EC-ttLbCas12a-i-rbcST+RZ-crRNA-CENH3-T1+GTV-CENH3-T1+PPTR,
pEx-EC-ttLbCas12a-i-rbcST+RZ-crRNA-CENH3-T3+GTV-CENH3-T3+PPTR.

To identify ALFA-tag integrated plants via *ip*GT (ALFA-CENH3 (GT)), primary transformants were selected and seeds were harvested. In the T_2 generation, a bulk screening approach (Rönspies et al., 2022a) was employed, initially testing pooled DNA samples for positive signals. In total, 15 lines for Target 1 and 16 lines for Target 3 were screened.

Bulk samples yielding positive signals were subsequently analyzed at the individual plant level using PCR-based screening, followed by Sanger sequencing (see Figure 3.14). While no ALFA-tag-integrated plants were obtained for Target 3, one heterozygous ALFA-tag-integrated plant was identified among 2,400 T2 individuals for Target 1, corresponding to a GT efficiency of 0.04%. Consistent with the *ip*GT strategy, the ALFA-tag was precisely inserted at the N-terminus of *At*CENH3. Molecular analysis confirmed accurate integration at the target locus.

Figure 3.13: *in planta* Gene Targeting (*ip*GT) workflow for ALFA-tag integration into CENTROMERIC HISTONE H3 (CENH3).

A) *in planta* Gene Targeting (*ip*GT) construct for ALFA-tag integration. The construct consists of sequences flanked by the left and right borders (LB and RB), enabling integration into the plant genome via *Agrobacterium*-mediated transformation of *Arabidopsis thaliana*. The *ip*GT constructs harbour a Cas expression cassette composed of an oocyte-specific promoter (pEC), the ttLbCas12a-i coding sequence, and the rbcS E9 terminator (T). In addition, gRNA expression cassette is included, consisting of CRISPR RNA (crRNA) sequence driven by the *Arabidopsis U6 SMALL NUCLEOLAR RNA26* (U6-26) promoter and terminated by Poly-T signal, which incorporates the spacer sequence. Furthermore, the construct contains a donor template, GT donor, comprising homologous arms flanked by protospacer sequences, along with a silent mutation and the 45 bp coding sequence of ALFA-tag. The ALFA-tag sequence is placed downstream of the start codon of CENH3 coding sequence. To facilitate selection of primary transformants, a resistance cassette, Phosphinothricin (PPTR), is also incorporated into the construct. **B) The mechanism of the *ip*GT system.** The Cas nuclease, expressed under the control of the pEC, induces double-strand breaks (DSBs) both at the genomic *CENH3* target locus and at the flanking sites of the GT donor. The GT donor is designed to contain the same target sequence and PAM motifs at its 5' and 3' ends, enabling Cas-mediated excision and release of the donor template. Following cleavage, the released donor DNA serves as a repair template for homology-directed repair (HDR) at the genomic target site, resulting in the precise integration of the ALFA-tag sequence into the *CENH3* locus.

Furthermore, the segregation analysis of the progeny derived from the heterozygous plant revealed 39 homozygous edited and 50 heterozygous individuals carrying the ALFA-tag, along with 59 non-edited individuals. This distribution significantly deviated from the expected Mendelian 1:2:1 segregation ratio according to a chi-square goodness-of-fit-test

($\chi^2 = 20.97$, df = 2, $p < 0.001$), indicating the segregation distortion. Homozygous ALFA-CENH3 (GT) plants showed no visible morphological differences compared with wild-type Col-0 plants (see Figure 3.15).

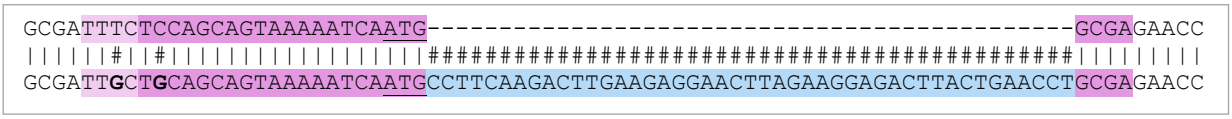

Figure 3.14: Sequence alignment illustrating the targeted ALFA-tag integration at the *Arabidopsis thaliana CENH3* locus.

The alignment shows the insertion of a 45 bp ALFA-tag coding sequence immediately downstream of the CENH3 start codon (underlined), resulting in N-terminal translational fusion. The upper sequence represents the unmodified genomic sequence at the target region, whereas the lower sequence represents the edited sequence containing the ALFA-tag integration and two silent mutations (indicated in bold). The CRISPR RNA (crRNA) spacer sequence is highlighted in dark pink, the corresponding Protospacer Adjacent Motif (PAM) sequences are indicated in light pink, and the inserted ALFA-tag sequence is highlighted in light blue. Two silent mutations were introduced within the PAM and seed regions to prevent Cas12a-mediated re-cleavage of the edited locus while preserving the CENH3 amino acid sequence. The alignment confirms the precise in-frame integration of the ALFA tag at the 5' end of the CENH3 coding sequence.

Following the successful integration of the ALFA-tag via *ip*GT, the subsequent experiments to evaluate haploid induction efficiency were conducted in collaboration with Prof. Dr. Andreas Houben's research group at the Leibniz Institute of Plant Genetics and Crop Plant Research (IPK) Gatersleben, Germany.

To confirm the functional integrity of the ALFA-tag, homozygous ALFA-CENH3 (GT) plants were used as female parents in crossed with glabrous mutant (*glabra1-1, gl1-1*) males. The recessive *gl1-1* allele, present Landsberg erecta Ler-0 background, and associated with a glabrous (trichome-less) phenotype, served as a phenotypic marker for haploid identification. Unlike randomly integrated ALFA-transgenes, which showed variable background activity, the *in-locus* tagged plants indicated no background haploid induction. This observation supports the rationale that ALFA-tagged plants maintain normal growth and development prior to activation of the degradation module. In this system, the ALFA-tag is introduced into the endogenous *CENH3* locus in a targeted configuration rather than a random transgenic insertion. Haploidization is then initiated by the subsequent introduction of an engineered degradation cassette, which encodes a fusion protein composed of the NbALFA and an E3 ubiquitin ligase. The nanobody recognizes the ALFA-tag with high affinity, whereas the E3 ligase domain recruits the plant ubiquitination machinery. Because this construct is driven by an egg-cell-specific promoter, the fusion protein is produced upon egg cell maturation. Within the egg cell, the nanobody domain binds to ALFA-tagged CENH3 proteins and directs them for degradation through lysine polyubiquitination and proteasome-mediated turnover. Upon fertilization of a CENH3-depleted egg cell by wild-type pollen, a pronounced CENH3

nucleosome asymmetry is established between the parental genomes in the resulting zygote. During early embryonic division, newly synthesized or residual CENH3 proteins preferentially associate with the CENH3-rich paternal chromosomes. In contrast, maternal chromosomes with insufficient centromeric CENH3 fail to maintain functional centromeres and are selectively eliminated. Consequently, targeted depletion of maternally inherited ALFA-tagged CENH3 enables the production of non-transgenic paternal haploid plants.

To implement this strategy, the non-plant-derived E3 ubiquitin ligase (Speckle-type POZ protein) SPOP (Ju Shin et al., 2015) was fused to an anti-ALFA nanobody (NbALFA), forming the EN-SPOP module. The randomly integrated ALFA-CENH3 transgene plant and the *in-locus* ALFA-CENH3 (GT) plant were combined with the EN-SPOP degradation module via genetic transformation, yielding haploid plants at a median rate of 4.11% and 16.38%, respectively, with both median values calculated across 11 independent lines (n = 11 per background).

Figure 3.15: 47-days old wild type Col-0 and ALFA-tagged homozygous *Arabidopsis thaliana.*

After the ALFA-tag-integrated heterozygous plants were grown to seed maturity in the botanical garden and their seeds were collected, the obtained seeds were sown on selection marker-free medium and cultivated in a growth chamber for 14 days under a 16 h light/8 h dark photoperiod at 22 °C. The homozygous plants were transferred to soil and cultivated in the botanical garden until seed maturity. When 47-day-old plants were photographed, no major phenotypic differences were observed between Arabidopsis wild-type Col-0 plants (left) and homozygous ALFA-tag integrated plants (right).

These results indicate that utilizing the *ip*GT system for precise *in-locus* tagging of endogenous genes, serves as a powerful tool to eliminate integration locus-dependent variation associated with transgenic approaches, thereby paving the way for a robust and highly efficient haploidization platform.

4 DISCUSSION

The CRISPR/Cas system has been widely adopted for genome editing and crop improvement because it enables sequence-specific induction of DSB more easily and effectively. CRISPR/Cas-based and derived methods offer a broad range of applications in plants, from small nucleotide modifications (Lin et al., 2020b; Zong et al., 2017) to large genomic rearrangement (Rönspies et al., 2025, 2022b), by exploiting different features of the system. In agriculture, these approaches enable genome modification for purposes such as the domestication of wild varieties and crop improvements, while overcoming several limitations of conventional breeding, including time and cost (Chen et al., 2019). Despite these advantages, CRISPR/Cas-based biotechnological tools still require further improvements because of limitations such as low efficiency and target site dependency.

While the use of CRISPR/Cas for targeted mutagenesis has overcome the problem of random mutation generation in conventional breeding by enabling sequence-specific modifications, alternative CRISPR/Cas-based systems have been developed for precise genome engineering. BE, PE and their derived systems allow precise gene editing; however, their editing windows remain narrow and the range of possible nucleotide substitutions and the insertion of large fragments into the genome remain limited (Tuncel et al., 2025). In contrast, HR-based gene targeting methods can enable large fragment integration by exploiting the cell's endogenous repair mechanisms. In this context, the development and improvement of the *ip*GT system represents an important advancement.

In the *ip*GT system, Cas nucleases generate site-specific breaks, while the HR donor template located within the T-DNA is released. The HR donor, which carries the desired modification, can then be integrated into the target region (Fauser et al., 2012). However, the major limitation of this system is the low efficiency of HR in somatic cells, indicating that further improvements are required for efficient GT and its broader applications.

4.1 Impact of Exonuclease Recruitment Strategies on The Outcome of Targeted Gene Editing

4.1.1 Direct fusion of 5' exonucleases to ttLbCas12a-i reduce *ip*GT efficiency independently of KU70

Previous strategies aimed at improving GT have focused on modifying different components that influence *ip*GT efficiency. These include the optimization of DSB induction, modification of the donor template, and promotion of HR during cell cycle phases favorable for HDR. Although these approaches have improved GT efficiency to some extent, the overall frequency of precise GT remains low. Therefore, additional factors that may influence GT outcomes need to be further investigated. (Huang and Puchta, 2019). While *ip*GT efficiency is influenced by the cleavage activity of the Cas nuclease, including its capacity to generate blunt (Jinek et al., 2012) or staggered ends (Zetsche et al., 2015), DSB repair pathway choice is also crucial for precise GT (Merker et al., 2024). Previous studies have shown that DSB repair outcomes can be biased toward specific pathways by manipulating key repair factors (Merker et al., 2024; Nishizawa-Yokoi et al., 2012; Y. Qi et al., 2013; Shaked et al., 2005). For example, an *ip*GT study using *ku70* and *polq* Arabidopsis mutants showed that, in the absence of KU70, the *ip*GT rate increased about 8-fold compared with wild-type Col-0 plants (Merker et al., 2024). This result suggests that impairment of the cNHEJ pathway may favour HR-mediated repair. Under normal conditions, KU70/KU80 heterodimers bind to cleaved DNA ends, and protects the ends from nucleolytic degradation, thereby promoting cNHEJ (Mimori and Hardin, 1986). In KU70-deficient plants, reduced KU70/KU80 activity may allow increased binding of the MRN complex, which competes for the DNA ends (Symington and Gautier, 2011; Tan et al., 2023). Therefore, absence or suppression of cNHEJ-associated proteins may provide an advantage for GT efficiency by shifting the repair pathway choice toward HR (Merker et al., 2024).

In previous studies, several exonucleases were tested with Cas9 and Cas12a endonucleases, and reported higher deletion sizes and mutagenesis efficiencies (Certo et al., 2012; Clements et al., 2017; Ordon et al., 2023; Wu et al., 2020; Zhang et al., 2020). Therefore, exonuclease fusion provides a validated strategy for increasing the mutagenesis efficiency. However, their contribution and impact on GT efficiency have been investigated only to a limited extent. In one of the previous studies it was shown that fusion of exonucleases to Cas9 resulted in 2.5-fold increase in HR in mammalian cells (Hackley, 2021). Moreover, several exonucleases were tested to generate longer 3' ssDNA and thereby increased GT efficiency with both Cas9 and

Cas12a nucleases (Schreiber et al., 2024). When 5’ exonucleases from herpes virus PapE, HSVUL12, and bacteriophage T7 families were fused to SpCas9i and ttLbCas12a-i, HR-based GT efficiency increased in plants. In a transient *Nicotiana benthamiana* assay based on tobacco mosaic virus replication, exonuclease-assisted Cas constructs markedly improved HDR, with the largest enhancement detected for the PapE-SpCas9i combination, reaching up to a 38-fold increase. Although ttLbCas12a-i variants carrying exonuclease fusions were also evaluated, the strongest improvement in this assay was linked to the SpCas9i-based configuration. In stable *Arabidopsis thaliana* experiments, coupling SpCas9i with a herpes virus-derived exonuclease increased knock-in recovery in T_1 plants by about 10-fold. The study further demonstrated that this strategy could generate stable, heritable knock-ins in wheat, with precise events detected in roughly 1% of primary transformants, supporting the use of exonuclease-assisted Cas platforms for scar-free GT of multi-kilobase DNA fragments.(Schreiber et al., 2024).

In this study, PapE and HSVUL12 exonucleases fused to N-terminal to ttLbCas12a-i, with a comparison of ttLbCas12a-i approach. The constructs were transformed both wild-type Col-0 and *ku70* mutant plants. Comparison in ttLbCas12a-i between the genotypes, 2.14-fold increase was observed in *ku70* mutants. This result was supported by the previous study in *ku70* (Merker et al., 2024). However, the increase in GT efficiency observed with ttLbCas12a-i alone highlights the importance of competition with cNHEJ as a limiting factor for precise GT. This observation is consistent with previous studies showing that reduced KU70 activity can enhance GT efficiency by limiting cNHEJ (H. Chen et al., 2022; Merker et al., 2024; Y. Qi et al., 2013). Interestingly, comparison between the exonuclease fused lines in both genotypes, respective constructs showed similar GT efficiency. While PapE-ttLbCas12a-i demonstrated 0.29% GT efficiency in Col-0, 0.25% GT efficiency was observed in *ku70* plants. Additionally, HSVUL12-ttLbCas12a-i indicated 0.58% and 0.43% GT efficiency in Col-0 and *ku70* backgrounds, respectively. Together, these results indicate that the reduced GT efficiency caused by PapE- and HSVUL12-ttLbCas12a-i is not rescued by the *ku70* background. Therefore, the negative effect of these exonuclease fusions is unlikely to be explained solely by KU70-dependent cNHEJ and may involve additional factors affecting DSB processing, donor-template stability, or Cas12a fusion functionality. Excessive or mistimed 5’ end resection may compromise productive HR, while resection of the excised donor template could reduce effective donor-target homology (Chapman et al., 2012; Eschbach and Kobbe, 2014; Schreiber et al., 2024). In addition, impaired Cas12a fusion functionality cannot be excluded, as Cas12a-mediated cleavage depends on coordinated R-loop formation, domain rearrangements, and positioning of the target and non-target DNA strands within the RuvC active site, the fusion

of a relatively large exonuclease domain may interfere with Cas12a conformational dynamics or DNA substrate positioning, thereby reducing nuclease functionality (Strohkendl et al., 2024).

After a Cas nuclease induces a DSB, the broken DNA ends can be rapidly processed by the cNHEJ pathway, which does not require a homologous repair template. In this pathway, the DNA ends are protected from 5'-end resection and maintained in close proximity by the dsDNA end-binding KU70/KU80 heterodimer. (Chapman et al., 2012). Therefore, the initiation of 5' end resection plays an important role in determining which repair pathway will be used, depending on the extent of resection and proteins involved (Beying et al., 2021). Addition to this, the recruitment of exonucleases might promotes this resection (Schreiber et al., 2024). The resection proceeds in 5'-3' direction and generates the 3' ssDNA end required for strand invasion (Eschbach and Kobbe, 2014). The MRN complex plays a critical role in the 5'-end resections required for HR-mediated repair by recognizing DSB sites and initiating DNA end processing. Through the nuclease activity of MRE11, a core component of the complex, MRN functions as an initiator of 5'-end resection (Chapman et al., 2012). In an *in vivo* study performed in *S. cerevisiae*, MRN was shown to introduce nicks up to 300 nucleotides away from the DSB site. Following nick formation, the exonuclease activity of MRE11 processes the nicked DNA strand back toward the break (Chapman et al., 2012; Garcia et al., 2011). In addition, competition between the MRN complex and the KU70/KU80 heterodimer, as well as MRN-mediated displacement of KU from DNA ends, can promote the initiation of HR-mediated repair pathways (Symington and Gautier, 2011; Tan et al., 2023). Although the initiation of the resection is shared among multiple repair pathways, they can be differed in their genetic dependencies and the length of homologous sequences involved. Typically, HDR pathways, including SSA, require more extensive end resection and depend on longer regions of homology (Deng et al., 2014; Kamoen et al., 2025; Sfeir and Symington, 2015).

In addition to the role of the MRN complex in DSB repair pathway regulation, studies in HSV-1 infected Vero cells, a mammalian cell culture system, have shown that the N-terminus of the HSV-1-encoded UL12 exonuclease physically interacts with the MRN complex and modulates its activity (Balasubramanian et al., 2010). The UL12-MRN interaction may influence the probability of resection at a DSB, as well as the recruitment of additional repair factors, ultimately affecting the choice of repair mechanism (Mimitou and Symington, 2009). Moreover, UL12 has also been shown to interact with Mismatch Repair (MMR) complexes. MMR proteins are known to prevent recombination between heterologous sequences and to facilitate flap removal during SSA (de Wind et al., 1995; Lyndaker and Alani, 2009; Schumacher et al., 2012). Consistent with this, a previous study demonstrated that UL12 is

necessary and sufficient to increase SSA, and that its 5'-to-3'exonuclease activity is required for this effect (Schumacher et al., 2012). Based on these findings, it has been proposed that interactions between UL12 and cellular DNA repair proteins may contribute to shifting DSB repair toward the SSA pathway (Schumacher et al., 2012). Given that the MRN complex is evolutionarily conserved, the physical interaction between UL12 and MRN suggested that recruitment of UL12 to Cas-induced DSBs could potentially enhance HR activity (Balasubramanian et al., 2010; Schreiber et al., 2024). However, in the *ip*GT system used in this study, direct fusion of HSVUL12 did not improve GT efficiency. In contrast to the increased knock-in frequency reported by Schreiber et al. (2024) for a herpes virus family exonuclease fused to SpCas9i at the Arabidopsis *thiC* locus, targeting the *ALS* locus in our system resulted in reduced GT efficiency compared with the control. This difference suggests that additional factors influencing GT efficiency need to be considered, including repair pathway competition, fusion architecture, and the possibility that direct fusion of UL12 may interfere with Cas nuclease activity or proper repair factor recruitment. Therefore, as previously suggested the time required for the fused exonuclease to begin processing Cas9-induced DSBs is likely to be a key determinant of the repair outcome (Schreiber et al., 2024). This requirement, together with overall exonuclease activity, may be influenced by several factors, including the spatial orientation of the exonuclease relative to the endonuclease, its affinity for DSB ends, the accessibility of the DNA substrate, the monomeric or oligomeric state of the exonuclease, and its processivity.

In their Arabidopsis system, the PapE and ME15E exonucleases were fused to SpCas9i. The PapE-Cas9 fusion resulted in an approximately 10-fold increase in GT efficiency in T_1 plants compared with the wild-type Cas9 control (Schreiber et al., 2024). In tobacco, Cas-exonuclease fusion experiments were performed using a tobacco mosaic virus-based transient assay system, in which a viral amplicon was used to provide high-copy T-DNA inserts. This setup resulted in substantially higher HDR efficiencies, approximately 20- to 40-fold higher than those observed in Arabidopsis (Schreiber et al., 2024). Based on these observations, Schreiber et al. associated the enhanced HDR efficiency with increased T-DNA copy number. In contrast, the *ip*GT system relies on the excision of the HR donor from a genomically integrated T-DNA followed by its insertion into the target locus. Therefore, in the absence of a viral amplicon system, the excised donor template was present as only a single copy, which may have limited GT efficiency in the *ip*GT setup.

Although the staggered ends generated by Cas12a have been shown to enhance *ip*GT efficiency (Huang et al., 2021; Merker et al., 2020a; Wolter et al., 2018), the lack of improvement observed

with UL12 and PapE exonuclease fusions suggests that these exonucleases may not have acted exclusively on the DSB ends at the target locus. Instead, they may also have promoted resection at the ends of the HR donor template. Such donor-end resection could reduce the effective homology between the donor and the target region, thereby impairing HR-mediated integration and contributing to the observed decrease in GT efficiency.

4.1.2 SunTag-mediated exonuclease recruitments in *ip*GT

Based on these previous results, the effect observed in *ku70* mutants and the impact of direct exonuclease fusion to ttLbCas12a-i on GT efficiency highlighted the importance of further investigating the mechanistic basis of the system, alternative recruitment strategies, and the effect of modulating protein stability through indirect fusion approaches. In this context, previous studies in which up to ten exonucleases were fused to Cas9 using the SunTag system and evaluated for mutagenesis efficiency and deletion size showed that HsTREX1 could influence editing outcomes and that deletion profiles could be altered when fused to SpCas9 (Capdeville et al., 2024). Therefore, in addition to the 5' exonucleases PapE and HSVUL12, the fusion or recruitment of the 3' exonuclease HsTREX1 to Cas12a became an interesting strategy to test in the *ip*GT system. For this purpose, following the design described by Capdeville et al. (2024), a 10 × GCN4 SunTag array was added to the C-terminal end of the ttLbCas12a-i coding sequence using a flexible GS linker, with the aim of recruiting exonucleases without direct fusion to the Cas nuclease. SunTag-mediated exonuclease recruitment was then tested in both Col-0 and *ku70* mutant backgrounds. This approach allowed to examine whether the reduction observed with direct exonuclease fusion, independent of KU70 status, would also occur under indirect recruitment conditions, or could be mitigated. In the *ip*GT experiments, the SunTag control showed a GT efficiency of 0.71% in Col-0, whereas SunTag-HsTREX1 showed a GT efficiency of 0.36%, corresponding to a 1.97-fold decrease compared with the control. Similarly, in the *ku70* mutant background, SunTag-HsTREX1 showed a GT efficiency of 0.61%, compared with 0.81% for the SunTag control, corresponding to a 1.33-fold decrease.

HsTREX1 is the most abundant mammalian 3'-5' DNA exonuclease and preferentially degrades single-stranded DNA as well as mispaired 3' termini in DNA duplexes (Höss et al., 1999; Mazur and Perrino, 2001; Miyazaki et al., 2014). Although its main function is associated with the degradation of cytosolic ssDNA to prevent the accumulation of immunostimulatory DNA, HsTREX1 has also been implicated in the DNA damage response. Upon DNA damage, HsTREX1 can translocate to the nucleus, associate with chromatin, and interact with PARP1,

a key factor involved in cellular responses to DNA damage and single-strand break repair through base excision repair mechanisms. This interaction was detected specifically under DNA damage conditions, suggesting that HsTREX1 may contribute to the regulation of DNA repair-associated processes following genotoxic stress (Gibson and Kraus, 2012; Miyazaki et al., 2014; Robert et al., 2009).

Based on these properties, recruitment of HsTREX1 to Cas12a-induced DSBs does not necessarily favour HR-mediated GT. Since productive HR requires the generation and maintenance of 3' ssDNA overhangs for homology search and strand invasion, the 3'-5' exonuclease activity of HsTREX1 could counteract this process by processing 3' DNA termini. In addition, exonuclease-mediated processing of ssDNA or exposed donor template ends may represent a general possibility; however, this effect may be more pronounced for HsTREX1, thereby reducing the availability or integrity of the HR donor required for efficient GT. Therefore, the reduction observed after SunTag-mediated HsTREX1 recruitment in both Col-0 and *ku70* backgrounds may reflect unfavorable processing of DSB ends or donor-template intermediates rather than enhanced repair pathway redirection toward GT.

However, the reduced magnitude of this decrease in the *ku70* background, together with the 1.69-fold increase observed for SunTag-HsTREX1 in *ku70* mutants compared with Col-0, suggests that the negative effect associated with direct exonuclease fusion to ttLbCas12a-i may be partially alleviated by the SunTag recruitment strategy. A similar trend was observed for SunTag-PapE, which showed a GT efficiency of 0.59% in Col-0 and 1% in *ku70* mutants, corresponding to a 1.69-fold increase in the *ku70* background. This observation supports the idea that the indirect recruitment strategy may reduce the adverse effects potentially caused by direct fusion and that removal of KU from the system can improve GT efficiency, consistent with the positive effect of KU deficiency on GT reported by Merker et al. (2024). In contrast, SunTag-HSVUL12 showed a different pattern. Compared with the respective SunTag controls, SunTag-HSVUL12 increased GT efficiency in both genetic backgrounds, from 0.71% to 1.12% in Col-0 and from 0.81% to 0.90% in *ku70* mutants, corresponding to 1.58-fold and 1.11-fold increases, respectively. However, when SunTag-HSVUL12 was compared between genotypes, GT efficiency was 1.24-fold lower in *ku70* mutants than in Col-0. This suggests that, unlike HsTREX1 and PapE, HSVUL12-mediated enhancement of GT may not benefit from the absence of KU70 and may depend on additional repair pathway interactions that are altered in the *ku70* mutant background.

UL12, well characterized 5'-to-3' exonuclease, interact with the MRN complex to influence resection. Moreover, its standalone overexpression has been shown to promote a 25-fold increase in SSA-mediated repair (Balasubramanian et al., 2010; Reuven et al., 2003; Schumacher et al., 2012). In HSV-infected human HEK293 cells, this increase in SSA was accompanied by a reduction in HR activity, suggesting that UL12 may shift DSB repair pathway choice from HR toward SSA (Schumacher et al., 2012).

Additionally, the interaction between UL12 and the MRN complex may affect DSB repair by modulating the likelihood of DNA end resection and by influencing the recruitment of additional repair factors (Schreiber et al., 2024). In addition to MRN, UL12 was reported to interact with two MMR complexes, MSH2-MSH6 and MSH2-MSH3. Since MMR proteins contribute both to the suppression of recombination between non-homologous sequences and to flap removal during SSA, these interactions may be relevant for repair pathway choice. It was further shown that UL12 is both necessary and sufficient to enhance SSA, and that this effect depends on its 5'-to-3' exonuclease activity. Based on these findings, it was suggested that UL12 may promote a shift in DSB repair toward the SSA pathway through its interactions with cellular DNA repair proteins. Although increased GT efficiency was reported when a herpesvirus-derived exonucleases were fused to SpCas9i and ttLbCas12a-i in tobacco, the limited and genotype-dependent increase observed in the *ip*GT system after the SunTag-mediated HSVUL12 recruitment to ttLbCas12a-i suggests that UL12-mediated repair modulation is context-dependent. In the *ip*GT setup, HSVUL12 recruitment may have altered the balance of DSB repair pathways in a manner that was not favorable for precise donor-mediated integration, potentially by promoting SSA-like repair, excessive or mistimed DSB-end resection, or processing of the excised donor template (Merker et al., 2020b; Schreiber et al., 2024; Schumacher et al., 2012; Strohkendl et al., 2024). Thus, rather than uniformly enhancing GT, UL12 activity may bias repair outcomes depending on the recruitment architecture, target locus, donor-template configuration, and timing of exonuclease activity.

4.1.3 Sequencing-based characterization of perfect and ectopic GT events following exonuclease recruitment

To verify the GT events identified on the basis of phenotypic analysis, molecular analyses were performed. A plant viable on IM-containing medium can arise as a result of a perfect, one-sided, or ectopic event (Hanin et al., 2001; Puchta et al., 1996; Wright et al., 2005). Perfect GT events can be identified using the molecular analysis described in Chapter 2.2.3.

Perfect GT events contain the intended S653N substitution with intact junctions, either in a homozygous or heterozygous state, and may also include the silent mutation. One-sided events contain the S653N substitution but show a mutated junction, whereas ectopic events are characterized by the absence of mutations at the target sequence.

In a perfect GT event, the DSB is repaired via SDSA using the provided donor. This can result either in a target sequence containing a silent mutation and the sequence encoding the S653N mutation, or in a target sequence containing only the sequence encoding the S653N mutation. If the DSB is repaired exclusively via SDSA, this results in a target sequence that contains only the coding sequence for the S653N mutation. A sequence carrying both modifications could be attributable to SDSA repair combined with second-end capture. In this process, synthesis from both 3’ overhangs result in the integration of one mutation in each case. After both synthesized 3’ overhangs dissociate from the template, the resulting mismatches can be integrated into the respective opposite strand by mismatch repair. Another possibility leading to a target sequence with both mutations is based on additional degradation of the 3’ends. As a result, the shortened 3’ overhang can invade the template upstream or downstream of the region homologous to the DSB induction site, whereby the newly synthesized 3’ overhang contains both mutations. The newly synthesized 3’ overhang can then dissociate from the template and be ligated to the other DSB end. One-sided events are based on both HR and NHEJ. In this case, the 3’ overhang synthesized during HR can subsequently be joined to the other end of the DSB via NHEJ (Puchta et al., 1996; Wright et al., 2005).

Ectopic events are likewise a combination of HR and NHEJ. Here, the selection marker on the donor sequence is first restored via HR using the target sequence, but is subsequently integrated into a random DSB in the genome via NHEJ (Hanin et al., 2001; Salomon and Puchta, 1998).

The molecular mechanisms underlying different *ip*GT repair outcomes are not yet fully understood. Although most DSBs generated in GT experiments using a T-DNA donor are thought to be repaired via SDSA, additional mechanisms may also contribute to events containing both intended mutations (Puchta, 1998). Moreover, the apparent frequency of GT outcome classes can be influenced by escape events, in which certain repair products bypass or are lost from the selection system. Therefore, molecular analysis is essential to validate phenotypically selected GT plants and to distinguish between different event types.

Based on this classification, the T_2 plants were analyzed to determine whether exonuclease fusion or recruitment altered not only the occurrence of GT events, but also the proportion of precise, perfect GT outcomes. Molecular analysis of the T_2 plants showed that the proportion

of perfect GT events varied depending on the fusion strategy and genetic background. In the direct fusion approach, the control ttLbCas12a-i produced 43% perfect GT events in Col-0 and 71% in *ku70*. However, PapE direct fusion reduced the proportion of perfect GT events in both Col-0 and *ku70* backgrounds, with 15% and 38%, respectively. HSVUL12 direct fusion showed a similar level to the control in Col-0, with 44% perfect GT events, but reduced the proportion in *ku70* to 55%. These results suggest that direct exonuclease fusion does not consistently improve perfect GT event formation and may negatively affect precise repair outcomes, particularly in the PapE fusion.

In contrast, SunTag-mediated exonuclease recruitment generally increased the proportion of perfect GT events compared with the SunTag control. In Col-0, the SunTag control showed 23% perfect GT events, whereas SunTag-HsTREX1, SunTag-PapE, and SunTag-HSVUL12 resulted in 57%, 55%, and 29%, respectively. A similar trend was observed in the *ku70* background, where the SunTag control showed 36% perfect GT events, while SunTag-HsTREX1, SunTag-PapE, and SunTag-HSVUL12 resulted in 60%, 53%, and 48%, respectively. Thus, indirect recruitment of exonucleases through the SunTag system appeared to improve the quality of GT outcomes compared with direct fusion, especially for HsTREX1 and PapE. These results together indicated that indirect exonuclease recruitment may better preserve Cas12a activity and promote more precise GT outcomes than direct fusion.

Taken together, the molecular analysis suggests that the effect of exonuclease recruitment on perfect GT formation depends strongly on the recruitment architecture. Direct fusion may place the exonuclease in very close proximity to the Cas12a-induced break, which could interfere with Cas12a function, alter DSB-end processing, or promote excessive processing of donor-associated repair intermediates. By contrast, SunTag-mediated recruitment may provide a more flexible spatial arrangement between Cas12a, the exonuclease, and the donor template, allowing exonuclease activity to support repair-intermediate processing without strongly compromising Cas12a activity. The stronger improvement observed for HsTREX1 and PapE under SunTag-mediated recruitment further suggests that the effect of exonuclease recruitment is not uniform across the tested exonucleases. Overall, these findings indicate that exonuclease recruitment can influence the quality of GT outcomes, but this effect is highly dependent on recruitment mode, exonuclease identity, and repair background.

4.1.4 Mutagenesis efficiency of SunTag-mediated exonuclease recruitment

When the *ip*GT results obtained through SunTag-mediated exonuclease recruitment to ttLbCas12a-i were examined, three different exonucleases were tested and were found to result in different GT efficiencies. Although GT efficiency varied depending on whether the recruited exonuclease had 5'-to-3'or 3'-to-5' polarity, differences were also observed between the two 5'-to-3' exonucleases, PapE and HSVUL12. In Col-0 lines, the SunTag control group showed a GT efficiency of 0.71%, whereas SunTag-PapE resulted in a decrease to 0.59%, and SunTag-HSVUL12 showed an increase to 1.12%. These differences suggested that it would be important to further investigate the effects of SunTag-mediated recruitment of these exonucleases to Cas12a in terms of mutagenesis efficiency and DSB repair pattern.

Previously, several exonucleases have been directly fused to different Cas endonucleases in various cell types and organisms, including mammalian cells, Arabidopsis, and zebrafish, and these approaches have been reported to increase mutation frequencies (Certo et al., 2012; Clements et al., 2017; Ordon et al., 2023; Wu et al., 2020; Zhang et al., 2020). This strategy has also been investigated in plants, particularly with respect to InDel formation and larger deletion profiles. For example, direct fusion of T5 exonuclease to the N-terminus of Cas9 was tested in rice protoplasts and was shown to increase deletion frequency compared with Cas9 alone. While Cas9 alone mostly generated 1-2 bp deletions, T5exo-Cas9 was able to induce deletions of up to 446 bp. Similarly, T5exo-Cas9 showed higher editing efficiency in rice seedlings (Zhang et al., 2020). In subsequent analyses using Cas12a, deletions were already the predominant mutation type with Cas12a alone, while insertions represented only 6.2-11.2%. T5exo-Cas12a further increased the deletion frequency to 98.6-99.8% and reduced insertion events to 0.2-1.4% (Zhang et al., 2020).

As an alternative to direct exonuclease fusion, indirect SunTag-mediated exonuclease recruitment was first applied with SpCas9 using HsTREX2, HsTREX1, and *E. coli* Exo1. In this system, SunTag-mediated recruitment of the 3'-to-5' exonuclease HsTREX1 increased deletion size, with deletions of approximately 20-40 bp around the cut site being reported (Capdeville et al., 2024).

Based on these findings, the mutagenesis efficiency and deletion frequency of SunTag-mediated exonuclease recruitment were analyzed in this study. After targeting three different genomic regions, ADH1, ECA3, and Cen4, mutation induction efficiency was found to be comparable between the control group and the exonuclease recruitment approaches.

However, the heterochromatic Cen4 region showed the lowest mutation efficiency, ranging between 33.7% and 36.5%, compared with the euchromatic regions ECA3 and ADH1, which ranged between 43.7% and 75.5% and between 63.9% and 75.3%, respectively. Several studies have shown that chromatin accessibility strongly influences CRISPR nuclease activity. Cas binding and cleavage are reduced when target sites are embedded within nucleosomes or heterochromatic regions, whereas open chromatin is generally more permissive for editing. This has been demonstrated *in vitro* and *in vivo* for Cas9, in plant systems such as Arabidopsis, and more recently for Cas12a, indicating that closed chromatin can limit target accessibility and reduce genome editing efficiency (Horlbeck et al., 2016; Schep et al., 2021; Weiss et al., 2022).

On the other hand, several mechanistic factors may explain why the Cas12a-based SunTag-mediated exonuclease recruitment approach did not produce an enhancement comparable to those reported in other systems. First, unlike Cas9, Cas12a generates staggered DNA ends (Zetsche et al., 2015), which may alter the physical and chemical nature of the DNA termini accessible to the recruited exonucleases. In addition, the prolonged association of Cas12a with the target DNA, particularly around the PAM-proximal region, may restrict access to the cleaved DNA ends. This could be especially limiting for exonucleases with defined polarity, such as the 3'-5' DNA exonuclease HsTREX1. Thus, although the SpCas9-SunTag-HsTREX1 system has been reported to increase deletion frequency (Capdeville et al., 2024), the absence of a similar effect with ttLbCas12a-i-SunTag-HsTREX1 may be attributable to differences in cleavage geometry, DNA-end accessibility, and exonuclease polarity. Second, Cas9 and Cas12a differ in their cleavage-site architecture and PAM orientation (Chen et al., 2025). Therefore, although SunTag-mediated recruitment may increase the local concentration of exonucleases at the target locus, the catalytic domains may not be positioned at an optimal distance or orientation relative to the DNA break ends, thereby limiting their ability to process the cleaved DNA.

Previous studies have shown that, compared with Cas9, Cas12a can generate larger deletions due to its ability to produce staggered DNA ends at the target site (Zetsche et al., 2015). In addition, fusion of exonucleases to Cas9 or Cas12a has been applied as a strategy to increase deletion size and modify repair outcomes (Wang et al., 2025). However, in the present study, targeting ADH1, ECA3, and CEN4 resulted in deletion frequency profiles with distinct patterns depending on both the genomic target site and the recruited exonuclease. SunTag-mediated exonuclease recruitment produced target- and exonuclease-dependent effects. For example, SunTag-mediated recruitment of HsTREX1 modestly increased deletion frequencies at the CEN4 and ADH1 targets, whereas SunTag-mediated recruitment of PapE showed a higher

deletion frequency at ECA3. These observations suggest that the effect of exonuclease recruitment is not uniform across genomic loci, but is likely influenced by genomic context.

In addition, the deletion sizes generated by the SunTag-exonuclease approaches showed comparable changes across the different target sites. This indicates that, although exonuclease recruitment can influence deletion frequency, it did not strongly or consistently increase deletion size under the tested conditions. This may reflect that Cas12a-mediated cleavage is already sufficient to generate robust DSBs at these targets, thereby limiting the additional impact of recruited exonuclease activity on deletion size.

Moreover, the positional distribution of deleted bases within a 40 bp window surrounding the DSB revealed a pattern that differed from previously reported outcomes using SunTag-mediated recruitment of exonucleases with SpCas9. In the SpCas9-based system, recruited exonucleases shifted deletion frequencies toward the PAM-distal region (Capdeville et al., 2024). In contrast, in the present ttLbCas12a-i SunTag-mediated exonuclease recruitment system, deleted bases were mainly positioned around the DSB cleavage site. This difference may be explained by the distinct cleavage properties and post-cleavage DNA binding behaviors of Cas9 and Cas12a. Cas9 generally generates a blunt DSB close to the PAM-proximal region and can remain tightly associated with both cleaved DNA ends, which may limit direct end accessibility and favor more directional exonuclease-mediated processing when exonucleases are recruited. In SpCas9-based system, this could contribute to extended or asymmetric DNA end processing, resulting in a shift of deletions toward the PAM-distal side (Capdeville et al., 2024). By contrast, Cas12a generates staggered ends distal to the PAM, and may leave one cleaved DNA end more accessible after cleavage, which could already facilitate DNA end processing by endogenous repair factors. Therefore, in the ttLbCas12a-i system, recruited exonucleases may process DNA ends primarily near the original cleavage site rather than shifting deletion formation further away from the target region. Therefore, in the ttLbCas12a-i system, recruited exonucleases may increase mutagenic activity or influence deletion frequency without necessarily driving deletion formation away from the original cleavage site. Instead, exonuclease activity may remain concentrated near the accessible Cas12a-generated break ends. This suggests that SunTag-mediated exonuclease recruitment can alter repair outcomes, but that its effect is strongly shaped by the choice of the exonuclease. Overall, these findings indicate that exonuclease recruitment does not produce a universal deletion profile, but instead results in context-dependent editing outcomes that differ between Cas9- and Cas12a-based systems.

The mutagenesis efficiency and deletion frequency analyses therefore provide an important link to the *ip*GT results, as they indicate that exonuclease recruitment can influence repair outcomes in a target- and exonuclease-dependent manner without uniformly enhancing Cas12a-induced editing. In the context of *ip*GT, this suggests that improving GT efficiency requires not only efficient DSB induction, but also controlled DSB end processing, preservation of donor template integrity, and favorable repair pathway choice. Thus, the *ip*GT system should be evaluated through an integrated approach that considers the combination of various effects. Although *ip*GT remains limited by relatively low efficiency, it provides a precise and promising strategy for targeted genome modification. To better exploit this system, future strategies should include optimizing Cas nuclease activity, testing alternative exonuclease fusion or recruitment configurations, characterizing their activity at target loci, and modulating proteins or complexes involved in DNA repair pathways to enhance GT efficiency. Further improvements in *ip*GT could be particularly valuable for breeding and crop improvement, where precise targeted modification of plant genomes may offer an alternative to more complex genome engineering strategies while reducing time requirements and technical complexity.

4.2 *ip*GT-Mediated Endogenous CENH3 Tagging as a Strategy for Transgene-Free Haploid Induction

Although several strategies have been developed to improve *ip*GT, achieving consistently high frequencies of precise HR remains challenging. Nevertheless, the significance of *ip*GT should not be assessed solely on the basis of its frequency. For functionally sensitive loci, its major advantage lies in the possibility of introducing defined modifications directly into the endogenous genomic context, thereby avoiding the positional and expression-related effects associated with random transgene insertion.

The results of this study demonstrate that precise endogenous tagging of *AtCENH3* by *ip*GT provides a functional route to overcome one of the major limitations of transgene-based CENH3 haploid induction systems: the uncontrolled variation caused by random transgene integration. Previous CENH3-based haploid induction strategies have shown that modification or depletion of CENH3 can trigger uniparental chromosome elimination during early embryogenesis, thereby producing haploid progeny. However, these systems are highly sensitive to the structural and expression context of CENH3, because centromere function depends on accurate CENH3 deposition, stability, and kinetochore assembly. In this context, the present work

addresses a central technical and biological problem: how to introduce a small, non-disruptive tag into endogenous *CENH3* in a way that preserves normal plant development but enables inducible, targeted CENH3 depletion for haploid induction.

DH technology represents a highly valuable strategy in modern plant breeding, as it enables the rapid production of completely homozygous lines. By generating genetically fixed material at an early stage of the breeding cycle, DH technology allows breeders to evaluate desirable traits more efficiently and to accelerate the development of improved cultivars (Forster et al., 2007; Jacquier et al., 2020). This technology consists mainly of two steps: first, the production of haploid embryos or plantlets, and second, chromosome doubling to obtain diploid and fully homozygous plants (Jacquier et al., 2020). The ability to generate haploid plants has been shown to substantially shorten the breeding process while reducing both time and cost (Demidov et al., 2022). Haploids are generally produced either through *in vitro* haploid technologies or through the selective loss of one parental chromosome set after hybridization. DH technology usually requires only two to three generations and is therefore widely used in crop breeding programs (Demidov et al., 2022; Qu et al., 2024). Accordingly, haploid induction constitutes a critical component of DH technology, as it facilitates the rapid generation of homozygous lines compared with conventional breeding schemes and contributes to the accelerated development of new cultivars (Li et al., 2025).

Despite the considerable advantages of DH technology in accelerating the production of homozygous lines, its broad application remains constrained in many crop species. A major limitation is the lack of efficient and widely applicable haploid induction systems. In several crops, viable haploid technology is either not available, restricted to a narrow range of genotypes, or associated with prohibitively high costs (Demidov et al., 2022). Although chromosome doubling also presents technical challenges, the principal barrier to the generalized use of DH technology in plant breeding is the limited availability of reliable methods for inducing haploidy across diverse crop species and genetic backgrounds (Dunwell, 2010; Forster et al., 2007). The most commonly used haploidization approaches have relied on the *in vitro* culture of haploid gametophytic tissues, particularly male gametophytic tissues through androgenesis, although gynogenesis from female gametophytic tissues is also employed (Jacquier et al., 2020; Maluszynski et al., 2003). These approaches require culture conditions that enable gametophytic cells to be reprogrammed toward embryogenic development. However, despite substantial improvements, *in vitro* protocols remain labor-intensive, and their broader application is still constrained by species- and genotype-dependent responses (Davey, 2009; Jacquier et al., 2020). Alternative *in vivo* strategies, including distant hybridization,

haploid inducer genotypes, and pollination with physically (radiation and high temperature) or chemically (phosphatidylcholine or methimazole) treated pollen, have also been developed (Forster et al., 2007; Ishii et al., 2016; C. Jiang et al., 2022; Katayama, 1934; Li et al., 2025; Mathur et al., 1980). Nevertheless, their wider use is restricted by factors such as inducer availability, species recalcitrance, and genotype-dependent regeneration bottlenecks (Li et al., 2025).

In this context, haploid inducer lines represent a particularly promising *in planta* alternative, as they enable haploid production without the requirement for tissue culture. Unlike conventional regeneration-based approaches, haploid inducer lines can generate haploid embryos and plantlets through simple intraspecific crosses, thereby allowing haploids to be recovered directly from seeds. These specialized genotypes produce viable seeds containing haploid embryos, which can subsequently develop into haploid plantlets upon germination (Gilles et al., 2017; Jacquier et al., 2020; Kalinowska et al., 2019). Consequently, haploid inducer lines are regarded as a central component of DH technology, because they facilitate the production of haploid progeny when crossed with diverse germplasm (Qu et al., 2024). Such *in vivo* haploid induction systems have therefore gained increasing importance as tools for accelerating crop improvement (Li et al., 2025). Mechanistically, haploid inducer approaches can be broadly categorized into centromere-based and non-centromere-based systems (Somasundaram et al., 2026). In centromere-based systems, haploidization is generally achieved through the preferential elimination of one parental chromosome set after fertilization, often as a consequence of altered centromere identity, centromere strength, or chromosome segregation fidelity. By contrast, non-centromere-based systems act mainly by disrupting specific events during double fertilization, including sperm cell integrity, plasmogamy, karyogamy, early cell division, or embryogenesis activation, thereby enabling the development of an embryo containing only one parental genome. Nevertheless, haploid formation remains a rare and highly specialized outcome of double fertilization, and only a limited number of genetic factors have been successfully exploited for haploid induction to date, with the molecular mechanisms underlying some of these factors still incompletely understood (Li et al., 2025).

Recent approaches have combined CRISPR/Cas editing with *in planta* haploid inducer lines. Systems such as Haploid induction-Edit (Kelliher et al., 2019) and haploid-inducer-mediated genome editing (IMGE) (Wang et al., 2019) use haploid inducer lines carrying a transgenic CRISPR/Cas cassette, which are crossed with elite cultivars to deliver edits directly into breeding materials while avoiding stable inheritance of the editing transgene (Jacquier et al., 2020). This coordinated use of genome editing and haploid induction can accelerate the

transmission of desired edits into advanced germplasm and reduce the delays and costs associated with conventional introgression. Therefore, continued development of genome editing platforms across crop species is essential for fully integrating genetic engineering with haploid induction-based breeding strategies (Li et al., 2025).

Beyond naturally occurring inducer variation, targeted biotechnological manipulation has provided an additional route for developing haploid inducer systems. In particular, modification of CENH3 led to the establishment of a novel class of haploid inducer lines in *Arabidopsis thaliana* (Ravi and Chan, 2010). CENH3 is regarded as the defining component of centromeres in most eukaryotes and plays a fundamental role in centromere identity and function (Talbert and Henikoff, 2020). As a centromere-specific histone H3 variant, CENH3 replaces canonical histone H3 in centromeric chromatin and provides the epigenetic foundation required for kinetochore assembly (Demidov et al., 2022; Malik and Henikoff, 2003; Ravi and Chan, 2010). Because kinetochores mediate microtubule attachment and ensure accurate chromosome movement during mitosis and meiosis, proper CENH3 loading is essential for faithful chromosome segregation (Jacquier et al., 2020; Li et al., 2025; Wang and Dawe, 2018). Accordingly, the absence or functional impairment of CENH3 leads to defective kinetochores, centromere dysfunction, chromosome mis-segregation, and, in severe cases, embryo lethality (Allshire and Karpen, 2008; Demidov et al., 2022). Importantly, errors in CENH3 transcription, translation, post-translational modification, or incorporation into centromeres can disturb the interaction between centromeres and the mitotic spindle, thereby promoting selective centromere dysfunction and chromosome loss (Li et al., 2025). This mechanistic sensitivity explains why engineered alterations of CENH3, such as CENH3-based haploid inducer systems, can trigger haploid formation through chromosome elimination.

A key experimental breakthrough in CENH3-mediated haploid induction was the development of the transgenic GFP-tailswap system in *Arabidopsis thaliana*. In this approach, the native N-terminal tail of CENH3 was replaced by GFP fused to the N-terminal tail of conventional histone H3.3, which partially complemented the lethal phenotype of a *cenh3 null* mutant (Ravi and Chan, 2010). Remarkably, when this GFP-tailswap line was used as the female parent and fertilized with wild-type pollen, approximately 30% of the resulting embryos were haploid and contained only the paternal wild-type genome (Ravi and Chan, 2010). This finding established modified CENH3 as one of the most widely used haploid induction genes, since mutation or transgenic expression of CENH3 variants can promote the elimination of chromosomes derived from the mutant parent and thereby generate haploid progeny (Qu et al., 2024; Ravi and Chan, 2010). At the molecular level, direct or indirect alteration of CENH3 is thought to create a weak

centromere, causing chromosomes carrying defective centromeres to be selectively lost during early zygotic or embryonic development (Demidov et al., 2022; Li et al., 2025). Consequently, when CENH3-defective plants are crossed with wild-type plants, chromosome segregation becomes imbalanced, leading to uniparental genome elimination and haploid embryo formation (Comai and Tan, 2019; Jacquier et al., 2020). However, efficient CENH3-mediated haploid induction has so far been developed mainly in *A. thaliana*, indicating that broader application in crop species remains challenging (Demidov et al., 2022). Despite its conceptual strength, the original tailswap strategy was reproduced in maize, but the average haploid induction frequency was below 1%, which is insufficient for routine breeding applications (Ravi and Chan, 2010). More generally, CENH3-based systems show a strong parental-effect bias: when wild-type female plants are pollinated with CENH3-engineered pollen, maternal haploid induction is very low, and the basis of this reduced efficiency through the male remains unclear (Jacquier et al., 2020; Kalinowska et al., 2019). Although modified CENH3 approaches have now been tested in several crops (Han et al., 2024; Lv et al., 2020; Manape et al., 2024; Wang et al., 2024), their efficiency is generally much lower than in *Arabidopsis* (Li et al., 2025). In maize, haploid induction using AcGREEN-tailswap-CENH3 reached up to 3.6%. Crosses involving *cenh3/+* heterozygous plants showed a parent-of-origin effect, producing approximately 5% haploids when *cenh3/+* plants were used as the maternal parent, whereas their use as the paternal parent resulted in only 0.5% haploid induction (Wang et al., 2021). In wheat, genome-edited *TaCENH3a* heteroallelic combinations were reported to induce haploids at a frequency of approximately 7% (Lv et al., 2020). Lower efficiencies have also been reported in switchgrass, with 0.5-1.4% haploids, and in several other crops including tomato, rice, cucumber, melon, onion, cauliflower, kale, and broccoli (Han et al., 2024; Li et al., 2025; Lv et al., 2020; Manape et al., 2024; Wang et al., 2024). These limitations may reflect species-specific differences in CENH3 deposition, stability, and developmental regulation, as CENH3 functions during mitosis, meiosis, and multiple developmental stages (Li et al., 2025). Therefore, although modified CENH3 remains a promising basis for engineering haploid inducer lines, most crop species still lack an efficient CENH3-based haploid induction technology, and species-specific optimization is required (Demidov et al., 2022; Li et al., 2025).

Building on this rationale, precise modification of CENH3 at its endogenous locus represents a particularly relevant strategy for improving the control and interpretability of CENH3-based haploid induction systems. Endogenous tagging provides an opportunity to evaluate the functional compatibility of a tag under native regulatory control, while minimizing the influences associated with ectopic transgene expression. This is consistent with the proposal

that targeted insertion of tags into endogenous CENH3 by knock-in approaches, followed by controlled degradation, could provide a feasible route for haploid production, although its broader implementation depends on the development of efficient genome editing technologies in different plant species (Li et al., 2025). A related strategy for CENH3-based haploid induction has been developed through nanobody-mediated degradation of tagged CENH3 proteins. Previous work demonstrated nucleus-specific depletion of EYFP-tagged CENH3 from *A. thaliana* in *Nicotiana tabacum*, establishing that a nanobody-based system can be used to target CENH3 fusion proteins for degradation (Demidov et al., 2022). This concept was subsequently applied in Arabidopsis, where an EYFP-CENH3 transgene in a *cenh3* mutant background was combined with an anti-GFP nanobody linked to the ubiquitin-proteasome pathway, resulting in depletion of the tagged CENH3 protein and successful haploid production (Demidov et al., 2022). These findings provided important proof of principle that targeted CENH3 degradation can trigger chromosome elimination and haploidization. However, the EYFP-based system also illustrates several limitations that motivate the present work. For instance, the earlier approach relied on engineered E3 ligases encoded by the paternal genome to degrade maternally inherited EYFP-CENH3 and eliminate maternal chromosomes, but it required transgenes in both parents, generated transgenic haploids that are less suitable for breeding applications, and showed relatively low efficiency compared with established CENH3 manipulation systems in Arabidopsis. Moreover, the use of a large fluorescent tag and randomly integrated transgenes may introduce additional complications, including tag-dependent interference with CENH3 function, transgene-position effects, and background haploid induction (Somasundaram et al., 2026). Therefore, while EYFP-CENH3 degradation demonstrated the feasibility of nanobody-directed haploid induction, it also highlighted the need for a cleaner and more controllable endogenous tagging strategy.

This study directly addresses this strategy by using *ip*GT to insert the 45 bp ALFA-tag coding sequence into the endogenous *AtCENH3* locus. Two CRISPR/Cas12a target sites were selected within Exon 1: Target 1, with the predicted DSB upstream of the start codon, and Target 3, with the predicted DSB downstream of the start codon. T_2 progeny from both target-site lines were screened to identify ALFA-tag integration events and evaluate the practical efficiency of the *ip*GT strategy. While no ALFA-tag integration was detected for Target 3, one heterozygous ALFA-CENH3 (GT) plant was identified for Target 1, corresponding to a GT efficiency of 0.04%. The heterozygous plant was subsequently self-crossed, and homozygous ALFA-CENH3 (GT) plants were identified. Nevertheless, the observed segregation distortion among edited progeny should be considered carefully. The ratio of

39 homozygous edited:50 heterozygous:59 non-edited plants deviated significantly from the expected Mendelian segregation pattern ($\chi^2 = 20.97$, $df = 2$, $p < 0.001$), suggesting that even precise endogenous modification of CENH3 may affect allele transmission, gametophytic or zygotic viability, or may be subject to selection or segregation bias. Although this did not manifest as an obvious developmental phenotype, it may represent a biologically relevant effect requiring further investigation.

On the other hand, the choice of the ALFA-tag is not only a technical detail but also a key interpretive point. Previous EYFP-CENH3 degradation systems used a much larger 26.7 kDa tag and showed background haploid induction before E3-ligase activation, with reported frequencies of 5.54-20.34% (Demidov et al., 2022; Somasundaram et al., 2026). By contrast, the 1.9 kDa ALFA-tag was selected to minimize structural interference with CENH3. This approach is further supported by the observation that randomly integrated ALFA-CENH3 transgenes displayed variable background haploid induction activity, ranging from 0% to 15.15%, whereas endogenous ALFA-CENH3 (GT) lines showed no background haploid induction prior to activation of the degradation system. Thus, endogenous CENH3 tagging by *ip*GT provides a more controlled framework for separating tag-related effects from transgene-position influences.

In the present study, endogenous ALFA-CENH3 (GT) plants displayed no visible morphological abnormalities and did not show background haploid induction (Somasundaram et al., 2026), indicating that the ALFA-tag is compatible with essential CENH3 function when inserted at the native *AtCENH3* locus and expressed under endogenous regulatory control. This is a critical distinction from randomly integrated transgene-based systems, because the absence of spontaneous haploid formation before EN-SPOP introduction suggests that endogenous ALFA-CENH3 (GT) does not constitutively generate a weak-centromere state under normal conditions. Instead, haploidization appears to depend on conditional activation of the degradation module.

Importantly, after introduction of EN-SPOP, the endogenous ALFA-CENH3 (GT) background produced a median haploid induction rate of 16.38%, compared with 4.11% in random ALFA-CENH3 transgene backgrounds, based on 11 independent lines per background. This demonstrates that precise endogenous tagging not only minimizes background activity but also improves inducible haploidization efficiency. Functionally, egg-cell-specific EN-SPOP expression is expected to deplete maternal ALFA-CENH3, creating parental CENH3 asymmetry after fertilization. As the paternal genome is contributed by wild-type pollen and

remains CENH3-competent, maternal chromosomes carrying depleted ALFA-CENH3 likely behave as weak-centromere chromosomes and are selectively eliminated during early embryogenesis (Somasundaram et al., 2026).

Although endogenous ALFA tagging improved inducible haploidization efficiency in this study, CENH3-based haploid induction is influenced by additional genetic, developmental, and environmental factors. Therefore, further improvement of this system will likely require combining precise endogenous tagging with complementary strategies that enhance induction efficiency and reduce unintended effects. Several studies indicate that altered CENH3 function can be achieved through different routes. For example, CENH3 point mutations can be introduced through non-transgenic approaches such as targeting-induced local lesions in genomes (TILLING). In addition, CRISPR-mediated in-frame deletions have been reported to generate haploid progeny at frequencies reaching 25.7% (Kuppu et al., 2020). These findings suggest that controlled modification of CENH3 can be an effective strategy for triggering chromosome elimination without necessarily relying on large transgenic constructs. Additional genetic factors may also modulate haploid induction efficiency. For instance, haploid induction efficiency was improved by combining the *cenh3-1* GFP-tailswap system with a mutation in LIG4, a conserved component of the cNHEJ pathway. This suggests that DNA repair mechanisms may contribute to the efficiency and outcome of CENH3-mediated genome elimination (Tan et al., 2015). Environmental conditions can further affect induction efficiency: higher growth temperatures have been reported to increase haploid induction, although this is accompanied by reduced pollen viability, whereas lower temperatures tend to decrease haploid induction while improving pollen performance (Ahmadli et al., 2023; Jin et al., 2023; Li et al., 2025; Wang et al., 2023). These observations demonstrate that CENH3-based haploidization is not determined solely by the engineered CENH3 allele itself, but is also shaped by genetic background, DNA repair capacity, reproductive fitness, and the developmental environment. Despite these advances, several limitations continue to restrict the broad application of CENH3- and CRISPR-based haploid induction systems. Disruption of CENH3 function is a proven route to uniparental chromosome elimination during early embryogenesis, before the first mitotic division of the unicellular embryo, and this strategy has been applied in several plant species (Kelliher et al., 2019; Li et al., 2025; Lv et al., 2020; Wang et al., 2021). Nevertheless, chromosome elimination mediated by CENH3 modification is largely biased toward the maternal genome. In contrast, paternal genome elimination has thus far been documented only in *Arabidopsis* and maize, where its efficiency is approximately 10-fold lower than that of maternal chromosome elimination (Ravi and Chan, 2010; Wang et al., 2021).

Because maternal haploid production is particularly relevant for modern breeding, improving the efficiency and reliability of this pathway remains an important objective (Li et al., 2025). CRISPR-mediated haploid induction also offers a rapid and powerful route for generating homozygous lines, but its implementation across crop species faces several unresolved barriers (Liu et al., 2021). These include inconsistent induction efficiency across species and even among cultivars of the same species, difficulties in delivering CRISPR components into plant cells (Mao et al., 2019), possible off-target mutations with unpredictable developmental or agronomic consequences (Zhu et al., 2020), and regulatory or public acceptance concerns surrounding genome-edited crops (Ahmad et al., 2021; He et al., 2022; Li et al., 2025). Therefore, future development of haploid induction technologies will need to prioritize systems that are efficient, genotype-flexible, minimally disruptive, and, where possible, compatible with non-transgenic final products (Li et al., 2025).

Within this broader context, the present work does not solve all challenges associated with crop-wide deployment, species-specific transformation barriers, or regulatory acceptance of genome editing. However, it addresses a central conceptual and technical limitation in the model system: how to engineer a clean, endogenous, nanobody-addressable CENH3 substrate that remains functionally compatible under normal conditions but can be efficiently converted into a haploid-inducing state upon targeted degradation. This distinction is important because many earlier CENH3-based systems rely on constitutively altered CENH3 variants, large fluorescent tags, or randomly integrated transgenes, all of which may generate background centromere weakness before experimental activation. By contrast, the endogenous ALFA-CENH3 (GT) configuration avoids visible developmental defects and background haploid induction prior to EN-SPOP activation, suggesting that the ALFA-tagged protein does not behave as a permanently weakened centromere component under native regulation. At the same time, the system supports strong inducible haploidization after degradation-module introduction. Thus, while further optimization will be required before similar strategies can be translated broadly to crop species, these results provide a controlled framework for separating tag compatibility, endogenous CENH3 function, and inducible chromosome elimination. This represents an important step toward more precise, conditional, and potentially cleaner CENH3-based haploid induction systems. To achieve this, the *ip*GT system, which was developed for precise GT in plants, offers a valuable opportunity due to its adaptability and practical applicability. Although its efficiency remains relatively low, this study demonstrates that *ip*GT can introduce the desired modification through accurate and effective targeting. Importantly, this study provides the first practical demonstration of *ip*GT application and

confirms its successful use in achieving the intended genetic modification. Overall, *ip*GT represents a promising alternative because it can be adapted to different plant species, allows target-specific design, and is straightforward to design and implement. Furthermore, the findings of this study support the potential of *ip*GT as a valuable tool for crop improvement.

5 SUMMARY

GT is an important tool for plant breeding because it enables precise genome modifications. CRISPR/Cas systems, which induce sequence-specific DNA breaks, have become a key platform for improving GT efficiency in plants. However, GT efficiency remains low, requiring further optimizations. Therefore, this study investigated the effects of direct and indirect exonuclease recruitment on *ip*GT. The direct fusion of PapE and HSVUL12 to ttLbCas12a-i reduced GT efficiency compared with the control in both Col-0 and *ku70* backgrounds. Similar GT efficiencies in both backgrounds suggest that this reduction was not primarily dependent on the DNA repair background. Instead, direct exonuclease fusion may compromise the editing complex by affecting Cas12a stability, folding, target binding, or cleavage activity. Based on these observations, an indirect SunTag-mediated exonuclease recruitment strategy was tested. In this system, the 5' exonucleases PapE and HSVUL12, together with the 3' exonuclease HsTREX1, were recruited to ttLbCas12a-i, and their effects on GT efficiency were examined. This approach partially overcame the reduction observed with direct PapE and HSVUL12 fusion. However, HsTREX1 resulted in lower GT efficiency than the 5' exonucleases, possibly because its 3'-5' exonuclease activity may resect free 3' ssDNA ends required for HR. Moreover, genome editing efficiency was further evaluated, and the SunTag-mediated exonuclease recruitment showed comparable mutagenesis efficiencies across different genomic regions. Although deletion frequencies varied in a target- and exonuclease-dependent manner, the deleted bases mainly accumulated around the Cas12a cleavage site rather than toward the PAM-distal region. These results indicate that exonuclease selection is an important parameter for system optimization toward achieving higher *ip*GT efficiencies. Nevertheless, *ip*GT is valuable for plant breeding. Importantly, this study demonstrates, for the first time, the practical applicability of *ip*GT by introducing a desired modification into an endogenous gene. In this study, the small ALFA tag was introduced into the endogenous *AtCENH3* locus using *ip*GT. This modification enabled subsequent E3 ligase-mediated degradation of CENH3, providing a basis for inducible haploidization. Therefore, *ip*GT offers a promising route for precise endogenous modification and potentially transgene-free haploid induction systems.

6 REFERENCES

Ahmad, S., Tang, L., Shahzad, R., Mawia, A.M., Rao, G.S., Jamil, S., Wei, C., Sheng, Z., Shao, G., Wei, X., Hu, P., Mahfouz, M.M., Hu, S., Tang, S., 2021. CRISPR-Based Crop Improvements: A Way Forward to Achieve Zero Hunger. J. Agric. Food Chem. 69, 8307–8323. https://doi.org/10.1021/acs.jafc.1c02653

Ahmadli, U., Kalidass, M., Khaitova, L.C., Fuchs, J., Cuacos, M., Demidov, D., Zuo, S., Pecinkova, J., Mascher, M., Ingouff, M., Heckmann, S., Houben, A., Riha, K., Lermontova, I., 2023. High temperature increases centromere-mediated genome elimination frequency and enhances haploid induction in *Arabidopsis*. Plant Communications 4, 100507. https://doi.org/10.1016/j.xplc.2022.100507

Allen, A., Cooper, B.H., Singh, J., Rohs, R., Qin, P.Z., 2025. PAM-adjacent DNA flexibility tunes CRISPR-Cas12a off-target binding. Sci Rep 15, 4930. https://doi.org/10.1038/s41598-025-87565-9

Allshire, R.C., Karpen, G.H., 2008. Epigenetic regulation of centromeric chromatin: old dogs, new tricks? Nat Rev Genet 9, 923–937. https://doi.org/10.1038/nrg2466

Altae-Tran, H., Kannan, S., Demircioglu, F.E., Oshiro, R., Nety, S.P., McKay, L.J., Dlakić, M., Inskeep, W.P., Makarova, K.S., Macrae, R.K., Koonin, E.V., Zhang, F., 2021. The widespread IS200/IS605 transposon family encodes diverse programmable RNA-guided endonucleases. Science 374, 57–65. https://doi.org/10.1126/science.abj6856

Anders, C., Niewoehner, O., Duerst, A., Jinek, M., 2014. Structural basis of PAM-dependent target DNA recognition by the Cas9 endonuclease. Nature 513, 569–573. https://doi.org/10.1038/nature13579

Andres, S.N., Modesti, M., Tsai, C.J., Chu, G., Junop, M.S., 2007. Crystal Structure of Human XLF: A Twist in Nonhomologous DNA End-Joining. Molecular Cell 28, 1093–1101. https://doi.org/10.1016/j.molcel.2007.10.024

Anzalone, A.V., Gao, X.D., Podracky, C.J., Nelson, A.T., Koblan, L.W., Raguram, A., Levy, J.M., Mercer, J.A.M., Liu, D.R., 2022. Programmable deletion, replacement, integration and inversion of large DNA sequences with twin prime editing. Nat Biotechnol 40, 731–740. https://doi.org/10.1038/s41587-021-01133-w

Anzalone, A.V., Randolph, P.B., Davis, J.R., Sousa, A.A., Koblan, L.W., Levy, J.M., Chen, P.J., Wilson, C., Newby, G.A., Raguram, A., Liu, D.R., 2019. Search-and-replace genome editing without double-strand breaks or donor DNA. Nature 576, 149–157. https://doi.org/10.1038/s41586-019-1711-4

Arezi, B., Hogrefe, H., 2009. Novel mutations in Moloney Murine Leukemia Virus reverse transcriptase increase thermostability through tighter binding to template-primer. Nucleic Acids Res 37, 473–481. https://doi.org/10.1093/nar/gkn952

Asik, E., Kashif, S.Z., Oztas, O., 2026. Plant tolerance mechanisms to DNA-damaging UV stress. J Exp Bot 77, 27–50. https://doi.org/10.1093/jxb/eraf272

Atia, M., Jiang, W., Sedeek, K., Butt, H., Mahfouz, M., 2024. Crop bioengineering via gene editing: reshaping the future of agriculture. Plant Cell Rep 43, 98. https://doi.org/10.1007/s00299-024-03183-1

Atkins, P.A., Voytas, D.F., 2020. Overcoming bottlenecks in plant gene editing. Curr Opin Plant Biol 54, 79–84. https://doi.org/10.1016/j.pbi.2020.01.002

Auerbach, C., Robson, J.M., 1946. Chemical Production of Mutations. Nature 157, 302–302. https://doi.org/10.1038/157302a0

Authority (EFSA), E.F.S., Paraskevopoulos, K., Federici, S., 2021. Overview of EFSA and European national authorities' scientific opinions on the risk assessment of plants developed through New Genomic Techniques. EFSA Journal 19, e06314. https://doi.org/10.2903/j.efsa.2021.6314

Awan, M.J.A., Amin, I., Mansoor, S., 2022. CRISPR-Cas12c: a noncleaving DNA binder with minimal PAM requirement. Trends in Biotechnology 40, 1141–1143. https://doi.org/10.1016/j.tibtech.2022.07.005

Balasubramanian, N., Bai, P., Buchek, G., Korza, G., Weller, S.K., 2010. Physical Interaction between the Herpes Simplex Virus Type 1 Exonuclease, UL12, and the DNA Double-Strand Break-Sensing MRN Complex. Journal of Virology 84, 12504–12514. https://doi.org/10.1128/jvi.01506-10

Baltes, N.J., Gil-Humanes, J., Cermak, T., Atkins, P.A., Voytas, D.F., 2014. DNA replicons for plant genome engineering. Plant Cell 26, 151–163. https://doi.org/10.1105/tpc.113.119792

Baranauskas, A., Paliksa, S., Alzbutas, G., Vaitkevicius, M., Lubiene, J., Letukiene, V., Burinskas, S., Sasnauskas, G., Skirgaila, R., 2012. Generation and characterization of new highly thermostable and processive M-MuLV reverse transcriptase variants. Protein Eng Des Sel 25, 657–668. https://doi.org/10.1093/protein/gzs034

Baranova, S.V., Zhdanova, P.V., Pestryakov, P.E., Chernonosov, A.A., Koval, V.V., 2025. Key thermodynamic characteristics of Cas9 and Cas12a endonucleases' cleavage of a DNA substrate containing a nucleotide mismatch in the region complementary to RNA. Biochemical and Biophysical Research Communications 768, 151892. https://doi.org/10.1016/j.bbrc.2025.151892

Barco, B., Dong, S., Matsuba, Y., Crook, A., Xu, R., Zhang, Yingxiao, Zhang, C., Carlin, R., Potter, K., Rigoulot, S.B., Park, J., Seaberry, E.M., Parrish, A., Elumalai, S., Nalapalli, S., Schuller, C., Prairie, A., Mangum, A., Mei, K., Wu, H., Murray, M., Setliff, K., Johnson, F., McNamara, D., Zhu, L., Rose, M., Gu, W., Hu, H., Zhang, Yuanji, Jiang, Y., Wang, W., Tang, G., Geng, L., Xu, J., Shi, W., Nichols, J., Kelliher, T., Shi, L., Jepson, I., Que, Q., 2025. Development of efficient targeted insertion mediated by CRISPR-Cas12a and homology-directed repair in maize. Front. Genome Ed. 7. https://doi.org/10.3389/fgeed.2025.1713347

Barrangou, R., Fremaux, C., Deveau, H., Richards, M., Boyaval, P., Moineau, S., Romero, D.A., Horvath, P., 2007. CRISPR provides acquired resistance against viruses in prokaryotes. Science 315, 1709–1712. https://doi.org/10.1126/science.1138140

Beying, N., Schmidt, C., Puchta, H., 2021. Double strand break (DSB) repair pathways in plants and their application in genome engineering, in: Cornell University, USA, Willmann, M.R. (Eds.), Burleigh Dodds Series in Agricultural Science. Burleigh Dodds Science Publishing, pp. 27–62. https://doi.org/10.19103/AS.2020.0082.04

Bhargava, R., Onyango, D.O., Stark, J.M., 2016. Regulation of Single-Strand Annealing and its Role in Genome Maintenance. Trends in Genetics 32, 566–575. https://doi.org/10.1016/j.tig.2016.06.007

Bhaya, D., Davison, M., Barrangou, R., 2011. CRISPR-Cas Systems in Bacteria and Archaea: Versatile Small RNAs for Adaptive Defense and Regulation. Annu. Rev. Genet. 45, 273–297. https://doi.org/10.1146/annurev-genet-110410-132430

Bonnet, S., Knoll, A., Hartung, F., Puchta, H., 2013. Different functions for the domains of the Arabidopsis thaliana RMI1 protein in DNA cross-link repair, somatic and meiotic recombination. Nucleic Acids Res 41, 9349–9360. https://doi.org/10.1093/nar/gkt730

Boulton, S.J., Jackson, S.P., 1996. Saccharomyces cerevisiae Ku70 potentiates illegitimate DNA double-strand break repair and serves as a barrier to error-prone DNA repair pathways. EMBO J 15, 5093–5103.

Bronstein, J.C., Weber, P.C., 1996. Purification and characterization of herpes simplex virus type 1 alkaline exonuclease expressed in Escherichia coli. Journal of Virology 70, 2008–2013. https://doi.org/10.1128/jvi.70.3.2008-2013.1996

Butler, N.M., Baltes, N.J., Voytas, D.F., Douches, D.S., 2016. Geminivirus-Mediated Genome Editing in Potato (Solanum tuberosum L.) Using Sequence-Specific Nucleases. Front Plant Sci 7, 1045. https://doi.org/10.3389/fpls.2016.01045

Cao, Z., Sun, W., Qiao, D., Wang, J., Li, S., Liu, X., Xin, C., Lu, Y., Gul, S.L., Wang, X.-C., Chen, Q.-J., 2024. PE6c greatly enhances prime editing in transgenic rice plants. Journal of Integrative Plant Biology 66, 1864–1870. https://doi.org/10.1111/jipb.13738

Capdeville, N., Schindele, P., Puchta, H., 2024. Increasing deletion sizes and the efficiency of CRISPR/Cas9-mediated mutagenesis by SunTag-mediated TREX1 recruitment. The Plant Journal 118, 277–287. https://doi.org/10.1111/tpj.16586

Capdeville, N., Schindele, P., Puchta, H., 2023. Getting better all the time — recent progress in the development of CRISPR/Cas-based tools for plant genome engineering. Current Opinion in Biotechnology 79, 102854. https://doi.org/10.1016/j.copbio.2022.102854

Cardi, T., Murovec, J., Bakhsh, A., Boniecka, J., Bruegmann, T., Bull, S.E., Eeckhaut, T., Fladung, M., Galovic, V., Linkiewicz, A., Lukan, T., Mafra, I., Michalski, K., Kavas, M., Nicolia, A., Nowakowska, J., Sági, L., Sarmiento, C., Yıldırım, K., Zlatković, M., Hensel, G., Van Laere, K., 2023. CRISPR/Cas-mediated plant genome editing: outstanding challenges a decade after implementation. Trends in Plant Science 28, 1144–1165. https://doi.org/10.1016/j.tplants.2023.05.012

Ceccaldi, R., Cejka, P., 2025. Mechanisms and regulation of DNA end resection in the maintenance of genome stability. Nat Rev Mol Cell Biol 26, 586–599. https://doi.org/10.1038/s41580-025-00841-4

Čermák, T., Baltes, N.J., Čegan, R., Zhang, Y., Voytas, D.F., 2015. High-frequency, precise modification of the tomato genome. Genome Biol 16, 232. https://doi.org/10.1186/s13059-015-0796-9

Certo, M.T., Gwiazda, K.S., Kuhar, R., Sather, B., Curinga, G., Mandt, T., Brault, M., Lambert, A.R., Baxter, S.K., Jacoby, K., Ryu, B.Y., Kiem, H.-P., Gouble, A., Paques, F., Rawlings, D.J., Scharenberg, A.M., 2012. Coupling endonucleases with DNA end–processing enzymes to drive gene disruption. Nat Methods 9, 973–975. https://doi.org/10.1038/nmeth.2177

Chang, A.K., Duggleby, R.G., 1998. Herbicide-resistant forms of Arabidopsis thaliana acetohydroxyacid synthase: characterization of the catalytic properties and sensitivity to inhibitors of four defined mutants. Biochem J 333 (Pt 3), 765–777. https://doi.org/10.1042/bj3330765

Chang, H.H.Y., Pannunzio, N.R., Adachi, N., Lieber, M.R., 2017. Non-homologous DNA end joining and alternative pathways to double-strand break repair. Nat Rev Mol Cell Biol 18, 495–506. https://doi.org/10.1038/nrm.2017.48

Chang, H.H.Y., Watanabe, G., Gerodimos, C.A., Ochi, T., Blundell, T.L., Jackson, S.P., Lieber, M.R., 2016. Different DNA End Configurations Dictate Which NHEJ Components Are Most Important for Joining Efficiency. J Biol Chem 291, 24377–24389. https://doi.org/10.1074/jbc.M116.752329

Chapman, J.R., Taylor, M.R.G., Boulton, S.J., 2012. Playing the End Game: DNA Double-Strand Break Repair Pathway Choice. Molecular Cell 47, 497–510. https://doi.org/10.1016/j.molcel.2012.07.029

Charbonnel, C., Gallego, M.E., White, C.I., 2010. Xrcc1-dependent and Ku-dependent DNA double-strand break repair kinetics in Arabidopsis plants. The Plant Journal 64, 280–290. https://doi.org/10.1111/j.1365-313X.2010.04331.x

Chatterjee, N., Walker, G.C., 2017. Mechanisms of DNA damage, repair and mutagenesis. Environ Mol Mutagen 58, 235–263. https://doi.org/10.1002/em.22087

Chen, H., Lisby, M., Symington, L.S., 2013. RPA Coordinates DNA End Resection and Prevents Formation of DNA Hairpins. Molecular Cell 50, 589–600. https://doi.org/10.1016/j.molcel.2013.04.032

Chen, H., Neubauer, M., Wang, J.P., 2022. Enhancing HR Frequency for Precise Genome Editing in Plants. Front. Plant Sci. 13. https://doi.org/10.3389/fpls.2022.883421

Chen, J., Li, S., He, Y., Li, J., Xia, L., 2022. An update on precision genome editing by homology-directed repair in plants. Plant Physiol 188, 1780–1794. https://doi.org/10.1093/plphys/kiac037

Chen, K., Wang, Y., Zhang, R., Zhang, H., Gao, C., 2019. CRISPR/Cas Genome Editing and Precision Plant Breeding in Agriculture. Annual Review of Plant Biology 70, 667–697. https://doi.org/10.1146/annurev-arplant-050718-100049

Chen, R.-D., Yang, Y., Liu, K.-M., Hu, J.-Z., Feng, Y.-L., Yang, C.-Y., Jiang, R.-R., Liu, S.-C., Wang, Y., Han, P.-A., Tian, R.-G., Wang, Y.-L., Xu, S.-M., Xie, A.-Y., 2025. Post-cleavage target residence determines asymmetry in non-homologous end joining of Cas12a-induced DNA double strand breaks. Genome Biol 26, 96. https://doi.org/10.1186/s13059-025-03567-w

Chen, S.H., Plank, J.L., Willcox, S., Griffith, J.D., Hsieh, T., 2014. Top3α Is Required during the Convergent Migration Step of Double Holliday Junction Dissolution. PLoS One 9, e83582. https://doi.org/10.1371/journal.pone.0083582

Chen, X., Zaro, J., Shen, W.-C., 2013. Fusion Protein Linkers: Property, Design and Functionality. Adv Drug Deliv Rev 65, 1357–1369. https://doi.org/10.1016/j.addr.2012.09.039

Chiolo, I., Altmeyer, M., Legube, G., Mekhail, K., 2025. Nuclear and genome dynamics underlying DNA double-strand break repair. Nat Rev Mol Cell Biol 26, 538–557. https://doi.org/10.1038/s41580-025-00828-1

Choi, J., Chen, W., Suiter, C.C., Lee, C., Chardon, F.M., Yang, W., Leith, A., Daza, R.M., Martin, B., Shendure, J., 2022. Precise genomic deletions using paired prime editing. Nat Biotechnol 40, 218–226. https://doi.org/10.1038/s41587-021-01025-z

Chung, Y.-T., Hsu, W., 1996. Functional expression of the bovine herpesvirus 1 alkaline deoxyribonuclease (UL12) inEscherichia coli. Archives of Virology 141, 2457–2464. https://doi.org/10.1007/BF01718643

Chylinski, K., Le Rhun, A., Charpentier, E., 2013. The tracrRNA and Cas9 families of type II CRISPR-Cas immunity systems. RNA Biology 10, 726–737. https://doi.org/10.4161/rna.24321

Clement, K., Rees, H., Canver, M.C., Gehrke, J.M., Farouni, R., Hsu, J.Y., Cole, M.A., Liu, D.R., Joung, J.K., Bauer, D.E., Pinello, L., 2019. CRISPResso2 provides accurate and rapid genome editing sequence analysis | Nature Biotechnology [WWW Document]. URL https://www.nature.com/articles/s41587-019-0032-3 (accessed 10.20.25).

Clements, T.P., Tandon, B., Lintel, H.A., McCarty, J.H., Wagner, D.S., 2017. RICE CRISPR: Rapidly increased cut ends by an exonuclease Cas9 fusion in zebrafish. genesis 55, e23044. https://doi.org/10.1002/dvg.23044

Clough, S.J., Bent, A.F., 1998. Floral dip: a simplified method for Agrobacterium-mediated transformation of Arabidopsis thaliana. Plant J 16, 735–743. https://doi.org/10.1046/j.1365-313x.1998.00343.x

Comai, L., Tan, E.H., 2019. Haploid Induction and Genome Instability. Trends in Genetics 35, 791–803. https://doi.org/10.1016/j.tig.2019.07.005

Conant, D., Hsiau, T., Rossi, N., Oki, J., Maures, T., Waite, K., Yang, J., Joshi, S., Kelso, R., Holden, K., Enzmann, B.L., Stoner, R., 2022. Inference of CRISPR Edits from Sanger Trace Data. CRISPR J 5, 123–130. https://doi.org/10.1089/crispr.2021.0113

Dahan-Meir, T., Filler-Hayut, S., Melamed-Bessudo, C., Bocobza, S., Czosnek, H., Aharoni, A., Levy, A.A., 2018. Efficient in planta gene targeting in tomato using geminiviral replicons and the CRISPR/Cas9 system. The Plant Journal 95, 5–16. https://doi.org/10.1111/tpj.13932

Davey, M.R., 2009. Advances in haploid production in higher plants. Ann Bot 104, x. https://doi.org/10.1093/aob/mcp248

De Saeger, J., Park, J., Chung, H.S., Hernalsteens, J.-P., Van Lijsebettens, M., Inzé, D., Van Montagu, M., Depuydt, S., 2021. *Agrobacterium* strains and strain improvement: Present and outlook. Biotechnology Advances 53, 107677. https://doi.org/10.1016/j.biotechadv.2020.107677

de Wind, N., Dekker, M., Berns, A., Radman, M., te Riele, H., 1995. Inactivation of the mouse Msh2 gene results in mismatch repair deficiency, methylation tolerance, hyperrecombination, and predisposition to cancer. Cell 82, 321–330. https://doi.org/10.1016/0092-8674(95)90319-4

Deltcheva, E., Chylinski, K., Sharma, C.M., Gonzales, K., Chao, Y., Pirzada, Z.A., Eckert, M.R., Vogel, J., Charpentier, E., 2011. CRISPR RNA maturation by trans-encoded small RNA and host factor RNase III. Nature 471, 602–607. https://doi.org/10.1038/nature09886

Demidov, D., Lermontova, I., Moebes, M., Kochevenko, A., Fuchs, J., Weiss, O., Rutten, T., Sorge, E., Zuljan, E., Giehl, R.F.H., Mascher, M., Somasundaram, S., Conrad, U., Houben, A., 2022. Haploid induction by nanobody-targeted ubiquitin-proteasome-based degradation of EYFP-tagged CENH3 in Arabidopsis thaliana. J Exp Bot 73, 7243–7254. https://doi.org/10.1093/jxb/erac359

Deng, S.K., Gibb, B., de Almeida, M.J., Greene, E.C., Symington, L.S., 2014. RPA antagonizes microhomology-mediated repair of DNA double-strand breaks. Nat Struct Mol Biol 21, 405–412. https://doi.org/10.1038/nsmb.2786

Dong, H., Huang, Y., Wang, K., 2021. The Development of Herbicide Resistance Crop Plants Using CRISPR/Cas9-Mediated Gene Editing. Genes 12. https://doi.org/10.3390/genes12060912

Dorn, A., Röhrig, S., Papp, K., Schröpfer, S., Hartung, F., Knoll, A., Puchta, H., 2018. The topoisomerase 3α zinc-finger domain T1 of Arabidopsis thaliana is required for targeting the enzyme activity to Holliday junction-like DNA repair intermediates. PLoS Genet 14, e1007674. https://doi.org/10.1371/journal.pgen.1007674

Doudna, J.A., Charpentier, E., 2014. The new frontier of genome engineering with CRISPR-Cas9. Science 346, 1258096. https://doi.org/10.1126/science.1258096

Dunwell, J.M., 2010. Haploids in flowering plants: origins and exploitation. Plant Biotechnology Journal 8, 377–424. https://doi.org/10.1111/j.1467-7652.2009.00498.x

Edwards, K., Johnstone, C., Thompson, C., 1991. A simple and rapid method for the preparation of plant genomic DNA for PCR analysis. Nucleic Acids Res 19, 1349. https://doi.org/10.1093/nar/19.6.1349

Eid, A., Alshareef, S., Mahfouz, M.M., 2018. CRISPR base editors: genome editing without double-stranded breaks. Biochem J 475, 1955–1964. https://doi.org/10.1042/BCJ20170793

Endo, A., Masafumi, M., Kaya, H., Toki, S., 2016. Efficient targeted mutagenesis of rice and tobacco genomes using Cpf1 from Francisella novicida. Sci Rep 6, 38169. https://doi.org/10.1038/srep38169

Endo, M., Mikami, M., Toki, S., 2016. Biallelic Gene Targeting in Rice. Plant Physiology 170, 667–677. https://doi.org/10.1104/pp.15.01663

Eschbach, V., Kobbe, D., 2014. Different Replication Protein A Complexes of Arabidopsis thaliana Have Different DNA-Binding Properties as a Function of Heterotrimer Composition. Plant Cell Physiol 55, 1460–1472. https://doi.org/10.1093/pcp/pcu076

Even-Faitelson, L., Samach, A., Melamed-Bessudo, C., Avivi-Ragolsky, N., Levy, A.A., 2011. Localized egg-cell expression of effector proteins for targeted modification of the Arabidopsis genome. Plant J 68, 929–937. https://doi.org/10.1111/j.1365-313X.2011.04741.x

Evenson, R.E., Gollin, D., 2003. Assessing the Impact of the Green Revolution, 1960 to 2000. Science 300, 758–762. https://doi.org/10.1126/science.1078710

Fauser, F., Roth, N., Pacher, M., Ilg, G., Sánchez-Fernández, R., Biesgen, C., Puchta, H., 2012. *In planta* gene targeting. Proc. Natl. Acad. Sci. U.S.A. 109, 7535–7540. https://doi.org/10.1073/pnas.1202191109

Fauser, F., Schiml, S., Puchta, H., 2014. Both CRISPR/Cas-based nucleases and nickases can be used efficiently for genome engineering in Arabidopsis thaliana. The Plant Journal 79, 348–359. https://doi.org/10.1111/tpj.12554

Feng, W., Peng, H., Xu, J., Liu, Y., Pabbaraju, K., Tipples, G., Joyce, M.A., Saffran, H.A., Tyrrell, D.L., Babiuk, S., Zhang, H., Le, X.C., 2021. Integrating Reverse Transcription Recombinase Polymerase Amplification with CRISPR Technology for the One-Tube Assay of RNA. Anal Chem 93, 12808–12816. https://doi.org/10.1021/acs.analchem.1c03456

Feng, Z., Scott, S.P., Bussen, W., Sharma, G.G., Guo, G., Pandita, T.K., Powell, S.N., 2011. Rad52 inactivation is synthetically lethal with BRCA2 deficiency. Proceedings of the National Academy of Sciences 108, 686–691. https://doi.org/10.1073/pnas.1010959107

Fonfara, I., Richter, H., Bratovič, M., Le Rhun, A., Charpentier, E., 2016. The CRISPR-associated DNA-cleaving enzyme Cpf1 also processes precursor CRISPR RNA. Nature 532, 517–521. https://doi.org/10.1038/nature17945

Forster, B.P., Heberle-Bors, E., Kasha, K.J., Touraev, A., 2007. The resurgence of haploids in higher plants. Trends in Plant Science 12, 368–375. https://doi.org/10.1016/j.tplants.2007.06.007

Forster, B.P., Thomas, W.T.B., 2005. Doubled Haploids in Genetics and Plant Breeding, in: Plant Breeding Reviews. John Wiley & Sons, Ltd, pp. 57–88. https://doi.org/10.1002/9780470650301.ch3

Freese, N.H., Norris, D.C., Loraine, A.E., 2016. Integrated genome browser: visual analytics platform for genomics. Bioinformatics 32, 2089–2095. https://doi.org/10.1093/bioinformatics/btw069

Gaillochet, C., Peña Fernández, A., Goossens, V., D'Halluin, K., Drozdzecki, A., Shafie, M., Van Duyse, J., Van Isterdael, G., Gonzalez, C., Vermeersch, M., De Saeger, J., Develtere, W., Audenaert, D., De Vleesschauwer, D., Meulewaeter, F., Jacobs, T.B., 2023. Systematic optimization of Cas12a base editors in wheat and maize using the ITER platform. Genome Biol 24, 6. https://doi.org/10.1186/s13059-022-02836-2

Gallagher, D.N., Pham, N., Tsai, A.M., Janto, N.V., Choi, J., Ira, G., Haber, J.E., 2020. A Rad51-independent pathway promotes single-strand template repair in gene editing. PLOS Genetics 16, e1008689. https://doi.org/10.1371/journal.pgen.1008689

Gao, C., 2018. The future of CRISPR technologies in agriculture. Nat Rev Mol Cell Biol 19, 275–276. https://doi.org/10.1038/nrm.2018.2

Garcia, M.D., Nouwens, A., Lonhienne, T.G., Guddat, L.W., 2017. Comprehensive understanding of acetohydroxyacid synthase inhibition by different herbicide families. Proceedings of the National Academy of Sciences 114, E1091–E1100. https://doi.org/10.1073/pnas.1616142114

Garcia, V., Phelps, S.E.L., Gray, S., Neale, M.J., 2011. Bidirectional resection of DNA double-strand breaks by Mre11 and Exo1. Nature 479, 241–244. https://doi.org/10.1038/nature10515

Gasiunas, G., Barrangou, R., Horvath, P., Siksnys, V., 2012. Cas9–crRNA ribonucleoprotein complex mediates specific DNA cleavage for adaptive immunity in bacteria. Proc Natl Acad Sci U S A 109, E2579–E2586. https://doi.org/10.1073/pnas.1208507109

Gaudelli, N.M., Komor, A.C., Rees, H.A., Packer, M.S., Badran, A.H., Bryson, D.I., Liu, D.R., 2017. Programmable base editing of A•T to G•C in genomic DNA without DNA cleavage. Nature 551, 464–471. https://doi.org/10.1038/nature24644

Gehrke, F., Schindele, A., Puchta, H., 2021. Nonhomologous end joining as key to CRISPR/Cas-mediated plant chromosome engineering. Plant Physiol 188, 1769–1779. https://doi.org/10.1093/plphys/kiab572

Gibson, B.A., Kraus, W.L., 2012. New insights into the molecular and cellular functions of poly(ADP-ribose) and PARPs. Nat Rev Mol Cell Biol 13, 411–424. https://doi.org/10.1038/nrm3376

Gilles, L.M., Martinant, J.-P., Rogowsky, P.M., Widiez, T., 2017. Haploid induction in plants. Current Biology 27, R1095–R1097. https://doi.org/10.1016/j.cub.2017.07.055

Gnügge, R., Symington, L.S., 2021. DNA end resection during homologous recombination. Current Opinion in Genetics & Development, Mechanisms of Homologous Recombination 71, 99–105. https://doi.org/10.1016/j.gde.2021.07.004

González, M.N., Salaria, N., Friberg, M., Liu, Y., Alverup, J., Andersson, M., Hofvander, P., 2025. Single-stranded DNA (ssDNA) donor repair templates and CRISPR/Cas9 enable a high-frequency of targeted insertions in potato. Front. Genome Ed. 7. https://doi.org/10.3389/fgeed.2025.1661829

Götzke, H., Kilisch, M., Martínez-Carranza, M., Sograte-Idrissi, S., Rajavel, A., Schlichthaerle, T., Engels, N., Jungmann, R., Stenmark, P., Opazo, F., Frey, S., 2019. The ALFA-tag is a highly versatile tool for nanobody-based bioscience applications. Nat Commun 10, 4403. https://doi.org/10.1038/s41467-019-12301-7

Gronenborn, A.M., Filpula, D.R., Essig, N.Z., Achari, A., Whitlow, M., Wingfield, P.T., Clore, G.M., 1991. A novel, highly stable fold of the immunoglobulin binding domain of streptococcal protein G. Science 253, 657–661. https://doi.org/10.1126/science.1871600

Guha, S., Maheshwari, S.C., 1964. In vitro Production of Embryos from Anthers of Datura. Nature 204, 497–497. https://doi.org/10.1038/204497a0

Gupta, D., Bhattacharjee, O., Mandal, D., Sen, M.K., Dey, D., Dasgupta, A., Kazi, T.A., Gupta, R., Sinharoy, S., Acharya, K., Chattopadhyay, D., Ravichandiran, V., Roy, S., Ghosh, D., 2019. CRISPR-Cas9 system: A new-fangled dawn in gene editing. Life Sci 232, 116636. https://doi.org/10.1016/j.lfs.2019.116636

Gurel, F., Wu, Y., Pan, C., Cheng, Y., Li, G., Zhang, T., Qi, Y., 2023. On- and Off-Target Analyses of CRISPR-Cas12b Genome Editing Systems in Rice. The CRISPR Journal 6, 62–74. https://doi.org/10.1089/crispr.2022.0072

Gürel, F., Zhang, Y., Sretenovic, S., Qi, Y., 2020. CRISPR-Cas nucleases and base editors for plant genome editing: CRISPR-Cas nucleases and base editors for plant genome editing. aBIOTECH 1, 74–87. https://doi.org/10.1007/s42994-019-00010-0

Hackley, C.R., 2021. A Novel Set of Cas9 Fusion Proteins to Stimulate Homologous Recombination: Cas9-HRs. The CRISPR Journal 4, 253–263. https://doi.org/10.1089/crispr.2020.0034

Haft, D.H., Selengut, J., Mongodin, E.F., Nelson, K.E., 2005. A guild of 45 CRISPR-associated (Cas) protein families and multiple CRISPR/Cas subtypes exist in prokaryotic genomes. PLoS Comput Biol 1, e60. https://doi.org/10.1371/journal.pcbi.0010060

Hajiahmadi, Z., Movahedi, A., Wei, H., Li, D., Orooji, Y., Ruan, H., Zhuge, Q., 2019. Strategies to Increase On-Target and Reduce Off-Target Effects of the CRISPR/Cas9 System in Plants. International Journal of Molecular Sciences 20. https://doi.org/10.3390/ijms20153719

Han, F., Zhang, X., Liu, Yuxiang, Liu, Yumei, Zhao, H., Li, Z., 2024. One-step creation of CMS lines using a BoCENH3-based haploid induction system in Brassica crop. Nat. Plants 10, 581–586. https://doi.org/10.1038/s41477-024-01643-w

Hanin, M., Volrath, S., Bogucki, A., Briker, M., Ward, E., Paszkowski, J., 2001. Gene targeting in Arabidopsis. The Plant Journal 28, 671–677. https://doi.org/10.1046/j.1365-313x.2001.01183.x

Hartung, F., Suer, S., Knoll, A., Wurz-Wildersinn, R., Puchta, H., 2008. Topoisomerase 3alpha and RMI1 suppress somatic crossovers and are essential for resolution of meiotic recombination intermediates in Arabidopsis thaliana. PLoS Genet 4, e1000285. https://doi.org/10.1371/journal.pgen.1000285

He, Y., Mudgett, M., Zhao, Y., 2022. Advances in gene editing without residual transgenes in plants. Plant Physiol 188, 1757–1768. https://doi.org/10.1093/plphys/kiab574

Hermans, P.W., van Soolingen, D., Bik, E.M., de Haas, P.E., Dale, J.W., van Embden, J.D., 1991. Insertion element IS987 from Mycobacterium bovis BCG is located in a hot-spot integration region for insertion elements in Mycobacterium tuberculosis complex strains. Infect Immun 59, 2695–2705. https://doi.org/10.1128/iai.59.8.2695-2705.1991

Hess, G.T., Tycko, J., Yao, D., Bassik, M.C., 2017. Methods and Applications of CRISPR-Mediated Base Editing in Eukaryotic Genomes. Molecular Cell 68, 26–43. https://doi.org/10.1016/j.molcel.2017.09.029

Hillary, V.E., Ceasar, S.A., 2023. A Review on the Mechanism and Applications of CRISPR/Cas9/Cas12/Cas13/Cas14 Proteins Utilized for Genome Engineering. Mol Biotechnol 65, 311–325. https://doi.org/10.1007/s12033-022-00567-0

Horlbeck, M.A., Witkowsky, L.B., Guglielmi, B., Replogle, J.M., Gilbert, L.A., Villalta, J.E., Torigoe, S.E., Tjian, R., Weissman, J.S., 2016. Nucleosomes impede Cas9 access to DNA in vivo and in vitro. eLife 5, e12677. https://doi.org/10.7554/eLife.12677

Höss, M., Robins, P., Naven, T.J., Pappin, D.J., Sgouros, J., Lindahl, T., 1999. A human DNA editing enzyme homologous to the Escherichia coli DnaQ/MutD protein. EMBO J 18, 3868–3875. https://doi.org/10.1093/emboj/18.13.3868

Hu, X., Wang, C., Liu, Q., Fu, Y., Wang, K., 2017. Targeted mutagenesis in rice using CRISPR-Cpf1 system. Journal of Genetics and Genomics 44, 71–73. https://doi.org/10.1016/j.jgg.2016.12.001

Huang, T., Armstrong, B., Schindele, P., Puchta, H., 2021. Efficient gene targeting in *Nicotiana tabacum* using CRISPR/SaCas9 and temperature tolerant LbCas12a. Plant Biotechnology Journal 19, 1314–1324. https://doi.org/10.1111/pbi.13546

Huang, T.-K., Puchta, H., 2019. CRISPR/Cas-mediated gene targeting in plants: finally a turn for the better for homologous recombination. Plant Cell Rep 38, 443–453. https://doi.org/10.1007/s00299-019-02379-0

Hwang, H.-Y., Gim, D., Yi, H., Jung, H., Lee, J., Kim, D., 2024. Precise editing of pathogenic nucleotide repeat expansions in iPSCs using paired prime editor. Nucleic Acids Res 52, 5792–5803. https://doi.org/10.1093/nar/gkae310

Hwarari, D., Radani, Y., Ke, Y., Chen, J., Yang, L., 2024. CRISPR/Cas genome editing in plants: mechanisms, applications, and overcoming bottlenecks. Funct Integr Genomics 24, 50. https://doi.org/10.1007/s10142-024-01314-1

Ishii, T., Karimi-Ashtiyani, R., Houben, A., 2016. Haploidization via Chromosome Elimination: Means and Mechanisms. Annual Review of Plant Biology 67, 421–438. https://doi.org/10.1146/annurev-arplant-043014-114714

Ishino, Y., Shinagawa, H., Makino, K., Amemura, M., Nakata, A., 1987. Nucleotide sequence of the iap gene, responsible for alkaline phosphatase isozyme conversion in Escherichia coli, and identification of the gene product. Journal of Bacteriology 169, 5429–5433. https://doi.org/10.1128/jb.169.12.5429-5433.1987

Jacquier, N.M.A., Gilles, L.M., Pyott, D.E., Martinant, J.-P., Et., A., 2020. Puzzling out plant reproduction by haploid induction for innovations in plant breeding. Nature Plants. https://doi.org/10.1038/s41477-020-0664-9

Jansen, R., Embden, J.D.A. van, Gaastra, W., Schouls, L.M., 2002. Identification of genes that are associated with DNA repeats in prokaryotes. Mol Microbiol 43, 1565–1575. https://doi.org/10.1046/j.1365-2958.2002.02839.x

Jia, Q., Bundock, P., Hooykaas, P.J.J., de Pater, S., 2012. Agrobacterium tumefaciens T-DNA Integration and Gene Targeting in Arabidopsis thaliana Non-Homologous End-Joining Mutants. Journal of Botany 2012, 989272. https://doi.org/10.1155/2012/989272

Jiang, C., Sun, J., Li, R., Yan, S., Chen, W., Guo, L., Qin, G., Wang, P., Luo, C., Huang, W., Zhang, Q., Fernie, A.R., Jackson, D., Li, X., Yan, J., 2022. A reactive oxygen species burst causes haploid induction in maize. Molecular Plant 15, 943–955. https://doi.org/10.1016/j.molp.2022.04.001

Jiang, F., Doudna, J.A., 2017. CRISPR–Cas9 Structures and Mechanisms. Annual Review of Biophysics 46, 505–529. https://doi.org/10.1146/annurev-biophys-062215-010822

Jiang, F., Doudna, J.A., 2015. The structural biology of CRISPR-Cas systems. Curr Opin Struct Biol 30, 100–111. https://doi.org/10.1016/j.sbi.2015.02.002

Jiang, T., Zhang, X.-O., Weng, Z., Xue, W., 2022. Deletion and replacement of long genomic sequences using prime editing. Nat Biotechnol 40, 227–234. https://doi.org/10.1038/s41587-021-01026-y

Jiang, W., Feng, S., Huang, S., Yu, W., Li, G., Yang, G., Liu, Y., Zhang, Y., Zhang, L., Hou, Y., Chen, Jia, Chen, Jieping, Huang, X., 2018. BE-PLUS: a new base editing tool with broadened editing window and enhanced fidelity. Cell Res 28, 855–861. https://doi.org/10.1038/s41422-018-0052-4

Jiang, Y., Chai, Y., Qiao, D., Wang, J., Xin, C., Sun, W., Cao, Z., Zhang, Y., Zhou, Y., Wang, X.-C., Chen, Q.-J., 2022. Optimized prime editing efficiently generates glyphosate-resistant rice plants carrying homozygous TAP-IVS mutation in *EPSPS*. Molecular Plant 15, 1646–1649. https://doi.org/10.1016/j.molp.2022.09.006

Jin, C., Sun, L., Trinh, H.K., Danny, G., 2023. Heat stress promotes haploid formation during CENH3-mediated genome elimination in Arabidopsis. Plant Reprod 36, 147–155. https://doi.org/10.1007/s00497-023-00457-8

Jinek, M., Chylinski, K., Fonfara, I., Hauer, M., Doudna, J.A., Charpentier, E., 2012. A Programmable Dual-RNA–Guided DNA Endonuclease in Adaptive Bacterial Immunity. Science 337, 816–821. https://doi.org/10.1126/science.1225829

Ju Shin, Y., Kyun Park, S., Jung Jung, Y., Na Kim, Y., Sung Kim, K., Kyu Park, O., Kwon, S.-H., Ho Jeon, S., Trinh, L.A., Fraser, S.E., Kee, Y., Joon Hwang, B., 2015. Nanobody-targeted E3-ubiquitin ligase complex degrades nuclear proteins. Sci Rep 5, 14269. https://doi.org/10.1038/srep14269

Kalinowska, K., Chamas, S., Unkel, K., Demidov, D., Lermontova, I., Dresselhaus, T., Kumlehn, J., Dunemann, F., Houben, A., 2019. State-of-the-art and novel developments of in vivo haploid technologies. Theor Appl Genet 132, 593–605. https://doi.org/10.1007/s00122-018-3261-9

Kalter, N., Fuster-García, C., Silva, A., Ronco-Díaz, V., Roncelli, S., Turchiano, G., Gorodkin, J., Cathomen, T., Benabdellah, K., Lee, C., Hendel, A., 2025. Off-target effects in CRISPR-Cas genome editing for human therapeutics: Progress and challenges. Molecular Therapy Nucleic Acids 36, 102636. https://doi.org/10.1016/j.omtn.2025.102636

Kamoen, L., de Bruin, D.A., Kralemann, L.E.M., Roos, K., Wildhagen, M.M.D.A., van Schendel, R., Hooykaas, P.J.J., de Pater, S., Tijsterman, M., 2025. Division of labor within polymerase theta in repair of CRISPR-induced DNA breaks in Arabidopsis thaliana. PNAS Nexus 4, pgaf183. https://doi.org/10.1093/pnasnexus/pgaf183

Karanam, K., Kafri, R., Loewer, A., Lahav, G., 2012. Quantitative live cell imaging reveals a gradual shift between DNA repair mechanisms and a maximal use of HR in mid S phase. Mol Cell 47, 320–329. https://doi.org/10.1016/j.molcel.2012.05.052

Katayama, Y., 1934. Haploid Formation by X-rays in Triticum monococcum. CYTOLOGIA 5. https://doi.org/10.1508/cytologia.5.235

Kelliher, T., Starr, D., Su, X., Tang, G., Chen, Z., Carter, J., Wittich, P.E., Dong, S., Green, J., Burch, E., McCuiston, J., Gu, W., Sun, Y., Strebe, T., Roberts, J., Bate, N.J., Que, Q., 2019. One-step genome editing of elite crop germplasm during haploid induction. Nat Biotechnol 37, 287–292. https://doi.org/10.1038/s41587-019-0038-x

Kelliher, T., Starr, D., Wang, W., McCuiston, J., Zhong, H., Nuccio, M., Martin, B., 2016. Maternal Haploids Are Preferentially Induced by CENH3-tailswap Transgenic Complementation in Maize. Frontiers in Plant Science 7. https://doi.org/10.3389/fpls.2016.00414

Kent, T., Mateos-Gomez, P.A., Sfeir, A., Pomerantz, R.T., 2016. Polymerase θ is a robust terminal transferase that oscillates between three different mechanisms during end-joining. eLife 5, e13740. https://doi.org/10.7554/eLife.13740

Khan, H., Ochi, T., 2023. Plant PAXX has an XLF-like function and stimulates DNA end joining by the Ku-DNA ligase IV/XRCC4 complex. The Plant Journal 116, 58–68. https://doi.org/10.1111/tpj.16359

Kieffer, S.R., Lowndes, N.F., 2022. Immediate-Early, Early, and Late Responses to DNA Double Stranded Breaks. Front Genet 13, 793884. https://doi.org/10.3389/fgene.2022.793884

Knoll, A., Fauser, F., Puchta, H., 2014a. DNA recombination in somatic plant cells: mechanisms and evolutionary consequences. Chromosome Res 22, 191–201. https://doi.org/10.1007/s10577-014-9415-y

Knoll, A., Schröpfer, S., Puchta, H., 2014b. The RTR complex as caretaker of genome stability and its unique meiotic function in plants. Front Plant Sci 5, 33. https://doi.org/10.3389/fpls.2014.00033

Kölreuter, J.G., 1761. D. Joseph Gottlieb Kölreuters Vorläufige Nachricht von einigen das Geschlecht der Pflanzen betreffenden Versuchen und Beobachtungen [WWW Document]. -, Kölreuter, Joseph Gottlieb: D. Joseph Gottlieb Kölreuters Vorläufige Nachricht von einigen das Geschlecht der Pflanzen betreffenden Versuchen und Beobachtungen, -: Gleditsch -. URL https://haab-digital.klassik-stiftung.de/viewer/toc/3571520300/1/ (accessed 11.16.25).

Komor, A.C., Badran, A.H., Liu, D.R., 2018. Editing the Genome Without Double-Stranded DNA Breaks. ACS Chem Biol 13, 383–388. https://doi.org/10.1021/acschembio.7b00710

Komor, A.C., Kim, Y.B., Packer, M.S., Zuris, J.A., Liu, D.R., 2016. Programmable editing of a target base in genomic DNA without double-stranded DNA cleavage. Nature 533, 420–424. https://doi.org/10.1038/nature17946

Koncz, C., Schell, J., 1986. The promoter of TL-DNA gene 5 controls the tissue-specific expression of chimaeric genes carried by a novel type of Agrobacterium binary vector. Molec Gen Genet 204, 383–396. https://doi.org/10.1007/BF00331014

Kosicki, M., Allen, F., Steward, F., Tomberg, K., Pan, Y., Bradley, A., 2022. Cas9-induced large deletions and small indels are controlled in a convergent fashion. Nat Commun 13, 3422. https://doi.org/10.1038/s41467-022-30480-8

Kozak, J., West, C.E., White, C., da Costa-Nunes, J.A., Angelis, K.J., 2009. Rapid repair of DNA double strand breaks in *Arabidopsis thaliana* is dependent on proteins involved in chromosome structure maintenance. DNA Repair 8, 413–419. https://doi.org/10.1016/j.dnarep.2008.11.012

Krenning, L., Berg, J. van den, Medema, R.H., 2019. Life or Death after a Break: What Determines the Choice? Molecular Cell 76, 346–358. https://doi.org/10.1016/j.molcel.2019.08.023

Krishna, T.P.A., Veeramuthu, D., Maharajan, T., Soosaimanickam, M., 2023. The Era of Plant Breeding: Conventional Breeding to Genomics-assisted Breeding for Crop Improvement. Curr Genomics 24, 24–35. https://doi.org/10.2174/1389202924666230517115912

Kuang, Y., Li, S., Ren, B., Yan, F., Spetz, C., Li, X., Zhou, X., Zhou, H., 2020. Base-Editing-Mediated Artificial Evolution of *OsALS1 In Planta* to Develop Novel Herbicide-Tolerant Rice Germplasms. Molecular Plant 13, 565–572. https://doi.org/10.1016/j.molp.2020.01.010

Kumar, R., Das, S.P., Choudhury, B.U., Kumar, A., Prakash, N.R., Verma, R., Chakraborti, M., Devi, A.G., Bhattacharjee, B., Das, R., Das, Bapi, Devi, H.L., Das, Biswajit, Rawat, S., Mishra, V.K., 2024. Advances in genomic tools for plant breeding: harnessing DNA molecular markers, genomic selection, and genome editing. Biol Res 57, 80. https://doi.org/10.1186/s40659-024-00562-6

Kuppu, S., Ron, M., Marimuthu, M.P.A., Li, G., Huddleson, A., Siddeek, M.H., Terry, J., Buchner, R., Shabek, N., Comai, L., Britt, A.B., 2020. A variety of changes, including CRISPR/Cas9-mediated deletions, in CENH3 lead to haploid induction on outcrossing. Plant Biotechnology Journal 18, 2068–2080. https://doi.org/10.1111/pbi.13365

Kweon, J., Hwang, H.-Y., Ryu, H., Jang, A.-H., Kim, D., Kim, Y., 2023. Targeted genomic translocations and inversions generated using a paired prime editing strategy. Molecular Therapy 31, 249–259. https://doi.org/10.1016/j.ymthe.2022.09.008

Lainšček, D., Forstnerič, V., Mikolič, V., Malenšek, Š., Pečan, P., Benčina, M., Sever, M., Podgornik, H., Jerala, R., 2022. Coiled-coil heterodimer-based recruitment of an exonuclease to CRISPR/Cas for enhanced gene editing. Nat Commun 13, 3604. https://doi.org/10.1038/s41467-022-31386-1

LaRossa, R.A., Schloss, J.V., 1984. The sulfonylurea herbicide sulfometuron methyl is an extremely potent and selective inhibitor of acetolactate synthase in Salmonella typhimurium. Journal of Biological Chemistry 259, 8753–8757. https://doi.org/10.1016/S0021-9258(17)47217-6

Laxa, M., 2017. Intron-Mediated Enhancement: A Tool for Heterologous Gene Expression in Plants? Front. Plant Sci. 7. https://doi.org/10.3389/fpls.2016.01977

Lee, J., Kweon, J., Kim, Y., 2025. Emerging trends in prime editing for precision genome editing. Exp Mol Med 57, 1381–1391. https://doi.org/10.1038/s12276-025-01463-8

Lee, J.-H., Paull, T.T., 2004. Direct Activation of the ATM Protein Kinase by the Mre11/Rad50/Nbs1 Complex. Science 304, 93–96. https://doi.org/10.1126/science.1091496

Li, B., Sun, C., Li, J., Gao, C., 2024. Targeted genome-modification tools and their advanced applications in crop breeding. Nat Rev Genet 25, 603–622. https://doi.org/10.1038/s41576-024-00720-2

Li, C., Zhang, R., Meng, X., Chen, S., Zong, Y., Lu, C., Qiu, J.-L., Chen, Y.-H., Li, J., Gao, C., 2020a. Targeted, random mutagenesis of plant genes with dual cytosine and adenine base editors. Nat Biotechnol 38, 875–882. https://doi.org/10.1038/s41587-019-0393-7

Li, C., Zhu, H., Jin, S., Maksoud, L.M., Jain, N., Sun, J., Gao, Y., 2023. Structural basis of DNA polymerase θ mediated DNA end joining. Nucleic Acids Res 51, 463–474. https://doi.org/10.1093/nar/gkac1201

Li, C., Zong, Y., Jin, S., Zhu, H., Lin, D., Li, S., Qiu, J.-L., Wang, Y., Gao, C., 2020b. SWISS: multiplexed orthogonal genome editing in plants with a Cas9 nickase and engineered CRISPR RNA scaffolds. Genome Biol 21, 141. https://doi.org/10.1186/s13059-020-02051-x

Li, T., Wang, C., Pan, J., Tabusam, J., Li, Y., Yao, J., Chen, W., Wang, Y., Gao, W., Rong, J., Ahmad, Z., Houben, A., Zhu, S., Jin, S., Zhang, Y., 2025. Exploring potential strategies for haploid induction based on double fertilization in plants. Plant Biotechnology Journal 23, 4000–4016. https://doi.org/10.1111/pbi.70197

Li, T., Yang, X., Yu, Y., Si, X., Zhai, X., Zhang, H., Dong, W., Gao, C., Xu, C., 2018. Domestication of wild tomato is accelerated by genome editing. Nat Biotechnol 36, 1160–1163. https://doi.org/10.1038/nbt.4273

Li, X., Wang, Y., Liu, Y., Yang, B., Wang, X., Wei, J., Lu, Z., Zhang, Y., Wu, J., Huang, X., Yang, L., Chen, J., 2018. Base editing with a Cpf1–cytidine deaminase fusion. Nat Biotechnol 36, 324–327. https://doi.org/10.1038/nbt.4102

Li, Y., Li, S., Li, C., Zhang, C., Yan, L., Li, J., He, Y., Guo, Y., Lin, Y., Zhang, Y., Xia, L., 2023. Engineering a plant A-to-K base editor with improved performance by fusion with a transactivation module. Plant Communications, Focus Issue on Climate Change and Food Security: Plant Science Roles 4, 100667. https://doi.org/10.1016/j.xplc.2023.100667

Liang, Z., Chen, K., Li, T., Zhang, Y., Wang, Y., Zhao, Q., Liu, J., Zhang, H., Liu, C., Ran, Y., Gao, C., 2017. Efficient DNA-free genome editing of bread wheat using CRISPR/Cas9 ribonucleoprotein complexes. Nat Commun 8, 14261. https://doi.org/10.1038/ncomms14261

Liao, H., Wu, J., VanDusen, N.J., Li, Y., Zheng, Y., 2024. CRISPR-Cas9-mediated homology-directed repair for precise gene editing. Mol Ther Nucleic Acids 35, 102344. https://doi.org/10.1016/j.omtn.2024.102344

Lieber, M.R., 2010. The Mechanism of Double-Strand DNA Break Repair by the Nonhomologous DNA End-Joining Pathway. Annual Review of Biochemistry 79, 181–211. https://doi.org/10.1146/annurev.biochem.052308.093131

Lieber, M.R., Ma, Y., Pannicke, U., Schwarz, K., 2003. Mechanism and regulation of human non-homologous DNA end-joining. Nat Rev Mol Cell Biol 4, 712–720. https://doi.org/10.1038/nrm1202

Lin, Q., Jin, S., Zong, Y., Yu, H., Zhu, Z., Liu, G., Kou, L., Wang, Y., Qiu, J.-L., Li, J., Gao, C., 2021. High-efficiency prime editing with optimized, paired pegRNAs in plants. Nat Biotechnol 39, 923–927. https://doi.org/10.1038/s41587-021-00868-w

Lin, Q., Zong, Y., Xue, C., Wang, S., Jin, S., Zhu, Z., Wang, Y., Anzalone, A.V., Raguram, A., Doman, J.L., Liu, D.R., Gao, C., 2020a. Prime genome editing in rice and wheat. Nat Biotechnol 38, 582–585. https://doi.org/10.1038/s41587-020-0455-x

Lin, Q., Zong, Y., Xue, C., Wang, S., Jin, S., Zhu, Z., Wang, Y., Anzalone, A.V., Raguram, A., Doman, J.L., Liu, D.R., Gao, C., 2020b. Prime genome editing in rice and wheat. Nat Biotechnol 38, 582–585. https://doi.org/10.1038/s41587-020-0455-x

Lindahl, T., Barnes, D.E., Yang, Y.-G., Robins, P., 2009. Biochemical properties of mammalian TREX1 and its association with DNA replication and inherited inflammatory disease. Biochem Soc Trans 37, 535–538. https://doi.org/10.1042/BST0370535

Liu, J., Liang, D., Yao, L., Zhang, Y., Liu, C., Liu, Y., Wang, Y., Zhou, H., Kelliher, T., Zhang, X., Bandyopadhyay, A., 2021. Rice Haploid Inducer Development by Genome Editing, in: Bandyopadhyay, A., Thilmony, R. (Eds.), Rice Genome Engineering and Gene Editing: Methods and Protocols. Springer US, New York, NY, pp. 221–230. https://doi.org/10.1007/978-1-0716-1068-8_14

Liu, L., Zhang, Z., Wang, C., Yan, F., Sun, W., Zhou, X., Miao, W., Zhou, H., 2024. Developing guanine base editors for G-to-T editing in rice. Journal of Integrative Plant Biology 66, 1557–1560. https://doi.org/10.1111/jipb.13729

Liu, X., Gu, D., Zhang, Y., Jiang, Y., Xiao, Z., Xu, R., Qin, R., Li, J., Wei, P., 2024. Conditional knockdown of OsMLH1 to improve plant prime editing systems without disturbing fertility in rice. Genome Biol 25, 131. https://doi.org/10.1186/s13059-024-03282-y

Lonhienne, T., Low, Y.S., Garcia, M.D., Croll, T., Gao, Y., Wang, Q., Brillault, L., Williams, C.M., Fraser, J.A., McGeary, R.P., West, N.P., Landsberg, M.J., Rao, Z., Schenk, G., Guddat, L.W., 2020. Structures of fungal and plant acetohydroxyacid synthases. Nature 586, 317–321. https://doi.org/10.1038/s41586-020-2514-3

Loureiro, A., da Silva, G.J., 2019. CRISPR-Cas: Converting A Bacterial Defence Mechanism into A State-of-the-Art Genetic Manipulation Tool. Antibiotics (Basel) 8, 18. https://doi.org/10.3390/antibiotics8010018

Loveless, A., 1958. Increased Rate of Plaque-type and Host-range Mutation following Treatment of Bacteriophage in vitro with Ethyl Methane Sulphonate. Nature 181, 1212–1213. https://doi.org/10.1038/1811212a0

Lowder, L.G., Zhang, D., Baltes, N.J., Paul, J.W., Tang, X., Zheng, X., Voytas, D.F., Hsieh, T.-F., Zhang, Y., Qi, Y., 2015. A CRISPR/Cas9 Toolbox for Multiplexed Plant Genome Editing and Transcriptional Regulation. Plant Physiol 169, 971–985. https://doi.org/10.1104/pp.15.00636

Lv, J., Yu, K., Wei, J., Gui, H., Liu, C., Liang, D., Wang, Y., Zhou, H., Carlin, R., Rich, R., Lu, T., Que, Q., Wang, W.C., Zhang, X., Kelliher, T., 2020. Generation of paternal haploids in wheat by genome editing of the centromeric histone CENH3. Nat Biotechnol 38, 1397–1401. https://doi.org/10.1038/s41587-020-0728-4

Lyndaker, A.M., Alani, E., 2009. A Tale of Tails: Insights into the Coordination of 3′ End Processing during Homologous Recombination. Bioessays 31, 315–321. https://doi.org/10.1002/bies.200800195

Ma, C.J., Kwon, Y., Sung, P., Greene, E.C., 2017. Human RAD52 interactions with replication protein A and the RAD51 presynaptic complex. Journal of Biological Chemistry 292, 11702–11713. https://doi.org/10.1074/jbc.M117.794545

Makarova, K.S., Haft, D.H., Barrangou, R., Brouns, S.J.J., Charpentier, E., Horvath, P., Moineau, S., Mojica, F.J.M., Wolf, Y.I., Yakunin, A.F., van der Oost, J., Koonin, E.V., 2011. Evolution and classification of the CRISPR–Cas systems. Nat Rev Microbiol 9, 467–477. https://doi.org/10.1038/nrmicro2577

Makarova, K.S., Shmakov, S.A., Wolf, Y.I., Mutz, P., Altae-Tran, H., Beisel, C.L., Brouns, S.J.J., Charpentier, E., Cheng, D., Doudna, J., Haft, D.H., Horvath, P., Moineau, S., Mojica, F.J.M., Pausch, P., Pinilla-Redondo, R., Shah, S.A., Siksnys, V., Terns, M.P., Tordoff, J., Venclovas, Č., White, M.F., Yakunin, A.F., Zhang, F., Garrett, R.A., Backofen, R., van der Oost, J., Barrangou, R., Koonin, E.V., 2025. An updated evolutionary classification of CRISPR–Cas systems including rare variants. Nat Microbiol 10, 3346–3361. https://doi.org/10.1038/s41564-025-02180-8

Makarova, K.S., Wolf, Y.I., Alkhnbashi, O.S., Costa, F., Shah, S.A., Saunders, S.J., Barrangou, R., Brouns, S.J.J., Charpentier, E., Haft, D.H., Horvath, P., Moineau, S., Mojica, F.J.M., Terns, R.M., Terns, M.P., White, M.F., Yakunin, A.F., Garrett, R.A., van der Oost, J., Backofen, R., Koonin, E.V., 2015. An updated evolutionary classification of CRISPR-Cas systems. Nat Rev Microbiol 13, 722–736. https://doi.org/10.1038/nrmicro3569

Makarova, K.S., Wolf, Y.I., Iranzo, J., Shmakov, S.A., Alkhnbashi, O.S., Brouns, S.J.J., Charpentier, E., Cheng, D., Haft, D.H., Horvath, P., Moineau, S., Mojica, F.J.M., Scott, D., Shah, S.A., Siksnys, V., Terns, M.P., Venclovas, Č., White, M.F., Yakunin, A.F., Yan, W., Zhang, F.,

Garrett, R.A., Backofen, R., Van Der Oost, J., Barrangou, R., Koonin, E.V., 2020. Evolutionary classification of CRISPR–Cas systems: a burst of class 2 and derived variants. Nat Rev Microbiol 18, 67–83. https://doi.org/10.1038/s41579-019-0299-x

Makarova, K.S., Wolf, Y.I., Koonin, E.V., 2022. Evolutionary Classification of CRISPR-Cas Systems, in: Crispr. John Wiley & Sons, Ltd, pp. 13–38. https://doi.org/10.1002/9781683673798.ch2

Makharashvili, N., Tubbs, A.T., Yang, S.-H., Wang, H., Barton, O., Zhou, Y., Deshpande, R.A., Lee, J.-H., Lobrich, M., Sleckman, B.P., Wu, X., Paull, T.T., 2014. Catalytic and Noncatalytic Roles of the CtIP Endonuclease in Double-Strand Break End Resection. Molecular Cell 54, 1022–1033. https://doi.org/10.1016/j.molcel.2014.04.011

Malik, H.S., Henikoff, S., 2003. Phylogenomics of the nucleosome. Nat Struct Mol Biol 10, 882–891. https://doi.org/10.1038/nsb996

Maluszynski, M., Kasha, K.J., Forster, B.P., Szarejko, I. (Eds.), 2003. Doubled Haploid Production in Crop Plants: A Manual. Springer Netherlands, Dordrecht. https://doi.org/10.1007/978-94-017-1293-4

Malzahn, A.A., Tang, X., Lee, K., Ren, Q., Sretenovic, S., Zhang, Yingxiao, Chen, H., Kang, M., Bao, Y., Zheng, X., Deng, K., Zhang, T., Salcedo, V., Wang, K., Zhang, Yong, Qi, Y., 2019. Application of CRISPR-Cas12a temperature sensitivity for improved genome editing in rice, maize, and Arabidopsis. BMC Biol 17, 9. https://doi.org/10.1186/s12915-019-0629-5

Manape, T.K., Satheesh, V., Somasundaram, S., Soumia, P.S., Khade, Y.P., Mainkar, P., Mahajan, V., Singh, M., Anandhan, S., 2024. RNAi-mediated downregulation of AcCENH3 can induce in vivo haploids in onion (Allium cepa L.). Sci Rep 14, 14481. https://doi.org/10.1038/s41598-024-64432-7

Mao, Y., Botella, J.R., Liu, Y., Zhu, J.-K., 2019. Gene editing in plants: progress and challenges. Natl Sci Rev 6, 421–437. https://doi.org/10.1093/nsr/nwz005

Mao, Z., Bozzella, M., Seluanov, A., Gorbunova, V., 2008. Comparison of nonhomologous end joining and homologous recombination in human cells. DNA Repair 7, 1765–1771. https://doi.org/10.1016/j.dnarep.2008.06.018

Mari, P.-O., Florea, B.I., Persengiev, S.P., Verkaik, N.S., Brüggenwirth, H.T., Modesti, M., Giglia-Mari, G., Bezstarosti, K., Demmers, J.A.A., Luider, T.M., Houtsmuller, A.B., van Gent, D.C., 2006. Dynamic assembly of end-joining complexes requires interaction between Ku70/80 and XRCC4. Proceedings of the National Academy of Sciences 103, 18597–18602. https://doi.org/10.1073/pnas.0609061103

Marks, J.D., Hoogenboom, H.R., Bonnert, T.P., McCafferty, J., Griffiths, A.D., Winter, G., 1991. By-passing immunization. Human antibodies from V-gene libraries displayed on phage. J Mol Biol 222, 581–597. https://doi.org/10.1016/0022-2836(91)90498-u

Mathur, D.S., Aman, M.A., Sarkar, K.R., 1980. Induction of Maternal Haploids in Maize Through Heat Treatment of Pollen. Current Science 49, 744–746.

Mazur, D.J., Perrino, F.W., 2001. Excision of 3′ Termini by the Trex1 and TREX2 3′→5′ Exonucleases: CHARACTERIZATION OF THE RECOMBINANT PROTEINS*. Journal of Biological Chemistry 276, 17022–17029. https://doi.org/10.1074/jbc.M100623200

McCarty, N.S., Graham, A.E., Studená, L., Ledesma-Amaro, R., 2020. Multiplexed CRISPR technologies for gene editing and transcriptional regulation. Nat Commun 11, 1281. https://doi.org/10.1038/s41467-020-15053-x

Mendel, G., 1866. Versuche über Pflanzen-Hybriden, 1. Auflage. ed, Verhandlungen des Naturforschenden Vereines in Brünn. Naturforschender Verein, Brünn.

Meng, X., Hu, X., Liu, Q., Song, X., Gao, C., Li, J., Wang, K., 2018. Robust genome editing of CRISPR-Cas9 at NAG PAMs in rice. Sci. China Life Sci. 61, 122–125. https://doi.org/10.1007/s11427-017-9247-9

Merker, L., Feller, L., Dorn, A., Puchta, H., 2024. Deficiency of both classical and alternative end-joining pathways leads to a synergistic defect in double-strand break repair but not to an increase in homology-dependent gene targeting in Arabidopsis. The Plant Journal 118, 242–254. https://doi.org/10.1111/tpj.16604

Merker, L., Schindele, P., Huang, T.-K., Wolter, F., Puchta, H., 2020a. Enhancing in planta gene targeting efficiencies in Arabidopsis using temperature-tolerant CRISPR/LbCas12a. Plant Biotechnol J 18, 2382–2384. https://doi.org/10.1111/pbi.13426

Merker, L., Schindele, P., Puchta, H., 2020b. Using CRISPR/tt *Lb* Cas12a for *in planta* Gene Targeting in *A. thaliana*. CP Plant Biology 5, e20117. https://doi.org/10.1002/cppb.20117

Mikami, M., Toki, S., Endo, M., 2016. Precision Targeted Mutagenesis via Cas9 Paired Nickases in Rice. Plant Cell Physiol 57, 1058–1068. https://doi.org/10.1093/pcp/pcw049

Miki, D., Zhang, W., Zeng, W., Feng, Z., Zhu, J.-K., 2018. CRISPR/Cas9-mediated gene targeting in Arabidopsis using sequential transformation. Nat Commun 9, 1967. https://doi.org/10.1038/s41467-018-04416-0

Mimitou, E.P., Symington, L.S., 2009. DNA end resection: many nucleases make light work. DNA Repair (Amst) 8, 983–995. https://doi.org/10.1016/j.dnarep.2009.04.017

Mimori, T., Hardin, J.A., 1986. Mechanism of interaction between Ku protein and DNA. Journal of Biological Chemistry 261, 10375–10379. https://doi.org/10.1016/S0021-9258(18)67534-9

Miyazaki, T., Kim, Y.-S., Yoon, J., Wang, H., Suzuki, T., Morse, H.C., 2014. The 3'-5' DNA exonuclease TREX1 directly interacts with poly(ADP-ribose) polymerase-1 (PARP1) during the DNA damage response. J Biol Chem 289, 32548–32558. https://doi.org/10.1074/jbc.M114.547331

Mojica, F.J.M., Díez-Villaseñor, C., Soria, E., Juez, G., 2000. Biological significance of a family of regularly spaced repeats in the genomes of Archaea, Bacteria and mitochondria. Molecular Microbiology 36, 244–246. https://doi.org/10.1046/j.1365-2958.2000.01838.x

Molinier, J., Stamm, M.-E., Hohn, B., 2004. SNM-dependent recombinational repair of oxidatively induced DNA damage in Arabidopsis thaliana. EMBO Rep 5, 994–999. https://doi.org/10.1038/sj.embor.7400256

Moreno-Mateos, M.A., Fernandez, J.P., Rouet, R., Vejnar, C.E., Lane, M.A., Mis, E., Khokha, M.K., Doudna, J.A., Giraldez, A.J., 2017. CRISPR-Cpf1 mediates efficient homology-directed repair and temperature-controlled genome editing. Nat Commun 8, 2024. https://doi.org/10.1038/s41467-017-01836-2

Muller, H.J., 1927. Artificial Transmutation of the Gene. Science 66, 84–87. https://doi.org/10.1126/science.66.1699.84

Naeem, M., Alkhnbashi, O.S., 2023. Current Bioinformatics Tools to Optimize CRISPR/Cas9 Experiments to Reduce Off-Target Effects. Int J Mol Sci 24, 6261. https://doi.org/10.3390/ijms24076261

Nakata, A., Amemura, M., Makino, K., 1989. Unusual nucleotide arrangement with repeated sequences in the Escherichia coli K-12 chromosome. J Bacteriol 171, 3553–3556. https://doi.org/10.1128/jb.171.6.3553-3556.1989

Nelson, J.W., Randolph, P.B., Shen, S.P., Everette, K.A., Chen, P.J., Anzalone, A.V., An, M., Newby, G.A., Chen, J.C., Hsu, A., Liu, D.R., 2022. Engineered pegRNAs improve prime editing efficiency. Nat Biotechnol 40, 402–410. https://doi.org/10.1038/s41587-021-01039-7

Neugebauer, M.E., Hsu, A., Arbab, M., Krasnow, N.A., McElroy, A.N., Pandey, S., Doman, J.L., Huang, T.P., Raguram, A., Banskota, S., Newby, G.A., Tolar, J., Osborn, M.J., Liu, D.R., 2023. Evolution of an adenine base editor into a small, efficient cytosine base editor with low off-target activity. Nat Biotechnol 41, 673–685. https://doi.org/10.1038/s41587-022-01533-6

Newsom, S., Parameshwaran, H.P., Martin, L., Rajan, R., 2021. The CRISPR-Cas Mechanism for Adaptive Immunity and Alternate Bacterial Functions Fuels Diverse Biotechnologies. Front. Cell. Infect. Microbiol. 10. https://doi.org/10.3389/fcimb.2020.619763

Ni, P., Zhao, Y., Zhou, X., Liu, Z., Huang, Z., Ni, Z., Sun, Q., Zong, Y., 2023. Efficient and versatile multiplex prime editing in hexaploid wheat. Genome Biol 24, 156. https://doi.org/10.1186/s13059-023-02990-1

Nick McElhinny, S.A., Snowden, C.M., McCarville, J., Ramsden, D.A., 2000. Ku Recruits the XRCC4-Ligase IV Complex to DNA Ends. Molecular and Cellular Biology 20, 2996–3003. https://doi.org/10.1128/MCB.20.9.2996-3003.2000

Nishimasu, H., Cong, L., Yan, W.X., Ran, F.A., Zetsche, B., Li, Y., Kurabayashi, A., Ishitani, R., Zhang, F., Nureki, O., 2015. Crystal Structure of Staphylococcus aureus Cas9. Cell 162, 1113–1126. https://doi.org/10.1016/j.cell.2015.08.007

Nishimasu, H., Ran, F.A., Hsu, P.D., Konermann, S., Shehata, S.I., Dohmae, N., Ishitani, R., Zhang, F., Nureki, O., 2014. Crystal structure of Cas9 in complex with guide RNA and target DNA. Cell 156, 935–949. https://doi.org/10.1016/j.cell.2014.02.001

Nishizawa-Yokoi, A., Nonaka, S., Saika, H., Kwon, Y.-I., Osakabe, K., Toki, S., 2012. Suppression of Ku70/80 or Lig4 leads to decreased stable transformation and enhanced homologous recombination in rice. New Phytologist 196, 1048–1059. https://doi.org/10.1111/j.1469-8137.2012.04350.x

Offringa, R., de Groot, M.J., Haagsman, H.J., Does, M.P., van den Elzen, P.J., Hooykaas, P.J., 1990. Extrachromosomal homologous recombination and gene targeting in plant cells after Agrobacterium mediated transformation. EMBO J 9, 3077–3084. https://doi.org/10.1002/j.1460-2075.1990.tb07504.x

Ordon, J., Kiel, N., Becker, D., Kretschmer, C., Schulze-Lefert, P., Stuttmann, J., 2023. Targeted gene deletion with SpCas9 and multiple guide RNAs in Arabidopsis thaliana: four are better than two. Plant Methods 19, 30. https://doi.org/10.1186/s13007-023-01010-4

Pan, W., Zhu, Y., Li, P., Li, Z., Xu, C., Jin, M., Tang, X., 2026. Natural and artificial evolution of acetolactate synthase for crop breeding. The Crop Journal 14, 95–106. https://doi.org/10.1016/j.cj.2025.04.014

Park, J., Lim, K., Kim, J.-S., Bae, S., 2017. Cas-analyzer: an online tool for assessing genome editing results using NGS data. Bioinformatics 33, 286–288. https://doi.org/10.1093/bioinformatics/btw561

Paszkowski, J., Baur, M., Bogucki, A., Potrykus, I., 1988. Gene targeting in plants. EMBO J 7, 4021–4026. https://doi.org/10.1002/j.1460-2075.1988.tb03295.x

Paul, B., Montoya, G., 2020. CRISPR-Cas12a: Functional overview and applications. Biomedical Journal 43, 8–17. https://doi.org/10.1016/j.bj.2019.10.005

Pédelacq, J.-D., Cabantous, S., Tran, T., Terwilliger, T.C., Waldo, G.S., 2006. Engineering and characterization of a superfolder green fluorescent protein. Nat Biotechnol 24, 79–88. https://doi.org/10.1038/nbt1172

Piatek, A., Ali, Z., Baazim, H., Li, L., Abulfaraj, A., Al-Shareef, S., Aouida, M., Mahfouz, M.M., 2015. RNA-guided transcriptional regulation in planta via synthetic dCas9-based transcription factors. Plant Biotechnology Journal 13, 578–589. https://doi.org/10.1111/pbi.12284

Pingali, P.L., 2012. Green Revolution: Impacts, limits, and the path ahead [WWW Document]. https://doi.org/10.1073/pnas.0912953109

Puchta, H., 1998. Repair of genomic double-strand breaks in somatic plant cells by one-sided invasion of homologous sequences. The Plant Journal 13, 331–339. https://doi.org/10.1046/j.1365-313X.1998.00035.x

Puchta, H., Dujon, B., Hohn, B., 1996. Two different but related mechanisms are used in plants for the repair of genomic double-strand breaks by homologous recombination. Proceedings of the National Academy of Sciences 93, 5055–5060. https://doi.org/10.1073/pnas.93.10.5055

Puchta, H., Dujon, B., Hohn, B., 1993. Homologous recombination in plant cells is enhanced by in vivo induction of double strand breaks into DNA by a site-specific endonuclease. Nucleic Acids Res 21, 5034–5040. https://doi.org/10.1093/nar/21.22.5034

Puchta, H., Hohn, B., 1991a. The mechanism of extrachromosomal homologous DNA recombination in plant cells. Molec. Gen. Genet. 230, 1–7. https://doi.org/10.1007/BF00290641

Puchta, H., Hohn, B., 1991b. A transient assay in plant cells reveals a positive correlation between extrachromosomal recombination rates and length of homologous overlap. Nucleic Acids Research 19, 2693–2700. https://doi.org/10.1093/nar/19.10.2693

Qi, L.S., Larson, M.H., Gilbert, L.A., Doudna, J.A., Weissman, J.S., Arkin, A.P., Lim, W.A., 2013. Repurposing CRISPR as an RNA-Guided Platform for Sequence-Specific Control of Gene Expression. Cell 152, 1173–1183. https://doi.org/10.1016/j.cell.2013.02.022

Qi, Y., Zhang, Y., Zhang, F., Baller, J.A., Cleland, S.C., Ryu, Y., Starker, C.G., Voytas, D.F., 2013. Increasing frequencies of site-specific mutagenesis and gene targeting in Arabidopsis by manipulating DNA repair pathways. Genome Res 23, 547–554. https://doi.org/10.1101/gr.145557.112

Qu, Y., Fernie, A.R., Liu, J., Yan, J., 2024. Doubled haploid technology and synthetic apomixis: Recent advances and applications in future crop breeding. Molecular Plant 17, 1005–1018. https://doi.org/10.1016/j.molp.2024.06.005

Quiroz, L.F., Gondalia, N., Brychkova, G., McKeown, P.C., Spillane, C., 2024. Haploid rhapsody: the molecular and cellular orchestra of in vivo haploid induction in plants. New Phytologist 241, 1936–1949. https://doi.org/10.1111/nph.19523

Ran, F.A., Cong, L., Yan, W.X., Scott, D.A., Gootenberg, J.S., Kriz, A.J., Zetsche, B., Shalem, O., Wu, X., Makarova, K.S., Koonin, E.V., Sharp, P.A., Zhang, F., 2015. In vivo genome editing using Staphylococcus aureus Cas9. Nature 520, 186–191. https://doi.org/10.1038/nature14299

Ran, F.A., Hsu, P.D., Lin, C.-Y., Gootenberg, J.S., Konermann, S., Trevino, A.E., Scott, D.A., Inoue, A., Matoba, S., Zhang, Y., Zhang, F., 2013. Double nicking by RNA-guided CRISPR Cas9 for enhanced genome editing specificity. Cell 154, 1380–1389. https://doi.org/10.1016/j.cell.2013.08.021

Rananaware, S.R., Vesco, E.K., Shoemaker, G.M., Anekar, S.S., Sandoval, L.S.W., Meister, K.S., Macaluso, N.C., Nguyen, L.T., Jain, P.K., 2023. Programmable RNA detection with CRISPR-Cas12a. Nat Commun 14, 5409. https://doi.org/10.1038/s41467-023-41006-1

Rausch, T., Fritz, M.H.-Y., Untergasser, A., Benes, V., 2020. Tracy: basecalling, alignment, assembly and deconvolution of sanger chromatogram trace files. BMC Genomics 21, 230. https://doi.org/10.1186/s12864-020-6635-8

Ravi, M., Chan, S.W.L., 2010. Haploid plants produced by centromere-mediated genome elimination. Nature 464, 615–618. https://doi.org/10.1038/nature08842

Rees, H.A., Liu, D.R., 2018. Base editing: precision chemistry on the genome and transcriptome of living cells. Nat Rev Genet 19, 770–788. https://doi.org/10.1038/s41576-018-0059-1

Renkawitz, J., Lademann, C.A., Kalocsay, M., Jentsch, S., 2013. Monitoring Homology Search during DNA Double-Strand Break Repair In Vivo. Molecular Cell 50, 261–272. https://doi.org/10.1016/j.molcel.2013.02.020

Reuven, N., Adler, J., Broennimann, K., Myers, N., Shaul, Y., 2019. Recruitment of DNA Repair MRN Complex by Intrinsically Disordered Protein Domain Fused to Cas9 Improves Efficiency of CRISPR-Mediated Genome Editing. Biomolecules 9, 584. https://doi.org/10.3390/biom9100584

Reuven, N.B., Staire, A.E., Myers, R.S., Weller, S.K., 2003. The Herpes Simplex Virus Type 1 Alkaline Nuclease and Single-Stranded DNA Binding Protein Mediate Strand Exchange In Vitro. J Virol 77, 7425–7433. https://doi.org/10.1128/JVI.77.13.7425-7433.2003

Robert, I., Dantzer, F., Reina-San-Martin, B., 2009. Parp1 facilitates alternative NHEJ, whereas Parp2 suppresses IgH/c-myc translocations during immunoglobulin class switch recombination. J Exp Med 206, 1047–1056. https://doi.org/10.1084/jem.20082468

Rodgers, K., McVey, M., 2016. Error-Prone Repair of DNA Double-Strand Breaks. Journal of Cellular Physiology 231, 15–24. https://doi.org/10.1002/jcp.25053

Rohatgi, N., Fortin, J.-P., Lau, T., Ying, Y., Zhang, Y., Lee, B.L., Costa, M.R., Reja, R., 2024. Seed sequences mediate off-target activity in the CRISPR-interference system. Cell Genomics 4, 100693. https://doi.org/10.1016/j.xgen.2024.100693

Röhrig, S., Dorn, A., Enderle, J., Schindele, A., Herrmann, N.J., Knoll, A., Puchta, H., 2018. The RecQ-like helicase HRQ1 is involved in DNA crosslink repair in Arabidopsis in a common pathway with the Fanconi anemia-associated nuclease FAN1 and the postreplicative repair ATPase RAD5A. New Phytologist 218, 1478–1490. https://doi.org/10.1111/nph.15109

Rönspies, M., Khosravi, S., Helia, O., Valisi, A., Fajkus, J., Fojtová, M., Houben, A., Puchta, H., 2025. CRISPR-Cas–mediated heritable chromosome fusions in Arabidopsis. Science 390, 843–848. https://doi.org/10.1126/science.adz8505

Rönspies, M., Schindele, P., Wetzel, R., Puchta, H., 2022a. CRISPR–Cas9-mediated chromosome engineering in Arabidopsis thaliana. Nat Protoc 17, 1332–1358. https://doi.org/10.1038/s41596-022-00686-7

Rönspies, M., Schmidt, C., Schindele, P., Lieberman-Lazarovich, M., Houben, A., Puchta, H., 2022b. Massive crossover suppression by CRISPR–Cas-mediated plant chromosome engineering. Nat. Plants 8, 1153–1159. https://doi.org/10.1038/s41477-022-01238-3

Rose, A.B., 2008. Intron-Mediated Regulation of Gene Expression, in: Reddy, A.S.N., Golovkin, M. (Eds.), Nuclear Pre-mRNA Processing in Plants. Springer, Berlin, Heidelberg, pp. 277–290. https://doi.org/10.1007/978-3-540-76776-3_15

Roth, D.B., Wilson, J.H., 1986. Nonhomologous recombination in mammalian cells: role for short sequence homologies in the joining reaction. Mol Cell Biol 6, 4295–4304. https://doi.org/10.1128/mcb.6.12.4295

Salas, T.R., Petruseva, I., Lavrik, O., Bourdoncle, A., Mergny, J.-L., Favre, A., Saintomé, C., 2006. Human replication protein A unfolds telomeric G-quadruplexes. Nucleic Acids Res 34, 4857–4865. https://doi.org/10.1093/nar/gkl564

Salomon, S., Puchta, H., 1998. Capture of genomic and T-DNA sequences during double-strand break repair in somatic plant cells. EMBO J 17, 6086–6095. https://doi.org/10.1093/emboj/17.20.6086

Sartori, A.A., Lukas, C., Coates, J., Mistrik, M., Fu, S., Bartek, J., Baer, R., Lukas, J., Jackson, S.P., 2007. Human CtIP promotes DNA end resection. Nature 450, 509–514. https://doi.org/10.1038/nature06337

Schep, R., Brinkman, E.K., Leemans, C., Vergara, X., van der Weide, R.H., Morris, B., van Schaik, T., Manzo, S.G., Peric-Hupkes, D., van den Berg, J., Beijersbergen, R.L., Medema, R.H., van Steensel, B., 2021. Impact of chromatin context on Cas9-induced DNA double-strand break repair pathway balance. Molecular Cell 81, 2216-2230.e10. https://doi.org/10.1016/j.molcel.2021.03.032

Schiml, S., Fauser, F., Puchta, H., 2014. The CRISPR / C as system can be used as nuclease for *in planta* gene targeting and as paired nickases for directed mutagenesis in A rabidopsis resulting in heritable progeny. The Plant Journal 80, 1139–1150. https://doi.org/10.1111/tpj.12704

Schindele, P., 2020. Etablierung und Optimierung von CRISPR/Cas-Systemen in Pflanzen [WWW Document]. URL https://publikationen.bibliothek.kit.edu/1000127856 (accessed 10.20.25).

Schindele, P., Merker, L., Schreiber, T., Prange, A., Tissier, A., Puchta, H., 2023. Enhancing gene editing and gene targeting efficiencies in *Arabidopsis thaliana* by using an intron-containing version of TT *LB* CAS12A . Plant Biotechnology Journal 21, 457–459. https://doi.org/10.1111/pbi.13964

Schindele, P., Puchta, H., 2020. Engineering CRISPR/LbCas12a for highly efficient, temperature-tolerant plant gene editing. Plant Biotechnol J 18, 1118–1120. https://doi.org/10.1111/pbi.13275

Schmidt, C., Pacher, M., Puchta, H., 2019. Efficient induction of heritable inversions in plant genomes using the CRISPR /Cas system. The Plant Journal 98, 577–589. https://doi.org/10.1111/tpj.14322

Schreiber, T., Prange, A., Schäfer, P., Iwen, T., Grützner, R., Marillonnet, S., Lepage, A., Javelle, M., Paul, W., Tissier, A., 2024. Efficient scar-free knock-ins of several kilobases in plants by engineered CRISPR-Cas endonucleases. Mol Plant 17, 824–837. https://doi.org/10.1016/j.molp.2024.03.013

Schröpfer, S., Kobbe, D., Hartung, F., Knoll, A., Puchta, H., 2014. Defining the roles of the N-terminal region and the helicase activity of RECQ4A in DNA repair and homologous recombination in Arabidopsis. Nucleic Acids Res 42, 1684–1697. https://doi.org/10.1093/nar/gkt1004

Schubert, M.S., Thommandru, B., Woodley, J., Turk, R., Yan, S., Kurgan, G., McNeill, M.S., Rettig, G.R., 2021. Optimized design parameters for CRISPR Cas9 and Cas12a homology-directed repair. Sci Rep 11, 19482. https://doi.org/10.1038/s41598-021-98965-y

Schumacher, A.J., Mohni, K.N., Kan, Y., Hendrickson, E.A., Stark, J.M., Weller, S.K., 2012. The HSV-1 Exonuclease, UL12, Stimulates Recombination by a Single Strand Annealing Mechanism. PLOS Pathogens 8, e1002862. https://doi.org/10.1371/journal.ppat.1002862

Scully, R., Panday, A., Elango, R., Willis, N.A., 2019. DNA double-strand break repair-pathway choice in somatic mammalian cells. Nat Rev Mol Cell Biol 20, 698–714. https://doi.org/10.1038/s41580-019-0152-0

Séguéla-Arnaud, M., Crismani, W., Larchevêque, C., Mazel, J., Froger, N., Choinard, S., Lemhemdi, A., Macaisne, N., Van Leene, J., Gevaert, K., De Jaeger, G., Chelysheva, L., Mercier, R., 2015. Multiple mechanisms limit meiotic crossovers: TOP3α and two BLM homologs antagonize crossovers in parallel to FANCM. Proc Natl Acad Sci U S A 112, 4713–4718. https://doi.org/10.1073/pnas.1423107112

Seol, J.-H., Shim, E.Y., Lee, S.E., 2018. Microhomology-mediated end joining: Good, bad and ugly. Mutation Research/Fundamental and Molecular Mechanisms of Mutagenesis 809, 81–87. https://doi.org/10.1016/j.mrfmmm.2017.07.002

Serra, H., Da Ines, O., Degroote, F., Gallego, M.E., White, C.I., 2013. Roles of XRCC2, RAD51B and RAD51D in RAD51-Independent SSA Recombination. PLoS Genet 9, e1003971. https://doi.org/10.1371/journal.pgen.1003971

Sfeir, A., Symington, L.S., 2015. Microhomology-mediated end joining: a back-up survival mechanism or dedicated pathway? Trends Biochem Sci 40, 701–714. https://doi.org/10.1016/j.tibs.2015.08.006

Sfeir, A., Tijsterman, M., McVey, M., 2024. Microhomology-Mediated End-Joining Chronicles: Tracing the Evolutionary Footprints of Genome Protection. Annu Rev Cell Dev Biol 40, 195–218. https://doi.org/10.1146/annurev-cellbio-111822-014426

Shaked, H., Melamed-Bessudo, C., Levy, A.A., 2005. High-frequency gene targeting in Arabidopsis plants expressing the yeast RAD54 gene. Proceedings of the National Academy of Sciences 102, 12265–12269. https://doi.org/10.1073/pnas.0502601102

Shaner, D.L., Anderson, P.C., Stidham, M.A., 1984. Imidazolinones: potent inhibitors of acetohydroxyacid synthase. Plant Physiol 76, 545–546. https://doi.org/10.1104/pp.76.2.545

Shaul, O., 2017. How introns enhance gene expression. The International Journal of Biochemistry & Cell Biology, Splicing 91, 145–155. https://doi.org/10.1016/j.biocel.2017.06.016

Shi, J., Lai, J., 2015. Patterns of genomic changes with crop domestication and breeding. Current Opinion in Plant Biology 24, 47–53. https://doi.org/10.1016/j.pbi.2015.01.008

Shou, J., Li, J., Liu, Y., Wu, Q., 2018. Precise and Predictable CRISPR Chromosomal Rearrangements Reveal Principles of Cas9-Mediated Nucleotide Insertion. Molecular Cell 71, 498-509.e4. https://doi.org/10.1016/j.molcel.2018.06.021

Slaman, E., Kottenhagen, L., de Martines, W., Angenent, G.C., de Maagd, R.A., 2024. Comparison of Cas12a and Cas9-mediated mutagenesis in tomato cells. Sci Rep 14, 4508. https://doi.org/10.1038/s41598-024-55088-4

Somasundaram, S., Yaşar, S., Fuchs, J., Cuacos, M., Claassen, J., Weiss, O., Kochevenko, A., Lamb, J.C., Li, T., Capdeville, N., Puchta, H., Houben, A., 2026. Targeted CENH3 protein depletion in egg cells enables highly efficient haploid induction. Plant Comm 0. https://doi.org/10.1016/j.xplc.2026.101837

Sprunck, S., Rademacher, S., Vogler, F., Gheyselinck, J., Grossniklaus, U., Dresselhaus, T., 2012. Egg Cell–Secreted EC1 Triggers Sperm Cell Activation During Double Fertilization. Science 338, 1093–1097. https://doi.org/10.1126/science.1223944

Sretenovic, S., Liu, S., Li, G., Cheng, Y., Fan, T., Xu, Y., Zhou, J., Zheng, X., Coleman, G., Zhang, Y., Qi, Y., 2021. Exploring C-To-G Base Editing in Rice, Tomato, and Poplar. Front. Genome Ed. 3. https://doi.org/10.3389/fgeed.2021.756766

Stadler, L.J., 1928. Genetic Effects of X-Rays in Maize. Proc Natl Acad Sci U S A 14, 69–75. https://doi.org/10.1073/pnas.14.1.69

Steinert, J., Schiml, S., Fauser, F., Puchta, H., 2015. Highly efficient heritable plant genome engineering using Cas9 orthologues from Streptococcus thermophilus and Staphylococcus aureus. The Plant Journal 84, 1295–1305. https://doi.org/10.1111/tpj.13078

Stinson, B.M., Loparo, J.J., 2021. Repair of DNA Double-Strand Breaks by the Non-homologous End Joining Pathway. Annu Rev Biochem 90, 137–164. https://doi.org/10.1146/annurev-biochem-080320-110356

Strohkendl, I., Saha, A., Moy, C., Nguyen, A.-H., Ahsan, M., Russell, R., Palermo, G., Taylor, D.W., 2024. Cas12a domain flexibility guides R-loop formation and forces RuvC resetting. Molecular Cell 84, 2717-2731.e6. https://doi.org/10.1016/j.molcel.2024.06.007

Sun, C., Lei, Y., Li, B., Gao, Q., Li, Yunjia, Cao, W., Yang, C., Li, H., Wang, Z., Li, Yan, Wang, Y., Liu, J., Zhao, K.T., Gao, C., 2024. Precise integration of large DNA sequences in plant genomes using PrimeRoot editors. Nat Biotechnol 42, 316–327. https://doi.org/10.1038/s41587-023-01769-w

Sun, Y., Zhang, X., Wu, C., He, Y., Ma, Y., Hou, H., Guo, X., Du, W., Zhao, Y., Xia, L., 2016. Engineering Herbicide-Resistant Rice Plants through CRISPR/Cas9-Mediated Homologous Recombination of Acetolactate Synthase. Molecular Plant 9, 628–631. https://doi.org/10.1016/j.molp.2016.01.001

Sung, P., 1997. Function of Yeast Rad52 Protein as a Mediator between Replication Protein A and the Rad51 Recombinase*. Journal of Biological Chemistry 272, 28194–28197. https://doi.org/10.1074/jbc.272.45.28194

Swarts, D.C., van der Oost, J., Jinek, M., 2017. Structural Basis for Guide RNA Processing and Seed-Dependent DNA Targeting by CRISPR-Cas12a. Molecular Cell 66, 221-233.e4. https://doi.org/10.1016/j.molcel.2017.03.016

Swoboda, P., Gal, S., Hohn, B., Puchta, H., 1994. Intrachromosomal homologous recombination in whole plants. EMBO J 13, 484–489. https://doi.org/10.1002/j.1460-2075.1994.tb06283.x

Symington, L.S., 2016. Mechanism and Regulation of DNA End Resection in Eukaryotes. Crit Rev Biochem Mol Biol 51, 195–212. https://doi.org/10.3109/10409238.2016.1172552

Symington, L.S., Gautier, J., 2011. Double-strand break end resection and repair pathway choice. Annu Rev Genet 45, 247–271. https://doi.org/10.1146/annurev-genet-110410-132435

Szostak, J.W., Orr-Weaver, T.L., Rothstein, R.J., Stahl, F.W., 1983. The double-strand-break repair model for recombination. Cell 33, 25–35. https://doi.org/10.1016/0092-8674(83)90331-8

Talbert, P.B., Henikoff, S., 2020. What makes a centromere? Experimental Cell Research 389, 111895. https://doi.org/10.1016/j.yexcr.2020.111895

Tamura, K., Adachi, Y., Chiba, K., Oguchi, K., Takahashi, H., 2002. Identification of Ku70 and Ku80 homologues in Arabidopsis thaliana: evidence for a role in the repair of DNA double-strand breaks. The Plant Journal 29, 771–781. https://doi.org/10.1046/j.1365-313X.2002.01258.x

Tan, E.H., Henry, I.M., Ravi, M., Bradnam, K.R., Mandakova, T., Marimuthu, M.P., Korf, I., Lysak, M.A., Comai, L., Chan, S.W., 2015. Catastrophic chromosomal restructuring during genome elimination in plants. Elife 4, e06516. https://doi.org/10.7554/eLife.06516

Tan, J., Sun, X., Zhao, H., Guan, H., Gao, S., Zhou, P.-K., 2023. Double-strand DNA break repair: molecular mechanisms and therapeutic targets. MedComm (2020) 4, e388. https://doi.org/10.1002/mco2.388

Tanenbaum, M.E., Gilbert, L.A., Qi, L.S., Weissman, J.S., Vale, R.D., 2014. A Protein-Tagging System for Signal Amplification in Gene Expression and Fluorescence Imaging. Cell 159, 635–646. https://doi.org/10.1016/j.cell.2014.09.039

Tang, X., Lowder, L.G., Zhang, T., Malzahn, A.A., Zheng, X., Voytas, D.F., Zhong, Z., Chen, Y., Ren, Q., Li, Q., Kirkland, E.R., Zhang, Y., Qi, Y., 2017. A CRISPR–Cpf1 system for efficient genome editing and transcriptional repression in plants. Nature Plants 3, 17018. https://doi.org/10.1038/nplants.2017.18

Tao, J., Bauer, D.E., Chiarle, R., 2023. Assessing and advancing the safety of CRISPR-Cas tools: from DNA to RNA editing. Nat Commun 14, 212. https://doi.org/10.1038/s41467-023-35886-6

Tao, R., Wang, Y., Hu, Y., Jiao, Y., Zhou, L., Jiang, L., Li, L., He, X., Li, M., Yu, Y., Chen, Q., Yao, S., 2022a. WT-PE: Prime editing with nuclease wild-type Cas9 enables versatile large-scale genome editing. Sig Transduct Target Ther 7, 108. https://doi.org/10.1038/s41392-022-00936-w

Tao, R., Wang, Y., Jiao, Y., Hu, Y., Li, L., Jiang, L., Zhou, L., Qu, J., Chen, Q., Yao, S., 2022b. Bi-PE: bi-directional priming improves CRISPR/Cas9 prime editing in mammalian cells. Nucleic Acids Res 50, 6423–6434. https://doi.org/10.1093/nar/gkac506

Terns, M.P., Terns, R.M., 2011. CRISPR-Based Adaptive Immune Systems. Curr Opin Microbiol 14, 321–327. https://doi.org/10.1016/j.mib.2011.03.005

Toh, M., Ngeow, J., 2021. Homologous Recombination Deficiency: Cancer Predispositions and Treatment Implications. Oncologist 26, e1526–e1537. https://doi.org/10.1002/onco.13829

Tuncel, A., Pan, C., Clem, J.S., Liu, D., Qi, Y., 2025. CRISPR–Cas applications in agriculture and plant research. Nat Rev Mol Cell Biol 26, 419–441. https://doi.org/10.1038/s41580-025-00834-3

Uanschou, C., Siwiec, T., Pedrosa-Harand, A., Kerzendorfer, C., Sanchez-Moran, E., Novatchkova, M., Akimcheva, S., Woglar, A., Klein, F., Schlögelhofer, P., 2007. A novel plant gene essential for meiosis is related to the human CtIP and the yeast COM1/SAE2 gene. EMBO J 26, 5061–5070. https://doi.org/10.1038/sj.emboj.7601913

ViennaRNA Web Services [WWW Document], n.d. URL http://rna.tbi.univie.ac.at/ (accessed 4.14.26).

Voytas, D.F., 2013. Plant Genome Engineering with Sequence-Specific Nucleases. Annual Review of Plant Biology 64, 327–350. https://doi.org/10.1146/annurev-arplant-042811-105552

Voytas, D.F., Gao, C., 2014. Precision Genome Engineering and Agriculture: Opportunities and Regulatory Challenges. PLOS Biology 12, e1001877. https://doi.org/10.1371/journal.pbio.1001877

Vu, T.V., Nguyen, N.T., Kim, J., Song, Y.J., Nguyen, T.H., Kim, J.-Y., 2024. Optimized dicot prime editing enables heritable desired edits in tomato and Arabidopsis. Nat. Plants 10, 1502–1513. https://doi.org/10.1038/s41477-024-01786-w

Vu, T.V., Sivankalyani, V., Kim, E.-J., Doan, D.T.H., Tran, M.T., Kim, J., Sung, Y.W., Park, M., Kang, Y.J., Kim, J.-Y., 2020. Highly efficient homology-directed repair using CRISPR/Cpf1-

geminiviral replicon in tomato. Plant Biotechnology Journal 18, 2133–2143. https://doi.org/10.1111/pbi.13373

Wang, B., Zhu, L., Zhao, B., Zhao, Y., Xie, Y., Zheng, Z., Li, Y., Sun, J., Wang, H., 2019. Development of a Haploid-Inducer Mediated Genome Editing System for Accelerating Maize Breeding. Molecular Plant 12, 597–602. https://doi.org/10.1016/j.molp.2019.03.006

Wang, G., Zong, M., Han, S., Zhao, H., Duan, M., Liu, X., Guo, N., Liu, F., 2024. In vivo haploid induction in cauliflower, kale, and broccoli. Journal of Integrative Plant Biology 66, 1823–1826. https://doi.org/10.1111/jipb.13730

Wang, J., He, Z., Wang, G., Zhang, R., Duan, J., Gao, P., Lei, X., Qiu, H., Zhang, C., Zhang, Y., Yin, H., 2022. Efficient targeted insertion of large DNA fragments without DNA donors. Nat Methods 19, 331–340. https://doi.org/10.1038/s41592-022-01399-1

Wang, M., Lu, Y., Botella, J.R., Mao, Y., Hua, K., Zhu, J.-K., 2017. Gene Targeting by Homology-Directed Repair in Rice Using a Geminivirus-Based CRISPR/Cas9 System. Mol Plant 10, 1007–1010. https://doi.org/10.1016/j.molp.2017.03.002

Wang, N., Dawe, R.K., 2018. Centromere Size and Its Relationship to Haploid Formation in Plants. Molecular Plant, Genome Biology 11, 398–406. https://doi.org/10.1016/j.molp.2017.12.009

Wang, N., Gent, J.I., Dawe, R.K., 2021. Haploid induction by a maize cenh3 null mutant. Sci Adv 7, eabe2299. https://doi.org/10.1126/sciadv.abe2299

Wang, X., Clem, J., Malzahn, A., Qi, Y., 2025. Increasing Cas12a- and Cas9-mediated deletion sizes with exonucleases. Plant Physiol 199, kiaf507. https://doi.org/10.1093/plphys/kiaf507

Wang, Z., Chen, M., Yang, H., Hu, Z., Yu, Y., Xu, H., Yan, S., Yi, K., Li, J., 2023. A simple and highly efficient strategy to induce both paternal and maternal haploids through temperature manipulation. Nat. Plants 9, 699–705. https://doi.org/10.1038/s41477-023-01389-x

Wang, Z.-P., Xing, H.-L., Dong, L., Zhang, H.-Y., Han, C.-Y., Wang, X.-C., Chen, Q.-J., 2015. Egg cell-specific promoter-controlled CRISPR/Cas9 efficiently generates homozygous mutants for multiple target genes in Arabidopsis in a single generation. Genome Biol 16, 144. https://doi.org/10.1186/s13059-015-0715-0

Waters, C.A., Strande, N.T., Pryor, J.M., Strom, C., Mieczkowski, P., Burkhalter, M.D., Oh, S., Qaqish, B.F., Moore, D.T., Hendrickson, E.A., Ramsden, D.A., 2014. The fidelity of the ligation step determines how ends are resolved during Nonhomologous end joining. Nat Commun 5, 4286. https://doi.org/10.1038/ncomms5286

Weiss, T., Crisp, P.A., Rai, K.M., Song, M., Springer, N.M., Zhang, F., 2022. Epigenetic features drastically impact CRISPR–Cas9 efficacy in plants. Plant Physiol 190, 1153–1164. https://doi.org/10.1093/plphys/kiac285

Weiss, T., Wang, C., Kang, X., Zhao, H., Gamo, M.E., Starker, C.G., Crisp, P.A., Zhou, P., Springer, N.M., Voytas, D.F., Zhang, F., 2020. Optimization of multiplexed CRISPR/Cas9 system for highly efficient genome editing in Setaria viridis. The Plant Journal 104, 828–838. https://doi.org/10.1111/tpj.14949

Wiedenheft, B., Sternberg, S.H., Doudna, J.A., 2012. RNA-guided genetic silencing systems in bacteria and archaea. Nature 482, 331–338. https://doi.org/10.1038/nature10886

Wiedenheft, B., Zhou, K., Jinek, M., Coyle, S.M., Ma, W., Doudna, J.A., 2009. Structural Basis for DNase Activity of a Conserved Protein Implicated in CRISPR-Mediated Genome Defense. Structure 17, 904–912. https://doi.org/10.1016/j.str.2009.03.019

Wolter, F., Klemm, J., Puchta, H., 2018. Efficient in planta gene targeting in Arabidopsis using egg cell-specific expression of the Cas9 nuclease of Staphylococcus aureus. The Plant Journal 94, 735–746. https://doi.org/10.1111/tpj.13893

Wolter, F., Puchta, H., 2019. *In planta* gene targeting can be enhanced by the use of CRISPR/Cas12a. The Plant Journal 100, 1083–1094. https://doi.org/10.1111/tpj.14488

Wolter, F., Schindele, P., Beying, N., Scheben, A., Puchta, H., 2021. Different DNA repair pathways are involved in single-strand break-induced genomic changes in plants. Plant Cell 33, 3454–3469. https://doi.org/10.1093/plcell/koab204

Wörn, A., Auf der Maur, A., Escher, D., Honegger, A., Barberis, A., Plückthun, A., 2000. Correlation between in vitro stability and in vivo performance of anti-GCN4 intrabodies as cytoplasmic inhibitors. J Biol Chem 275, 2795–2803. https://doi.org/10.1074/jbc.275.4.2795

Wright, D.A., Townsend, J.A., Winfrey, R.J., Irwin, P.A., Rajagopal, J., Lonosky, P.M., Hall, B.D., Jondle, M.D., Voytas, D.F., 2005. High-frequency homologous recombination in plants

mediated by zinc-finger nucleases. Plant J 44, 693–705. https://doi.org/10.1111/j.1365-313X.2005.02551.x

Wright, W.D., Shah, S.S., Heyer, W.-D., 2018. Homologous recombination and the repair of DNA double-strand breaks. J Biol Chem 293, 10524–10535. https://doi.org/10.1074/jbc.TM118.000372

Wu, Y., Yuan, Q., Zhu, Y., Gao, X., Song, J., Yin, Z., 2020. Improving FnCas12a Genome Editing by Exonuclease Fusion. The CRISPR Journal 3, 503–511. https://doi.org/10.1089/crispr.2020.0073

Xu, R., Ma, C., Sheng, J., Zhu, J., Wang, D., Liu, X., Wang, Q., Li, J., Qin, R., Wei, P., 2024. Engineering PE6 prime editors to efficiently insert tags in rice. Plant Biotechnology Journal 22, 3383–3385. https://doi.org/10.1111/pbi.14456

Xu, R., Qin, R., Li, H., Li, D., Li, L., Wei, P., Yang, J., 2017. Generation of targeted mutant rice using a CRISPR-Cpf1 system. Plant Biotechnology Journal 15, 713–717. https://doi.org/10.1111/pbi.12669

Xue, C., Greene, E.C., 2021. DNA Repair Pathway Choices in CRISPR-Cas9-Mediated Genome Editing. Trends in Genetics 37, 639–656. https://doi.org/10.1016/j.tig.2021.02.008

Yamamoto, H., Hirasawa, A., 2022. Homologous Recombination Deficiencies and Hereditary Tumors. International Journal of Molecular Sciences 23, 348. https://doi.org/10.3390/ijms23010348

Yan, J., Oyler-Castrillo, P., Ravisankar, P., Ward, C.C., Levesque, S., Jing, Y., Simpson, D., Zhao, A., Li, H., Yan, W., Goudy, L., Schmidt, R., Solley, S.C., Gilbert, L.A., Chan, M.M., Bauer, D.E., Marson, A., Parsons, L.R., Adamson, B., 2024. Improving prime editing with an endogenous small RNA-binding protein. Nature 628, 639–647. https://doi.org/10.1038/s41586-024-07259-6

Yan, W.X., Hunnewell, P., Alfonse, L.E., Carte, J.M., Keston-Smith, E., Sothiselvam, S., Garrity, A.J., Chong, S., Makarova, K.S., Koonin, E.V., Cheng, D.R., Scott, D.A., 2019. Functionally diverse type V CRISPR-Cas systems. Science 363, 88–91. https://doi.org/10.1126/science.aav7271

Yarnall, M.T.N., Ioannidi, E.I., Schmitt-Ulms, C., Krajeski, R.N., Lim, J., Villiger, L., Zhou, W., Jiang, K., Garushyants, S.K., Roberts, N., Zhang, L., Vakulskas, C.A., Walker, J.A., Kadina, A.P., Zepeda, A.E., Holden, K., Ma, H., Xie, J., Gao, G., Foquet, L., Bial, G., Donnelly, S.K., Miyata, Y., Radiloff, D.R., Henderson, J.M., Ujita, A., Abudayyeh, O.O., Gootenberg, J.S., 2023. Drag-and-drop genome insertion of large sequences without double-strand DNA cleavage using CRISPR-directed integrases. Nat Biotechnol 41, 500–512. https://doi.org/10.1038/s41587-022-01527-4

Yu, H., Li, J., 2022. Breeding future crops to feed the world through de novo domestication. Nat Commun 13, 1171. https://doi.org/10.1038/s41467-022-28732-8

Yu, H., Lin, T., Meng, X., Du, H., Zhang, J., Liu, G., Chen, Mingjiang, Jing, Y., Kou, L., Li, X., Gao, Q., Liang, Yan, Liu, X., Fan, Z., Liang, Yuntao, Cheng, Z., Chen, Mingsheng, Tian, Z., Wang, Y., Chu, C., Zuo, J., Wan, J., Qian, Q., Han, B., Zuccolo, A., Wing, R.A., Gao, C., Liang, C., Li, J., 2021. A route to *de novo* domestication of wild allotetraploid rice. Cell 184, 1156-1170.e14. https://doi.org/10.1016/j.cell.2021.01.013

Zetsche, B., Gootenberg, J.S., Abudayyeh, O.O., Slaymaker, I.M., Makarova, K.S., Essletzbichler, P., Volz, S.E., Joung, J., van der Oost, J., Regev, A., Koonin, E.V., Zhang, F., 2015. Cpf1 Is a Single RNA-Guided Endonuclease of a Class 2 CRISPR-Cas System. Cell 163, 759–771. https://doi.org/10.1016/j.cell.2015.09.038

Zhang, A., Shan, T., Sun, Y., Chen, Z., Hu, J., Hu, Z., Ming, Z., Zhu, Z., Li, X., He, J., Liu, S., Jiang, L., Dong, X., Wu, Y., Wang, Y., Liu, Y., Li, C., Wan, J., 2023. Directed evolution rice genes with randomly multiplexed sgRNAs assembly of base editors. Plant Biotechnology Journal 21, 2597–2610. https://doi.org/10.1111/pbi.14156

Zhang, H., Li, T., Sun, Y., Yang, H., 2021. Perfecting Targeting in CRISPR. Annu. Rev. Genet. 55, 453–477. https://doi.org/10.1146/annurev-genet-071719-030438

Zhang, J., Yu, H., Li, J., 2023. *De novo* domestication: retrace the history of agriculture to design future crops. Current Opinion in Biotechnology 81, 102946. https://doi.org/10.1016/j.copbio.2023.102946

Zhang, K., Duan, X., Cai, P., Gao, L., Wu, X., Yao, L., Zhou, Y.J., 2022. Fusing an exonuclease with Cas9 enhances homologous recombination in Pichia pastoris. Microb Cell Fact 21, 182. https://doi.org/10.1186/s12934-022-01908-z

Zhang, Q., Yin, K., Liu, G., Li, S., Li, M., Qiu, J.-L., 2020. Fusing T5 exonuclease with Cas9 and Cas12a increases the frequency and size of deletion at target sites. Sci. China Life Sci. 63, 1918–1927. https://doi.org/10.1007/s11427-020-1671-6

Zhang, S., Zhang, R., Gao, J., Song, G., Li, J., Li, W., Qi, Y., Li, Y., Li, G., 2021. CRISPR/Cas9-mediated genome editing for wheat grain quality improvement. Plant Biotechnology Journal 19, 1684–1686. https://doi.org/10.1111/pbi.13647

Zhang, Y., Malzahn, A.A., Sretenovic, S., Qi, Y., 2019. The emerging and uncultivated potential of CRISPR technology in plant science. Nat. Plants 5, 778–794. https://doi.org/10.1038/s41477-019-0461-5

Zhao, B., Rothenberg, E., Ramsden, D.A., Lieber, M.R., 2020. The molecular basis and disease relevance of non-homologous DNA end joining. Nat Rev Mol Cell Biol 21, 765–781. https://doi.org/10.1038/s41580-020-00297-8

Zhong, Z., Zhang, Yingxiao, You, Q., Tang, X., Ren, Q., Liu, S., Yang, L., Wang, Y., Liu, X., Liu, B., Zhang, T., Zheng, X., Le, Y., Zhang, Yong, Qi, Y., 2018. Plant Genome Editing Using FnCpf1 and LbCpf1 Nucleases at Redefined and Altered PAM Sites. Molecular Plant 11, 999–1002. https://doi.org/10.1016/j.molp.2018.03.008

Zhou, Z., Xiao, J., Yin, S., Chen, Y., Yuan, Y., Zhang, J., Xiong, L., Xie, K., 2025. Cas9-Rep fusion tethers donor DNA in vivo and boosts the efficiency of HDR-mediated genome editing. Plant Biotechnol J 23, 2006–2017. https://doi.org/10.1111/pbi.70036

Zhu, H., Li, C., Gao, C., 2020. Applications of CRISPR–Cas in agriculture and plant biotechnology. Nat Rev Mol Cell Biol 21, 661–677. https://doi.org/10.1038/s41580-020-00288-9

Zong, Y., Liu, Y., Xue, C., Li, B., Li, X., Wang, Y., Li, J., Liu, G., Huang, X., Cao, X., Gao, C., 2022a. An engineered prime editor with enhanced editing efficiency in plants. Nat Biotechnol 40, 1394–1402. https://doi.org/10.1038/s41587-022-01254-w

Zong, Y., Liu, Y., Xue, C., Li, B., Li, X., Wang, Y., Li, J., Liu, G., Huang, X., Cao, X., Gao, C., 2022b. An engineered prime editor with enhanced editing efficiency in plants. Nat Biotechnol 40, 1394–1402. https://doi.org/10.1038/s41587-022-01254-w

Zong, Y., Wang, Y., Li, C., Zhang, R., Chen, K., Ran, Y., Qiu, J.-L., Wang, D., Gao, C., 2017. Precise base editing in rice, wheat and maize with a Cas9-cytidine deaminase fusion. Nat Biotechnol 35, 438–440. https://doi.org/10.1038/nbt.3811

Zsögön, A., Čermák, T., Naves, E.R., Notini, M.M., Edel, K.H., Weinl, S., Freschi, L., Voytas, D.F., Kudla, J., Peres, L.E.P., 2018. De novo domestication of wild tomato using genome editing. Nat Biotechnol 36, 1211–1216. https://doi.org/10.1038/nbt.4272

Zsögön, A., Cermak, T., Voytas, D., Peres, L.E.P., 2017. Genome editing as a tool to achieve the crop ideotype and *de novo* domestication of wild relatives: Case study in tomato. Plant Science 256, 120–130. https://doi.org/10.1016/j.plantsci.2016.12.012

7 SUPPLEMENTARY

7.1 Plasmids and Oligonucleotides Used in This Study

Table 7.1: Cloned entry and destination vectors.

Entry and destination vectors cloned in this study and their corresponding backbone vectors.

Name	Backbone
entry vectors	
pEn-RZ-LbcrRNA-ALS	pEn-RZ-LbcrRNA (Wolter and Puchta, 2019)
pEn-UBI-scFv-sfGFP-GB1-nosT	pEn-SagRNA+UBI-scFv-sfGFP-GB1-nosT (BioCat GmbH, Heidelberg)
pEn-UBI+scFv-sfGFP-HsTREX1-GB1-nosT	pEn-UBI-scFv-sfGFP-GB1-nosT
pEn-UBI+scFv-sfGFP-HSVUL12-GB1-nosT	pEn-UBI-scFv-sfGFP-GB1-nosT
pEn-UBI+scFv-sfGFP-PapE-GB1-nosT	pEn-UBI-scFv-sfGFP-GB1-nosT
pEn-EC-scFv-sfGFP-GB1-rbcST	pEn-UBI-scFv-sfGFP-GB1-nosT
pEn-EC-scFv-sfGFP-HsTREX1-GB1-rbcST	pEn-EC-scFv-sfGFP-GB1-rbcST
pEn-EC-scFv-sfGFP-HSVUL12-GB1-rbcST	pEn-EC-scFv-sfGFP-GB1-rbcST
pEn-EC-scFv-sfGFP-PapE-GB1-rbcST	pEn-EC-scFv-sfGFP-GB1-rbcST
pEn-RZ-LbcrRNA-Cen4	pEn-RZ-LbcrRNA (Wolter and Puchta, 2019)
pEn-RZ-LbcrRNA-ECA3	pEn-RZ-LbcrRNA (Wolter and Puchta, 2019)
pEn-RZ-LbcrRNA-ADH1	pEn-RZ-LbcrRNA (Wolter and Puchta, 2019)
destination vectors	
pDe-EC-ttLbCas12a-i-rbcST+ccdB+ALS+GTVc12+PPTR	pDe-EC-ttLbCas12a-i-rbcST+ccdB+PPTR (Schindele et al., 2023)
pDe-EC-Omega-ttLbCas12a-i-GCN4-rbcST+ccdB+ALS+GTVc12+PPTR	pDe-EC-ttLbCas12a-i-rbcST+ccdB+ALS+GTVc12+PPTR
pDe-UBI-Omega-ttLbCas12a-i-GCN4-pea3A+ccdB+PPTR	pDe-UBI-Omega-SaCas9-GCN4-pea3A+ccdB+PPTR (Capdeville et al., 2024)
pDe-UBI-Omega-ttLbCas12a-i-GCN4-pea3A+ccdB+Cen4+PPTR	pDe-UBI-Omega-ttLbCas12a-i-GCN4-pea3A+ccdB+PPTR
pDe-UBI-Omega-ttLbCas12a-i-GCN4-pea3A+ccdB+ECA3+PPTR	pDe-UBI-Omega-ttLbCas12a-i-GCN4-pea3A+ccdB+PPTR
pDe-UBI-Omega-ttLbCas12a-i-GCN4-pea3A+ccdB+ADH1+PPTR	pDe-UBI-Omega-ttLbCas12a-i-GCN4-pea3A+ccdB+PPTR
pDe-EC-ttLbCas12a-i-rbcST+GTV-CENH3-T1+PPTR	pDe-EC-ttLbCas12a-i-rbcST+ccdB+PPTR (Schindele et al., 2023)
pDe-EC-ttLbCas12a-i-rbcST+GTV-CENH3-T3+PPTR	pDe-EC-ttLbCas12a-i-rbcST+ccdB+PPTR (Schindele et al., 2023)

Table 7.2: Cloned expression vectors.

Expression vectors cloned in this study and their corresponding backbone vectors.

Name	Backbone
expression vectors	
pEx-EC-HSVUL12-ttLbCas12a-i+ALS+GTVc12+GentR	pEx-EC-ttLbCas12a-i+ALS+GTVc12+GentR (Schindele et al., 2023)
pEx-EC-PapE-ttLbCas12a-i+ALS+GTVc12+GentR	pEx-EC-ttLbCas12a-i+ALS+GTVc12+GentR (Schindele et al., 2023)
pEx-EC-Omega-ttLbCas12a-i-GCN4+scFv-sfGFP-HsTREX1-GB1+ALS+GTVc12+PPTR	pDe-EC-Omega-ttLbCas12a-i-GCN4-rbcST+ccdB+ALS+GTVc12+PPTR
pEx-EC-Omega-ttLbCas12a-i-GCN4+scFv-sfGFP-HSVUL12-GB1-ALS-GTVc12+PPTR	pDe-EC-Omega-ttLbCas12a-i-GCN4-rbcST+ccdB+ALS+GTVc12+PPTR
pEx-EC-Omega-ttLbCas12a-i-GCN4+scFv-sfGFP-PapE-GB1+ALS+GTVc12+PPTR	pDe-EC-Omega-ttLbCas12a-i-GCN4-rbcST+ccdB+ALS+GTVc12+PPTR
pEx-EC-Omega-ttLbCas12a-i-GCN4+scFv-sfGFP-GB1+ALS+GTVc12+PPTR	pDe-EC-Omega-ttLbCas12a-i-GCN4-rbcST+ccdB+ALS+GTVc12+PPTR
pEx-UBI-Omega-ttLbCas12a-i-GCN4-pea3A+Cen4+scFv-sfGFP-HsTREX1-GB1+PPTR	pDe-UBI-Omega-ttLbCas12a-i-GCN4-pea3A+ccdB+Cen4+PPTR
pEx-UBI-Omega-ttLbCas12a-i-GCN4-pea3A+Cen4+scFv-sfGFP-HSVUL12-GB1+PPTR	pDe-UBI-Omega-ttLbCas12a-i-GCN4-pea3A+ccdB+Cen4+PPTR
pEx-UBI-Omega-ttLbCas12a-i-GCN4-pea3A+Cen4+scFv-sfGFP-PapE-GB1+PPTR	pDe-UBI-Omega-ttLbCas12a-i-GCN4-pea3A+ccdB+Cen4+PPTR
pEx-UBI-Omega-ttLbCas12a-i-GCN4-pea3A+Cen4+scFv-sfGFP-GB1+PPTR	pDe-UBI-Omega-ttLbCas12a-i-GCN4-pea3A+ccdB+Cen4+PPTR
pEx-UBI-Omega-ttLbCas12a-i-GCN4-pea3A+ECA3+scFv-sfGFP-HsTREX1-GB1+PPTR	pDe-UBI-Omega-ttLbCas12a-i-GCN4-pea3A+ccdB+ECA3+PPTR
pEx-UBI-Omega-ttLbCas12a-i-GCN4-pea3A+ECA3+scFv-sfGFP-HSVUL12-GB1+PPTR	pDe-UBI-Omega-ttLbCas12a-i-GCN4-pea3A+ccdB+ECA3+PPTR
pEx-UBI-Omega-ttLbCas12a-i-GCN4-pea3A+ECA3+scFv-sfGFP-PapE-GB1+PPTR	pDe-UBI-Omega-ttLbCas12a-i-GCN4-pea3A+ccdB+ECA3+PPTR
pEx-UBI-Omega-ttLbCas12a-i-GCN4-pea3A+ECA3+scFv-sfGFP-GB1+PPTR	pDe-UBI-Omega-ttLbCas12a-i-GCN4-pea3A+ccdB+ECA3+PPTR
pEx-UBI-Omega-ttLbCas12a-i-GCN4-pea3A+ADH1+scFv-sfGFP-HsTREX1-GB1+PPTR	pDe-UBI-Omega-ttLbCas12a-i-GCN4-pea3A+ccdB+ADH1+PPTR
pEx-UBI-Omega-ttLbCas12a-i-GCN4-pea3A+ADH1+scFv-sfGFP-HSVUL12-GB1+PPTR	pDe-UBI-Omega-ttLbCas12a-i-GCN4-pea3A+ccdB+ADH1+PPTR
pEx-UBI-Omega-ttLbCas12a-i-GCN4-pea3A+ADH1+scFv-sfGFP-PapE-GB1+PPTR	pDe-UBI-Omega-ttLbCas12a-i-GCN4-pea3A+ccdB+ADH1+PPTR
pEx-UBI-Omega-ttLbCas12a-i-GCN4-pea3A+ADH1+scFv-sfGFP-GB1+PPTR	pDe-UBI-Omega-ttLbCas12a-i-GCN4-pea3A+ccdB+ADH1+PPTR

Table 7.3: List of spacer sequences used in this study.

The name, 5'-3' sequence and the target sites of the spacer oligonucleotides are stated. Overhangs required for integration of the spacers into the entry vectors are represented by lowercase letters.

Name	Sequence 5'→3'
ALS Cas12a target forward	agatTCCGCACCAAGAACATGTGTTGC
ALS Cas12a target reverse	ggccGCAACACATGTTCTTGGTGCGGA
Cen4 Cas12a target forward	agatACTATAATTTATTTTACTTAATTT
Cen4 Cas12a target reverse	ggccAAATTAAGTAAAATAAATTATAGT
ECA3 Cas12a target forward	agatTGATTCTCAGGTATGAACCTGTTG
ECA3 Cas12a target reverse	ggccCAACAGGTTCATACCTGAGAATCA
ADH1 Cas12a target forward	agatCCGGAGAATGTGGGGAGTGTCGTC
ADH1 Cas12a target reverse	ggccGACGACACTCCCCACATTCTCCGG
CENH3 Cas12a target1 forward	agatTCCAGCAGTAAAAATCAATGGCGA
CENH3 Cas12a target1 reverse	ggccTCGCCATTGATTTTTACTGCTGGA
CENH3 Cas12a target3 forward	agatAGATACCAGTTTGATTCCGAGGTT
CENH3 Cas12a target3 reverse	ggccAACCTCGGAATCAAACTGGTATCT

Table 7.4: List of primer sequences used for molecular analysis.

The table shows the names and 5'-3'sequences of the primers used for the molecular analysis.

Name	Sequence 5'→3'
ALS Cas12a target molecular analysis forward	AGTACGTTGATGGGGCTGG
ALS Cas12a target molecular analysis reverse	CCAATGTCTGATTAGTGCTTCTGG
ALS screening forward	ACCAGCATCTTGGCATGGTTA
CENH3 Cas12a target molecular analysis forward	CTATCCTCGGTAATGACCAG
CENH3 Cas12a target molecular analysis reverse	CCTGTCTGGATCTCTTAGCC
CENH3 screening forward	CTAACAATCGAGTCGAACCC

Table 7.5: List of primer sequences for Gibson Assembly.

Listed are the overhang primers used in this study for cloning by Gibson assembly. For each oligonucleotide, the name and sequence are provided in the 5'-3' orientation. Overhang sequences are indicated by lowercase letters, and restriction enzyme recognition sites are highlighted in red.

Name	Sequence 5'→3'
HSVUL12 with AscI site and EC promoter-OH forward	tatcaatctgttgagaaggtaccggcgcgccATGGAATCTACTGTGGGTCC
PapE with AscI site and EC promoter-OH forward	tatcaatctgttgagaaggtaccggcgcgccATGCAGACTACTACCCCTGTGG
ttLbCas12a-i with AscI site and rbcST-OH reverse	gaacgaaagctctgagctcggcgcgccTCACGAACCCTTTTTCTTTTTTGCC
Omega with EC promoter-OH forward	atctgttgagaagaattcGGATCATCAACAAGTTTGTAC
Omega-OH reverse	TTTTTTTGTAATTGTAAATAGTAATTGTAATG
ttLbCas12a-i with Omega-OH forward	actatttacaattacaaaaaaaGGCGCGCCATGAGCAAGC
ttLbCas12a-i with GCN4-OH reverse	agggataggcTTTCTTCTTCTTAGCCTGACCAGCTTTCTTAG
rbcST with pEn-OH forward	gcctacgccatggccgtaacCAGAGCTTTCGTTCGTATC
rbcST with pEn-OH reverse	tgcggccgctctagacctagAGCTCGTTGTCAATCAATTG
GCN4 with ttLbCas12a-i-OH forward	gaagaagaaaGCCTATCCCTATGACGTGCC
GCN4 with rbcST-OH reverse	atgatacgaacgaaagctctGAGCTCGGCGCGCCTTAC
ttLbCas12a-i with Omega-OH forward	actatttacaattacaaaaaaaGGCGCGCCATGAGCAAGCTC
ttLbCas12a-i with rbcST-OH reverse	aaagctctgagctcggcgcgCCTCATTTCTTCTTCTTAGCCTGACC
HSVUL12 with sfGFP-OH forward	cggtcgtacgggcggtggcgATGGAATCTACTGTGGGTCC
HSVUL12 with GB1-OH reverse	ccctccgccaccgccggatcTCTAGATGACCTGCCGGTG
PapE with sfGFP-OH forward	cggtcgtacgggcggtggcgATGCAGACTACTACCCCTG
PapE with GB1-OH reverse	ccctccgccaccgccggatcCGAAGAAGTTTCGCCAGC

Table 7.6: Primer sequences used for ONT analysis.

Listed are the primers used in this study to generate amplicons for ONT analysis. For each oligonucleotide, the name and corresponding sequence are provided in the 5'-3' orientation.

Name	Sequence 5'→3'
ONT Cen4 forward	CTACGAGTGCAGGAGCGACGAGTG
ONT Cen4 reverse	CCGAGATCATGGATGCATCAGG
ONT ECA3 forward	GAGGATCATGAGTGGTGACAACG
ONT ECA3 reverse	CAGAACCAGTTTCCAGAATGGCG
ONT ADH1 forward	GCAACACCACGGCGTGACCATC
ONT ADH1 reverse	CTCAAGCTCCAGCTCCTATGTC

Table 7.7: Primer sequences for screening ALFA-tag-integrated plants.

The primers were used to generate amplicons for identifying heterozygous and homozygous ALFA-tag-integrated plants. Primer names and corresponding sequences are provided in the 5'-3' orientation.

Name	Sequence 5'→3'
Arabidopsis upstream of CENH3 forward	CTATCCTCGGTAATGACCAG
ALFA-tag reverse	CCTCTTCAAGTCTTGAAGG

Table 7.8: Primers used for sequencing cloned constructs.

Listed are the primers used in this study for sequencing cloned constructs. For each primer, the name and corresponding sequence are provided in the 5'-3' orientation.

Name	Sequence 5'→3'
ttLbCas12a-i 1 forward	CTACCTGAGCTTCATCAACG
ttLbCas12a-i 2 forward	GGTTCTGAGCGATCGTGAG
ttLbCas12a-i 3 forward	GAGACTAATAGGGACGAGTC
ttLbCas12a-i 4 forward	GATGCATATTTGTGATGAG
ttLbCas12a-i 5 forward	GGTTGAGAAGCAGGTCTACC
ttLbCas12a-i 6 forward	CGGCGCTTACAACATTGCC
ttLbCas12a-i 1 reverse	GCCTCTTCGCTGAACATGTT
ttLbCas12a-i 2 reverse	GTCATCGTACTCAGCATTCC
ttLbCas12a-i 3 reverse	GGTAGTACTTAGAGCCGTAC
ttLbCas12a-i 4 reverse	GTCGAACAGCAGCTTGAAGT
ttLbCas12a-i 5 reverse	GCTTGTCGATGAGCATCTTC
ttLbCas12a-i 6 reverse	CAGCATTCTTCGGCAGGATT
pre-promoter region forward	GCCAATACGCAAACCGCC
EC promoter 1 forward	TGCGTTTGGTTTATCATTGCG
EC promoter 2 reverse	GAGTAGAAGTTGCTTTGGTTG
UBI promoter forward	GTGTGTGTATATGTGTGTTCTG
rbcST 1 forward	CTCATGGATTTGTAGTTGAG
rbcST 2 reverse	CTCGTTGTCAATCAATTGGC
rbcST 3 forward	GTAACCAGAGCTTTCGTTC
rbcST 3 reverse	GAACGAAAGCTCTGGTTAC
GCN4 forward	GGAGGAGTTGCTGAGCAA
scFV 1 forward	GAATTCATGGGCCCCGACAT
scFv 1 reverse	ATGTCGGGGCCCATGAATTC
scFV 2 reverse	GTGAAAAGTTCTTCTCCTTTGCT
sfGFP 1 forward	AGCAAAGGAGAAGAACTTTTCAC
sfGFP 2 forward	GCATGGATGAGCTCTACAAAGG
exonuclease end rev	TTTGGAGCCCCTCCGCCAC
HsTREX1 1 forward	CCTTCTGAACATGGACCTAG
HsTREX1 1 reverse	CTAGGTCCATGTTCAGAAGG
HsTREX1 2 reverse	GAAGACCTTCTCTACTAAGAGC

7.2 DNA Sequences of Synthetic Constructs

The sequences of the CENH3 ALFA-tag Target 1 and 3 GTVs are provided in the 5'-3' orientation. The sequences are flanked by protospacer sequences, highlighted in pink, and PAM sequences, highlighted in yellow. These elements are oriented such that the majority of the protospacer sequence is excised from the donor following Cas12a-mediated DSB induction. In addition, the GTVs contain two silent mutations in the PAM and seed region, shown in red and bold, which are required in the target sequence for DSB induction. The CENH3 start codon is shown in black and bold. Furthermore, the donor contains the coding sequence for the 45 bp ALFA-tag.

CENH3 ALFA-tag Target 1 GTV:

TTTCTCCAGCAGTAAAAATCAATGGCGAAACCTATGATTGGATGCTGAGAACTTGTAAAGAAT
CTGAGGCAGAAAGTTGAAAAACTGTGTCAATTTCATTAACTTGAAAAGATGAGCATAAATTGG
GAGAGAGAGAGAGAGACAAAGATTTTGAATTGAGGTTTAACGGTAAAACACACAAAACCTATT
CCCCTCTGTTTCCAATTTTCATCTAAACAAACAGGTACATATTTGAATGTAATATTGTATACA
GACCAGGGGTAAAACAGGAACTAAAGAAGGCTAACAATCGAGTCGAACCCTCTATGTGAAGCC
ACAGGTTTAGTGCAAATTGTAATAAGTTGTTCAGAGAGACTCTTGACTGAAACAAATTGTGAA
GCAGATTCGATTTTAAAATCAAAATTTGAGTGTCGAGCGGGAAAGTAAAAGTTCCGCTCCAAT
CTTCTAATCTTTTCGTATCTAGCGGGAAATTTCTCAGCAGGTGACTTTCATAATCGCAGTTTT
CGTCGATTCTCTTTTCCGATTTTACGATTCCTCTCTCTCTCTCATGGTGCGATTGCTGCAGCA
GTAAAAATCAATGCCTTCAAGACTTGAAGAGGAACTTAGAAGGAGACTTACTGAACCTGCGAG
AACCAAGCATCGCGTTACCAGGTCACAACCTCGGAATCAAACTGGTATCTTAAATCTGCTTTC
TCTTTCAATTTTTACTTCTGATTTTACCCAGAATTTTAGGTTTTTTATTTCGATTTTGTTAAC
CCTAGATTTCGAATCTGAAATTTGTAGATGCCGCCGGTGCTTCATCTTCTCAGGCGGCAGGTC
CAACTACGGTACGGCATCTTTTTCCGTCTTAGGGTTTCCAATGTTTCTTCCTTTTATCGTTAT
GATCAAATTTGTTTATCTATCGAAATTGAAGACCCCGACAAGGAGAGGCGGTGAAGGTGGAGA
TAATACTCAACAAAGTGAGTTTTTTATATTTGAAGTCTTTTTTTTCCCTCTTTTCATCTCTTT
TGTTTGTGAAGTTATTCTTTTGTAACATCTGCAGCAAATCCTACAACTTCACCAGCTACTGGT
ACAAGGGTAAGATTTTTGTGACCATTGCTTATGAACTGCTTCAACTTTGATTTCGTTATTAAG
CTGACAAAATTCTCGTTTTGGTTTCGCCATTGATTTTTACTGCTGGAGAAA

CENH3 ALFA-tag Target 3 GTV:

TTTAAGATACCAGTTTGATTCCGAGGTTAAGAATCTGAGGCAGAAAGTTGAAAAACTGTGTCA
ATTTCATTAACTTGAAAAGATGAGCATAAATTGGGAGAGAGAGAGAGAGACAAAGATTTTGAA
TTGAGGTTTAACGGTAAAACACACAAAACCTATTCCCCTCTGTTTCCAATTTTCATCTAAACA
AACAGGTACATATTTGAATGTAATATTGTATACAGACCAGGGGTAAAACAGGAACTAAAGAAG
GCTAACAATCGAGTCGAACCCTCTATGTGAAGCCACAGGTTTAGTGCAAATTGTAATAAGTTG
TTCAGAGAGACTCTTGACTGAAACAAATTGTGAAGCAGATTCGATTTTAAAATCAAAATTTGA
GTGTCGAGCGGGAAAGTAAAAGTTCCGCTCCAATCTTCTAATCTTTTCGTATCTAGCGGGAAA
TTTCTCAGCAGGTGACTTTCATAATCGCAGTTTTCGTCGATTCTCTTTTCCGATTTTACGATT
CCTCTCTCTCTCTCATGGTGCGATTTCTCCAGCAGTAAAAATCA**ATG**CCTTCAAGACTTGAAG
AGGAACTTAGAAGGAGACTTACTGAACCTGCGAGAACCAAGCATCGCGTTACCAGGTCACAAC
CTCGGAATCAAACTGGTA**T**TTT**G**AATCTGCTTTCTCTTTCAATTTTTACTTCTGATTTTACCC
AGAATTTTAGGTTTTTTATTTCGATTTTGTTAACCCTAGATTTCGAATCTGAAATTTGTAGAT
GCCGCCGGTGCTTCATCTTCTCAGGCGGCAGGTCCAACTACGGTACGGCATCTTTTTCCGTCT
TAGGGTTTCCAATGTTTCTTCCTTTTATCGTTATGATCAAATTTGTTTATCTATCGAAATTGA
AGACCCCGACAAGGAGAGGCGGTGAAGGTGGAGATAATACTCAACAAAGTGAGTTTTTTATAT
TTGAAGTCTTTTTTTTCCCTCTTTTCATCTCTTTTGTTTGTGAAGTTATTCTTTTGTAACATC
TGCAGCAAATCCTACAACTTCACCAGCTACTGGTACAAGGGTAAGATTTTTGTGACCATTGCT
TATGAACTGCTTCAACTTTGATTTCGTTATTAAGCTGACAAAATTCTCGTTTTGGTTAACCTC
GGAATCAAACTGGTATCTTAAA

7.3 Raw Data

Table 7.9: Overview of the GT efficiencies of the individual replicates from Chapter 3.1.

The table presents the tested approaches from Chapter 3.1, performed in two genotypes, including the replicate line numbers, the number of analyzed T_1 single lines, the GT efficiency of the replicates, the overall GT efficiency across all single lines, the number of T_1 single lines, the number of positive single lines, and the normalized GT efficiency of all single lines.

Genotype	Approach	Line number of the replicates	Number of T_1 lines	GT efficiency of replicates (%)	GT efficiency of all single lines (%)	Number of T_1 single lines	Number of positive lines	Normalized GT efficiency (%)
Col-0	**ttLbCas12a-i**	SY114-1	20	1.1	0.87	40	35	0.98
		SY114-2	20	0.59				
	ttLbCas12a-i-PapE	SY115-1	20	0.88	0.25	39	17	0.29
		SY115-2	19	0.14				
	ttLbCas12a-i-HSVUL12	SY116-1	19	0.58	0.51	39	27	0.58
		SY116-2	20	0.36				
ku70	**ttLbCas12a-i**	SY117-1	19	2.35	1.97	37	31	2.10
		SY117-2	18	1.41				
	ttLbCas12a-i-PapE	SY118-1	17	0.26	0.24	33	12	0.25
		SY118-2	16	0.16				
	ttLbCas12a-i-HSVUL12	SY119	19	0.73	0.4	39	17	0.43
		SY127	20	0.36				

Table 7.10: Overview of the GT efficiencies of the single lines from Chapter 3.1 in the Col-0 genotype.

The table presents the tested approaches using ttLbCas12a-i, ttLbCas12a-i-PapE and ttLbCas12a-i-HSVUL12 in Col-0 genotype, including the replicate numbers, seed numbers, the number of GT plants and GT efficiency.

Line number of replicates	Number of the T_1 single lines	Number of seeds	Number of GT plants	GT efficiency (%)	Normalized GT efficiency (%)	Line number of replicates	Number of the T_1 single lines	Number of seeds	Number of GT plants	GT efficiency (%)	Normalized GT efficiency (%)
Col-0::ttLbCas12a-i						**Col-0::ttLbCas12a-i-PapE**					
	1	1120	11	0.98	1.11		1	541	23	4.25	4.81
	2	1005	13	1.29	1.46		2	1188	7	0.59	0.67
	3	370	2	0.54	0.61		3	352	0	0.00	0.00
	4	385	1	0.26	0.29		4	381	0	0.00	0.00
	5	1290	4	0.31	0.35		5	672	3	0.45	0.50
	6	620	13	2.10	2.37		6	338	0	0.00	0.00
	7	1480	63	4.26	4.81		7	814	2	0.25	0.28
	8	665	0	0.00	0.00		8	1435	0	0.00	0.00
	9	675	0	0.00	0.00		9	425	0	0.00	0.00
	10	1770	5	0.28	0.32		10	410	6	1.46	1.65
SY114-1	11	1405	17	1.21	1.37	**SY115-1**	11	1093	2	0.18	0.21
	12	880	8	0.91	1.03		12	494	5	1.01	1.14
	13	1220	13	1.07	1.20		13	516	1	0.19	0.22
	14	975	11	1.13	1.28		14	385	0	0.00	0.00
	15	440	2	0.45	0.51		15	1035	3	0.29	0.33
	16	415	4	0.96	1.09		16	654	1	0.15	0.17
	17	835	15	1.80	2.03		17	657	0	0.00	0.00
	18	905	17	1.88	2.12		18	1017	0	0.00	0.00
	19	455	5	1.10	1.24		19	923	0	0.00	0.00
	20	605	9	1.49	1.68		20	305	0	0.00	0.00
	21	520	4	0.77	0.87		21	541	0	0.00	0.00
	22	425	1	0.24	0.27		22	926	0	0.00	0.00
	23	1325	20	1.51	1.71		23	1580	0	0.00	0.00
	24	1245	7	0.56	0.64		24	414	0	0.00	0.00
	25	1180	5	0.42	0.48		25	708	0	0.00	0.00
	26	1030	9	0.87	0.99		26	556	0	0.00	0.00
	27	1265	3	0.24	0.27		27	1097	0	0.00	0.00
	28	1855	19	1.02	1.16		28	643	1	0.16	0.18
	29	1110	17	1.53	1.73		29	1097	2	0.18	0.21
	30	655	3	0.46	0.52		30	937	3	0.32	0.36
SY114-2	31	1160	17	1.47	1.66	**SY115-2**	31	1359	0	0.00	0.00
	32	1375	6	0.44	0.49		32	1093	3	0.27	0.31
	33	650	2	0.31	0.35		33	534	3	0.56	0.64
	34	1895	5	0.26	0.30		35	418	0	0.00	0.00
	35	2785	10	0.36	0.41		36	552	0	0.00	0.00
	36	2950	0	0.00	0.00		37	661	6	0.91	1.03
	37	225	0	0.00	0.00		38	599	0	0.00	0.00
	38	255	0	0.00	0.00		39	694	0	0.00	0.00
	39	515	2	0.39	0.44		40	501	1	0.20	0.23
	40	1500	16	1.07	1.21						
Col-0::ttLbCas12a-i-HSVUL12											
	1	162	0	0.00	0.00		21	1021	0	0.00	0.00
	2	352	1	0.28	0.32		22	531	1	0.19	0.21
	3	548	0	0.00	0.00		23	948	4	0.42	0.48
	4	217	0	0.00	0.00		24	1131	2	0.18	0.20
	5	938	47	5.01	5.67		25	1014	5	0.49	0.56
	6	641	2	0.31	0.35		26	931	4	0.43	0.49
	7	828	0	0.00	0.00		27	369	1	0.27	0.31
	8	659	1	0.15	0.17		28	248	1	0.40	0.46
	9	514	2	0.39	0.44		29	800	6	0.75	0.85
	10	686	1	0.15	0.16		30	338	1	0.30	0.33
SY116-1	11	266	1	0.38	0.43	**SY116-2**	31	283		0.00	0.00
	12	924	0	0.00	0.00		32	1241	2	0.16	0.18
	13	417	0	0.00	0.00		33	1655	0	0.00	0.00
	14	938	2	0.21	0.24		34	538	0	0.00	0.00
	15	1148	9	0.78	0.89		35	1176	1	0.09	0.10
	16	524	7	1.34	1.51		36	800	3	0.38	0.42
	17	348	2	0.57	0.65		37	679	0	0.00	0.00
	18	293	0	0.00	0.00		38	817	23	2.81	3.18
	19	424	6	1.41	1.60		39	641	1	0.16	0.18
					0.00		40	834	1	0.12	0.14

Table 7.11: Overview of the GT efficiencies of the single lines from Chapter 3.1 in the *ku70* genotype.

The table presents the tested approaches using ttLbCas12a-i, ttLbCas12a-i-PapE and ttLbCas12a-i-HSVUL12 in *ku70* genotype, including the replicate numbers, seed numbers, the number of GT plants and GT efficiency.

Line number of replicates	Number of the T_1 single lines	Number of seeds	Number of GT plants	GT efficiency (%)	Normalized GT efficiency (%)	Line number of replicates	Number of the T_1 single lines	Number of seeds	Number of GT plants	GT efficiency (%)	Normalized GT efficiency (%)
***ku70*::ttLbCas12a-i**						***ku70*::ttLbCas12a-i-HSVUL12**					
	1	1464	19	1.30	1.39		1	585	10	1.71	1.83
	2	1588	1	0.06	0.07		2	344	17	4.94	5.28
	3	1028	63	6.13	6.55		3	883	0	0.00	0.00
	4	528	8	1.52	1.62		4	128	0	0.00	0.00
	5	1548	38	2.45	2.62		5	560	0	0.00	0.00
	6	92	2	2.17	2.32		6	387	0	0.00	0.00
	7	460	8	1.74	1.86		7	291	2	0.69	0.73
	8	700	4	0.57	0.61		8	1309	0	0.00	0.00
	9	588	0	0.00	0.00		10	454	2	0.44	0.47
SY117-1	10	1220	33	2.70	2.89	**SY119**	11	539	15	2.78	2.97
	11	872	27	3.10	3.31		12	1206	0	0.00	0.00
	12	976	15	1.54	1.64		13	1812	0	0.00	0.00
	13	1668	6	0.36	0.38		14	532	0	0.00	0.00
	14	2008	14	0.70	0.75		15	383	3	0.78	0.84
	16	1004	27	2.69	2.87		16	511	0	0.00	0.00
	17	1724	44	2.55	2.73		17	220	2	0.91	0.97
	18	1064	69	6.48	6.93		18	578	2	0.35	0.37
	19	1456	42	2.88	3.08		19	245	1	0.41	0.44
	20	1200	68	5.67	6.06		20	110	1	0.91	0.97
	21	1400	24	1.71	1.83		1	482	0	0.00	0.00
	22	708	0	0.00	0.00		2	2078	12	0.58	0.62
	23	688	0	0.00	0.00		3	362	0	0.00	0.00
	24	1632	0	0.00	0.00		4	965	0	0.00	0.00
	25	1060	14	1.32	1.41		5	461	0	0.00	0.00
	26	1220	37	3.03	3.24		6	2504	15	0.60	0.64
	27	816	21	2.57	2.75		7	1422	9	0.63	0.68
	28	1172	27	2.30	2.46		8	1241	8	0.64	0.69
	30	1288	32	2.48	2.65		9	259	5	1.93	2.06
	31	1332	34	2.55	2.73		10	1383	9	0.65	0.70
SY117-2	32	1748	30	1.72	1.83	**SY127**	11	1582	0	0.00	0.00
	33	252	7	2.78	2.97		12	1869	0	0.00	0.00
	34	560	11	1.96	2.10		13	535	2	0.37	0.40
	36	204	0	0.00	0.00		14	504	0	0.00	0.00
	37	560	7	1.25	1.34		15	918	6	0.65	0.70
	38	872	2	0.23	0.25		16	911	3	0.33	0.35
	39	980	14	1.43	1.53		17	809	0	0.00	0.00
	40	312	0	0.00	0.00		18	936	5	0.53	0.57
							19	780	2	0.26	0.27
							20	1699	0	0.00	0.00
***ku70*::ttLbCas12a-i-PapE**											
	1	594	0	0.00	0.00		21	1100	1	0.09	0.10
	2	566	0	0.00	0.00		22	344	0	0.00	0.00
	3	369	0	0.00	0.00		23	459	0	0.00	0.00
	4	769	0	0.00	0.00		24	366	0	0.00	0.00
	5	444	1	0.23	0.24		25	375	2	0.53	0.57
	6	334	0	0.00	0.00		27	509	2	0.39	0.42
	7	491	0	0.00	0.00		28	475	1	0.21	0.22
	8	606	1	0.16	0.18		30	1022	2	0.20	0.21
SY118-1	9	344	0	0.00	0.00	**SY118-2**	32	609	4	0.66	0.70
	10	112	0	0.00	0.00		33	722	2	0.28	0.30
	11	309	0	0.00	0.00		35	322	0	0.00	0.00
	13	272	0	0.00	0.00		36	534	0	0.00	0.00
	14	612	21	3.43	3.66		37	772	1	0.13	0.14
	15	553	0	0.00	0.00		38	334	0	0.00	0.00
	16	1188	0	0.00	0.00		39	881	0	0.00	0.00
	19	653	4	0.61	0.65		40	75	0	0.00	0.00
	20	575	0	0.00	0.00						

Table 7.12: Overview of the GT efficiencies of the individual replicates from Chapter 3.2.

The table presents the tested approaches from Chapter 3.2, performed in two genotypes, including the replicate line numbers, the number of analyzed T_1 single lines, the GT efficiency of the replicates, the overall GT efficiency across all single lines, the number of T_1 single lines, the number of positive single lines, and the normalized GT efficiency of all single lines.

Genotype	Approach	Line number of the replicates	Number of T_1 lines	GT efficiency of replicates (%)	GT efficiency of all single lines (%)	Number of T_1 single lines	Number of positive lines	Normalized GT efficiency (%)
Col-0	SunTag	SY202-1	15	0.41	0.46	71	53	0.71
		SY202-2	10	0.60				
		SY288	4	0.74				
		SY322	22	0.35				
		SY447	20	0.41				
	SunTag-HsTREX1	SY199-1	15	0.34	0.30	80	35	0.36
		SY199-2	16	0.29				
		SY310-1	17	0.05				
		SY310-2	24	0.62				
		SY489	8	0.17				
	SunTag-PapE	SY200-1	13	0.43	0.39	57	49	0.59
		SY200-2	8	0.23				
		SY276	10	1.54				
		SY329	14	0.26				
		SY442	20	0.48				
	SunTag-HSVUL12	SY201-1	19	0.63	0.76	74	59	1.12
		SY201-2	9	1.90				
		SY279	8	0.24				
		SY311	19	0.42				
		SY443	19	0.46				
ku70	SunTag	SY213	16	0.92	0.59	62	38	0.81
		SY224	5	1.66				
		SY289	7	0.63				
		SY321	14	0.20				
		SY448	20	0.48				
	SunTag-HsTREX1	SY210-1	7	0.53	0.49	61	37	0.61
		SY210-2	5	0.90				
		SY273-1	11	0.11				
		SY273-2	6	0.00				
		SY482	32	0.45				
	SunTag-PapE	SY211-1	7	0.38	0.72	57	40	1.00
		SY211-2	5	1.00				
		SY280	4	0.55				
		SY312	21	0.79				
		SY445	20	0.96				
	SunTag-HSVUL12	SY212	7	1.28	0.56	69	37	0.90
		SY287	8	0.76				
		SY319	35	0.17				
		SY446	19	0.79				

Table 7.13: Overview of the GT efficiencies of the individual lines from Chapter 3.2 in the Col-0 and *ku70* genotypes.

The table presents the tested approaches using SunTag, SunTag-HsTREX1, SunTag-PapE and SunTag-HSVUL12 in both Col-0 and *ku70* genotypes, including the replicate numbers, seed numbers, the number of GT plants, GT efficiency, and normalized GT efficiency of each line.

Line number of replicates	Number of the T1 single lines	Number of seeds	Number of GT plants	GT efficiency (%)	Normalized GT efficiency (%)	Line number of replicates	Number of the T1 single lines	Number of seeds	Number of GT plants	GT efficiency (%)	Normalized GT efficiency (%)
Col-0::SunTag											
SY202-1	1	7964	23	0.29	0.45	**SY322**	22	1334	0	0.00	0.00
	2	6210	0	0.00	0.00		23	1773	4	0.23	0.35
	3	7474	27	0.36	0.56		24	2731	2	0.07	0.11
	4	5886	75	1.27	1.99		26	352	0	0.00	0.00
	5	8519	26	0.31	0.48		28	1933	1	0.05	0.08
	6	6508	59	0.91	1.42		29	1053	0	0.00	0.00
	7	9623	14	0.15	0.23		30	1442	1	0.07	0.11
	8	5803	27	0.47	0.73		31	1143	4	0.35	0.55
	9	7306	57	0.78	1.22		32	2141	3	0.14	0.22
	10	9501	23	0.24	0.38		33	560	33	5.90	9.22
	11	4258	23	0.54	0.84		34	779	0	0.00	0.00
	12	1565	6	0.38	0.60		35	2853	0	0.00	0.00
	13	4739	10	0.21	0.33		36	571	0	0.00	0.00
	14	5244	9	0.17	0.27		37	2622	0	0.00	0.00
	15	8367	0	0.00	0.00		38	689	0	0.00	0.00
SY447	1	4727	5	0.11	0.17		39	620	1	0.16	0.25
	2	4132	5	0.12	0.19		40	3103	5	0.16	0.25
	3	7494	0	0.00	0.00		41	1366	0	0.00	0.00
	4	6703	61	0.91	1.42		42	1945	8	0.41	0.64
	5	2884	11	0.38	0.60		43	3905	3	0.08	0.12
	6	4152	13	0.31	0.49		44	626	1	0.16	0.25
	7	4626	47	1.02	1.59		45	1436	0	0.00	0.00
	8	6453	0	0.00	0.00	**SY202-2**	21	3847	28	0.73	1.14
	9	4269	10	0.23	0.37		22	8511	71	0.83	1.30
	10	4641	12	0.26	0.40		23	7564	31	0.41	0.64
	11	4719	10	0.21	0.33		24	1968	0	0.00	0.00
	12	5138	10	0.19	0.30		25	5733	108	1.88	2.94
	13	8187	0	0.00	0.00		26	9877	41	0.42	0.65
	14	8609	151	1.75	2.74		27	8414	0	0.00	0.00
	15	9419	103	1.09	1.71		28	7083	81	1.14	1.79
	16	7091	15	0.21	0.33		29	6163	1	0.02	0.03
	17	2332	8	0.34	0.54		30	4692	29	0.62	0.97
	18	4516	11	0.24	0.38	**SY288**	3	7251	48	0.66	1.03
	19	5103	0	0.00	0.00		6	4266	48	1.13	1.76
	20	8551	62	0.73	1.13		8	5009	34	0.68	1.06
					0.17		11	203	1	0.49	0.77

Line number of replicates	Number of the T_1 single lines	Number of seeds	Number of GT plants	GT efficiency (%)	Normalized GT efficiency (%)	Line number of replicates	Number of the T_1 single lines	Number of seeds	Number of GT plants	GT efficiency (%)	Normalized GT efficiency (%)
Col-0::SunTag-HsTREX1											
SY199-1	1	11704	88	0.75	0.91	**SY310-1**	2	9478	33	0.35	0.42
	2	1356	2	0.15	0.18		7	1339	0	0.00	0.00
	3	7617	2	0.03	0.03		9	948	3	0.32	0.38
	4	10634	21	0.20	0.24		10	148	0	0.00	0.00
	5	11138	76	0.68	0.82		11	591	1	0.17	0.20
	6	7556	11	0.15	0.18		12	643	0	0.00	0.00
	7	7539	10	0.13	0.16		13	452	0	0.00	0.00
	8	939	2	0.21	0.26		14	600	0	0.00	0.00
	9	9791	59	0.60	0.73		15	356	0	0.00	0.00
	10	9704	29	0.30	0.36		16	626	0	0.00	0.00
	11	13051	19	0.15	0.18		17	1704	0	0.00	0.00
	12	12617	61	0.48	0.58		18	191	0	0.00	0.00
	13	9373	13	0.14	0.17		44	261	0	0.00	0.00
	14	4400	29	0.66	0.80		45	200	0	0.00	0.00
	15	10869	56	0.52	0.62		46	183	0	0.00	0.00
SY199-2	21	16364	0	0.00	0.00		47	713	0	0.00	0.00
	22	9947	1	0.01	0.01		48	104	0	0.00	0.00
	23	14790	284	1.92	2.32	**SY310-2**	19	374	0	0.00	0.00
	24	7373	17	0.23	0.28		20	1469	0	0.00	0.00
	25	13460	40	0.30	0.36		21	843	0	0.00	0.00
	26	12686	0	0.00	0.00		22	504	0	0.00	0.00
	27	9452	0	0.00	0.00		23	5443	0	0.00	0.00
	28	10086	63	0.62	0.75		24	365	0	0.00	0.00
	29	11999	16	0.13	0.16		25	70	0	0.00	0.00
	30	15712	19	0.12	0.15		27	1139	0	0.00	0.00
	31	17	0	0.00	0.00		28	191	0	0.00	0.00
	32	1313	0	0.00	0.00		29	565	0	0.00	0.00
	33	1843	8	0.43	0.52		30	278	3	1.08	1.30
	34	2000	9	0.45	0.54		31	539	0	0.00	0.00
	35	6721	11	0.16	0.20		32	313	0	0.00	0.00
	36	1096	2	0.18	0.22		33	548	0	0.00	0.00
SY489	1	7852	0	0.00	0.00		34	1052	1	0.10	0.11
	2	23103	52	0.23	0.27		35	1400	0	0.00	0.00
	3	12477	0	0.00	0.00		36	435	0	0.00	0.00
	4	15686	133	0.85	1.02		37	278	0	0.00	0.00
	5	15399	39	0.25	0.31		38	861	6	0.70	0.84
	6	9712	0	0.00	0.00		39	191	0	0.00	0.00
	7	8026	0	0.00	0.00		40	157	0	0.00	0.00
	11	12947	0	0.00	0.00		41	1956	0	0.00	0.00
							42	409	0	0.00	0.00
							43	174	0	0.00	0.00

Line number of replicates	Number of the T_1 single lines	Number of seeds	Number of GT plants	GT efficiency (%)	Normalized GT efficiency (%)	Line number of replicates	Number of the T_1 single lines	Number of seeds	Number of GT plants	GT efficiency (%)	Normalized GT efficiency (%)
Col-0::SunTag-PapE											
SY200-1	1	8049	2	0.02	0.04	**SY200-2**	21	2625	2	0.08	0.11
	2	10189	55	0.54	0.80		23	6782	40	0.59	0.88
	3	5101	28	0.55	0.82		24	1617	7	0.43	0.65
	4	7027	31	0.44	0.66		25	7104	0	0.00	0.00
	5	2930	9	0.31	0.46		26	5269	6	0.11	0.17
	6	5519	0	0.00	0.00		27	8549	7	0.08	0.12
	7	5960	0	0.00	0.00		29	4529	18	0.40	0.59
	8	2766	16	0.58	0.86		30	3239	4	0.12	0.18
	9	7540	30	0.40	0.59	**SY442**	1	3761	5	0.13	0.20
	10	5492	32	0.58	0.87		2	6391	23	0.36	0.54
	12	8267	10	0.12	0.18		3	7245	0	0.00	0.00
	13	6450	82	1.27	1.89		4	2784	1	0.04	0.05
	14	6028	50	0.83	1.24		5	2735	9	0.33	0.49
SY276	1	3025	65	2.15	3.20		6	3025	75	2.48	3.70
	2	7204	67	0.93	1.39		7	4502	0	0.00	0.00
SY329	11	3502	7	0.20	0.30		8	1744	22	1.26	1.88
	12	254	0	0.00	0.00		9	1826	0	0.00	0.00
	13	3125	1	0.03	0.05		10	3966	17	0.43	0.64
	14	2448	3	0.12	0.18		11	9135	13	0.14	0.21
	15	2880	0	0.00	0.00		12	4129	9	0.22	0.32
	16	2648	1	0.04	0.06		13	3143	10	0.32	0.47
	17	949	8	0.84	1.26		14	6287	30	0.48	0.71
	18	4324	19	0.44	0.65		15	5074	13	0.26	0.38
	22	3148	27	0.86	1.28		16	5755	4	0.07	0.10
	1	2271	4	0.18	0.26		17	4252	81	1.91	2.84
	2	2698	2	0.07	0.11		18	5187	9	0.17	0.26
	3	2648	10	0.38	0.56		19	4352	23	0.53	0.79
	4	3461	3	0.09	0.13		20	627	3	0.48	0.71
	5	2688	9	0.33	0.50						

Line number of replicates	Number of the T_1 single lines	Number of seeds	Number of GT plants	GT efficiency (%)	Normalized GT efficiency (%)	Line number of replicates	Number of the T_1 single lines	Number of seeds	Number of GT plants	GT efficiency (%)	Normalized GT efficiency (%)
Col-0::SunTag-HSVUL12											
	1	4143	51	1.23	1.80		21	1335	0	0.00	0.00
	2	3083	0	0.00	0.00		22	4545	0	0.00	0.00
	3	1812	5	0.28	0.40		23	1267	2	0.16	0.23
	4	5976	37	0.62	0.90		24	431	0	0.00	0.00
	5	3969	84	2.12	3.09		25	602	0	0.00	0.00
	6	6920	30	0.43	0.63		26	1241	1	0.08	0.12
	7	5955	28	0.47	0.69		27	1965	22	1.12	1.64
	8	5489	59	1.07	1.57		28	680	0	0.00	0.00
	9	4702	58	1.23	1.80		29	936	3	0.32	0.47
SY201-1	10	5809	4	0.07	0.10	**SY311**	30	2606	112	4.30	6.28
	11	6122	23	0.38	0.55		31	2061	0	0.00	0.00
	12	5660	33	0.58	0.85		32	456	1	0.22	0.32
	13	3111	38	1.22	1.78		33	733	2	0.27	0.40
	14	6144	38	0.62	0.90		34	1299	16	1.23	1.80
	15	4713	13	0.28	0.40		36	997	1	0.10	0.00
	16	4827	10	0.21	0.30		37	651	0	0.00	0.15
	17	4958	18	0.36	0.53		38	331	0	0.00	0.00
	19	1289	10	0.78	1.13		39	1128	1	0.09	0.00
	20	6243	7	0.11	0.16		40	812	0	0.00	0.13
	21	5528	24	0.43	0.63		1	2744	4	0.15	0.21
	22	5289	51	0.96	1.41		2	4300	24	0.56	0.82
	23	6774	64	0.94	1.38		3	2072	4	0.19	0.28
	24	5407	54	1.00	1.46		4	4143	4	0.10	0.14
SY201-2	26	4353	238	5.47	7.99		6	2307	6	0.26	0.38
	27	3264	181	5.55	8.10		7	2186	11	0.50	0.74
	28	5642	86	1.52	2.23		8	2922	30	1.03	1.50
	29	5870	36	0.61	0.90		9	3972	15	0.38	0.55
	30	6678	41	0.61	0.90		10	4214	32	0.76	1.11
	2	4407	44	1.00	1.46	**SY443**	11	4499	51	1.13	1.66
	3	1068	9	0.84	1.23		12	6080	41	0.67	0.99
	12	993	0	0.00	0.00		13	4047	9	0.22	0.32
	16	2050	0	0.00	0.00		14	4140	4	0.10	0.14
	17	2082	1	0.05	0.07		15	5773	53	0.92	1.34
SY279	18	271	0	0.00	0.00		16	7023	29	0.41	0.60
	19	1481	1	0.07	0.10		17	420	0	0.00	0.00
	20	1641	0	0.00	0.00		18	2666	4	0.15	0.22
					1.80		19	5318	31	0.58	0.85
					0.00		20	5243	35	0.67	0.98

Line number of replicates	Number of the T_1 single lines	Number of seeds	Number of GT plants	GT efficiency (%)	Normalized GT efficiency (%)	Line number of replicates	Number of the T_1 single lines	Number of seeds	Number of GT plants	GT efficiency (%)	Normalized GT efficiency (%)
					***ku70*::SunTag**						
SY213	1	5645	0	0.00	0.00	**SY448**	1	4960	57	1.15	1.56
	2	7915	0	0.00	0.00		2	2690	22	0.82	1.11
	3	777	30	3.86	5.25		3	7442	0	0.00	0.00
	4	3134	0	0.00	0.00		4	7717	0	0.00	0.00
	5	908	11	1.21	1.65		5	2067	40	1.94	2.63
	6	840	6	0.71	0.97		6	4293	28	0.65	0.89
	7	8012	0	0.00	0.00		7	2912	0	0.00	0.00
	10	3395	120	3.53	4.81		8	6688	63	0.94	1.28
	11	2434	24	0.99	1.34		9	9113	0	0.00	0.00
	12	3182	17	0.53	0.73		10	4245	20	0.47	0.64
	13	5423	0	0.00	0.00		11	9132	11	0.12	0.16
	14	2265	7	0.31	0.42		12	7886	0	0.00	0.00
	15	6027	105	1.74	2.37		13	3240	4	0.12	0.17
	16	473	4	0.85	1.15		14	8977	210	2.34	3.18
	17	652	3	0.46	0.63		15	4892	47	0.96	1.31
	18	1154	6	0.52	0.71		16	10798	0	0.00	0.00
SY321	23	2096	0	0.00	0.00		17	7239	0	0.00	0.00
	24	580	2	0.35	0.47		18	9296	0	0.00	0.00
	25	2308	8	0.35	0.47		19	8354	0	0.00	0.00
	27	966	4	0.41	0.56		20	9615	0	0.00	0.00
	28	338	0	0.00	0.00	**SY224**	1	3028	51	1.68	2.29
	29	1188	1	0.08	0.11		6	1444	24	1.66	2.26
	30	473	0	0.00	0.00		7	4704	157	3.34	4.54
	31	1671	2	0.12	0.16		9	2197	9	0.41	0.56
	32	2052	0	0.00	0.00		10	5689	70	1.23	1.67
	33	2453	21	0.86	1.16	**SY289**	3	11976	0	0.00	0.00
	34	2304	5	0.22	0.30		5	6399	44	0.69	0.94
	35	362	0	0.00	0.00		8	7456	237	3.18	4.32
	36	1405	0	0.00	0.00		9	1796	1	0.06	0.08
	37	1371	6	0.44	0.60		17	270	0	0.00	0.00
							19	2690	14	0.52	0.71
							20	174	0	0.00	0.00

Line number of replicates	Number of the T_1 single lines	Number of seeds	Number of GT plants	GT efficiency (%)	Normalized GT efficiency (%)	Line number of replicates	Number of the T_1 single lines	Number of seeds	Number of GT plants	GT efficiency (%)	Normalized GT efficiency (%)
***ku70*::SunTag-HsTREX1**											
	3	1515	41	2.71	3.36		21	4771	0	0.00	0.00
	4	5950	0	0.00	0.00		22	2319	0	0.00	0.00
	5	6766	0	0.00	0.00		23	12022	204	1.70	2.11
SY210-1	9	3689	11	0.30	0.37		25	6147	1	0.02	0.02
	11	3470	9	0.26	0.32		26	10310	167	1.62	2.01
	16	1133	5	0.44	0.55		29	3811	65	1.71	2.12
	17	6037	0	0.00	0.00		30	12728	37	0.29	0.36
	21	856	2	0.23	0.29		31	6737	13	0.19	0.24
	24	6106	18	0.29	0.37		32	4233	7	0.17	0.21
SY210-2	25	4516	2	0.04	0.06		33	7009	53	0.76	0.94
	26	3030	119	3.93	4.88		34	8749	43	0.49	0.61
	27	1081	0	0.00	0.00		35	2556	10	0.39	0.49
	1	1041	0	0.00	0.00		36	2174	14	0.64	0.80
	2	1272	0	0.00	0.00		37	5181	26	0.50	0.62
	11	810	0	0.00	0.00		38	5256	36	0.68	0.85
	13	2041	1	0.05	0.06		39	7367	1	0.01	0.02
	14	902	0	0.00	0.00	**SY482**	40	5360	0	0.00	0.00
SY273-1	15	3117	15	0.48	0.60		41	6488	11	0.17	0.21
	16	1631	0	0.00	0.00		42	4730	0	0.00	0.00
	17	243	0	0.00	0.00		45	3337	0	0.00	0.00
	18	1717	12	0.70	0.87		46	10675	48	0.45	0.56
	19	2290	0	0.00	0.00		48	7934	74	0.93	1.16
	20	2290	0	0.00	0.00		49	2157	2	0.09	0.12
	21	1342	0	0.00	0.00		50	5869	1	0.02	0.02
	22	584	0	0.00	0.00		51	6633	47	0.71	0.88
	23	249	0	0.00	0.00		52	9802	83	0.85	1.05
	24	324	0	0.00	0.00		55	9900	36	0.36	0.45
SY273-2	25	1139	0	0.00	0.00		56	4557	0	0.00	0.00
	26	2492	0	0.00	0.00		57	5459	22	0.40	0.50
							58	4221	3	0.07	0.09
							59	6766	28	0.41	0.51
							60	11594	70	0.60	0.75

Line number of replicates	Number of the T_1 single lines	Number of seeds	Number of GT plants	GT efficiency (%)	Normalized GT efficiency (%)	Line number of replicates	Number of the T_1 single lines	Number of seeds	Number of GT plants	GT efficiency (%)	Normalized GT efficiency (%)
***ku70*::SunTag-PapE**											
SY211-1	3	3318	0	0.00	0.00	**SY445**	1	2618	31	1.18	1.64
	6	870	7	0.80	1.11		2	4910	40	0.81	1.13
	9	735	7	0.95	1.32		3	5846	85	1.45	2.01
	12	4296	0	0.00	0.00		4	1869	91	4.87	6.75
	15	3193	22	0.69	0.95		5	794	5	0.63	0.87
	16	2826	3	0.11	0.15		6	3343	58	1.74	2.40
	20	1241	1	0.08	0.11		7	3842	8	0.21	0.29
SY312	22	624	0	0.00	0.00		8	957	51	5.33	7.38
	23	572	1	0.17	0.24		9	5166	0	0.00	0.00
	24	999	8	0.80	1.11		10	2060	0	0.00	0.00
	25	569	1	0.18	0.24		11	1626	10	0.61	0.85
	26	798	14	1.76	2.43		12	76	0	0.00	0.00
	27	1404	50	3.56	4.93		13	2167	1	0.05	0.06
	28	583	31	5.32	7.37		14	4792	15	0.31	0.43
	29	579	4	0.69	0.96		15	1522	4	0.26	0.36
	30	413	7	1.70	2.35		16	2871	16	0.56	0.77
	31	142	0	0.00	0.00		17	700	2	0.29	0.40
	32	218	0	0.00	0.00		18	2992	18	0.60	0.83
	33	135	0	0.00	0.00		19	4573	17	0.37	0.51
	34	381	2	0.52	0.73		20	3925	0	0.00	0.00
	35	83	0	0.00	0.00	**SY211-2**	21	2899	29	1.00	1.39
	36	309	0	0.00	0.00		25	3492	65	1.86	2.58
	37	926	0	0.00	0.00		26	749	16	2.14	2.96
	38	350	1	0.29	0.40		29	1751	0	0.00	0.00
	39	1207	16	1.33	1.84		30	101	0	0.00	0.00
	17	1123	0	0.00	0.00	**SY280**	2	5409	0	0	0.00
	18	919	1	0.11	0.15		10	1130	11	0.97	1.35
	19	1661	4	0.24	0.33		13	5368	20	0.37	0.52
							16	5055	43	0.85	1.18

Line number of replicates	Number of the T_1 single lines	Number of seeds	Number of GT plants	GT efficiency (%)	Normalized GT efficiency (%)	Line number of replicates	Number of the T_1 single lines	Number of seeds	Number of GT plants	GT efficiency (%)	Normalized GT efficiency (%)
***ku70*::SunTag-HSVUL12**											
SY212	3	677	4	0.59	0.95	**SY319**	21	3161	0	0.00	0.00
	4	6846	0	0.00	0.00		22	1936	6	0.31	0.50
	6	6498	163	2.51	4.03		23	1871	6	0.32	0.52
	8	4761	67	1.41	2.26		24	941	0	0.00	0.00
	11	245	6	2.45	3.94		25	846	0	0.00	0.00
	19	6299	42	0.67	1.07		26	2843	0	0.00	0.00
	20	2886	39	1.35	2.17		27	796	24	3.02	4.85
SY287	7	2606	118	4.53	7.28		28	40402	14	0.03	0.06
	16	2736	16	0.58	0.94		29	2032	18	0.89	1.42
	17	762	6	0.79	1.27		30	1730	1	0.06	0.09
	18	2327	1	0.04	0.07		32	4060	7	0.17	0.28
	19	597	0	0.00	0.00		37	1140	0	0.00	0.00
	20	1393	0	0.00	0.00		38	1741	0	0.00	0.00
	61	4830	6	0.12	0.20		39	697	0	0.00	0.00
	62	6399	0	0.00	0.00		40	1045	0	0.00	0.00
SY446	1	2495	0	0.00	0.00		41	513	0	0.00	0.00
	2	2269	6	0.26	0.43		42	111	0	0.00	0.00
	3	4546	123	2.71	4.35		43	360	0	0.00	0.00
	4	3280	17	0.52	0.83		44	161	0	0.00	0.00
	5	1883	14	0.74	1.20		45	666	0	0.00	0.00
	6	4971	5	0.10	0.16		46	1339	0	0.00	0.00
	7	5400	96	1.78	2.86		47	471	0	0.00	0.00
	8	1221	3	0.25	0.40		48	482	1	0.21	0.33
	9	1355	9	0.66	1.07		49	494	0	0.00	0.00
	10	3636	0	0.00	0.00		50	1986	0	0.00	0.00
	11	1875	30	1.60	2.57		51	459	0	0.00	0.00
	13	4481	24	0.54	0.86		52	184	1	0.54	0.88
	14	6766	26	0.38	0.62		53	1623	1	0.06	0.10
	15	3655	120	3.28	5.28		54	310	0	0.00	0.00
	16	4895	0	0.00	0.00		55	1018	0	0.00	0.00
	17	6315	48	0.76	1.22		56	421	0	0.00	0.00
	18	7313	0	0.00	0.00		57	731	2	0.27	0.44
	19	3490	16	0.46	0.74		58	383	0	0.00	0.00
	20	4332	45	1.04	1.67		59	448	0	0.00	0.00
					0.00		60	107	0	0.00	0.00

Table 7.14: Raw ONT read counts for ADH1, CEN4, and ECA3 across SunTag-based editing approaches.

The table presents raw ONT read counts for the ADH1, CEN4, and ECA3 target sites. For each target site, read counts are shown for the SunTag approach and the SunTag-HsTREX1, SunTag-PapE, and SunTag-HSVUL12 exonuclease-recruitment approaches across three replicates. Reads are categorized as precise ligation, insertions, indels, deletions, total mutated reads, and total reads.

Mutation category	ADH1-SunTag			ADH1-SunTag-HsTREX1			ADH1-SunTag-PapE			ADH1-SunTag-HSVUL12		
	replicate 1	replicate 2	replicate 3	replicate 1	replicate 2	replicate 3	replicate 1	replicate 2	replicate 3	replicate 1	replicate 2	replicate 3
precise ligation	84	61	228	74	83	66	114	235	98	77	100	65
insertions	1	1	3	8	3	0	1	1	2	0	5	2
InDels	2	0	3	8	8	0	3	32	8	11	2	11
deletions	134	82	581	360	309	110	289	497	115	286	191	249
total mutated reads	137	83	587	376	320	110	293	530	125	297	198	262
total reads	221	144	815	450	403	176	407	765	223	374	298	327
Mutation category	**Cen4-SunTag**			**Cen4-SunTag-HsTREX1**			**Cen4-SunTag-PapE**			**Cen4-SunTag-HSVUL12**		
	replicate 1	replicate 2	replicate 3	replicate 1	replicate 2	replicate 3	replicate 1	replicate 2	replicate 3	replicate 1	replicate 2	replicate 3
precise ligation	1149	521	1588	767	1614	1812	638	731	1488	716	268	790
insertions	7	2	9	3	47	17	9	8	6	4	7	2
InDels	26	11	5	3	0	1	7	1	4	0	1	8
deletions	639	282	630	578	784	635	582	220	589	376	181	383
total mutated reads	672	295	644	584	831	653	598	229	599	380	189	393
total reads	1821	816	2232	1351	2445	2465	1236	960	2087	1096	457	1183
Mutation category	**ECA3-SunTag**			**ECA3-SunTag-HsTREX1**			**ECA3-SunTag-PapE**			**ECA3-SunTag-HSVUL12**		
	replicate 1	replicate 2	replicate 3	replicate 1	replicate 2	replicate 3	replicate 1	replicate 2	replicate 3	replicate 1	replicate 2	replicate 3
precise ligation	487	558	1194	472	559	1126	296	400	287	589	725	470
insertions	6	20	9	8	1	6	16	3	1	32	6	3
InDels	44	52	10	13	0	66	28	17	3	29	7	16
deletions	1146	862	1000	839	231	596	1343	912	816	658	685	1426
total mutated reads	1196	934	1019	860	232	668	1387	932	820	719	698	1445
total reads	1683	1492	2213	1332	791	1794	1683	1332	1107	1308	1423	1915

Table 7.15: Deletion frequency distribution around the DSB sites at the ADH1, CEN4, and ECA3 target regions.

The table shows the distribution of deletion frequencies around the double-strand break (DSB) sites at the ADH1, CEN4, and ECA3 target regions, with the respective cleavage site defined as position 0. Deletion counts are shown from 40 bp upstream to 40 bp downstream of the DSB site for the SunTag approach and the three exonuclease-recruitment approaches, SunTag-HsTREX1, SunTag-PapE, and SunTag-HSVUL12, across three replicates.

Position	ADH1-SunTag			ADH1-SunTag-HsTREX1			ADH1-SunTag-PapE			ADH1-SunTag-HSVUL12		
	replicate 1	replicate 2	replicate 3	replicate 1	replicate 2	replicate 3	replicate 1	replicate 2	replicate 3	replicate 1	replicate 2	replicate 3
-40	8	1	39	5	8	2	7	18	4	25	8	3
-39	8	1	38	5	8	2	7	17	3	25	8	2
-38	9	1	37	5	8	2	8	17	3	25	8	2
-37	8	1	38	5	8	3	9	17	3	25	8	5
-36	8	1	40	5	8	3	9	17	3	24	8	5
-35	10	10	47	18	12	5	15	50	13	27	24	5
-34	11	10	47	18	12	5	15	50	13	27	24	5
-33	11	10	48	21	16	6	19	53	13	28	25	5
-32	12	10	48	21	15	6	19	53	13	28	25	5
-31	9	11	50	21	15	7	20	53	15	28	25	7
-30	9	11	50	21	16	7	21	53	15	28	27	7
-29	8	12	52	25	17	7	23	57	16	29	27	11
-28	9	12	53	25	18	8	29	60	16	29	27	11
-27	12	13	65	47	35	10	42	73	18	39	29	24
-26	12	13	66	46	41	12	43	74	18	42	30	29
-25	11	13	67	46	41	11	43	75	19	43	30	30
-24	12	15	73	50	42	10	45	76	18	43	31	30
-23	20	19	137	125	80	26	79	212	28	69	47	38
-22	20	19	141	126	79	26	78	213	28	70	47	33
-21	20	18	204	141	82	26	80	215	29	72	50	33
-20	21	19	207	152	108	29	80	216	30	74	51	35
-19	22	19	207	155	109	35	84	212	28	80	53	35
-18	22	20	212	177	111	36	85	220	30	77	51	36
-17	20	20	214	180	114	34	88	217	31	80	51	38
-16	27	20	225	183	115	34	89	222	34	80	52	38
-15	24	20	226	182	114	34	88	221	29	82	55	69
-14	25	17	230	184	114	35	87	220	31	84	56	69
-13	25	17	243	186	113	37	90	221	32	85	55	71
-12	31	17	250	196	111	36	91	234	32	87	71	76
-11	32	17	260	198	112	36	90	236	33	88	71	77
-10	33	20	262	200	121	43	99	240	33	92	73	85
-9	34	20	273	201	123	44	111	243	33	95	73	90
-8	36	22	281	203	124	51	119	250	34	112	77	105
-7	50	23	292	211	137	55	125	262	37	120	79	108
-6	64	25	310	218	152	63	136	286	39	129	85	113
-5	80	40	410	246	208	73	164	309	52	188	102	127
-4	113	43	484	302	260	85	245	386	67	259	138	148
-3	138	46	528	318	316	91	271	461	87	296	150	163
-2	133	71	533	351	339	97	297	502	112	287	171	239
-1	138	82	554	363	346	111	310	526	112	302	191	254

Position	ADH1-SunTag			ADH1-SunTag-HsTREX1			ADH1-SunTag-PapE			ADH1-SunTag-HSVUL12		
	replicate 1	replicate 2	replicate 3	replicate 1	replicate 2	replicate 3	replicate 1	replicate 2	replicate 3	replicate 1	replicate 2	replicate 3
0	131	78	543	356	320	109	296	503	109	289	180	255
1	127	76	536	346	294	105	278	482	109	280	181	236
2	126	81	561	356	304	110	281	495	114	281	188	247
3	91	73	511	288	250	91	257	431	107	200	131	204
4	81	61	498	250	231	71	206	386	100	157	119	191
5	69	57	444	150	190	51	152	239	86	120	98	179
6	60	49	423	136	172	48	143	200	64	103	96	173
7	58	36	410	120	164	40	128	159	53	95	79	166
8	58	36	407	119	153	39	134	157	53	92	75	166
9	52	33	380	108	138	36	122	146	50	78	73	162
10	48	33	370	104	132	35	110	143	46	70	72	155
11	44	31	322	83	109	33	94	125	44	58	67	139
12	43	31	302	81	104	31	89	122	44	55	66	137
13	44	31	283	78	96	24	85	114	44	49	65	136
14	43	31	280	74	96	23	80	112	44	47	65	136
15	39	31	274	70	94	23	81	88	43	45	65	136
16	34	23	268	67	90	21	77	85	29	44	64	135
17	33	23	212	61	86	16	73	80	28	43	61	130
18	33	23	208	60	85	16	73	79	28	43	61	130
19	27	10	197	40	57	11	53	66	12	30	43	105
20	24	9	187	40	54	10	51	66	12	30	41	104
21	24	7	181	42	47	10	38	35	8	25	39	99
22	25	7	175	37	45	9	37	34	7	18	32	97
23	25	7	176	32	43	8	37	32	8	18	30	89
24	21	7	175	30	40	6	34	30	7	15	29	88
25	21	7	168	26	39	5	33	30	5	12	25	85
26	28	8	176	44	49	10	33	42	8	20	28	88
27	20	6	158	25	40	5	29	26	5	12	24	84
28	20	6	158	23	38	5	29	26	5	11	24	85
29	20	6	157	26	37	5	31	24	5	11	25	84
30	20	7	157	24	35	6	29	26	5	11	24	84
31	20	7	156	23	36	6	29	27	5	11	24	84
32	20	7	156	23	35	6	28	26	5	9	23	84
33	9	6	150	23	30	5	25	24	7	11	24	82
34	8	8	150	22	30	5	24	22	7	9	16	80
35	8	5	146	22	28	4	24	20	5	6	2	80
36	7	5	147	21	26	4	24	20	4	6	2	80
37	5	5	145	21	25	4	24	19	4	6	2	80
38	5	4	145	21	26	4	24	20	4	6	2	80
39	5	4	147	21	26	4	23	21	5	6	3	80
40	5	4	147	21	26	4	22	20	4	6	3	80

Position	Cen4-SunTag			Cen4-SunTag-HsTREX1			Cen4-SunTag-PapE			Cen4-SunTag-HSVUL12		
	replicate 1	replicate 2	replicate 3	replicate 1	replicate 2	replicate 3	replicate 1	replicate 2	replicate 3	replicate 1	replicate 2	replicate 3
-40	48	20	37	55	50	16	26	8	32	50	47	46
-39	48	22	39	55	52	20	26	8	32	50	48	46
-38	49	22	44	55	52	24	26	10	31	50	47	46
-37	51	22	43	57	54	25	26	10	30	52	46	45
-36	57	36	55	56	63	37	32	24	33	57	47	50
-35	57	36	54	58	63	37	33	24	35	57	46	51
-34	58	36	54	59	64	39	35	24	34	57	46	55
-33	59	37	53	59	67	38	34	24	34	59	46	56
-32	59	37	54	61	69	43	38	24	38	55	46	57
-31	58	35	54	60	65	40	38	24	35	54	47	57
-30	65	35	57	60	69	43	37	23	34	54	48	61
-29	67	36	56	65	79	46	41	24	41	54	47	60
-28	70	36	57	64	77	47	41	24	38	61	47	61
-27	70	37	61	64	80	44	42	24	36	63	47	63
-26	69	37	77	64	79	45	41	24	36	62	47	62
-25	70	37	78	63	78	45	58	24	39	59	46	62
-24	74	38	81	63	78	48	59	24	40	59	46	61
-23	76	40	82	70	78	53	64	25	42	61	48	62
-22	78	41	89	72	79	56	65	27	50	61	48	65
-21	84	43	93	75	83	61	69	33	53	62	49	67
-20	78	40	104	72	79	54	66	27	49	61	51	62
-19	76	41	102	72	81	51	65	25	54	62	51	61
-18	131	47	126	137	98	53	73	25	57	64	51	65
-17	135	49	128	135	101	57	74	26	57	65	51	66
-16	137	49	132	136	109	58	75	25	62	86	54	71
-15	140	49	134	138	125	60	79	26	63	88	54	71
-14	142	49	141	139	153	66	83	27	80	90	52	75
-13	166	51	150	140	166	67	97	29	89	92	52	78
-12	169	54	155	139	177	69	99	28	95	93	53	80
-11	174	58	159	145	194	73	137	28	96	93	54	84
-10	193	60	171	150	227	79	148	33	102	99	56	97
-9	215	87	221	169	327	113	179	57	124	132	56	115
-8	242	93	250	180	370	125	193	73	132	144	67	128
-7	257	99	266	185	378	133	224	86	145	132	74	133
-6	271	116	307	195	418	158	253	92	160	145	80	150
-5	338	136	377	275	495	249	348	107	296	192	96	194
-4	534	212	549	448	663	459	540	162	393	306	126	323
-3	867	383	902	725	1175	1097	883	251	692	482	191	565
-2	879	386	907	733	1184	1089	877	252	704	494	190	567
-1	860	363	860	700	1178	1069	793	238	659	464	180	556
0	911	408	932	746	1155	1120	835	261	770	510	226	549
1	625	272	581	554	754	614	537	197	555	362	173	367
2	517	247	575	474	688	567	524	200	504	340	167	317
3	492	235	528	456	626	445	474	181	462	311	154	232
4	321	160	359	285	527	303	362	150	296	236	116	197
5	182	102	197	188	307	131	178	64	112	114	67	104

Position	Cen4-SunTag			Cen4-SunTag-HsTREX1			Cen4-SunTag-PapE			Cen4-SunTag-HSVUL12		
	replicate 1	replicate 2	replicate 3	replicate 1	replicate 2	replicate 3	replicate 1	replicate 2	replicate 3	replicate 1	replicate 2	replicate 3
6	167	96	175	174	287	89	160	60	90	97	56	61
7	122	64	133	70	266	56	128	46	74	65	23	47
8	104	58	105	57	236	43	111	40	51	49	14	42
9	101	54	101	53	234	40	92	38	47	48	14	39
10	97	50	92	51	226	38	84	37	42	47	12	38
11	92	47	91	42	225	35	73	38	40	40	10	35
12	84	36	70	40	207	27	68	36	37	31	10	34
13	86	35	66	36	187	27	67	34	35	31	10	33
14	81	35	64	35	166	26	65	34	29	29	10	31
15	76	34	59	39	152	24	62	34	20	26	9	28
16	74	34	57	38	153	24	65	34	19	25	11	27
17	73	30	51	40	155	20	67	28	20	25	11	24
18	70	30	50	41	153	19	64	28	20	22	11	24
19	70	30	50	40	147	19	65	28	19	21	11	24
20	57	26	30	42	142	16	31	27	12	14	9	20
21	57	26	32	42	141	20	32	27	12	14	10	21
22	54	26	32	38	139	15	31	26	13	13	10	20
23	53	26	32	36	135	15	32	26	12	13	10	20
24	55	25	31	32	135	17	61	25	13	13	10	22
25	53	25	29	31	135	10	60	28	13	11	10	22
26	55	27	30	31	139	18	59	30	19	14	11	23
27	51	25	25	30	134	14	57	27	13	12	10	22
28	50	25	25	31	136	15	56	28	17	11	10	24
29	50	24	24	32	139	15	55	27	16	12	10	21
30	49	24	24	32	137	18	55	27	15	12	10	20
31	49	22	23	33	124	16	56	28	17	12	10	21
32	49	20	22	33	124	14	54	28	15	10	9	19
33	50	20	22	31	122	13	54	28	17	8	11	18
34	55	19	27	33	100	11	53	30	20	10	12	17
35	54	19	25	25	98	9	52	31	21	9	12	11
36	54	23	28	26	98	14	53	30	18	9	11	11
37	52	19	22	27	85	7	53	26	17	12	10	10
38	46	20	19	26	76	6	52	25	17	10	10	7
39	52	22	29	32	79	13	57	26	24	15	14	9
40	47	19	22	24	77	4	52	25	13	9	10	5

Position	ECA3-SunTag			ECA3-SunTag-HsTREX1			ECA3-SunTag-PapE			ECA3-SunTag-HSVUL12		
	replicate 1	replicate 2	replicate 3	replicate 1	replicate 2	replicate 3	replicate 1	replicate 2	replicate 3	replicate 1	replicate 2	replicate 3
-40	19	57	79	79	22	13	42	18	26	24	24	35
-39	20	57	80	80	23	11	42	17	26	24	24	34
-38	20	57	81	81	23	11	42	16	27	24	24	35
-37	21	58	101	81	23	15	51	15	31	24	32	42
-36	25	60	103	84	22	16	53	16	24	24	33	41
-35	34	64	104	90	23	17	56	15	27	25	37	47
-34	26	64	103	85	22	25	51	18	28	26	33	45
-33	28	61	107	86	22	26	58	18	29	28	39	46
-32	27	65	103	89	23	27	57	19	40	28	33	46
-31	34	65	105	90	25	31	69	21	40	28	35	56
-30	34	64	105	89	28	32	72	22	36	29	36	57
-29	40	68	116	93	30	39	85	26	43	37	43	76
-28	34	64	106	90	29	33	76	23	38	30	39	57
-27	36	66	106	110	30	33	74	25	40	30	38	59
-26	39	69	113	113	36	34	76	42	42	36	40	61
-25	36	67	108	108	35	33	75	39	42	34	38	62
-24	41	68	108	111	39	35	76	38	46	33	37	66
-23	40	66	110	112	41	37	72	38	46	37	37	67
-22	41	66	113	113	41	37	73	40	46	37	37	67
-21	43	68	119	119	42	29	75	67	48	39	37	70
-20	50	71	120	128	45	35	81	73	54	43	44	72
-19	53	73	124	130	47	33	85	74	66	50	45	74
-18	56	76	125	132	48	33	89	76	69	52	43	88
-17	57	89	121	133	49	34	90	81	82	50	46	83
-16	86	121	155	236	56	47	137	103	116	65	58	116
-15	88	123	164	247	58	56	141	108	123	71	61	122
-14	98	134	162	271	66	63	154	118	137	77	64	130
-13	106	172	164	261	69	80	163	117	138	77	75	137
-12	112	179	182	281	71	84	175	122	159	85	77	142
-11	109	130	176	304	70	76	175	123	160	85	80	142
-10	108	130	188	310	77	74	176	124	161	91	81	148
-9	114	138	220	320	87	80	180	126	171	98	83	159
-8	140	176	231	327	88	83	198	136	173	104	88	191
-7	249	324	317	390	140	230	309	222	209	188	127	261
-6	314	400	353	461	156	319	399	298	217	227	184	403
-5	522	576	687	606	190	440	698	446	317	361	296	739
-4	811	757	917	724	218	539	1011	728	536	526	513	1122
-3	1120	862	1059	817	257	706	1241	901	699	710	610	1430
-2	1197	945	1121	822	264	733	1336	969	724	756	655	1515
-1	1157	888	1075	811	259	713	1323	945	737	695	648	1450
0	1159	852	1037	810	259	704	1333	933	805	689	664	1455
1	1113	835	969	793	227	569	1309	889	789	633	661	1378
2	739	609	671	694	194	421	890	557	553	447	456	979
3	466	347	456	481	130	280	609	341	369	236	332	660
4	355	282	382	406	116	266	495	228	342	202	301	500
5	315	253	345	358	107	247	409	200	331	184	273	445

Position	ECA3-SunTag			ECA3-SunTag-HsTREX1			ECA3-SunTag-PapE			ECA3-SunTag-HSVUL12		
	replicate 1	replicate 2	replicate 3	replicate 1	replicate 2	replicate 3	replicate 1	replicate 2	replicate 3	replicate 1	replicate 2	replicate 3
6	263	212	289	263	95	175	324	164	282	153	237	338
7	235	200	279	251	86	143	307	157	264	137	233	314
8	205	177	264	237	83	114	282	132	252	119	220	281
9	171	155	247	234	78	106	245	116	170	102	191	258
10	163	145	242	211	76	97	235	106	152	97	185	221
11	159	141	237	204	66	91	231	102	147	93	183	206
12	111	116	218	197	60	78	181	80	121	77	155	164
13	99	106	199	182	52	56	159	70	102	62	141	137
14	83	98	188	177	51	51	146	64	88	59	137	123
15	75	93	168	162	50	51	139	60	82	57	133	120
16	51	76	120	143	46	37	104	55	74	48	119	79
17	46	56	93	136	37	32	100	50	70	44	115	74
18	38	55	43	129	36	30	99	49	67	40	112	66
19	33	51	36	120	32	31	93	45	65	40	109	63
20	32	44	37	116	32	33	92	45	65	41	107	63
21	31	42	78	110	30	31	85	44	62	38	104	52
22	31	43	77	107	31	27	81	45	58	32	95	52
23	29	41	78	107	27	30	79	44	56	32	94	54
24	27	37	74	106	27	28	77	43	53	30	94	50
25	24	37	28	103	27	29	72	45	54	29	100	48
26	23	37	29	103	33	26	73	45	27	28	94	49
27	23	37	26	101	29	25	71	42	21	26	79	45
28	20	38	25	96	30	27	71	41	21	23	80	45
29	18	34	27	96	26	22	71	40	20	23	78	46
30	16	34	22	64	24	21	70	36	16	20	75	43
31	16	32	19	63	24	19	69	37	16	20	74	43
32	17	32	19	65	24	19	72	37	18	21	76	41
33	18	33	18	66	26	18	75	41	16	21	74	45
34	15	31	18	64	24	19	70	35	15	20	73	41
35	17	32	20	61	24	19	71	38	15	21	74	41
36	15	30	19	57	23	18	54	37	12	20	72	40
37	13	29	19	56	23	15	50	36	12	15	61	38
38	12	29	18	57	23	16	50	36	12	15	61	38
39	13	27	20	57	23	17	50	33	15	15	61	41
40	16	29	18	57	24	16	49	34	13	15	61	37

7.4 Supplementary Results

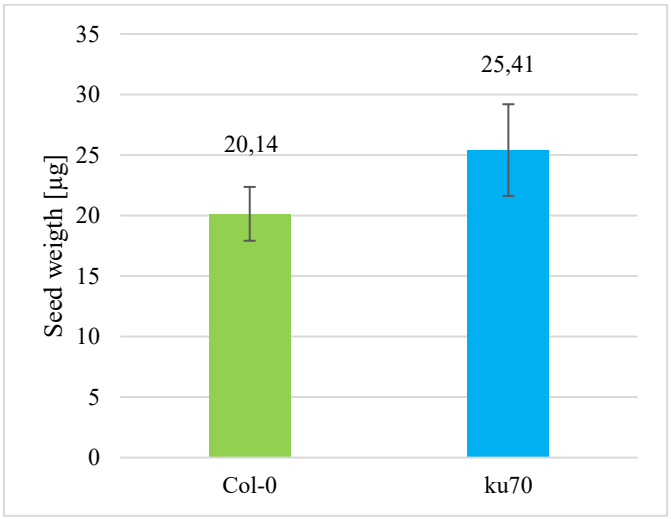

Figure 7.1: Seed weight of Col-0 wild type and *ku70* mutant plants used in Chapter 3.1.

The figure shows the determined weight of a single seed from Col-0 and *ku70* plants used in Chapter 3.1. Seed weight was determined from five replicates. Error bars indicate the standard deviation, and values above the bars represent the mean seed weight in µg.

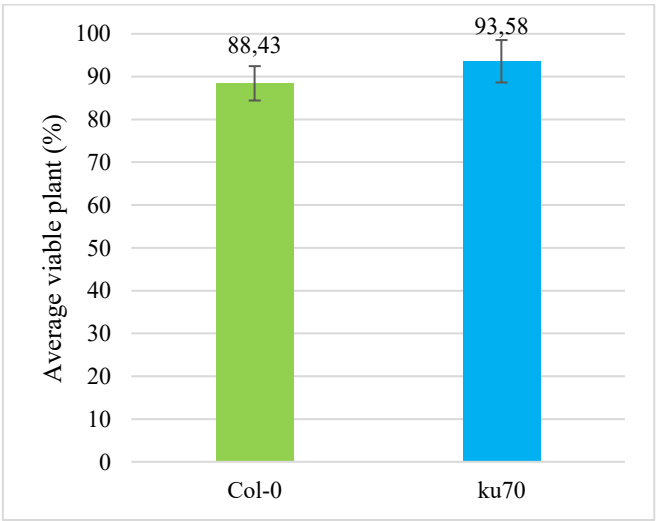

Figure 7.2: Average plant viability used for normalization of GT efficiency in Chapter 3.1.

Average plant viability is shown for Col-0 wild type and *ku70* plants based on six replicates. Error bars indicate the standard deviation, and values above the bars represent the mean viability in percent. The values were used to normalize the GT efficiencies in Chapter 3.1.

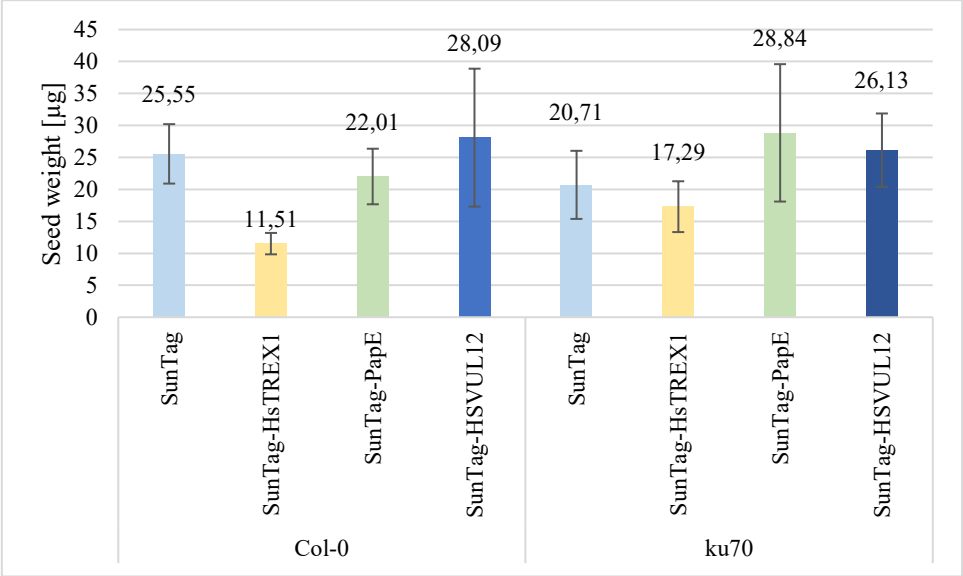

Figure 7.3: Seed weight of Col-0 wild type and *ku70* mutant plants used in Chapter 3.2.

The figure shows the mean seed weight of Col-0 and *ku70* lines carrying the SunTag, SunTag-HsTREX1, SunTag-PapE, and SunTag-HSVUL12 constructs used in Chapter 3.2. Bars represent the mean seed weight, and error bars indicate the standard deviation from five replicates. Values above the bars indicate the mean seed weight in µg.

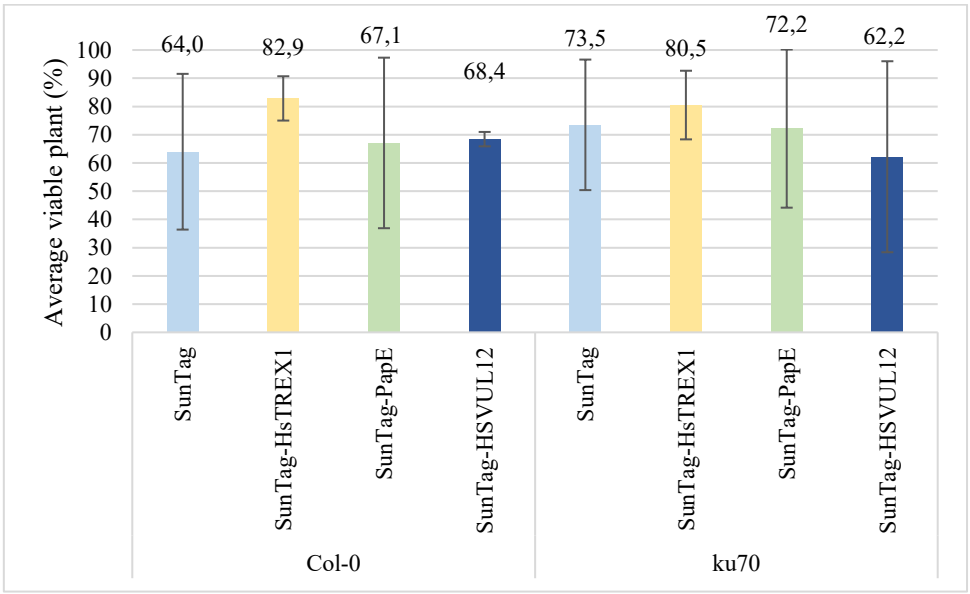

Figure 7.4: Average plant viability used for normalization of GT efficiency in Chapter 3.2.

Average plant viability is shown for Col-0 and *ku70* plants carrying the SunTag, SunTag-HsTREX1, SunTag-PapE, and SunTag-HSVUL12 constructs used in Chapter 3.2. Plant viability was determined based on six replicates. Error bars indicate the standard deviation, and values above the bars represent the mean viability in percent.